Domain Specific Interactions, Unfolding and Ultrafast Dynamics of Human and Bovine Serum Albumin: A Bulk and Single Molecular Level Study

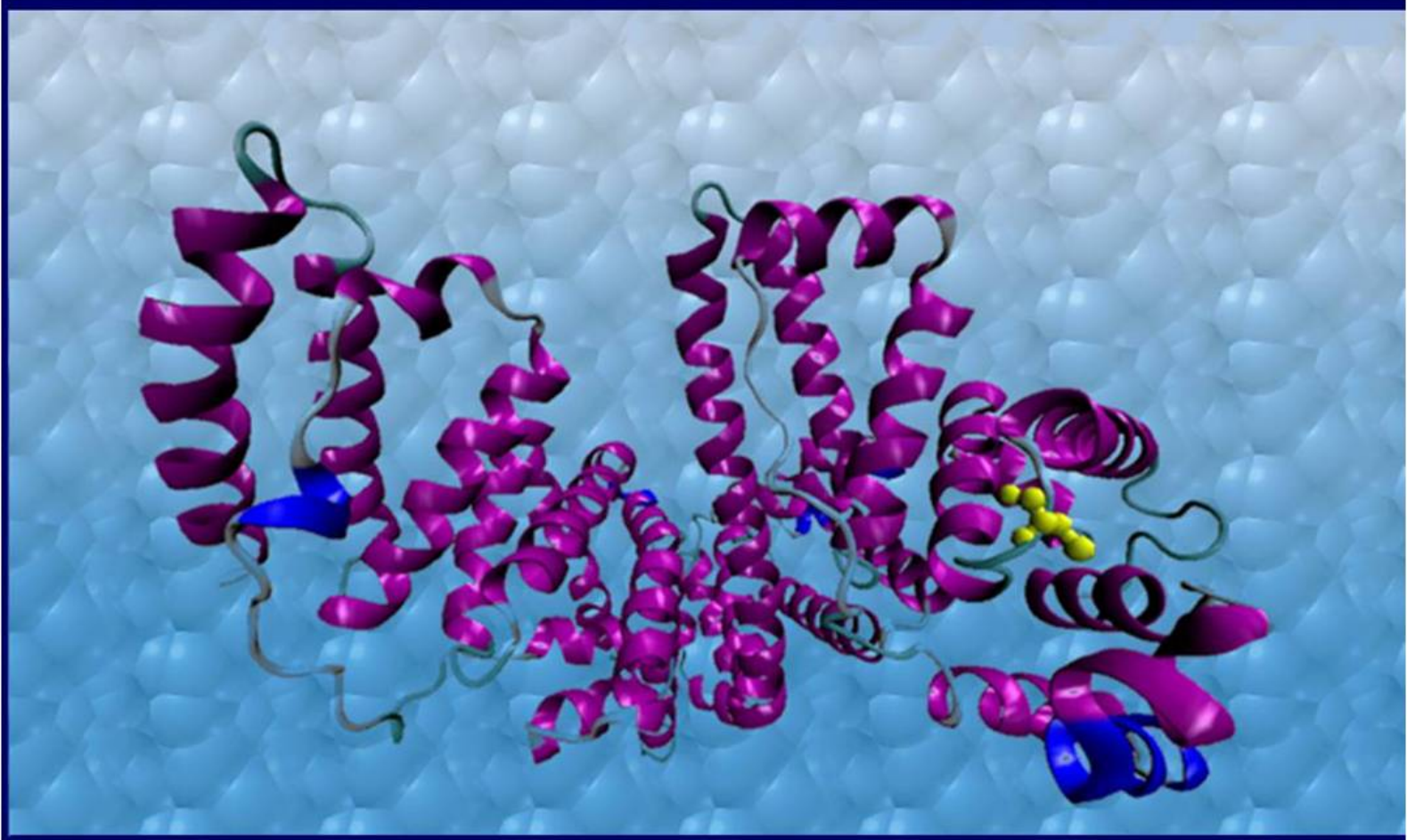

Rajeev Yadav

Department of Chemistry
Indian Institute of Technology Kanpur
Kanpur, India
May, 2014

Domain Specific Interactions, Unfolding and Ultrafast Dynamics of Human and Bovine Serum Albumin: A Bulk and Single Molecular Level Study

A Thesis

Submitted in Partial Fulfillment of the Requirements
for the Degree of

DOCTOR OF PHILOSOPHY

by

RAJEEV YADAV

to the

Department of Chemistry
Indian Institute of Technology Kanpur
Kanpur, India

May, 2014

STATEMENT

I hereby declare that the work manifested in the thesis entitled **"Domain Specific Interactions, Unfolding and Ultrafast Dynamics of Human and Bovine Serum Albumin: A Bulk and Single Molecular Level Study"** is the result of research carried out by me in the Department of Chemistry, Indian Institute of Technology Kanpur, India under the supervision of **Dr. Pratik Sen**.

In keeping with general practice of reporting scientific observations, due acknowledgements have been made whenever the work described is based on the findings of other investigators.

Rajeev Yadav

(Rajeev Yadav)

May, 2014
IIT Kanpur

CERTIFICATE

It is certified that the work reported in the thesis entitled **"Domain Specific Interactions, Unfolding and Ultrafast Dynamics of Human and Bovine Serum Albumin: A Bulk and Single Molecular Level Study"** has been carried out by **Mr. Rajeev Yadav** under my supervision and has not been submitted elsewhere for a degree.

Pratik Sen.

May, 2014
IIT Kanpur

(Dr. Pratik Sen)
Thesis Supervisor
Department of Chemistry
Indian Institute of Technology Kanpur
Kanpur - 208016, India

Dr. PRATIK SEN
Assistant Professor
Chemistry Department
Indian Institute of Technology, Kanpur
KANPUR U. P. 208 016

DEPARTMENT OF CHEMISTRY
INDIAN INSTITUTE OF TECHNOLOGY KANPUR

CERTIFICATE OF COURSE WORK

This is to certify that **Mr. Rajeev Yadav** has satisfactorily completed all the courses required for the Ph. D. degree. The courses include:

CHM631	Applications of Modern Instrumental Methods
CHM637	Molecular Spectroscopy
CHM636	Molecular Modelling in Chemistry
CHM621	Chemical Binding
CHM629	Principles of Physical Chemistry
CHM664	Modern Physical Methods in Chemistry
CHM 799	Research
CHM800	General Seminar
CHM801	Graduate Seminar

Mr. Rajeev Yadav was admitted to the candidacy of the Ph. D. degree in February, 2010 after he successfully completed the written and oral qualifying examinations.

P. K. Bharadwaj
Head
Department of Chemistry
Indian Institute of Technology Kanpur
Kanpur – 208016, India

P. K. Bharadwaj
Professor & Head
Department of Chemistry
I.I.T. Kanpur-208 016 (India)

Convenor, DPGC
Department of Chemistry
Indian Institute of Technology Kanpur
Kanpur – 208016, India

Actg. CONVENOR DPGC
DEPARTMENT OF CHEMISTRY
I.I.T. KANPUR

Dedicated to my Parents

Acknowledgements

First and foremost I owe my deepest gratitude and respect to my thesis supervisor, Dr. Pratik Sen for his precious guidance, unstinting encouragement, inspiration and amicable cooperation. It has been my pleasure to join the group as his first Ph.D. student. Since the day I joined, I have learnt a lot from him. I still remember the starting days, how he taught me all the skills necessary for an experimentalist, even the sample preparation, measurement, data analysis etc. He always gave me complete freedom to express my thoughts and provided useful hints to improve my scientific approach and has always been encouraging when difficulties arose. Apart from research skills he made me learn a lot of qualities necessary for life. The ardent devotion and enthusiasm he has for his research was fruitful and motivational for me and will always inspire me for future endeavours. I will always be indebted to him for shaping up the most important part of my scientific career. I am also grateful to madam Manila Sen for occasional parties and making us feel at home. Also lots of love to Suchismita, whose childishness will stay in my mind for a long time to come.

I am also thankful to Prof. Y. D. Vankar, Prof. A. Chandra, Prof. J. K. Bera, Prof. S. Manogaran, Prof. D. Goswami, Dr. M. Ranganathan for being my teacher during course work. From their informative and interesting courses, I have learned a lot. Special thanks Dr. Nisanth N. Nair for his kind help in MD Simulation.

I want to thank Professor Sudipta Maiti (TIFR, Mumbai), Dr. Sobhan Sen (JNU, New Delhi) for their considerable advises and help to construct FCS setup in our lab. I am also grateful to Sachin Dev Verma for his generous help to build this setup.

I wish to extend my sincere gratitude to the Department of Chemistry, IIT Kanpur for making me a part of it and also the current (Prof. P. K. Bharadwaj) and former (Prof. R. N. Mukherjee and Prof. V. Chandrashekhar) Heads of the Department for their cooperation. I am also thankful to all the faculty members of the department for their help and valuable suggestions from time to time. I express my thanks the office staff especially Sudha madam and Geeta madam for their cooperation and help whenever needed.

My heartfelt thanks to my lab mates Shradhey, Shahnawaz, Bhaswati, Puspal, Vaisakh, Vipin, Gyanesh and Faizi for their constant support and discussions related to research as well as social issues which made my years in the lab an experience that will stay with me forever. Many thanks to Shradhey and Shahnawaz, we enjoyed each other's company during the initial phase of setting up

our lab. I also want to acknowledge to the project students Shyamasish, Mainak, Soumen, Arghav, Nirmal, Snigdha, Sharmishta, Barun, Shubrangshu, Sayani, Ashish, Ankur, Sunil, Santosh and Indrani for your cooperation, help whenever I need.

I am very grateful to University Grant Commission (UGC), India for providing fellowship and also to Research and Development section IIT Kanpur for their best cooperation.

I would like to thank all my teachers in schools, college and university. I express my warm gratitude to the Department of Chemistry, Narain (P.G.) College Shikohabad, Firozabad from where I have completed my Bachelor's and Master's program. Sincere thanks to Dr. B. K. Shrivastava and Dr. R. K. Paliwal for being excellent teachers and their considerate advice and support. I am also thankful to Dr. Amar Srivastava (D.A.V. College Kanpur).

My time at IIT Kanpur was made enjoyable and has been blessed with the presence of many friends and groups that became a part of my life. I am grateful to Pardeep, Ashu, Ankit, Prashant, Ravi, Jhasaketan, Chetan, Amit, Akhilesh, Chandrajeet, Musheer, Archana, Ruchi, Sumit, Chandan, Keshav, Abhay, Samik, Ramesh, Sourav, Arvind, Asif, Akram, Akhilesh, Shashi, Rohan, Alok, Ganesh, Balu, Saikat, Shivin, Ramu, Sarvesh, Gurmeet, Pankaj, Awanish, Kamlesh and all my IITK friends. Friends from my home town most of these are with me from my schooling who always wishes and made me feel special, deserve a very warm acknowledgment, specially Onkar and Himanshu for their cooperation and support when needed.

Words fail to express my gratitude to my dearest parents whose teaching since childhood, unending love and affection, motivation, constant inspiration, and sacrifice has made me to complete my dissertation successfully. My mother who always be a torchbearer for me and taught the lesson of morality and transformed me into a good human being. I also want to acknowledge with my full heart to my late grandparents for their love and affection. A special thanks is due to my wife Priyanka for her unconditional faith, love and trust that made me feel special. Her altruistic support and motivation has always boosted my confidence. I would like to acknowledge my uncle Ramesh Chandra for his unforgettable support and encouragement. My heartfelt thanks to my brother, Sanjeev, my sisters, Sadhna, Nigam and in-laws Rishi, Mahender Singh and Ravindra for their love and constant support. I would like to express my greetings to all my relatives and other family members.

Finally, with humanity and sense of deep gratitude and a heavy heart, I bow down to almighty GOD for giving me health and energy to complete this research work successfully.

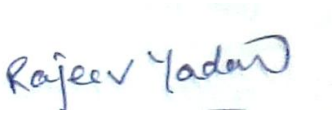

Rajeev Yadav

SYNOPSIS

Name of the Student:	Rajeev Yadav
Roll Number:	Y8207074
Degree for which the Thesis is Submitted:	Ph. D.
Department:	Chemistry
Supervisor:	Dr. Pratik Sen
Thesis Title:	Domain Specific Interactions, Unfolding and Ultrafast Dynamics of Human and Bovine Serum Albumin: A Bulk and Single Molecular Level Study
Month and Year of Submission:	May, 2014

The main focus of this thesis is to understand the domain specific response of multi-domain proteins towards molecular interactions, unfolding and dynamics. For this study, human serum albumin and bovine serum albumin have been taken as model proteins that contain three distinct domains. For the bulk measurements, mainly steady state and time resolved fluorescence spectroscopic methods have been used; while the measurements at single molecular level have been performed using fluorescence correlation spectroscopy (FCS) setup, which we constructed in our laboratory by assembling individual components. To study the different domains we used fluorescent markers that selectively bind (covalently and non-covalently) to different domains of serum albumin. Along with experimental studies molecular docking and molecular dynamics (MD) simulations have also been carried out to enunciate the findings.

Summary of the Work Done

(a) Static and Dynamic Aspects of Supramolecular Interaction of Coumarin 153 and Fluorescein with Bovine Serum Albumin

The binding phenomenon of two fluorescent organic dye molecules namely, coumarin 153 (C153) and fluorescein (FL) with bovine serum albumin (BSA) was studied using spectroscopic techniques. The spectral characteristics of both C153

and FL are remarkably modified upon binding with BSA. Binding stoichiometry and binding constant for both the probes with BSA have been determined using steady-state absorption or emission studies. Both the dyes were found to form 1:1 complex with BSA with binding constants 2.9×10^5 M^{-1} and 2.1×10^5 M^{-1} for C153 and FL, respectively. Site marker competitive experiment, steady-state FRET and molecular docking study reveal that C153 binds to domain IIIA of BSA, whereas FL binds at the surface of the protein. Urea induced denaturation study were done to understand the conformational stability of different sites of BSA compared to its global structure. The free energy of unfolding at zero denaturant concentration (ΔG_0) of global BSA is found to be 2 kcal mol^{-1} whereas for domain IIIA it is 2.2 kcal mol^{-1}. For non-specific FL-BSA complex, the free energy of unfolding at zero denaturant concentration is found to be 2.9 kcal mol^{-1}. The rate constants for binding of C153 and FL to BSA were estimated to be 8.8 sec^{-1} and 5.9 sec^{-1} respectively using stopped-flow method.

(b) Temperature Dependent Binding Modes of Coumarin 152 with Human Serum Albumin

The temperature dependent binding of coumarin 152 (C152) with human serum albumin (HSA) have been studied for a wide temperature range (from 278 K to 323 K) using spectroscopic techniques and the results were compared with computational studies. The spectroscopic results show that the binding affinity of C152 to HSA is almost unaffected until 298 K and decreases continuously on further increasing the temperature. Site marker competitive experiment, molecular docking study and Förster resonance energy transfer (FRET) experiment show that C152 binds to the digitoxin binding site in domain III of HSA and does not change with change in the temperature (278 K to 323 K). The calculated thermodynamic parameters show that at lower temperature the electrostatic and hydrophobic interactions predominate for association, whereas at higher temperature hydrogen bonding interaction plays a crucial role in the binding process.

(c) Direct Observation of Intermediate State(s) in the Mechanistic Investigation of Domain Specific Protein-Surfactant Interaction

Fluorescence spectroscopic techniques have been employed to study the interaction of two surfactants, an anionic (sodium dodecyl sulphate, SDS) and a cationic (cetyltrimethylammonium bromide, CTAB) with domain III of human serum albumin (HSA) using 8-anilino-1-naphthalene-sulphonate (ANS) as fluorescent marker, which specifically binds to domain III of HSA. The interaction of both the surfactants with HSA is found to be sequential in nature. The most important conclusion revealed from our study is that the nature of protein-surfactant interaction is not same throughout the entire protein. SDS is found to interact sequentially with the domain III of HSA having two detectable intermediate states in the binding process. In case of CTAB, we have observed only one intermediate state for its interaction with domain III. However, the overall conformational change of the HSA on addition of surfactants, studied by circular dichroism (CD) spectroscopy and the ANS-Trp distance, measured by FRET, could not resolve the presence of such intermediate states. The relative esterase activity of HSA towards the hydrolysis of *p*-nitrophenyl acetate (PNPA) in presence of surfactants for different reaction times also supports our observations. It has been proposed that different parts of the multi-domain HSA have different affinities with the surfactants. This study is expected to provide useful insight into the site-specific interaction of the polar molecules in biological systems.

(d) Mechanistic Investigation of Domain Specific Unfolding of Human Serum Albumin and the Effect of Sucrose

The steady-state and time-resolved fluorescence spectroscopy was employed to understand the domain wise unfolding mechanism of HSA, in absence and presence of the sucrose using domain specific marker molecules and is further being substantiated by molecular dynamics simulation. It was observed that, in water, domain III of HSA unfolds first in the denaturation process. The domain I and II unfolds thereafter almost simultaneously. The $[D]_{1/2}$ values of domain I, II

and III for GnHCl are estimated to be 2.3 M, 2.4 M, 1.6 M, respectively. In presence of sucrose the $[D]_{1/2}$ values are found to be 3.1 M, 3.0 M and 1.7 M GnHCl, respectively. The sequence of unfolding of HSA in sucrose medium is found to be same as compared to otherwise, however the $[D]_{1/2}$ values are shifted at higher GnHCl concentration. Clearly, addition of sucrose impose restriction in the GnHCl induced unfolding process for all the three domains but with different extent. The domain I and II are found to be stabilized more by sucrose as compared to domain III. The relative change in the RMSD and RMSF values obtained from MD simulation study also supports our experimental observations. This is to conclude that the unfolding behavior of different domains of a big protein is not uniform and the stabilizing effect of a stabilizer is different for different domains. The increase in the number of hydrogen bonds between the amino acid residues and water as well as the participation of sucrose in hydrogen bonding with protein indicate that broken glass hypothesis is in operation in the stabilization process.

(e) Conformational Fluctuation Dynamics of Domain I of Human Serum Albumin in the Course of Chemically and Thermally Induced Unfolding Using Fluorescence Correlation Spectroscopy

Fluorescence correlation spectroscopy (FCS) along with time resolved fluorescence measurements and CD spectroscopy were employed to study the global structural change as well as conformational fluctuation dynamics during chemically and thermally induced unfolding of HSA. Two fluorescent probes, tetramethylrhodamine-5-maleimide (TMR) and N-(7-dimethylamino-4-methylcoumarin-3-yl) iodoacetamide (DACIA) were used to selectively label the domain I of HSA through the reaction with cys-34 for these studies. The global structure of HSA has been associated with hydrodynamic radius of the protein (r_H), which changes in a similar trend as observed through CD spectroscopy. The value of r_H has been observed as 39.1 ± 2.5 Å in the native state of HSA, and on addition of GnHCl it remains unchanged till 1.85 M, which become 64.9 Å in presence of 4.5 M GnHCl. In FCS experiment, along with the diffusion time component an

exponential relaxation time component (τ_R) has been observed, and is ascribed to the concerted chain dynamics of domain I of HSA. The time scale of the concerted chain motion in the native state of HSA is found to be 27.5 ± 5 μs and remains similar till 1 M GnHCl. Afterward, an increment has been observed in the τ_R value which reaches to 52.4 ± 6 μs at 1.25 M GnHCl. On further increase in the GnHCl concentration till 1.85 M, the τ_R decreased to 31.2 μs. The τ_R value increases to 74.4 μs at 4.5 M GnHCl and remain similar till 6 M. Our analysis clearly indicates the involvement of two intermediate states during the GnHCl induced unfolding process of HSA, and domain I of HSA is primarily responsible for this subtle change in the overall structure of the protein in the intermediate states, as the fluorescent probe is located in domain I of HSA. $[D]_{1/2}$ values for the first ($N \leftrightarrow I_1$), second ($I_1 \leftrightarrow I_2$) and third ($I_2 \leftrightarrow D$) transitions are estimated to be 1.16 M, 1.52 M and 3.0 M respectively. The fluorescence lifetime measurement also supports these observations of intermediate states during the GnHCl induced unfolding of HSA. However for thermally induced unfolding of HSA, no such intermediate states were observed. It has been realized that to completely understand the unfolding mechanism of such massive protein, one needs to study the different fragments separately.

(f) Effect of Sucrose on Chemically and Thermally Induced Unfolding of Domain I of Human Serum Albumin: Solvation Dynamics and Time Resolved Fluorescence Anisotropy Study

In chapter 5 (section d of the synopsis), we have observed the differential stabilization effect of sucrose against GnHCl induced unfolding for different domains of HSA. Domain I was found to be stabilized more as compared to other two domains of HSA. To extend our knowledge, we have investigated the effect of sucrose on the solvation dynamics and orientation relaxation dynamics within the domain I of HSA during chemically as well as thermally induced unfolding. For this study, N-(7-dimethylamino-4-methylcoumarin-3-yl) iodoacetamide (DACIA) was selectively tagged with domain I of HSA. In absence of sucrose, the average

solvation time, $\langle \tau_s \rangle$, in domain I of HSA has been measured as 2300 ps in the native state, 230 ps (~0.1 times of the native state) in presence of 1.25 M GnHCl, 150 ps (~0.07 times of the native state) in presence of 3 M GnHCl concentration, and remains almost unchanged at higher concentration of GnHCl. Whereas, in presence of 1 M sucrose, $\langle \tau_s \rangle$ value decreases from 2500 ps in native state to 1800 ps (~0.75 times of the native state) and to 200 ps (~0.08 times of the native state) in presence 1.25 M GnHCl and 3 M GnHCl, respectively and remains almost similar at higher concentration of GnHCl. The effect of sucrose was found to be maximum for 1.25 M GnHCl concentration. Time resolved fluorescence anisotropy of DACIA labeled HSA was also measured and the data was analysed using "wobbling-in-cone" model to investigate the local motion in domain I. In the native state of HSA, the semicone angle of the local motion has been observed as 8.2°, which become 60° (~7.3 time increase) at 4.5 M GnHCl concentration, when sucrose is absent. In the initial concentration of GnHCl (till 1.75 M), the effect of sucrose on the semicone angle is very small. However, the semicone angle appreciably decreased at higher concentration of GnHCl in presence of sucrose.

These observations clearly indicates that the solvation dynamics plays an important role in the stabilization process at low concentration region; whereas environmental restriction is responsible for stabilizing the domain I of HSA at the higher concentration of GnHCl. On contrary, we have not observed any significant stabilizing effect of sucrose towards the temperature induced unfolding of domain I of HSA in the present temperature range.

TABLE OF CONTENTS

THESIS OUTLINE

This thesis is divided into following chapters

Chapter 1. This chapter describes a brief overview about the protein structure, stability and its folding mechanism with a brief introduction on the study of molecular interactions, denaturation and dynamics.

Chapter 2. This chapter deals with various experimental techniques and data analysis which have been used to understand our system along with the complete description of fluorescence correlation spectroscopy setup that we have built in our laboratory.

Chapter 3. This chapter is divided in two parts; first one describes the static and dynamic aspects of supramolecular interaction of coumarin 153 and fluorescein with bovine serum albumin and the second part describes the temperature dependent binding modes of coumarin 152 with human serum albumin.

Chapter 4. This chapter reports about the direct observation of intermediate state(s) in the mechanistic investigation of domain specific protein-surfactant interaction.

Chapter 5. This chapter deals with our work on mechanistic investigation of domain specific unfolding of human serum albumin and the effect of sucrose. Molecular dynamics simulations have also been carried out to enunciate our observations.

Chapter 6. In this chapter we have described the unfolding behaviour of domain I of HSA during chemically as well as thermally induced unfolding by measuring the conformational fluctuation dynamics of domain I using fluorescence correlation spectroscopy.

Chapter 7. In this chapter we have investigated the effect of sucrose on chemically and thermally induced unfolding of domain I of HSA using solvation dynamics and time resolved fluorescence anisotropy.

Chapter 1

Introduction

"Science is a part of culture. Indeed, it is the only truly global culture because protons and proteins are the same all over the world, and it's the one culture we can all share." ***Martin Rees***

1.1. Protein: An Overview

"Proteins are the machinery of living tissue that builds the structures and carries out the chemical reactions necessary for life." ***Michael Behe***

Proteins are the eminent molecules among those essential for life and are the most abundant biological macromolecules in cells. Their importance stems from the remarkable diversity of their functional roles within living organisms, like catalyzing biochemical reactions, replication of DNA, transporting molecules to appropriate sites, maintaining the structures of cells and organs, etc.[1-3] The basic structural unit of a protein is the polypeptide chain with a definite protein specific sequence of 20 commonly occurring amino acid residues linked by peptide bonds.[1-3] These amino acids, which contains a carboxyl group and an amino group bonded to the α-carbon atom, are α-amino acids. Each of these amino acid residues vary in structure, size and electric charges in physiological condition. Amino acid residues can be divided into two broad classes; hydrophilic and hydrophobic, those that are relatively more and less soluble in water, respectively. The hydrophilic side chains include electrically charged groups; while hydrophobic side chains are neutral and relatively non-polar. The amino acid sequence in the polypeptide chain is known as the primary structure of a protein. The specific sequence and the composition of amino acids in proteins differs the protein from one another.

1.1.1. Three-Dimensional Structure of Protein

The interactions among the amino acid residues guide a protein to fold into characteristic "native" three-dimensional structure. The native structure determines its specificity for interaction with other molecules, ability to function as an enzyme and to attain its stability.

A. Secondary, Tertiary, and Quaternary Structures of Protein

Secondary structure refers to the special arrangement of amino acid residue in a particular segment of polypeptide chain, whereas the tertiary structure includes

long range aspects of amino acid sequence. The α-helix, β-sheet and β-turns are the most common secondary structures and tertiary structure is the complete three dimensional structure of a polypeptide chain. The weak interactions, that are important in the folding of polypeptide chain into their secondary and tertiary structure, are mainly hydrophobic interactions, hydrogen bonding, ionic interactions, van der Waals forces, etc. Based on these structures, protein can be classified into two groups: fibrous proteins, where polypeptide chains are arranged in long strands or sheets and globular proteins, where the polypeptide chains are folded into a spherical or globular shape.[1] Some globular proteins are big and have distinct regions, called domains. Some proteins contain two or more separate polypeptide chains, or sub units, which may be identical or different and such higher order arrangement of these subunits is termed as quaternary structure. It is the highest level of organization in multimeric proteins.

B. Protein Domains

Domains are distinct parts of a protein that may response independently and are distinguishable from rest parts of the protein. In many cases it is convenient to describe a protein in terms of regions of the polypeptide chain that might fold autonomously. These regions are called domains and much of the discussion of tertiary structure centers on classification of these units of protein structure. Jane Richardson in 1981 has explained the three dimensional structure and domains of a protein in the article named as *"The anatomy and taxonomy of protein structure"*[4] and defined it as a part of polypeptide chain that can fold into a stable structure independently. Proteins may have one or more domains, depending on the amino acid sequence and the size of the polypeptide chain. Different domains often have distinct functions, such as binding of small molecules or interaction with other proteins, as a whole contributing to the overall role of a protein. In a variety of biological contexts, similar domains can be found in proteins with different functions.

1.1.2. Protein Stability

The term protein stability refers to the energy difference between the folded and unfolded state of the protein in solution. The free energy difference between these states is usually between 20 and 80 kJ mol^{-1}, which suggests that the active state of proteins are only marginally stable. A polypeptide chain can have enormous number of conformations, which results in high degree of conformational entropy for the unfolded state of protein. This entropy and the interactions of polypeptide chain with water molecules tend to maintain the unfolded state of the protein. Hence the protein stability is determined by an enormous number of weak interactions within and across the protein. These weak interacts are hydrogen bonds, hydrophobic interactions, ionic interactions, van der Waals forces, etc.

Among these forces, the major contribution comes from the hydrophobic interactions to stabilizing the globular form, whereas the hydrogen bonds and ionic interactions are responsible for thermodynamically more stable structure. The intra-molecular hydrogen bonds between polar groups found in the tertiary structure of the protein is largely canceled by the elimination of hydrogen bonds between polar groups and water. Thus hydrogen bonding is energetically neutral with respect to protein stability, whereas the release of structured water provides an entropic driving force for folding. Ionic interactions contribute very little to protein stability. The formation of S-S disulfide bridges between two cystein side chains also gives rigidity to the proteins. In this case, the stability appears to be entropic rather than enthalpic. This stabilizes the folded state by decreasing the entropy difference between the folded and unfolded state.

1.1.3. Protein Folding and Thermodynamics

Proteins need to exist in a three dimensional native structure that allow them to act as enzymes, transport agents, receptors etc. The means by which this biologically active folded structure is achieved remains one of the most important

questions in biochemistry and molecular biology and become a topic of considerable research interest from several decades.[1-10] The study of protein folding is focused on understanding the mechanism by which the protein attains its active folded structure. Hence, the kinetic and thermodynamic studies of protein folding may give answers to the questions- "By which pathway the final tertiary structure is formed?" and "How stable is the final folded structure and why?"

In late 1950s, Christian Anfinsen showed that a small protein (ribonuclease, contains 124 amino acid residues) folds spontaneously into its native state under normal physiological conditions.[5] He showed that the completely denatured ribonuclease (fully reduced randomly coiled polypeptide chain devoid of enzymetic activity) by treating with 8 M urea and β-mercaptoethanol could refold into a well defined unique structure, in which the biological activity was completely restored. He also performed other experiments by changing the environment of reduced ribonuclease and concluded that the folding process was driven by decrease in the free energy, where the native state is the most thermodynamically stable state with lowest free energy.[5] This study along with others leads to the thermodynamic hypothesis, which assumes that native state corresponds to the global free energy minimum of a protein. He also showed that the information needed to ascertain the native three dimensional structure of the protein is encoded in its amino acid sequence.[6] Subsequent studies have established the protein folding problem as "if the amino acids sequence is known, the conformation of the protein is possible to predict."

The stability of a protein in its native form is usually studied by observing the energetics of unfolding transitions as follows:

$$N \leftrightarrow U \tag{1.1}$$

$$K_{un} = [U]/[N] \tag{1.2}$$

$$\Delta G^0_{un} = -RT \ln K_{un} \tag{1.3}$$

where K_{un} is the equilibrium constant for a simple two-state transition between the native (*N*) and the unfolded (*U*) state. The degree of unfolding for most of the proteins as function of denaturant concentration (urea, guanidine hydrochloride, temperature etc.), suggests the involvement of two states with a sharp transition from native to the unfolded/denatured state without a detectable intermediate species. Protein folding and unfolding is considered to be a cooperative process.

The cooperative folding of protein, which is a thermodynamic property, reveals nothing about the kinetics and the mechanism of protein folding. Cyrus Levinthal mentioned that, even for a small protein, a long time would be required for the folding process by trying out all possible conformations in the polypeptide chain. Consider a small protein with 100 residues and if each residue is considered to have just three possible conformations, the total number of conformations would be 3^{100}, which is equal to 5×10^{47} conformations. If it takes 10^{-13} seconds for a conformational change, then the total search time required to sample all possible conformations would be $5 \times 10^{47} \times 10^{-13}$ seconds, which is equal to 5×10^{34} seconds or about 10^{27} years. Even the significant portion of these conformations are strictly forbidden, the folding time is still very large. However, the proteins are known to fold on the time scale of microseconds to hundreds of seconds. This huge difference between the actual time and the calculated time for protein folding is called *Levinthal's paradox*. It is impossible to sample all possible conformations during this time and is concluded that proteins must fold by specific pathways.[7]

To explain this problem, in 1990s people have used energy landscape theory (ELT).[8] According to this theory, folding is initiated by the spontaneous collapse of the polypeptide chain, mediated by hydrophobic interactions among the nonpolar residues, into a compact state. From this collapsed state, different polypeptides may take a variety of routes to fold into native state, with the number of different partly folded conformations or intermediate states. Thermodynamically, the folding process can be viewed as a kind of folding funnel or free energy funnel (see figure 1.1). All non-native conformations of the protein possess a high free energy and a

high degree of conformational entropy. The funnel contains many local minima in which a protein can fall during the folding process. Some of them represents productive intermediates (at the bottom of the funnel) that can be reduced to single native conformation of the protein.[9] The free energy funnel represents many folding pathways to reach the native state from any unfolded state quickly or slowly, depends on the shape and the gradient of the funnel which signifies the kinetic control of protein folding.

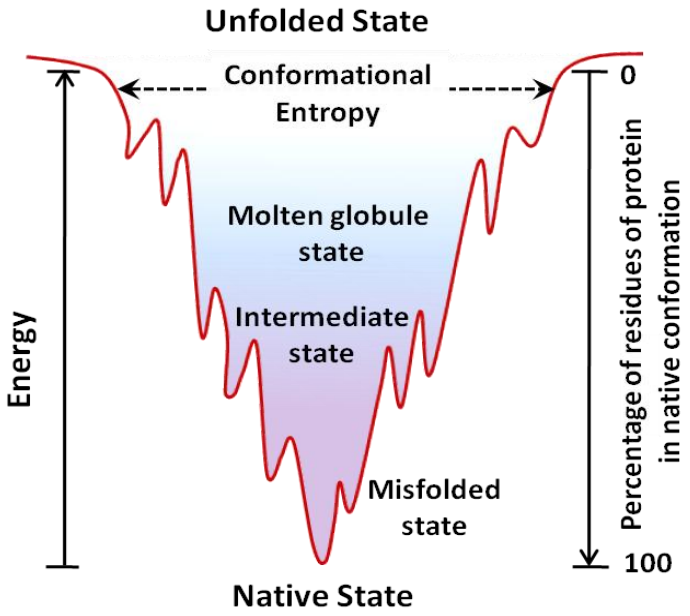

Figure 1.1. Free energy funnel for protein folding contains many local minima, in which the protein can fall during the folding process.

Till date, protein folding studies are mainly focused on the small or single domain proteins which follow a reversible two state process. However, the folding pathway of a large multi-domain protein is unquestionably complicated. For a multi-domain protein, different domains often have distinct functions, such as binding of small molecules or interaction with other proteins. Hence after getting prior knowledge of fluorescent molecules that can selectively bind to different domains, we can study the change in the conformations of different domains independently.

1.2. Interaction of Ligands with Protein

The function of many proteins involves the reversible binding of the ligands to the binding site. Among more than one binding sites of a protein, the actual ligand binding site depends on the nature of the ligand, i.e. size, shape as well as its hydrophilic or hydrophilic character. Hence a protein can have distinguished binding site for different ligands. Human and bovine serum albumin (HSA and BSA) have two major binding sites, recognized as site I and site II, which are located in sub-domain IIA and IIIA respectively. These binding sites are commonly referred as Sudlow's site I or warfarin binding site and Sudlow's site II or indole-benzodiazepine binding site, respectively.[10] Another binding site has been recognized as digitoxin drug binding site, which is also located in sub-domain IIIA of HSA.[10]

1.2.1. Interaction of Drugs

The binding of drugs to the proteins has been a subject of burgeoning interest for long time.[10-20] Serum albumins interact with a wide variety of endogenous and exogenous compounds such as fatty acids, bile acids, thyroxin and a broad range of drugs.[6,11,13-20] In the binding study, the important factor is to understand the kinetics and dynamic properties for a drug binds to the protein.[14,15]

Spectroscopic methods are eminent tools to study the interactions in biological and chemical systems because of its sensitivity for very low concentrations of the substances. Using fluorescence and UV-Vis spectroscopy, Xiao and co-workers have studied the binding properties of medicinal herb, berberine with HSA.[14] Stern-Volmer quenching and site marker competitive experiments were used to determine binding constant and binding site, respectively. They observed that berberine binds to the Sudlow's binding site I of HSA and the electrostatic interactions play a major role in the binding process.[14] Mukherjee and co-workers have studied the binding of a common antibiotic tetracycline hydrochloride (TC) to BSA and HSA using steady-state fluorescence,

time-resolved fluorescence, and circular dichroism (CD) spectroscopy. The gradual decrease in Trp fluorescence intensity occurs due to static quenching as well as fluorescence resonance energy transfer in both the proteins, of course, with different values of efficiency of energy transfer. Various thermodynamic parameters associated with such TC–protein interactions have been estimated and they concluded that the binding of TC to both the proteins is enthalpy driven.[16] In another work, they have used Ciprofloxacin Hydrochloride (CpH) to understand the nature of binding as a function of pH of the medium. Here they observed that the fluorescence quenching of Trp is mostly dynamic in nature at pH 7.4 and 9.2, whereas at pH 4.5, the quenching is mainly static in nature. Thermodynamic parameters of binding suggest that hydrophobic and van der Waals forces play an important role in the process of CpH-BSA interaction at three different pH values.[17] Datta and co-workers have studied the binding of two drugs, chlorine-p6 and purpurin-18 with HSA and determined that both the drugs are binding to Sudlow's Site I of HSA, using fluorescence quenching of single tryptophanyl residue, site marker competitive experiment and FRET. The principal driving force for the interaction was found to be the hydrophobic and the quenching of intrinsic fluorescence rendered by the added drug was static in nature.[18] Using fluorescence, Fourier transform infrared (FT-IR) and CD spectroscopy, Zhang and co-workers showed that puerarin, which exerts many pharmacological activities as antioxidant, binds to the sub-domain IIA of HSA with an alteration in the secondary structure.[19] Bosca and Tormos have studied the interaction of colchicine (COL), colchiceine (CEI), N-deacetylcol-chiceine and (DCEI) with HSA using laser flash photolysis (LFP). They observed that COL binds to the Sudlow’s site I of HSA with very low biding affinity, whereas CEI and DCEI binds to the Sudlow’s site II with relatively high binding affinity.[20]

1.2.2. Interaction of Dyes

Molecular dyes are routinely used as fluorescent probes for the study of complex chemical and biological systems.[21-27] The selective interaction of dye with

a certain part of biological macromolecule has an enormous scope to pursue a site specific study. Samanta and co-workers have studied the interaction of two classes of dyes, aminocoumarins and aminonitrobenzoxadiazoles with BSA by monitoring the spectral and temporal behavior of the intramolecular charge transfer fluorescence of the system. Molecular docking has been performed to locate the binding sites.[21c] Mishra and co-workers have showed the interaction behavior of 7-aminocoumarins with HSA using fluorescence spectroscopic technique and modeling studies and observed a large change in fluorescence spectral parameters on binding these dyes with the protein. Strong binding constant has been observed for all the dyes with different binding locations for different coumarins.[24] Ramaiah and co-workers have studied the binding of squaraine dyes, bis(2,4,6-trihydroxyphenyl) squaraine, bis (3,5-dibromo-2,4,6-trihydroxyphenyl) squaraine, and bis(3,5-diiodo-2,4,6-trihydroxyphenyl) squaraine with HSA and BSA. They demonstrated that on increase in molecular size of these dyes, the binding affinity increased towards the binding site II over the site I, indicating that the steric factors play a prominent role in binding of the squaraine dyes with HSA and BSA.[25]

1.2.3. Interaction of Surfactants

The interaction of surfactants with protein is of great interest among the researchers and is also well documented.[28-33] For the first time, in 1948 Duggan and Luck showed that serum albumin can be protected from urea induced denaturation by addition of small concentration of sodium dodecyl sulfate (SDS).[28] Moriyama and Takeda have also established the protective nature of double tailed surfactant, sodium bis(2-ethylhexyl) sulfosuccinate for HSA and BSA from thermal denaturation using CD spectroscopy. They have showed that the helicity of HSA decreased from 66 % to 44 % at 65 °C in the absence of surfactant, however the presence of low concentration of surfactant prevent such decrement in the helicity of HSA.[29b] Mukherjee and co-workers have studied the interaction of SDS with HSA using steady-state fluorescence, time-resolved fluorescence and CD spectroscopy and observed that the addition of SDS to HSA takes place in a

sequential manner depending on the concentration of SDS. The Trp-214 fluorescence intensity and lifetime in HSA decreased with the increasing concentration of SDS and they concluded that the surfactant molecules act as quencher for Trp fluorescence. Their data suggest that the interaction of SDS to HSA takes place in three different stages followed by a saturation stage.[31] Vlasova and co-workers studied the interaction of CTAB (cetyl trimethyl ammonium bromide) with HSA at different pH values using Trp fluorescence and revealed that at pH 3.5-8, the deepest denaturation of HSA reached at 4 mM of CTAB and the denaturation takes place in one step.[32] Apart from using intrinsic Trp fluorescence, many researchers have also used extrinsic fluorescent probes to monitor the interaction behavior of protein-surfactant assembly.[33-35] Bhattacharyya and co-workers have studied the interaction of SDS (very low concentration) with HSA using extrinsic fluorescent probe, 2,6-p-toluidinonaphthalene sulfonate (TNS). They observed that the solvation dynamics (discussed in section 1.5.1) becomes faster, when SDS binds to HSA, attributed to the displacement of the bound water molecules by SDS in the close vicinity of the fluorescent probe.[33a] In another work they have used covalently attached external fluorescent probe, CPM (7-dimethylamino-3-(4-maleimidophenyl)-4-methyl Coumarin) and observed that on addition of SDS the local water dynamics in HSA became faster by 1.3 times due to binding of SDS to HSA.[33b] Lu and co-workers have used ANS (8-anilino-1-naphthalene-sulphonic acid) as fluorescent probe to understand the interaction behavior of cationic (CTAB), anionic (SDS) and nonionic (Tween 20) surfactants with BSA.[34a] They observed that fluorescence intensity of ANS increases with a blue shift in the spectrum on addition of CTAB and Tween 20 to the protein solution, whereas SDS caused less increase in ANS fluorescence and less blue shift in emission maximum compared to CTAB and Tween 20.[34a]

1.2.4. Interaction of Other Molecules

Interaction of the other molecules (other than drugs, dyes and surfactants) like dendrimers, nanomaterials, ionic liquids, lipids, vesicles etc. with the proteins

has also drawn a considerable interest among the researchers.[36-46] Nanomaterials and dendrimers have huge scope of application in drug delivery system,[41,47] whereas lipid and vesicle serve as an elegant model for biological cell.[44] Room temperature ionic liquids (RTIL) have found applications in the biology ranging from bioanalysis to cellulose processing and also for biosensors and biocatalysis.[48] Bhattacharyya and co-workers have studied the effect of RTIL, 1-pentyl-3-methyl-imidazolium, on unfolding of HSA using fluorescence correlation spectroscopy (FCS). For this study they used coumarin 153 (C153) as fluorescent probe, that non-covalently binds to the protein. They showed that the presence of RTIL alters the structure and dynamics of protein during unfolding by GnHCl.[36a] In another work they have used covalently attached external fluorescent probe (CPM) and showed that 1-pentyl-3-methylimidazolium bromide ([pmim][Br]) act as denaturant in the native state of HSA, whereas in the unfolded state it acts as stabilizing agent.[36b] Wang and co-workers have studied the interaction behavior of three different RTILs (dibutylimidazolium chloride, 1-butyl-3-methylimida-zolium chloride, and 1-butyl-3-methylimidazolium nitrate) with BSA by using intrinsic fluorescence on exciting at 230 nm as well as 280 nm. The fluorescence quenching has been observed when excited at 230 nm, however, no fluorescence quenching is observed within the same region when excited at 280 nm. Thermodynamic investigations reveal that the combination between ILs and BSA is entropy driven by predominantly hydrophobic and electrostatic interactions, leading to the unfolding of polypeptides within BSA.[37]

Exploring the interaction behavior of nanomaterials with serum albumin has become a topic of great interest because of its widespread applications in biology.[38-40] Gao and co-workers have studied the interaction of pristine C_{60} nanoparticle with HSA and BSA using UV-Vis, fluorescence and dynamic light scattering techniques. They observed that the fluorescence of both the proteins was quenched on addition of C_{60} nanoparticles with small change in the secondary structure and explained in terms of change in the microenvironment in the close

proximity of Trp.[38a] Chakrabarti and co-workers have studied the interaction of gold nanoparticles and gold nanorods (GNP and GNR) with BSA using thermodynamic parameters of binding. They observed that the binding of GNP with BSA was enthalpy driven without any alteration in the secondary structure of the protein, whereas the interaction was entropically favored for GNR with a substantial loss in the secondary and tertiary structures of BSA.[39a] In another work, they have investigated the interaction of polyethyleneimine-functionalized ZnO nanoparticles with BSA and observed that the functionalized ZnO nanoparticles bind to the BSA with an alteration in the secondary structure as observed by CD and FT-IR spectroscopy.[39b]

Seto and co-workers have used zwitterionic lipid, dipalmitoyl-sn-glycero-3-phosphocholine (DPPC) at the air–water interface to see the interaction behavior with BSA. They revealed that the interaction of BSA with the lipid monolayer takes place at all pH below and above the isoelectric point of BSA (pH ≈ 4.8) and the nature of the water molecules in and around a biological assembly were different from that in bulk.[43] Cardenas and co-workers have studied the interaction of model cell membranes (giant unilamellar vesicles and supported lipid bilayers) with BSA, hemoglobin and lysozyme. They used fetal bovine serum as a good representative of a biomimetic protein mixture, to mimic the extracellular environment more closely. The interactions between a model cell membrane and these proteins were determined by their physico-chemical characteristics, mainly their dipolar character. They have also shown an additional role of glycolipids in cell membranes in reducing the effects of non-specific adsorption of soluble proteins on the cell membrane.[44a] Moreno and co-workers have synthesized lipidic α-amino acid with 11 carbons in the alkyl lateral chain (α-aminotridecanoic acid) that has been conjugated with a fluorescent polar group (7-nitrobenz-2-oxa-1,3-diazol-4-yl), to mimic drug conjugates, and its association with serum proteins and lipid bilayers was characterized. They concluded that the conjugation of polar drugs with lipidic amino acids is an efficient approach to increase their affinity for

biomembranes because a good aqueous solubility can be maintained while the affinity for biological membrane is strongly increased.[44b]

1.3. Protein Denaturation

The three dimensional structure and the function of a protein can be demolished by its unfolding. Some proteins can fold spontaneously to its biologically active form (native form), that depends both on the intrinsic properties of the amino acids sequence as well as on multiple contributing factors from crowded cellular environment.[1,49] The enormous complexity in the structure of native protein and a very limited understanding of the mechanism of the denaturation process makes it difficult to understand the protein folding completely. Since the folding and unfolding phenomenon of the protein is reversible in nature, the complete understanding of unfolding/denaturation process of protein will ultimately manifest the mechanism of protein folding.

The folding pathway of big proteins, HSA and BSA is a complex process by virtue of the presence different domains that folds independently. However, scientists have made considerable efforts for elucidating such mechanisms of folding and unfolding from last few decades.[49-57] Traditionally, most of the studies of protein folding in solution are based on the exploration of the induced denaturation of the protein from its native form. Proteins can be denatured by variety of external conditions such as changes in pH, temperature, pressure and also addition of chemical denaturants like urea, guanidine hydrochloride (GnHCl), surfactants, etc.[50-60]

1.3.1. pH Induced Denaturation

Most of the proteins have net negative charge at physiological pH, whereas the net charge will be zero at their iso-electric point (pI). Below pI the protein will lose its negative charge and contains only positive charges and vice versa. The large density of intra-molecular repulsion between charges is the main cause of

unfolding the protein. Mukhopadhyay and co-workers used fluorescence spectroscopic technique to study the effect of pH on conformation of BSA. For this study they used intrinsic (tryptophan) and extrinsic (ANS, pyrene) fluorophores and showed that at pH 3 a partially-folded, 'molten-globule-like' state is being populated. In addition, equilibrium unfolding studies indicated that the 'molten-globule-like' state unfolds in a non-cooperative fashion and is thermodynamically less stable than the native state.[55a] Bhattacharyya and co-workers used Forster resonance energy transfer (FRET) to study the GnHCl, pH and RTIL induced unfolding of HSA labeled with CPM (donor, D) and Alexa Fluor 488 (acceptor, A). They observed the presence of multiple conformers in equilibrium in the non-native state of HSA. In case of GnHCl and RTIL induced unfolding, the separation between the two domains (I and II) was found to increase considerably. In contrast, two acid induced molten globule states of HSA (formed at pH 2 and 4) were detected with high FRET efficiency, indicating a short D-A distance. In the presence of both GdnHCl and RTIL, the protein undergoes compaction and the D-A distance is found to be larger than that in the native state of the protein.[55b]

1.3.2. Temperature Induced Denaturation

Most of the proteins denature by heat, which makes the inter-residue interactions (primarily hydrogen bonds) much weaker. On heat treatment, the protein obtains a more flexible structure and the groups are more exposed to the solvent. As these bonds are broken, the water molecules make new hydrogen bonds with the polar heads of amino acids. The presence of water further weakens nearby hydrogen bonds due to increase in the effective dielectric constant. Once the secondary structure unfolds, hydrophobic groups are exposed to the solvent.

Havenith and co-workers have studied the temperature induced unfolding and refolding kinetics of HSA using CD and Terahertz (THz) spectroscopy. They showed that until 55 °C a marginal change occurs in the secondary structure of HSA which undergoes a transition from native to extended state. Whereas, at 70 °C

the protein undergoes a significant irreversible disruption of structure and assumes an unfolded form. THz data also support these observations and exhibit a reversible change in the THz absorption up to 55 °C.[56a] Fu and co-workers have studied the isotopic substitution effect on the structural and thermodynamic stability of BSA in aqueous solution over the temperature range of 5-90 °C using CD spectroscopy. They showed that BSA possesses similar conformations in H_2O and D_2O at temperatures below 50 °C but follows different unfolding pathways at higher temperatures. On incubation over a period of few minutes at 90 °C, D_2O causes a rapid aggregation of BSA molecules, which was not observed in H_2O.[56b]

1.3.3. Chemical Induced Denaturation

Proteins can be denatured by addition of external solutes like urea, guanidine hydrochloride (GnHCl), surfactants, and RTIL**s** etc. During the chemical induced denaturation of a protein, no covalent bond in the polypeptide chain is broken. Whereas the non-covalent bonds that are responsible for the stable native state of protein, disrupted by adding chemicals capable for building equally or stronger bonds with the groups holding the segments together.

The effects of denaturants such as urea and GnHCl on protein are complex, and currently are best thought as these denaturants bind to the protein preferentially.[57] Although many of the research have make efforts to understand the unfolding mechanism, yet it is a topic of considerable guess and controversy.[57,58] Urea is uncharged whereas GdHCl is ionic in nature and the mechanism of the action may be totally different.[58a] Bennion and Daggett have showed that urea denatures the proteins by direct binding and by indirect effect through water structure weakening,[58c] whereas Dempsey and co-workers have studied the interaction of GnHCl with a model peptide and showed that guanidinium ions (GnH^+ of GnHCl) binds to Arg, Trp, Glu side chains.[58d] Kumaran and Ramamurthy have used several urea derivatives to study the denaturation of BSA and observed that hydrogen-bonding interaction occurs

between N-H moiety of urea and carbonyl oxygen of the peptide backbone of BSA, which results in the unfolding process. They have also concluded that the water–water hydrogen-bonding network get perturbed on addition of urea to the protein.[59a] Hodges and co-workers showed the GnHCl induced denaturation is a function of its concentration. At low concentration, GnHCl ionizes in aqueous solution to GnH^+ and Cl^- ions which then mask the positively and negatively charged amino acid side chains. This in turn reduces or even eliminates any stabilizing or destabilizing electrostatic interactions. Whereas, at high concentrations, the binding of GnH^+ ions to the proteins predominate and it is thought to shift the equilibrium towards the unfolded state.[59b] Panda and co-workers have studied the folding and unfolding pathways of HSA using multiple probes. They showed that GnHCl induced unfolding of HSA follow a two step process when probed by CD spectroscopy, intrinsic Trp fluorescence and bilirubin absorbance. However, it follows a three state process with an intermediate state during folding and unfolding when probed by environment sensitive Nile red fluorescence.[60a] In another work they have studied the unfolding and folding of all three domains of HSA separately, using probes N-(1-pyrene) maleimide conjugated with cys 34, Trp residue and p-nitrophenyl anthranilate conjugated with Tyr 411 for domain I, II and III respectively. They observed that GnHCl induced unfolding of HSA occurs sequentially, where domain II unfolds first, followed by domain III and I.[60b] Recently Mukherjee and co-workers have studied the GnHCl induced unfolding and the subsequent refolding mechanism of BSA using steady state, time resolved fluorescence and CD spectroscopy.

1.4. Solvation Dynamics

Solvation is defined as the stabilization of a solute molecule by interaction with the surrounding solvent molecules and the solvation dynamics refers to the dynamics of this process.[61-63] To study solvation dynamics using fluorescence spectroscopy, a solute molecule (solvatochromic dye) having low ground state dipole moment and a high excited state dipole moment is used as a probe molecule. In ground state, solvent molecules remain randomly oriented around the solute molecule. A dipole is created within the solute molecule due to redistribution of charges at its electronically excited state through optical excitation by an ultra-short optical pulse. Following excitation, the solvent molecules reorganize around the instantaneously created dipole to stabilize the system.

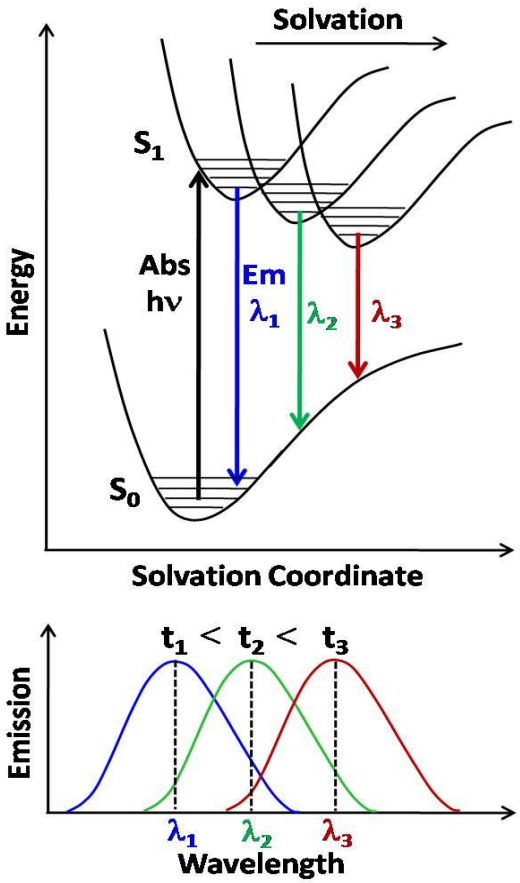

Figure 1.2. Schematic representation of solvation (top) and time dependent fluorescence Stokes' shift (bottom).

Immediately after the change in dipole, the energy of the system is very high because of the randomly oriented solvent dipoles around the instantaneously created solute dipole. The consequent energy relaxation is manifested in the gradual red shift of the emission spectrum (Fig. 1.3). This phenomenon is known as time dependent fluorescence Stokes' shift (TDFSS).[61,62] In case of solvation dynamics, the fluorescence decay exhibits a marked wavelength dependence. Sharp decays at shorter wavelengths and rise followed by decays at higher wavelengths are the typical signature that proves the probe experiencing the surrounding solvent

relaxation. At shorter wavelength, decay is observed which corresponds to the decay of unsolvated species, while at longer wavelengths a rise precedes the decay due to formation of fully solvated species. The rise at a longer wavelength is a clear manifestation of solvation dynamics (Figure 1.3).

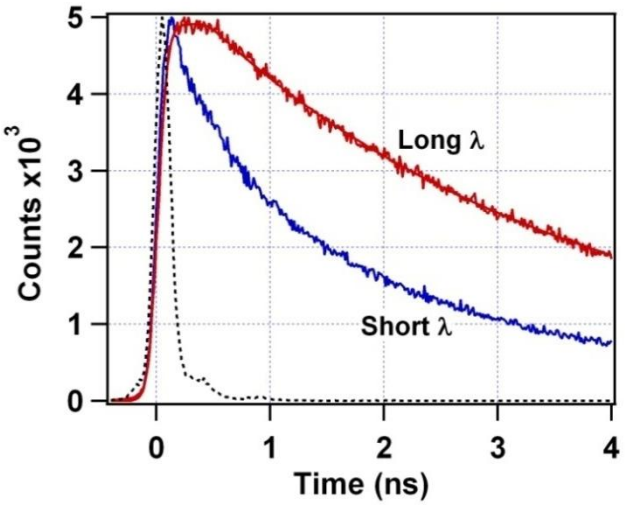

Figure 1.3. Wavelength dependence of fluorescence decays.

The time-dependent shift in fluorescence spectrum is called the time-resolved emission spectra (TRES). The TRES can be obtained from the fitted parameters of fluorescence decays at wavelength dependent, normalized with the steady-state fluorescence intensity of the solute. Finally the TDFSS is expressed in terms of shift in frequency with time followed by constructing the solvation correlation function $C(t)$ (see chapter 2).

The dynamics of water in biological systems can have a crucial influence on its biochemical function.[62] It dramatically affects the reaction which essentially involves a polar transition state. The development of ultrafast laser spectroscopy (with a time dependent fluorescence Stokes shift analysis) greatly improved our understanding about the nature of biological water. Recent experiments revealed that the dynamics of water associated with protein is significantly retarded compared to the bulk water. Corresponding development of theory and computer simulation suggests that the disruption of the extended water H-bonding network and formation of new H-bonds between water and biological molecule is mainly responsible for the slow water dynamics in protein.[64] The slow response of biological water may help a protein to retain its structure under adverse condition.

The solvation dynamics in a protein can be studied using an intrinsic fluorescent probe (Trp) and several extrinsic probes attached to the protein.[64-68]

The principle advantage of Trp is that if it is used as a probe, one can study a protein in the native state without worrying about the change in its structure or biological activity cause by incorporation of an external probe. Zewail and co-workers observed a time constant of 38 ps and 16 ps for solvation dynamics of Trp in two proteins, subtilisin Carlsberg and monellin, respectively. They also observed that in bulk water Trp exhibits a solvation time of 1.1 ps.[62d] Though, Trp is otherwise a very attractive probe, its photo physics is complicated by the interconversion of rotamers/electronic states in > 100 ps time scale.[62d] In another article Zhong and Zewail and their co-workers have studied the solvation dynamics in HSA at different pH values using intrinsic fluorescent probe, Trp and observed a ~100 ps solvation time at neutral pH. A similar temporal behavior was observed at acidic pH, whereas at basic pH a faster dynamics of 25 – 45 ps was observed.[65]

Several groups studied the solvation dynamics using extrinsic fluorescent probes that binds to the proteins covalently and non-covalently.[66-68] Bright and co-workers studied acrylodan labeled serum albumin in a water pool of a microemulsion using phase modulation of fluorescence and detected a nanosecond component.[67a] Zewail and co-workers studied the solvation dynamics of different domains of HSA using probes, acrylodan and prodan that binds to cys-34 of domain I covalently and non-covalently to domain II, respectively. They observed the time scale of dynamically ordered water as 57 ps for domain I and 32 ps for domain II. On unfolding, the solvation time was found to become faster and the time constant has been observed as 13 ps for domain I.[67b] Bhattacharyya and co-workers studied temperature dependent solvation dynamics using ANS as fluorescent probe that binds to the domain III of BSA non-covalently. They observed a short time component of 300 ps which is independent of temperature in the range of 278 – 318 K and a long component which decreases from 5800 ps at 278 K to 3600 ps at 318 K. The short time component was ascribed for dynamic exchange of bound to free water with a low barrier.[68a] In another work they measured the effect of RTIL on the native and denatured state of HSA using CMP

(7-dimethylamino-3-(4-maleimidophenyl)-4-methyl Coumarin) as fluorescent probe covalently attached to cys-34 of HSA and observed an average solvation time of 650 ps in the native state of HSA, 260 ps in presence of 1.5 M RTIL, 60 ps in presence of 6 M GnHCl and 30 ps in presence of 1.5 M RTIL along with 6 M GnHCl.[68b] However, they have suggested in their previous article that in presence of RTIL, the global structure of HSA become stabilize from GnHCl induced denaturation.[36b] Hence they concluded that the protein is structurally more compact, but the local environment of CPM is very different from that in native state when both RTIL and GnHCl are present in the system.[68b] Moreover, many theoretical calculations have also been performed to understand the dynamics of biological water.[62a, 64, 69]

1.5. Protein Dynamics

It is now well accepted that to understand the functions of a complex biological processes, information regarding the structure and dynamics of biological macromolecules are of great importance. Proteins are generally thought to adopt three dimensional structures determined by their amino acid sequences. However, the covalent backbone of a typical protein contains several individual bonds and the free rotation is possible around these bonds. Thus the protein can adopt a large number of conformations. As a consequence, the proteins are not strictly static in nature, but rather dynamic in nature. Protein dynamics dealt with such transitions that occur within the time window from nanoseconds (ns) to seconds (s).[70,71] It's also associated with the conformational change of bio-macromolecules on binding and release of ligands. Among the several methods the fluorescence based methods have become an elegant tool to investigate the protein dynamics by virtue of its sensitivity, selectivity and large temporal range.

On the basis of the size, the protein dynamics can be divided into two parts as **local conformational change** as well as **global structural change** with time. The local dynamics is associated with the change in the environment close to the

fluorescent tag molecule, whereas the global dynamics is associate with change in the overall protein. In the present scenario, the fluorescence-based methods like anisotropy decay kinetics, FRET, single molecule fluorescence resonance energy transfer (smFRET) and fluorescence correlation spectroscopy (FCS) are the prominent tools to study the local as well as global conformational dynamics of a protein.[72-79] Here smFRET and FCS are the tools that used for the study of protein dynamics at single molecular level. Many of the researchers have used time resolved fluorescence anisotropy for the structural characterization of macromolecules.[68a,72-74] Krishnamoorthy and co-workers have studied the motional dynamics of a covalently attached probe (acrylodan) to a protein (barstar) at various locations using fluorescence anisotropy decay kinetics. They have observed that the correlation times for global as well as local motion, which ranges from sub-nanoseconds to hundreds of nanoseconds, depends on the location of the fluorophore and are also different for different forms of the protein.[72b] Bohne and co-workers have studied the photocyclodimerization of 2-anthracenecarboxylate (AC) in the chiral binding site of human serum albumin (HSA) and concluded that the long rotational correlation time of 36 ns for AC bound to HSA is responsible for the high enantiomeric excess in photocyclodemerization reaction.[73b] Bright and co-workers have studied the dynamics of domain I of HSA in presence of ionic liquids (IL/2 % H_2O vol/vol) by using fluorescence anisotropy and showed that domain I of HSA was more significantly denatured in comparison when dissolve in aqueous solution of 8 M GnHCl. On increasing water loading they observed a progressive refolding of domain I followed by other domains.[74c]

Although the information from the bulk measurements is important; it fails to offer a complete description of molecular behavior due to the ensemble averaging, which is implicit in the measurement itself. For example, the fluctuation within the protein is impossible to monitor from ensemble measurements. Whereas, the measurements at single molecular level can evoke essential information that are hidden in the ensemble of molecules being studied, which are highly complex and

heterogeneous in nature. Single molecule fluorescence spectroscopy is an elegant and sensitive technique, which has been used to study such complex biological problems and has a long standing interest in the biophysical chemistry. **FCS and smFRET** are such fluorescence techniques for studying the conformational dynamics of proteins at single molecular level.[75-78] FCS is based on temporal fluctuations in the fluorescence intensity of a fluorescent probe attached to such macromolecules in the observation volume. The fluctuations of fluorescence intensity observed in FCS result either from the translational diffusion of the molecule in and out of the observation volume and/or other processes that are faster than the diffusion time, e.g. intersystem crossing, cis-trans isomerization, chemical reaction, quenching of fluorescence, etc. and as well the conformational fluctuations. The intensity fluctuations of a fluorescent tag attached to a protein can also arise from the quenching of the fluorescence signal of the fluorescent tag by some amino acid residues (act as quenchers), which is momentarily brought closer to the fluorescent tag by the conformational fluctuation of the side chain, and can be studied by FCS.[55b,79] smFRET is a technique that is used to measure the distances between donor and acceptor within a single biomolecule; and can be carried out either on surface immobilized molecules, or on the molecules freely diffusing in solution.[78] Webb and co-workers have analyzed the conformational fluctuations of apomyoglobin (apoMb) as a function of acid-induced unfolding by FCS.[75a] They have showed that as the pH of the medium decreases from 6.3 (native state) to 4.1 (molten globule state), both the fluctuation time scales and their amplitudes increase. On further decrease in the pH to 2.6 (unfolded state), the longer fluctuation time component as well as its amplitude remain constant, however the amplitude of the shorter component increases from 11 % to 17 %.[75a] They have reported the two time constants of conformational fluctuation of the native state as 8 μs and 100 μs. Frieden and co-workers have studied the kinetics of conformational fluctuation of a intestinal fatty acid binding protein and showed that the conformational fluctuations have a relaxation time component of 35 μs at pH 7.3 and become 2.5 μs at pH 2.[75b,c]

1.6. Model Proteins

Human Serum Albumin and Bovine Serum Albumin have served as model globular proteins for the present studies.

Human Serum Albumin (HSA). HSA is a multi-domain protein consisting of 585 amino acids residue and is the major protein found in our circulatory system (see figure 1.4).[80] The amino acid sequence contains a large number of disulphide bonds (17 in total), one free –SH group (cys-34) and a single tryptophan (trp-214).[10a] The secondary structure of HSA consists of about 67 % α-helical content and the molecular weight is ~65 kDa. The principal function of HSA is to transport fatty acids, but it is also capable of binding a great variety of metabolites and drugs.[81,82] The three dimensional structure of HSA has been determined crystallographically with a resolution of 2.8 Å by He *et al.*[10a] in 1992 and further at 2.5 Å resolution by Curry *et al.*[82] in 1998. The crystallographic data shows three structurally similar α-helical domains I, II and III that assemble to form a heart-shaped structure. Each domain is divided into two sub-domains (denoted A & B) possessing some common structural motifs.[10a,81-83] The single tryptophan unit of HSA is located in domain II of HSA.[10a,80] There are two known major drug binding sites (site I and site II) in HSA, located in sub-domain IIA and IIIA.[10a-c] Some of the drugs like warfarin, phenyl butazone, etc. are known to bind to the site I, whereas drugs like ibuprofen, diazapam, etc. selectively bind to the site II of HSA.[81,84] However, some drugs like digitoxin bind to another site of HSA, which

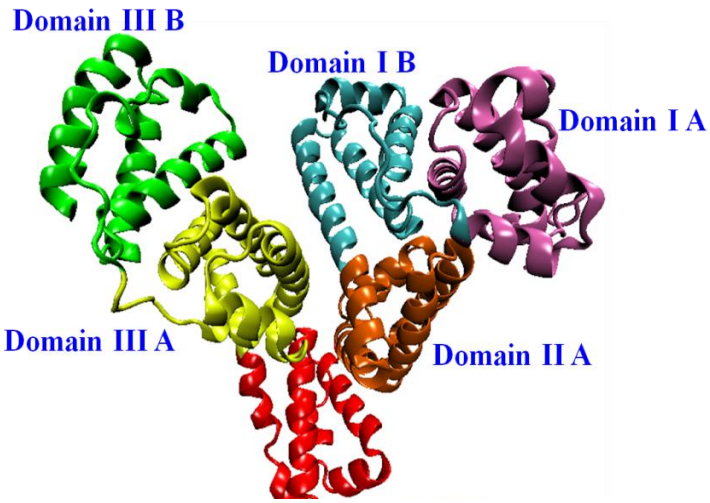

Figure 1.4. Schematic representation of human serum albumin, showing domain I, II and III; each is divided into two sub-domains A and B (PDB ID: 1HA2).

is named as digitoxin binding site or site III.[10b]

Bovine Serum Albumin (BSA). BSA shares approximately 80% sequence homology with HSA, and the repeating pattern of disulphide bonds which strictly conserved in both these serum albumins. It also has a single polypeptide chain, consisting 585 amino acid residues. The fundamental difference between both the serum albumins is that HSA contains only one tryptophan amino acid residue, Trp-214, whereas BSA contains two tryptophan residues, Trp-212 and Trp-135.[10c, 81] The spectral properties of HSA and BSA are not same in their native states due to the presence of an extra Trp-135 residue in BSA.

As discussed in section 1.1.1. that some globular proteins are big with distinct regions, called domains. These are distinct parts of a protein that may response independently and are distinguishable from rest parts of the protein. Different domains can impart different functions, such as binding of small molecules or interaction with other proteins, as a whole contributing to the overall role of the protein. Hence domain or site-specific investigation is necessary to understand the complete protein, which is not yet studied well. The structural details of HSA and BSA show that both the proteins are very big with three distinct domains. Each domain is structurally independent with the characteristics of a small globular protein. Hence, we choose these proteins as model proteins for domain specific study which can give a more precise knowledge about the actual functioning of these proteins. This thesis is devoted to understand the domain specific interactions, unfolding and dynamics of HSA and BSA. For these studies, mainly I have used fluorescent tag methods because fluorescent molecule selectively binds to a specific domain, and fluorescence response depends on change in its local environment.

References

1. Cox, M. M.; Nelson, D. L. *Lehninger, Principles of Biochemistry*, 5th Ed. W. H. Freeman Co. NY, **2008**.
2. Berg, J. M.; Tymoczko, J. L.; Stryer, L. *Biochemistry*, 5th Ed. W.H. Freeman Co. NY, **2002**.
3. (a) Eftink, M.; Pedigo, S. *Protein folding, Encyclopedia of physical science and technology*, 3rd Ed. (Biochemistry), p. 179.
   (b) Rayment, I. *Protein structure, Encyclopedia of physical science and technology*, 3rd Ed. (Biochemistry), p 191.
4. Richardson J. S. *Adv. Protein Chem.* **1981**, *34*,167.
5. Anfinsen, C. B. *Science*, **1973**, *181*, 223-230.
6. Anfinsen, C. B.; Haber, E.; Sela, M.; White, J. F. H. *Proc. Natl. Acad. Sci. U.S.A.* **1961**, *47*, 1309.
7. Levinthal, C. *J. Chem. Phys*. **1968**, *65*, 44.
8. (a) Bryngelson, J. D.; Onuchic, J. N.; Socci, N. D.; Wolynes, P. G. *Proteins: Struct. Funct. Gen.* **1995**, *21*, 167.
   (b) Wolynes, P. G.; Onuchic, J. N.; Thirumalai, D. *Science* **1995**, *267*, 1619.
9. (a) Clark, P. L. *Trends in Biochem. Sci.* **2004**, *29*, 527-534.
   (b) Schultz, C. P. *Nat. Struct. Biol*. **2000**, *7*, 7-10.
10. (a) He, X. M., and Carter, D. C. *Nature* **1992**, *358*, 209-215.
    (b) Sudlow, G.; Birkett, D. J.; Wade, D. N. *Mol. Pharmacol*. **1975**, *11*, 824.
    (c) Peters, T. Jr., *Adv. Protein Chem*. **1985**, *37*, 161-245.
11. Kregh-Hansen, U. *Dan. Med. Bull*. **1990**, *37*, 57.
12. Carter, D. C.; Ho, J. X. *Adv. Protein Chem*. **1994**, *45*, 152.
13. Kregh-Hansen, U.; Chuang, V. T. G.; Otagiri, M. *Biol. Pharm. Bull.* **2002**, *25*, 695.
14. Hu, Y.; Liu, Y.; Xiao, X. *Biomacromolecules* **2009**, *10*, 517.
15. Lazaro, E.; Lowe, P. J.; Briand, X.; Faller, B. *J. Med. Chem*. **2008**, *51*, 2009.
16. Anand, U.; Jash, C.; Boddepalli, R. K.; Shrivastava, A.; Mukherjee, S. *J. Phys. Chem. B* **2011**, *115*, 6312.

17. Anand, U.; Kurup, L.; Mukherjee, S. *Phys. Chem. Chem. Phys.* **2012**, *14*, 4250.
18. Patel, S.; Datta, A. *J. Phys. Chem. B*, **2007**, *111*, 10557.
19. Zhang, G.; Zhao, N.; Wang, L. *J. Lumines*. **2011**, *131*, 2716.
20. Bosca, F.; Tormos, R. *J. Phys. Chem. B* **2013**, *117*, 7528.
21. (a) Bhattacharyya, K. *Acc. Chem. Res.* **2003**, *36*, 95.
    (b) Das, K.; Jain, B.; Gupta, P. K. *Chem. Phys. Lett.* **2005**, *410*, 160.
    (c) Bhattacharya, B.; Srinivas, S.; Guruprasad, L.; Samanta, A. *J. Phys. Chem. B* **2009**, *113*, 2143.
22. Shreve, R. N.; Swaney, M. W.; Riechers, E. H. *J. Am. Chem. Soc.* **1943**, *65*, 2241.
23. (a) Kalkhambkar, R. G.; Kulkarni, G. M.; Kamanavalli, C. M.; Premkumar, N.; Asdaq, S. M. B.; Sun, C. M. *Eur. J. Med. Chem*. **2008**, *43*, 2178.
    (b) Wu, L.; Wang, X.; Xu, W.; Farzaneh, F.; Xu, R. *Curr. Med. Chem*. **2009**, *16*, 4236.
    (c) Basanagouda, M.; Shivashankar, K.; Kulkarni, M. V.; Rasal, V. P.; Patel, H.; Mutha, S. S.; Mohite, A. A. *Eur. J. Med. Chem*. **2010**, *45*, 1151.
24. Shobini, J.; Mishra, A. K.; Sandhya, K.; Chandra, N. *Spectrochim Acta A* **2001**, *57*, 1133.
25. Jisha, V. S.; Arun, K. T.; Hariharan, M.; D. Ramaiah, *J. Phys. Chem. B* **2010**, *114*, 5912.
26. (a) Martin, C.; Cohen, B.; Gaamoussi, I.; Ijjaali, M.; Douhal, A. *J. Phys. Chem. B* **2014**, DOI: 10.1021/jp5026575.
    (b) Grabolle, M.; Pauli, J.; Brehm, R.; Resch-Genger, U. *Dyes and Pigments* **2014**, *103*, 118.
27. (a) Peng, W.; Ding, F.; Peng, Y.; Jiang, Y.; Zhang, L. *J. Agric. Food Chem*., **2013**, *61*, 12415.
    (a) Simpson, M. J.; Poblete, H.; Griffith, M.; Alarcon, E. I.; Scaiano, J. C. *Photochem. Photobiol*. **2013**, *89*, 1433.
28. Duggan, E. L.; Luck, F. M. *J. Biologic. Chem.* **1948**, *172*, 205.
29. (a) Moriyama, Y.; Takeda, K. *Langmuir* **1999**, *15*, 2003.

(b) Moriyama, Y.; Takeda, K. *Langmuir* **2005**, *21*, 5524.

(c) Moriyama, Y.; Watanabe, E.; Kobayashi, K.; Harano, H.; Inui, E.; Takeda, K. *J. Phys. Chem. B* **2008**, *51*, 16585.

30. Ospinal-Jimenez, M.; Pozzo, D. C. *Langmuir* **2012**, *28*, 17749.
31. Anand, U.; Jash, C.; Mukherjee, S. *J. Phys. Chem. B* **2010**, *114*, 15839.
32. Vlasova, I. M.; Vlasov, A. A.; Saletsky, A.M. *J. Mol. Struct.* **2010**, *984*, 332.
33. (a) Mukherjee, S.; Sen, P.; Halder, A.; Sen, S.; Dutta, P.; Bhattacharyya, K. *Chem. Phys. Lett.* **2003**, *379*, 471.

(b) Mandal, U.; Ghosh, S.; Mitra, G.; Adhikari, A.; Dey, S.; Bhattacharyya, K. *Chem. -An Asian J.* **2008**, *3*, 1430.

34. (a) Qu, P.; Lu, H.; Yan, S.; Zhou, D.; Lu, Z. *J. Mol. Struct.* **2009**, *936*, 187.

(b) Kun, R.; Kis, L.; Dekany, I. *Colloids Surf. B* **2010**, *70*, 61.

35. Zhou, T.; Ao, M.; Xu, G.; Liu, T.; Zhang, J. J. *Colloid Interface Sci*. **2013**, *389*, 175.
36. (a) Mojumdar, S. S.; Chowdhury, R.; Chattoraj, S.; Bhattacharyya, K. *J Phys. Chem. B* **2012**, *116*, 12189.

(b) Sasmal, D. K.; Mondal, T.; Majumdar, S. S.; Choudhury, A.; Banerjee, R.; Bhattacharyya, K. *J. Phys. Chem. B* **2011**, *115*, 13075.

37. Shu, Y.; Liu, M.; Chen, S.; Chen, X.; Wang, J. *J.Phys.Chem.B* **2011**, *115*, 12306.
38. (a) Liu, S.; Sui, Y.; Guo, K.; Yin Z.; Gao, X. *Nanoscale Res. Lett*. **2012**,*7*, 433.

(b) Anand, U.; Ghosh, S.; Mukherjee, S. *J. Phys. Chem. Lett*. **2012,** *3*, 3605.

39. (a) Chakraborti, S.; Joshi, P.; Chakravarty, D.; Shanker, V.; Ansari, Z. A.; Singh, S. P.; Chakrabarti, P. *Langmuir* **2011**, *27*, 7722.

(b) Chakraborti, S.; Joshi, P.; Chakravarty, D.; Shanker, V.; Ansari, Z. A.; Singh, S. P.; Chakrabarti, P. *Langmuir* **2012**, *28*, 11142.

40. Schaefer, J.; Schulze, C.; Marxer, E. E. J.; Schaefer, U. F.; Wohlleben, W.; Bakowsky, U.; Lehr, C.M. *ACS Nano* **2012,** *6*, 4603.
41. (a) Giri, J.; Diallo, M. S., Simpson, A. J.; Liu, Y.; Goddard, W. A.; Kumar, R.; Woods, G.C. *ACS Nano* **2011**, *5*, 3456.

(b) Froehlich, E.; Mandeville, J. S.; Jennings, C. J.; Sedaghat-Herati, R.; Tajmir-Riahi, H. A. *J. Phys. Chem. B* **2009**, *113*, 6986.

42. (a) Biedermann, F.; Rauwald, U.; Zayed, J. K.; Scherman, O. A. *Chem. Sci*. **2011**, *2*, 279.

(b) Li, X.; Fang, Y.; Al-Assaf, S.; Phillips, G. O.; Jiang, F. *J. Colloid Interface Sci.* **2012**, *388*, 103.

43. Kundu, S.; Matsuoka, H.; Seto, H. *Colloids Surf. B* **2012**, *93*, 215–218.

44. (a) Ruggeri, F.; Zhang, F.; Lind, T.; Bruce, E. D.; Lau, B. L. T.; Cardenas, M. *Soft Matter* **2013**, *9*, 4219.

(b) Filipe, H. A. L.; Coreta-Gomes, F. M.; Velazquez-Campoy, A.; Almeida, A. R.; Peixoto, A. F.; Pereira, M. M.; Vaz, W. L. C.; and Moreno, M. J. *J. Phys. Chem. B* **2013**, *117*, 3439.

45. Dutta, P.; Sen, P.; Mukherjee, S.; Bhattacharyya, K. *Chem. Phys. Lett*. **2003**, *382*, 426.

46. Cheng, Z. *Mol. Biol. Rep*. **2012**, *39*, 9493.

47. (a) Luo, P.G.; Stutzenberger, F.J. *Adv. Appl. Microbiol*. **2008**, 63, 145.

(b) Buzea, C.; Blandino, I. I. P.; Robbie, K. *Biointerphases* **2007**, *2*, MR17–MR172.

(c) Sharifi, S,; Behzadi, S.; Laurent, S.; Forrest, M. L.; Stroeve, P.; Mahmoudi, M. *Chem. Soc. Rev.* **2012**, *41*, 2323.

48. (a) Horvath, I. T.; Anastas, P. T. *Chem. Rev*. **2007**, *107*, 2169.

(b) van Rantwijk, F.; Sheldon, R. A. *Chem. Rev*. **2007**, *107*, 2757.

(c) Wei, D.; Ivaska, A. *Anal. Chim. Acta* **2008**, *607*, 126.

49. (a) Dobson, C. M. *Nature* **2003**, *426*, 884.

(b) Seckler, R.; Jaenicke, R. *FASEB J*. **1992**, *6*, 2545.

50. (a) Santoro, M. M.; Bolen, D. W. *Biochemistry* **1988**, *27*, 8063.

(b) Klotz, I. M. *Proc. Natl. Acad. Sci. U.S.A.* **1996**, *93*, 14411.

(c) Varshney, A.; Ahmad, B.; Khan, R. H. *Int. J. Biol. Macromol*. **2008**, *42*, 438.

(d) Muzammil, S.; Kumar, Y.; Tayyab, S. *Proteins: Struc. Funct. Genet.* **2000**, *40*, 29.

51. (a) Ghosh, S.; Guchhait, N. *ChemPhysChem* **2009**, *10*, 1664.
(b) Tanford, C. *Adv Protein Chem*. **1968**, *23*, 121.

52. (a) Otzen, D. E.; Sehgal, P.; Westh, P. *J. Colloid Interface Sci*. **2009**, *329*, 273.
(b) Andersen, K. K.; Otzen, D. E. J. *Phys. Chem. B* **2009**, *113*, 13942.

53. (a) Kamal, J. K. A.; Zhao, L.; Zewail, A. H. *Proc. Natl. Acad. Sci. U.S.A.* **2004**, *101*, 13411.
(b) Tayyab, S., Siddiqui, M. U., and Ahmad, N. *Biochem. Ed.* **1995**, *23*, 162.

54. (a) Mitra, R. K.; Sinha, S. S.; Pal, S. K. *Langmuir* **2007**, *23*, 10224.
(b) Shaw, A. K.; Pal, S. K. *J. Photochem. Photobiol., B* **2008**, *90*, 69.
(c) Shaw, A. K.; Pal, S. K. *J. Photochem. Photobiol. B* **2008**, *90*, 187.

55. (a) Bhattacharya, M.; Jain, N.; Bhasne, K.; Kumari, V.; Mukhopadhyay, S. *J. Fluoresc.* **2011**, *1*, 1083.
(b) Chowdhury, R.; Chattoraj, S.; Mojumdar, S. S.; Bhattacharyya, K. *Phys. Chem. Chem. Phys*. **2013**, *15*, 16286.

56. (a) Luong, T. Q.; Verma, P. K.; Mitra, R.K.; Havenith, M. *Biophys. J*. **2011**, *101*, 925.
(b) Fu, L.; Villette, S.; Petoud, S.; Fernandez-Alonso, F.; Saboungi, M. L. *J. Phys. Chem. B* **2011**, *115*, 1881.

57. (a) Lee, J. C.; Timasheff, S. N. *Biochemistry* **1974**, *13*, 257.
(b) Miyawaki, O. *Biophys. Chem*. **2009**, 144, 46.

58. (a) Lim, W. K.; Rösgen, J.; Englander, S. W. *Proc. Natl. Acad. Sci. U.S.A.* **2009,** *106*, 2595.
(b) M. Roseman, W.P. Jencks, *J. Am. Chem. Soc.* **1975**, *97*, 631.
(c) Bennion, B. J.; Daggett, V. *Proc. Natl. Acad. Sci. U.S.A.* **2003**, *100*, 5142.
(d) Mason, P. E.; Brady, J. W.; Neilson, G. W.; Dempsey, C. E. *Biophys. J.* **2007**, *93*, L04 - L06.

59. (a) Kumaran, R.; Ramamurthy, P. *J. Fluoresc*. **2011**, *21*, 1499.
(b) Monera, O. D.; Kay, C. M.; Hodges, R. S. *Protein Sci*. **1994**, *3*, 1984.

60. (a) Santra, M. K.; Banerjee, A.; Krishnakumar, S. S.; Rahaman, O.; Panda, D. *Eur. J. Biochem.* **2004**, *271*, 1789.

(b) Santra, M. K.; Banerjee, A.; Rahaman, O.; Panda, D. *Int. J. Biol. Macromol.* **2005**, *37*, 200.

(c) Anand, U.; Jash, C.; Mukherjee, S. *Phys. Chem. Chem. Phys.* **2011**, *13*, 20418.

61. (a) Jimenez, R.; Fleming, G. R.; Kumar, P. V.; Maroncelli, M. *Nature* **1994**, *369*, 471.

(b) Bhattacharyya, K. *Acc. Chem. Res*. **2003**, *36*, 95.

(c) Bhattacharyya, K. *Chem. Comm*. **2008**, 2848.

62. (a) Nandi, N.; Bhattacharyya, K.; Bagchi, B. *Chem. Rev*. **2000**, *100*, 1013.

(b) Pal, S. K.; Peon, J.; Zewail, A. H. *Proc. Natl. Acad. Sci. U.S.A.* **2002,** *99*, 1763.

(c) Pal, S. K.; Peon, J.; Bagchi, B.; Zewail, A. H. *J. Phys. Chem. B* **2002**, *106*, 12376.

(d) Pal, S. K.; Zewail, A. H. *Chem. Rev*. **2004**, *104*, 2099.

63. Samaddar, S.; Mandal, A. K.; Mondal, S. K.; Sahu, K.; Bhattacharyya, K.; Roy, S. *J. Phys. Chem. B*, **2006**, *110*, 21210.

64. Nandi, N.; Bagchi, *B. J. Phys. Chem. B* **1997**, *101*, 10954.

65. Qui, W.; Zhang, L.; Okobiah, O.; Yang, Y.; Wang, L.; Zhong, D.; Zewail, A. H. *Phys. Chem. B*, **2006**, *110*, 20540.

66. (a) Chang, C. W.; He, T. F.; Guo, L.; Stevens, J. A.; Li, T.; Wang, L.; Zhong, D. *J. Am. Chem. Soc*. **2010**, *132*, 12741.

(b) Chang, C. W.; Guo, L.; Kao, T. H.; Li, T.; Saxena, C.; Liu, Z.; Wang, L.; Sancar, A.; Zhong, D. *Proc. Natl. Acad. Sci. U.S.A.* **2010,** *107*, 2914.

67. (a) Lundgren, J. S.; Heitz, M. P.; Bright, F. V. *Anal. Chem*. **1995**, *67*, 3775.

(b) Kamal, J. K. A.; Zhao, L.; Zewail, A. H. *Proc. Natl. Acad. Sci. U.S.A.* **2004,** *101*, 13411.

68. (a) Sahu, K.; Mondal, S. K.; Ghosh, S.; Roy, D.; Bhattacharyya, K. *J. Chem. Phys.* **2006**, *124*, 124909.

(b) Chowdhury, R.; Majumdar, S. S.; Chattoraj, S.; K. Bhattacharyya, *J. Chem. Phys.* **2012**, *137*, 55104.

69. Fogarty, A. C.; Dijon, E. D.; Sterpone, F.; Hynes J. T.; Laage, D. Biomolecular hydration dynamics: a jump model perspective. *Chem. Soc. Rev*., **2013**, *42*, 5672.
70. (a) Fraser, J. S., Clarkson, M. W., Degnan, S. C., Erion, R., Kern, D., Alber, T. *Nature* **2009**, *462*, 669.

(b) Frauenfelder, H., Sligar, S. G., and Wolynes, P. G. *Science* **1991**, *254*, 1598.

71. Weininger, U.; Brath, U.; Modig, K.; Teilum, K.; Akke, M. *J. Biomolecular NMR* **2014**, *59*, 23.
72. (a) Rami, B. R.; Krishnamoorthy, G.; Udgaonkar, J. B. *Biochemistry* **2003**, *42*, 7986.

(b) Jha, A.; Ishii, K.; Udgaonkar, J. B.; Tahara, T.; Krishnamoorthy, G. *Biochemistry* **2011**, *50*, 397.

73. (a) Naidu, K. T.; Prabhu, N. P. *J. Phys. Chem. B* **2011**, *115*, 14760.

(b) Fuentealba, D.; Kato, H.; Nishijima, M.; Fukuhara, G.; Mori, T.; Inoue, Y.; Bohne, C. *J. Am. Chem. Soc*. **2013**, *135*, 203.

74. (a) Jha, A.; Udgaonkar, J. B.; Krishnamoorthy, G. *J. Mol. Biol*. **2009**, *393*, 735.

(b) Flora, K.; Brennan, J. D.; Baker, G. A.; Doody, M. A.; Bright, F. V. *Biophys. J*. **1998**, *75*, 1084.

(c) Page, T. A.; Kraut, N. D.; Page, P. M.; Baker, G. A.; Bright, F. V. *J. Phys. Chem. B* **2009**, *113*, 12825.

75. (a) Chen, H.; Rhoades, E.; Butler, J. S.; Loh, S. N.; Webb, W. W. *Proc. Natl. Acad. Sci. U.S.A.* **2007**, *104*, 10459.

(b) Chattopadhyay, K.; Saffarian, S.; Elson, E. L.; Frieden, C. *Natl. Acad. Sci. USA* **2002**, *99*, 14171.

(c) Chattopadhyay, K.; Elson, E. L.; Frieden, C. *Proc. Natl. Acad. Sci. U.S.A.* **2005**, *102*, 2385.

76. (a) Haldar, S.; Mitra, S.; Chattopadhyay, K. *J. Biol. Chem*. **2010**, *285*, 25314.

(b) Haldar, S.; Chattopadhyay, K. *J. Biol. Chem*. **2012**, *287*, 11546.

77. (a) Pabbathi, A.; Patra, S.; Samanta, A. *ChemPhysChem* **2013**, *14*, 2441.

(b) Patra, S.; Santhosh, K.; Pabbathi, A.; Samanta, A. *RSC Advances* **2012**, *2*, 6079.

78. (a) Banerjee, P. R.; Deniz, A. A. *Chem. Soc. Rev*. 2014, *43*, 1172.

(b) Roy, R.; Hohng S.; Ha, T. *Nat. Methods* **2008**, *5*, 507.

79. (a) Neuweiler, H.; Banachewicz, W.; Fersht, A. R. *Proc. Natl. Acad. Sci. U.S.A.* **2010**, *107*, 22106.

(b) Neuweiler, H.; Johnson, C. M.; Fersht, A. R. *Proc. Natl. Acad. Sci. U.S.A.* **2009**, *106*, 18569.

80. Dugiaczyk, A.; Law, S.; Dennison, O. E. *Proc. Natl. Acad. Sci. U.S.A.* **1982**, *79*, 71.

81. Peters, T. Jr. *All about albumin: Biochemistry, Genetics, and Medical Applications*, Academic press, San Diego, **1996**.

82. Curry, S.; Mandelkow, H.; Brick, P.; Franks, N. *Nature Struc. Biol*. **1998**, *5*, 827.

83. Sugio, S.; Kashima, A.; Mochizuki, S.; Noda, M.; Kobayashi, K. *Protein Eng*. **1999**, *12*, 439.

84. (a) Kragh-Hansen, U.; Chuang, V. T. G.; Otagiri, M. *Biol. Pharm. Bull*. **2002**, *25*, 695.

(b) Kosa, T.; Moruyama, T.; Otagiri, M. *Pharm. Res*. **1997**, *14*, 1607.

Chapter 2

Experimental Methods

This chapter describes the experimental methods which have been used in carrying out the research work presented in this thesis. I will mainly describe the fundamental theory, basic principles and the instrumental details of one time resolved fluorescence spectroscopic technique, namely time correlated single photon counting (TCSPC) and a single molecule spectroscopic technique, namely fluorescence correlation spectroscopy (FCS). I will also describe the construction of a working FCS setup with high sensitivity by assembling different opto-mechanical components. Atomistic molecular dynamic simulations (classical MD simulations) and method of molecular docking are also discussed in brief in this chapter.

2.1. Steady State Measurements

The steady state absorption spectra of samples were recorded in Schimadzu 2450 spectrophotometer. Steady state emission spectra were recorded in Shimadzu RF5301, FluoroLog 3-21, Jobin Yvon, and Fluoromax-4, Jobin Yvon spectrofluorimeter. Circular dichroism spectra were recorded in Jasco J-815 CD Spectrometer. A stopped-flow apparatus (Applied Photo Physics, RX 2000) was connected to spectrophotometer or spectrofluorimeter as needed for the kinetic studies.

2.2. Time Resolved Fluorescence Measurements

There are various techniques such as time-correlated single photon counting (TCSPC), fluorescence up-conversion, and Streak camera that can be used for time resolved fluorescence measurements. These techniques differ in time resolutions, time window and sensitivity. For example, TCSPC has the time-resolution of the order of few tens of picoseconds (ps), Streak camera has the time-resolution of ~1-5 picoseconds (ps), and the fluorescence up-conversion has the time resolution of the order of hundreds of femtoseconds (fs). For the present work, I have used only TCSPC technique.

2.2.1. Time Correlated Single Photon Counting (TCSPC) Setup

TCSPC is a well established and commonly used technique for fluorescence lifetime measurements, which works on principle of detection of a single photon for each excitation pulse and measuring its arrival time with respect to a reference signal.[1,2] It's based on the probability distribution for the emission of a single photon after an excitation event yields the actual intensity against time distribution of all the photons emitted as a result of the excitation. By sampling the single photon emission for a large number of excitation pulses, the experiment reconstructs the probability distribution.[1,3]

A schematic representation of TCSPC setup is shown in figure 2.1. The samples were excited by high repetition rate low intensity picosecond diode laser and nano LED. A trigger pulse from the same diode laser or nano LED synchronous with excitation laser pulse is used as a start pulse for TAC (time to amplitude converter) and generates a voltage ramp, which increases linearly with time. An optical filter was used to block the exciting light and the sample fluorescence was dispersed to the monochromator. The fluorescence transient was collected at magic angle polarization, i.e. 54.7° from vertical excitation polarization using micro-channel plate photomultiplier tube (MCP-PMT). The output of the detector is used as stop pulse to the TAC after passing through constant fraction discriminator (CFD), which accurately measures the arrival time of pulse. The TAC generates voltage proportional to the time difference between the excitation of the sample and detected photon. The voltage is amplified and converted to numerical value using programmable gain amplifier (PGA) and analog-to-digital convertor (ADC), respectively. By repeating this process many times and by keeping the number of detected fluorescence photons low relative to the number of excitation pulses (2% or less), the fluorescence decay of the sample was obtained. The decays were best fitted with deconvolution method using commercial softwares, DAS6 and FAST. For recording the lamp profile, a scattering solution (Ludox) was used in place of the sample.

The main function of CFD is to measure the arrival time of photoelectron pulse with the highest resolution time. It is the first component which encounters with photoelectron pulse. CFD is being used to minimize the time jitter originated from the amplitude jitter by the detector. To minimize the pulse height distribution for the arrival time of the pulse, CFD eliminates the pulses which has height lower than a given threshold (voltage) and allows passing through only those pulses with higher height for further signal processing. After this, it splits the incoming pulse into two parts; one part of the pulse is inverted and the other part is delayed by the

half of the pulse width. Followed this, the two parts are recombined, where the time jitter of the zero crossing point is decreased dramatically.

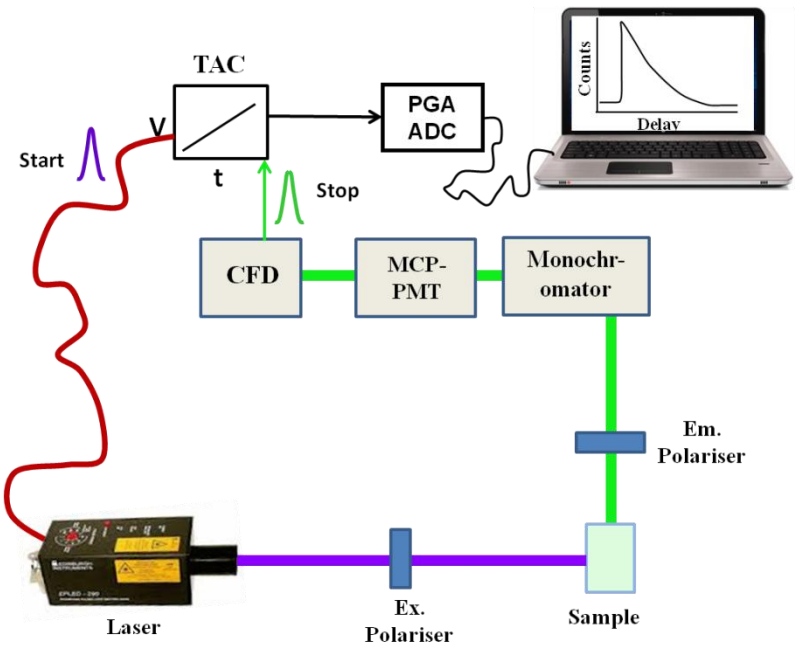

Figure 2.1. A schematic representation of time correlated single photon counting (TCSPC) setup.

After passing through the CFD, the photoelectron pulse is encountered with TAC, which is considered as the heart of TCSPC. The main role of TAC is to generate the voltage ramp by charging the capacitor inside TAC which is proportional to the time between the excitation and first arriving of emission photon. As the start pulse reaches to the TAC, the capacitor inside TAC get started to charge from 0 to 10 volts over a picosecond to microsecond time range and stopped by the stop pulse (first arriving emission pulse). The voltage which increases linearly with time completely depends on the arrival time of the stop pulse. Once the growth of voltage is stopped, now the TAC contains a voltage proportional to the time difference between the excitation of the sample and the emitted photon. The TAC output pulse can then be amplified and converted to numerical value using PGA and ADC, respectively. Multichannel analyzer (MCA) now measures the voltage signal from the TAC and classify it according to the counts at each particular voltage (time); and therefore put into different time bins in the MCA. The width of the time bins (i.e. time per channel) is the ratio of the full time-range of the TAC and the number of channels in MCA determined by the resolution of ADC. For the present work, we have used two

commercial TCSPC setups, Life Spec II from Edinburgh Instruments, UK and FluoroLog 3-21 fom Jobin Yvon, USA.

2.2.2. Data Processing

When the decay time is much larger compared to that of excitation pulse, the excitation may be described as a δ function. In case where the excitation pulse is larger compared to decay time, the measured data will depart from the actual fluorescence response due to a finite decay time of the pump pulse, response time of the photomultiplier tube and associated electronics. However, the measured fluorescence decay of the system is a convolution of the fluorescence from the molecule and the instrument response function. In order to extract actual fluorescence lifetime from measured fluorescence lifetime decay, it is necessary to deconvolute the experimental data obtained during the measurement. The measured fluorescence decay is mathematically represented by the following "convolution integral"

$$F(t) = \int_0^t I(t')P(t-t')dt' \qquad (2.1)$$

where, $F(t)$ is the fluorescence intensity at any time t, and $I(t')$ is the intensity of the exciting light at time t'. $P(t\text{-}t')$ is the response function of the experimental system. t' defines variable time delays (channel numbers) of infinitesimally small time-widths, dt' (channel widths). For single exponential decays, $P(t-t')$ can be written as $P(t-t') = \exp[-(t-t')/\tau]$, where τ is the actual fluorescence lifetime of the molecule. Thus, equation (2.1) is takes the form

$$F(t) = \exp(-t/\tau)\int_0^t I(t')\exp(t'/\tau)dt' \qquad (2.2)$$

Here, $F(t)$ is the observed fluorescence decay and $I(t')$ is the instrument response function, which are obtained experimentally by measuring fluorescence decays of sample and Rayleigh scattering from a LUDOX solution in water, respectively.

The deconvolution is based on an iterative least square regenerative convolution method.[1-4] An excitation pulse profile (i.e., IRF) and fluorescence lifetime decay are measured experimentally. Then the deconvolution starts with the mixing of the IRF and a projected decay to form a new reconvoluted function. This function is compared with the experimentally obtained fluorescence data and the difference is summed, generating the χ^2 function for the fit. The deconvolution proceeds through a series of such iterations until a significant change in χ^2 does not occur between two successive iterations. χ^2 is the measure for goodness of fitting and can be written as,

$$\chi^2 = \sum_{j=1}^{n} \frac{1}{\sigma_j^2} [F(t_j) - F_P(t_j)]^2 \qquad (2.3)$$

where $F(t_j)$ and $F_P(t_j)$ are the measured and projected data at different time-points, respectively. n is the number of data points or channels used in a particular analysis and σ_j is the standard deviation of each data point, which is the square root of the number of photon counts because TCSPC works on Poisson statistics, i.e. $\sigma_j = [N(t_j)]^{1/2}$.

The quality of fit is normally assessed by examining the reduced χ^2, plot of the weighted residuals and the autocorrelation function of residuals. Reduced χ^2 is defined as,

$$\chi_r^2 = \frac{\chi^2}{n-f} = \frac{\chi^2}{v} \qquad (2.4)$$

where n, p and $v = n\text{-}p$ are the number of data points, floating parameters and the number of degree of freedom, respectively.

We have to be careful for multi-exponential fitting, particularly where the difference between lamp and decay profile is small. Unless the data quality is very good, the fit was not satisfactory. An increase in the number of exponential terms is meaningful only when fitting is inappropriate with fewer numbers. There is

always a probability of reaching to a local minimum during deconvolution procedure and getting trapped there.

2.3. Time Resolved Emission Spectra

The emission spectra, at different times following the excitation, are called the time resolved emission spectra (TRES). These are obtained from the fluorescence decays, recorded at different wavelengths across the entire emission, and the steady state emission spectrum $I_{ss}(\lambda)$ of the fluorophore.[5-7] The best fits of decays at different wavelength by multi-exponential functions originate the time dependence of the fluorescence signal. Since the intensity depends on both wavelength and time, the total intensity can be written as a product of two functions individually dependent on wavelength and time as;

$$I(\lambda,t) = A(\lambda)B(t) \tag{2.5}$$

where, time dependent part $B(t)$ can be obtained from the best fits of the temporal decays; and the wavelength dependent part $A(\lambda)$ can be obtained from steady state emission spectrum $I_{ss}(\lambda)$, (emission intensity at the particular wavelength where the decay is measured). Thus it can be written as;

$$I_{ss}(\lambda) = \int_0^\infty I(\lambda,t)dt = A(\lambda)\int_0^\infty B(t)dt \tag{2.6}$$

where, $B(t) = \sum_{i=1}^{n} a_i \exp(-t/\tau_i)$ (2.7)

Thus, $A(\lambda) = \dfrac{I_{ss}(\lambda)}{\int_0^\infty B(t)dt} = \dfrac{I_{ss}(\lambda)}{\sum_i a_i\tau_i}$ (2.8)

In equation 2.7 and 2.8, a_i and τ_i are the i^{th} amplitude and decay constant of the temporal decay, respectively. Finally, the wavelength and time dependent fluorescence intensity can be written in the modified form as;

$$I(\lambda,t) = A(\lambda)B(t) = \frac{I_{ss}(\lambda)}{\sum_i a_i\tau_i}\sum_{i=1}^{n} a_i \exp(-t/\tau_i) \qquad (2.9)$$

This equation gives the fluorescence intensity at a particular wavelength and a particular instant of time. Once the time dependence of the intensity is obtained, the TRES are constructed by substituting the steady state fluorescence intensity and the fitting parameters of the decays at various wavelengths in equation 2.9. Because TRES contains only few data points over the entire emission spectrum, it is necessary to fit the data with some smooth function capable of modeling its line-shape. Lognormal line-shape function was employed to fit the TRES data and given by;[7-10]

$$g(\bar{\nu}) = g_0 \exp\left[-\ln(2)\left(\frac{\ln(1+2b(\bar{\nu}-\bar{\nu}_p)/\Delta)}{b}\right)^2\right], \; for\, \alpha > -1 \qquad (2.10)$$

and, $g(\bar{\nu}) = 0, \; for \; \alpha \le -1$ (2.11)

where, $\alpha = 2b(\bar{\nu}-\bar{\nu}_P)/\Delta$, g_0 is the peak height, $\bar{\nu}_p$ is the peak frequency in cm^{-1}, b is asymmetric factor and Δ is the width parameter usually of the order of few thousand cm^{-1}.

Time-dependent Stokes shift (TDSS), which can be constructed in terms of change in peak or mean frequency with time as obtained from fitted TRES data, can be a measure of solvation dynamics. TDSS is related to the theoretical function, solvation correlation function $C(t)$, which is normalized spectral shift and given by;

$$C(t) = \frac{\bar{\nu}(t)-\bar{\nu}(\infty)}{\bar{\nu}(0)-\bar{\nu}_p(\infty)} \qquad (2.12)$$

where, $\bar{\nu}(0)$, $\bar{\nu}(t)$, and $\bar{\nu}(\infty)$ represent the observed emission frequency denoted the peak of TRES at time zero, t and infinity, respectively.

2.4. Time Resolved Fluorescence Anisotropy

The fluorescence anisotropy is a powerful tool to investigate the dynamics of bimolecular systems in the condensed phase. The existence of transition moments for absorption and emission that lie along specific directions within the fluorophore structure is the main origin of anisotropy. The direction of the transition moments changes with the rotational diffusion of fluorophore. Fluorescence anisotropy reveals the average angular displacement of a fluorophore, occurs between the absorption and the subsequent emission of a photon. The rate and extent of rotational diffusion during excited state lifetime controls the angular displacement. It depends on the shape and size of the fluorophore and also on the viscosity of the medium. Upon excitation with a linearly polarized light, the fluorophores which are distributed isotropically in the fluid medium, the orientational distribution become nonuniform in the excited state. This nonuniformity induces anisotropy decays with the rotational relaxation of the fluorophore in the excited state with time.[3a]

Time resolved fluorescence anisotropy refers to the decay of optical anisotropy originated in an anisotropic ensemble of molecules by the excitation with a linearly polarized light. The time resolved fluorescence anisotropy is given by,

$$r(t) = \frac{I_{II}(t) - GI_{\perp}(t)}{I_{II}(t) + 2GI_{\perp}(t)} \qquad (2.13)$$

where, $I_{II}(t)$ and $I_{\perp}(t)$ denote time-dependent parallel and perpendicular components of the fluorescence decays to the vertically polarized excitation light respectively and G is the instrumental correction factor. During measurements, the analyzer was rotated at a regular interval to get parallel (I_{II}) and perpendicular ($I_{\perp}$) components of the decay. The G value was determined using tail matching method,[1] in which the intensity of the emitted light with parallel and perpendicular polarization should be equal at long time (i.e. $t = \infty$) so that $r = 0$.

2.5. Single Molecule Measurements

Although the information from the bulk measurements is important; but it fails to offer a complete description of molecular behavior due to the ensemble averaging, which is implicit in the measurement itself. Whereas, in single molecule spectroscopic study the properties of molecules can be investigated at a single molecular level; and has a long standing interest in the biophysical chemistry. Because of very high sensitivity and the bright signal against dark background, fluorescence becomes an obvious choice for single molecular spectroscopic techniques. There are various fluorescence based single molecule detection methods such as fluorescence correlation spectroscopy (FCS), single molecule FRET, and other methods of optical imaging based on various form of microscopy. For the present work, I used only FCS technique.

2.5.1. Fluorescence Correlation Spectroscopy (FCS)

The major concern of the current biological research is to determine the essential molecular interactions and precise physio-chemical characterization of elementary processes on the level of individual biological systems. Among several single molecule spectroscopic technique, FCS is an elegant technique that can monitor the molecular interactions, diffusion, chemical kinetics and conformational change in biological macromolecules at the single molecule level.[11-18] FCS is the method based on the observation of single molecule or a small number of molecules which are not immobilized like other single molecule spectroscopic methods. It detects the temporal fluctuation in the fluorescence intensity of the fluorophore in a focused laser beam.

FCS was first introduced by D. Magde, E. Elson and W.W. Webb in 1972 to study the binding kinetics of ethidium bromide (EtBr) with double-stranded DNA.[15] Employing the fluorescence fluctuation occurred due to the association and dissociation of EtBr with DNA as well as diffusion inside the observation volume; they observed the chemical reaction kinetic parameters along with

diffusion coefficients and diffusion-coupled reaction kinetics of EtBr interaction with DNA.

Although the principal ideas behind FCS as well as its main applications were already established in the early 70's; the experiments were still very hard to handle and suffered from the poor sensitivity (low signal-to-noise ratio due to the high background noise caused by the Raman scattering and Rayleigh scattering). The emerging utility of this method started only in the early 90's after introduction of the confocal detection scheme in FCS by Rigler *et al*. in 1993.[19] The basic concept behind the confocal detection scheme is to decrease the size of the detection volume, which may cause to minimize the background noise from scattered light and maximize the relative amplitude of fluorescence intensity fluctuations. That's why; the small observation volume is of utmost significance when performing the measurements at single molecular level. This can be achieved only when the laser light is focused tightly by using high numerical aperture (typically, NA > 1) objective to a diffraction-limited spot and also using a confocal pinhole with small diameter to reject signal from outside the desired volume. Using these optical conditions, the observation volume becomes ellipsoidal in shape elongated along the optical axis and become very small, typically of the order of femtoliter or less. Apart from the observation volume, the concentration of the sample (fluorophore) should be reduced so that a few molecules will present in the detection volume. This arrangement significantly increases the sensitivity of FCS by improving signal to noise ratio.[19-25] The main features of typical confocal FCS are as follows:

- **Create Small Focal Volume (Observation Volume)**
  - High *NA* Objective
  - Overfill back aperture
  - Small Pinhole diameter

Most crucial part in the FCS experiments is to create a small focal volume (typically less than a femtoliter) and detection of the fluorescence signal from this small volume. This can be achieved by tightly focused diffraction-limited spot of a Gaussian beam from the continuous wave laser source into the sample and subsequent confocal detection. The tight focusing of a laser beam can be achieved by using a high numerical aperture (*NA*) objective, which can be defined as,

$$NA = n\sin\theta \qquad (2.14)$$

where n is the refractive index of the medium, and θ is the half-angle of the cone formed at the focus point of the lens.

Except high numerical objective, the observation volume also depends on the beam diameter, fully or partially covering the back aperture of the objective. By using overfilled back aperture of the objective with the laser beam, the femtoliter observation volume can be achieved as shown in figure 2.2. Since the beam diameter of laser beam is generally very less, thus to overfilling of the back aperture of the objective expansion of the beam diameter is required.

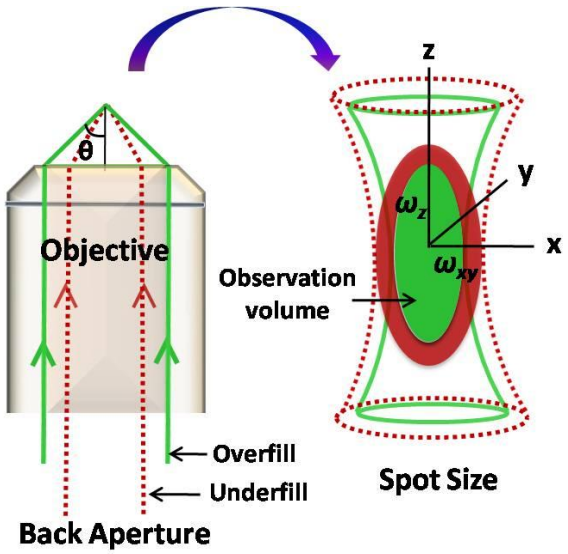

Figure 2.2. A schematic representation for variation in the focal volume with the change in beam diameter at the back aperture of the objective lens.

The fluorescence obtained from the observation volume is collected through the same objective lens in epi-fluorescence configuration. The epi-fluorescence is decoupled from the forward moving excitation light using dichroic mirror. The pinhole with small diameter was used after dichroic mirror to reject the undesired signal outside of the observation volume and reduce the lateral extent of the observation volume.

- **Collection of Fluorescence from Observation Volume**
  - Filtering the Fluorescence Signal from Background
  - Detection of Fluorescence

The collection of the fluorescence from observation volume is very sensitive in FCS experiments. The sample is excited by the tightly focused beam of laser light through the high *NA* objective and emitted photons form the tiny volume (observation volume) are collected by the same objective. The emitted light from the observation volume follows the same path in the reverse direction and separated by a dichroic mirror. Since in FCS experiment the concentration of the sample is very low (in nano-molar) and the observation volume is very small (femtoliter); hence it will very sensitive to stray light, residual excitation light, and Raman scattering from the solvent. These background signal cab be filtered out using a suitable band-pass filter that transmits light only within a small wavelength range. Afterward a confocal pinhole with small diameter is introduced in the image plane to limit the detection volume also in axial direction and which blocks all the light coming from outside the desired volume can be eliminated.

For the detection of fluorescence signal in FCS, a sensitive single-photon counting module is required because signal is not very strong. Generally single-photon avalanche photodiodes (SP-APD) are used to detect the fluorescence in the FCS experiments. These detectors collect single photons with high photon detection efficiencies and low dark noise. One can also use photomultiplier tube (PMT) for the detection. The APDs are more suitable in visible range due to its high sensitivity than PMT, whereas PMT can perform better in UV region.

- **Autocorrelation Analysis**

After detection, the signal is processed to the correlator card that can perform quasi real-time autocorrelation of the incoming signal and generate autocorrelation curve. Generally, the correlator cards are supplied with appropriate

driver software. It is the autocorrelation function (temporal) in which the correlation of signal occurs with itself for a series of time, shifted by time τ, as a function of t. This can be defined by the following equation.

$$G(\tau) = \frac{\langle \delta F(t)\delta F(t+\tau) + \delta F(t)\delta F(t+2\tau) + \cdots\cdots + \delta F(t)\delta F(t+n\tau)\rangle}{\langle F(t)\rangle^2} \quad (2.15)$$

Hence, the autocorrelation function is the product of signal at a certain time *t* with the signal at the time $t+\tau$ which describes the self-similarity of a fluctuating signal (see figure 2.3). After completion of autocorrelation analysis, autocorrelation curves were displayed using LabView program.

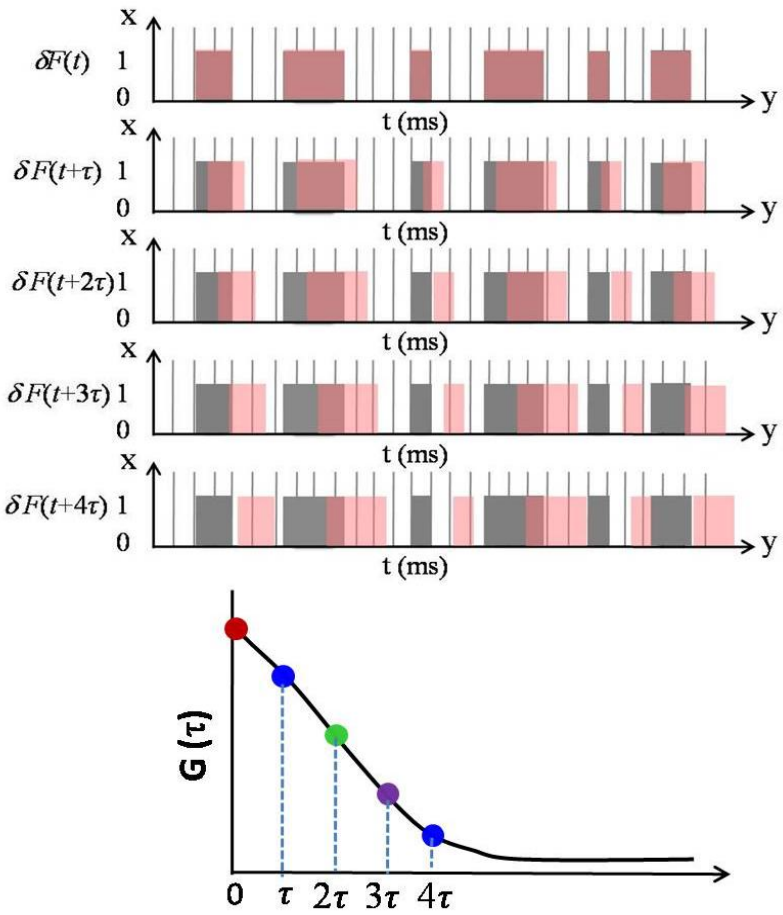

Figure 2.3. Representation for generate an autocorrelation curve from the fluctuations in the fluorescence intensity.

2.5.2. Theoretical Concepts of FCS

Fluctuations in the fluorescence signal, arises due to translational motion of the fluorescent species in-and-out of the observation volume and the chemical reaction or complex formation within the observation volume, have been evaluated to generate the autocorrelation curves. The Brownian motion of the fluorescent species within the samples is the main cause for the fluorescence fluctuations, whereas the average concentration of the molecules remains constant in space and time. The fluctuations in the fluorescence intensity obtained from FCS experiment are analyzed in terms of autocorrelation function $G(\tau)$ to obtain the information about the molecular processes as follows.[15,24-28]

$$G(\tau) = \frac{\langle \delta F(t) \delta F(t+\tau) \rangle}{\langle F(t) \rangle^2} \qquad (2.16)$$

where $\langle F(t) \rangle$ is the average fluorescence intensity, and $\delta F(t)$ and $\delta F(t+\tau)$ are the quantity of fluctuation in intensity around the mean value at time t and $t+\tau$ and are given by

$$\delta F(t) = F(t) - \langle F(t) \rangle \,,\ \delta F(t+\tau) = F(t+\tau) - \langle F(t) \rangle \qquad (2.17)$$

$$< F(t) >= \frac{1}{T} \int_0^T F(t) dt \qquad (2.18)$$

where, T is the data accumulation time or measurement time.

The fluorescence intensity from the sample depends on the concentration of fluorescent species in the observation volume and can be written as,

$$F(t) = B \int CEF(r) I_{ex}(r) C(r,t) dV \qquad (2.19)$$

$$B = q \varepsilon Q \qquad (2.20)$$

where, B is the brightness i.e. the number of emitted photons per second for a single fluorophore, which depends on detection efficiency of emitted photons (q),

molar absorbance (ε) and the quantum yield (Q). $CEF(r)$ is the collection efficiency function of the instrument as a function of position (r), $I_{ex}(r)$ is the excitation intensity and $C(r,t)$ is the concentration at position r at time t. For simplicity the position $\bar{r}$ is assumed as r for a vector. The excited fluorophore will be distributed in the three dimensional volume, in x-y plane and along z-axis.

Here another term can be used molecular detection efficiency $MDE(r)$, which is proportional to the intensity detected from a single emitter as function of its position r in the sample volume. It is calculated by multiplying the $CEF(r)$ and $I_{ex}(r)$ functions as follows.

$$p(r) = MDE(r) = CEF(r)I_{ex}(r) \tag{2.21}$$

The observation volume is defined by the intensity profile of focused laser beam and is assumed to be Gaussian (as shown in figure 2.2). For this configuration, the MDE can be approximated by a product of three-dimensional Gaussian.

$$p(r) = I_0 \exp[-2(x^2 + y^2)/{\omega_{xy}}^2]\exp(-2z^2/{\omega_z}^2) \tag{2.22}$$

where I_0 is the maximum intensity at the centre of the beam, ω_{xy} and ω_z refers to the distance in the lateral and axial directions at which the Gaussian profile decreases to I_0e^{-2}. We can assign the size of this volume which is normally defined by the effective volume V_{eff}.

$$\begin{aligned} V_{eff} &= \frac{(\int p(r)dV)^2}{\int p^2(r)dV} \\ &= \frac{(\int \exp[-2(x^2 + y^2)/{\omega_{xy}}^2]\exp(-2z^2/{\omega_z}^2)dV)^2}{\int \exp[-4(x^2 + y^2)/{\omega_{xy}}^2]\exp(-4z^2/{\omega_z}^2)dV} \approx \pi^{3/2}{\omega_{xy}}^2\omega_z \end{aligned} \tag{2.23}$$

All the fluctuations in the intensity arises only by the change in the concentration (δC) within the observation volume, can be written as,

$$\delta F(t) = B\int p(r)\delta C(r,t)dV \qquad (2.24)$$

The average intensity can be written as,

$$< F(t) >= BC\int p(r)dV \qquad (2.25)$$

Now the autocorrelation function for the intensity fluctuation cab be obtain by substituting equation 2.24 and 2.25 into equation 2.16.

$$G(\tau) = \frac{B^2 \iint p(r)\, p(r') < \delta C(r,0)\delta C(r',\tau) > dVdV'}{[BC\int p(r)dV]^2} \qquad (2.26)$$

where *r* and *r*' are the positions of the fluorophore at time $t = 0$ and $t = \tau$.

Considering the fluorescence property of the fluorophore due to reaction kinetic or complex formation is not changing within the observation volume and the fluorophore are freely diffusing in three dimensions with the diffusion coefficient *D*. The concentration correlation term for diffusion in three dimensions can be calculated as,[26]

$$< \delta C(r,0)\delta C(r',\tau) >= C(4\pi D\tau)^{3/2} \exp[-(r-r')^2 / 4D\tau] \qquad (2.27)$$

On substituting equation 2.27 and equation 2.23 into equation 2.26 and using some complex mathematics, one can easily calculate the autocorrelation function for freely diffusing molecules.[26, 27]

$$G(\tau) = \frac{1}{V_{eff}C} \cdot \frac{1}{(1+\tau/\tau_D)} \cdot \frac{1}{\sqrt{(1+(\omega_{xy}/\omega_z)^2 \cdot \tau/\tau_D)}} \qquad (2.28)$$

where the lateral diffusion time, $\tau_D = \omega_{xy}^2 / 4D$, which is the time that a molecule stay in the focal volume. The first term of equation 2.28 is exactly inverse of the average number of particles in the focal volume.

$$G(0) = \frac{1}{N} = \frac{1}{V_{eff}C} \qquad (2.29)$$

Finally, for a single component system diffusing in only three dimensions in solution phase, the diffusion time (τ_D) can be obtained by fitting the correlation function $G(\tau)$ using following equation.[3a]

$$G(\tau) = \frac{1}{N}\left(1+\frac{t}{\tau_D}\right)^{-1}\left(1+\frac{t}{\omega^2\tau_D}\right)^{-1/2} \qquad (2.30)$$

where N is the number of particles in the observation volume and $\omega = \omega_z/\omega_{xy}$ which is the depth to diameter ratio of 3D Gaussian volume. If the diffusing species undergoes an association chemical reaction or conformational change, which modulate its fluorescence intensity, with a relaxation time τ_R, then the correlation function can be written as,[29]

$$G(\tau) = \frac{1-A+A\exp(-t/\tau_R)}{N(1-A)}\left(1+\frac{t}{\tau_D}\right)^{-1}\left(1+\frac{t}{\omega^2\tau_D}\right)^{-1/2} \qquad (2.31)$$

where A is the amplitude of the process defined by τ_R.

2.5.3. Construction of FCS Setup

The motivation behind the construction of FCS setup in our laboratory is to make any alteration in the setup with ease and flexibly as per experimental demands and obviously saving the significant cost. For example, to perform the experiment at different excitation wavelength, along with excitation sources one need to change different optical as well as mechanical components that requires the realignment of the instrument. Similarly, for some experiments like reaction kinetics or conformational dynamics of a protein etc.; one needs to increase the size of the observation volume which can be achieved only by changing the beam diameter as well as the change in the confocal pinhole. These all modifications can only be possible with ease and flexibly in only home-build FCS setup. As a consequence, the complete understanding about the working principle and the rigorous alignment of the setup encourages us to exploration of new applications.

We construct our own home-built FCS setup using an inverted confocal microscope (Olympus IX71).

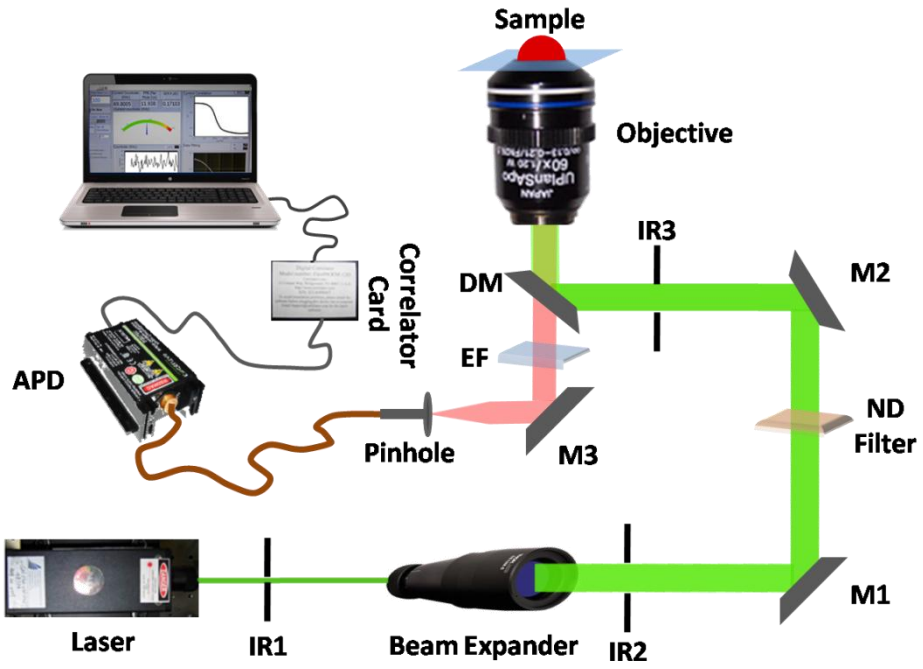

Figure 2.4. Schematic representation of fluorescence correlation spectroscopy (FCS) setup.

A schematic representation of home-built FCS setup is shown in figure 2.4. We used Olympus IX71 inverted microscope for this setup which contains three active ports in the left, right and back side of the microscope. The back-side port was used as entrance for the laser beam inside microscope to excite the sample; whereas left-side port was used as exit for the emitted light from the sample. The right-side port was kept closed. Along with active ports, the Olympus IX71 inverted microscope also contains slots for objective, dichroic mirror, emission filter and fluorescence focusing lens.

A CW laser source was used to excite the sample. As we have already discussed in section 2.5.1 that the back aperture of the objective should be overfilled (>10 mm for our instrument) to get a tiny observation volume. However, the beam diameter of laser source is very less which is insufficient to overfill the back aperture of the objective. In order to overfill the back aperture of objective, a

beam expander was used to expand the laser beam to a diameter of ~11 mm (see figure 2.4). To escape any photo-bleaching in the sample, we used neutral density (ND) filter in the path of the beam to control the intensity of the excitation light. Now with the help of mirrors, M1 and M2, the expended beam is processed to the dichroic mirror (DM) through the back port of the microscope and gets reflected to the back aperture of a 60X water immersion objective with high NA (NA ~1.2) objective. This high NA objective tightly focused the laser beam into the sample. The emitted photons were collected by the same objective and separated by the DM that blocks the excitation light and passes the fluorescence. The fluorescence is then focused to the confocal pinhole with diameter of 25μm of a multimode fiber patch chord after passing through an emission filter (EF). The holder of the fiber chord is mounted on a five-axis translational stage to make ease the alignment of confocal pinhole. Fluorescence signal was then directed towards a single photon counting module, avalanche photodiode (APD) through the fiber patch chord and then to the correlator card to generate the autocorrelation function $G(\tau)$. Finally autocorrelation curves were displayed using LabView program and further analysis is performed in IGOR Pro software.

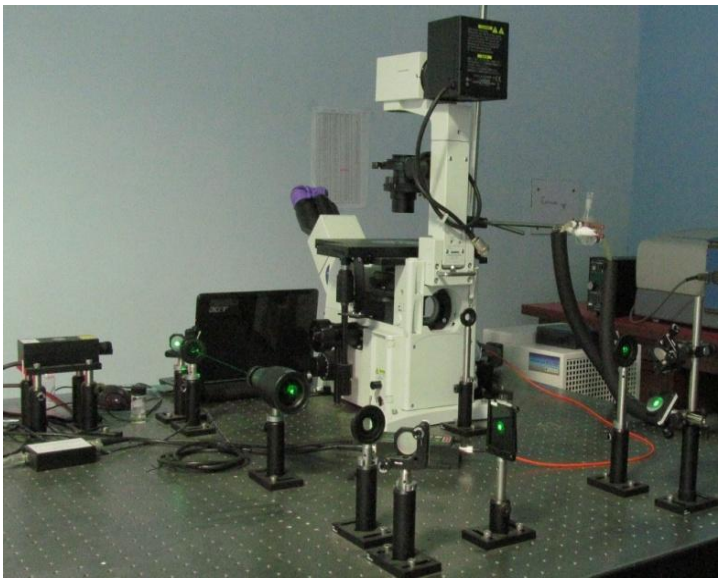

Figure 2.5. Photograph of fully functional FCS setup constructed in our laboratory

In FCS setups the detection efficiency of detectors (APD) is generally quite less than emitted by sample within the observation volume (< 1 of our instrument) and the sensitivity of FCS experiments is very high. Hence very small amount of light other than from the sample can

affect the measurements as well as damage the APD. To avoid these problems we placed it in complete dark room on an optical table. Since the detector is very sensitive and also expensive, a small fluctuation in the in the input light can damage the detector. An appropriate electric power supply was used which converts 12 Volt (DC) from a car battery to 5 Volt (DC) and supply to APD. A photograph of complete setup built in our laboratory is shown in figure 2.5.

➢ **List of Components Used for Construction of the Setup**

This microscope based FCS setup is constructed by assembling the commercially available components which are listed as follows:

- **Microscope**: Inverted confocal microscope; Olympus IX-71, Japan.
- **Objective**: 60X, Water immersion with NA 1.2; model: UPlanSAPO Olympus, Japan
- **Laser**: CW diode pump solid state laser @ 532 nm; Model SDL-532-LN-002T, Sanghai Dream Laser Tech, China.
- **Beam Expander**: 10X Optical beam expander, AR Coated: 400 - 650 nm; Model: BE10M-A, ThorLabs, USA.
- **Fiber Patch Chord**: Multimode fiber patch chord of 25 µm, 50 µm and 105 µm diameter; Model: M67L01 25µm 0.10NA, ThorLabs, USA.
- **Detector**: Single photon counting module, avalanche photodiode (APD); Model SPCM-AQRH-13-FC, Excelitas tech. Inc., Canada.
- **Correlator Card**: Hardware correlator; Model Flex99OEM-12/E, Correlator.com, USA
- **Optics: Dichroic Mirror**: ZT532rdc and **Emission Filter**: 605/70m both from Chroma tech. corp., USA; **ND filters**: Unmounted 2" x 2" Absorptive ND Filter, Optical density: 0.1 to 2 (NE201B to NE220B) and **Mirrors**: Ø1" (Ø25.4 mm) Protected Silver Mirror, 0.24" (6.0 mm) Thick (Silver PF10-03-P01) both from ThorLabs, USA.

➢ **Some Important Characteristic of the Setup**

- The back-side port was used as entrance for the laser beam inside microscope to excite the sample and the height of this back-port is ~18.6 cm from base. Hence to make the beam height same as the height of the back port of the microscope, we use a periscope, made by two mirrors, in place of M2 of figure 2.4.
- The collimation of beam was properly checked just after beam expander and a collimated beam diameter of 11 mm (to completely overfill the back aperture of objective) was adjusted using IR2 and IR3.
- To check whether the laser beam is vertical after passing through dichroic mirror, we used a scattering solution in cell that was prepared by pasting the base of 1 ml pipette tips on the cover slip. Now, by seeing the cone of illumination inside the scattering solution created by the tight focus of laser beam, we can make the light vertical by adjusting the mirrors.
- For the alignment of confocal pinhole, a high concentration solution of rhodamine 6G (R6G) as sample was used and the five axis translation stage, where the one side of fiber patch chord is attached, is adjusted until we can see the emitted light with naked eye from the other side of the chord. After this prior alignment, a fine alignment was done by seeing the count rate and autocorrelation curve of a very dilute R6G solution (within few nM) with the adjustments of x, y, z, θ_1, and θ_2 axis of five axis positioner.
- The collar correction has been done by changing the collar position from 0.13 to 0.22 and we observed maximum count rate, per particle brightness (PPB) and minimum diffusion time for R6G in water at collar position 0.14. For this position the observation volume has been calculated as ~ 0.6 fL.

2.6. Molecular Docking

Computational modeling of protein and ligand was carried out using Autodock Tools 4.2.[30] In this thesis we docked different ligands with HSA (PDB

code: 1HA2)[31] which gives the probable binding site of ligand inside the protein. The Autodock-tools were used to merge nonpolar hydrogens of protein and assign atomic charges. Also the nonpolar hydrogens of ligand were merged and rotatable bonds were assigned. Auto Grid was used to generate Grid-maps for each atom type.

2.7. Molecular Dynamics Simulations

Atomistic molecular dynamics (MD) simulations have been performed under the periodic boundary condition using Amber 9.[32] The initial coordinate of HSA was obtained from the Protein Data Bank (1HA2).[31] TIP3P water molecules[33] were used to solvate system and 14 Na^+ ions was added for the neutralization. AMBER 9 and general AMBER force field (GAFF) was used to model the protein and ligands (or any additives), respectively.[32,34a] First a 1000 steps of minimization was performed by holding the protein along with any solute molecule (if present) followed by 2500 steps of minimization without restrain any solute. Next a 20 ps initial equilibration has been done with restrained HSA along with any solute molecule. During the initial equilibration, each time step was 1 fs and the initial temperature of the systems was 0 K. Subsequently, the temperature of the system raised to room temperature in 6-7 ps time scale and maintained hereafter. Finally the MD simulations have been carried out by maintaining the final temperatures with the help of Langevin dynamics.[34b] Isotropic position scaling was used to maintain the pressure at 1 atm with a relaxation time of 2 ps.[34c] The SHAKE algorithm was employed to restrain the length of all covalent bonds involving hydrogen atom as well as the geometry of water molecule. [34d] A 2 fs time step was used to integrate the equation of motion. Particle Mesh Ewald method was employed to obtain the long range electrostatic interactions whereas a 10 Å cutoff was used for van der Waals interactions.[34e] It is worthy to note that during the simulation, the variation of potential energy and kinetic energy with time satisfied the energy conservation criteria. The Molecular Mechanics/Poisson−Boltzmann

Surface Area (MM-PBSA) approach from Amber Tools 12 was used to estimate the biding free energy of ligand with protein.[35f]

The MD simulations have been carried out for only two chapters, chapter 3b and chapter 5. For chapter 3b MD simulations have been performed at 293 K and 313 K for aqueous solution of HSA complexed with C152. For colligation of C152 to HSA, molecular docking study was performed using Autodock Tools 4.2.[30] In this system, after the initial equilibration, the temperature of the system raised to 293 K and 313 K in 6-7 ps time scale and maintained hereafter. Finally the MD simulation has been carried out for 2 ns. However for chapter 5, MD simulations have been performed for aqueous solution of HSA in presence and absence of 1M sucrose at 300 K.

2.8. Materials

Human serum albumin and bovine serum albumin both essentially fatty acid free, coumarin 153, coumarin 152, Fluorescein, 8-anilino-1-naphthalenesulfonic acid ammonium salt, tetramethylrhodamine-5-maleimide, warfarin, ibuprofen, digitoxin, sodium dodecyl sulphate, cetyltrimethyl ammonium bromide, p-nitrophenyl acetate, hemin from Porcine, guanidine hydrochloride and sucrose were purchased from Sigma-Aldrich, USA and used as such. N-(7-dimethylamino-4-methylcoumarin-3-yl) iodoacetamide has been purchased from Molecular Probes, Inc., USA and used as received. Urea was purchased from Spectrochem, India and was used after recrystallizing twice from aqueous ethanol. Analytical grade di-sodium hydrogen phosphate, sodium di-hydrogen phosphate, tris-buffer and hydrochloric acid were purchased from Merck, Mumbai, India and used for preparing the buffer solutions. Dialysis membrane tubing (12kDa cut-off) was purchased from Sigma-Aldrich, USA and used after removing the glycerol and sulfur compounds according to the procedure given by Sigma-Aldrich. Centrifugal filter units (Amicon Ultra, 10kDa cut-off) have been purchased from Merck Millipore, Germany.

References

1. O' Connor, D. V.; Phillips, D. *Time Correlated Single Photon Counting, Academic* Press: New York, **1984**.
2. (a) Becker, W. *Advanced Time-Correlated Single Photon Counting Techniques*, Springer, **2005**.
   (b) Tkachenko, N. V. *Optical Spectroscopy Methods and Instrumentations*, Elsevier **2006**.
3. (a) Lakowicz, J. R. *Principles of Fluorescence Spectroscopy*, 3rd Edition, Springer **2006**.
   (b) Fleming, G. R. *Chemical Applications of Ultrafast Spectroscopy*; Oxford University Press: New York, **1986**.
4. Bevington, P. R. *Data Reduction and Error Analyses for the Physical Sciences*, McGraw-Hill, **1969**.
5. Eastern, J. H.; DeTomma, R, P.; Brand, L. *Biophys, J.* **1976**, *16*, 571.
6. Badea, M. G.; Brand, L. *Methods Enzymol*. **1979**, *61*, 378.
7. Maroncelli, M.; Fleming, G. R. *J. Chem. Phys*. **1987**, *86*, 6221.
8. Fee, R.; Maroncelli, M. *Chem. Phys*. **1994**, *183*, 235.
9. Chapman, C.; Maroncelli, M. *J. Phys. Chem.* **1991**, *95*, 9095.
10. Fee, R. S.; Milsom, J. A.; Maroncelli, M. *J. Phys. Chem.* **1991**, *95*, 5170.
11. (a) Maiti, S.; Haupts, U.; Webb, W. W. Proc. Natl. Acad. Sci. USA **1997**, *94*, 11753.
    (b) Wohland, T.; Friedrich, K.; Hovius, R.; Vogel, H. *Biochemistry* **1999**, *38*, 8671.
12. Hess, S. T.; Huang, S.; Heikal, A. A.; Webb, W. W. *Biochemistry* **2002**, *41*, 697.
13. Sánchez, S. A.; Gratton, E. *Acc. Chem. Res.* **2005**, *38*, 469.
14. Haustein, E.; Schwille, P. Annu. Rev. *Biophys. Biomol. Struct.* **2007**, *36*, 151.
15. Magde, D.; Elson, E. L. Webb, W. W. *Phys. Rev. Lett.* **1972**, *29*, 705.
16. Magde, D.; Elson, E. L.; Webb, W. W. *Biopolymers* **1974**, *13*, 29.

17. Elson, E. L.; Magde, D. *Biopolymers* **1974**, *13*, 1.
18. Ehrenberg, M.; Rigler, R. *Phys. Chem.* **1974**, *4*, 390.
19. Rigler, R.; Mets, Ü.; Widengren, J.; Kask, P. *Eur. Biophys. J.* **1993**, *22*, 169.
20. Qian, H.; Elson, E. L. *Appl. Opt.* **1991**, *30*, 1185.
21. Zemanová, L.; Schenk, A.; Valler, M. J.; Nienhaus, G. U.; Heilker, R.
22. Drug Discovery Today 2003, 8, 1085.
23. Eigen, M.; Rigler, R. *Proc. Natl. Acad. Sci. U.S.A.* **1994**, *91*, 5740.
24. Rigler, R. *J. Biotechnol.* **1995**, *41*, 177.
25. Rigler, R.; Widengren, J.; Mets, Ü. *Fluorescence Spectroscopy: New Methods an Applications*, Ed. Wolfbeis, O S., Berlin, Springer **1992**, pp- 13.
26. Thompson, N.L.; in Topics in Fluorescence Spectroscopy, Lakowicz, J.R. ; Ed., Plenum Press, New York **1991**, *1*, 337.
27. Schwille, P. *In Fluorescence correlation spectroscopy. Theory and applications*, Elson, E.L.; Rigler, R. Eds., Springer, Berlin, p. 360, **2001**.
28. Widengren, J.; Mets, Ü. *Conceptual basis of fluorescence correlatrion spectroscopy and related techniques at tools in biosciences. In single molecule detection in solution*, Ed. Ch. Zander, J Enderlein, RA Keller. Wiley-VCD, Darmstadt, Germany, **2002**, pp 69-120.
29. (a) Widengren, J.; Rigler, R. *Cell. Mol. Biol.* **1998**, *44*, 857.
    (b) Palmer, A.G.; Thompson, N.L. *Biophys. J.* **1987**, *51*, 339.
30. (a) Morris, G. M.; Goodsell, D. S.; Halliday, R. S.; Huey, R.; Hart, H. E.; Belew, R. K.; Olson, A. J. *J. Comput. Chem*. **1998**, *19*, 1639.
    (b) Morris, G. M.; Huey, R.; Lindstrom, W.; Sanner, M. F.; Belew, R. K.; Goodsell, D. S.; Olson, A. J. *J. Comput. Chem*. **2009**, *16*, 2785.
31. Petitpas, I.; Bhattacharya, A. A.; Twine, S.; East, M.; Curry, S. *J. Biol. Chem.* **2001**, *276*, 22804.
32. (a) Ponder, J. W.; Case, D. A. *Adv. Prot. Chem*. **2003**, *66*, 27.
    (b) Case, D. A.; Cheatham, T.; Darden, T.; Gohlke, H.; Luo, R.; Merz, K. M.; Jr, Onufriev, A.; Simmerling, C.; Wang, B.; Woods, R. *J. Comput. Chem.* **2005**, *26*, 1668.

(c) Case, D. A.; Darden, T. A.; Cheatham, T. E.; III, Simmerling, C. L.; Wang, J.; Duke, R. E.; Luo, R.; Merz, K. M.; Pearlman, D. A.; Crowley, M.; Walker, R. C.; Zhang, W.; Wang, B.; Hayik, S.; Roitberg, A.; Seabra, G.; Wong, K. F.; Paesani, F.; Wu, X.; Brozell, S.; Tsui, V.; Gohlke, H.; Yang, L.; Tan, C.; Mongan, J.; Hornak, V.; Cui, G.; Beroza, P.; Mathews, D. H.; Schafmeister, C.; Ross, W. S.; Kollman, P. A. AMBER 9, University of California, San Francisco, **2006**.

(d) Popelier, P. L. A.; Aicken, F. M. *ChemPhysChem*. **2003**, *4*, 824.

33. Miyamoto, S.; Kollman, P. A. *J. Comput. Chem*. **1992** , *13*, 952.

34. (a) Wang, J.; Wolf, R. M.; Caldwell, J. W.; Kollamn, P. A.; Case, D. A. *J. Comput. Chem.* **2004**, *25*, 1157.

(b) Wu, X.; Brooks, B. R. *Chem. Phys. Lett.* **2003**, *381*, 512.

(c) Berendsen, H. J. C.; Postma, J. P. M.; van Gunsteren, W. F.; DiNola, A.; Haak, J. R. *J. Chem. Phys.* **1984**, *81*, 3684.

(d) Ryckaert, J. P.; Ciccotti, G.; Berendsen, H. J. C. *J. Comput. Phys*. **1977**, *23*, 327.

(e) Essmann, U.; Perera, L.; Berkowitz, M. L.; Darden, T.; Lee, H.; Pedersen, L. G. *J. Chem. Phys.* **1995**, *103*, 8577.

(f) Case, D. A.; Darden, T. A.; Cheatham, T. E.; III, Simmerling, C. L.; Wang, J.; Duke, R. E.; Luo, R.; Walker, R. C.; Zhang, W.; Merz, K.M.; Roberts, B.; Hayik, S.; Roitberg, A.; Seabra, G,; Swails, J.; Goetz, A. W.; Kolossváry, I.; Wong, K. F.; Paesani, F.; Vanicek, J.; Wolf, R. M.; Liu, J.; Wu, X.; Brozell, S. R.; Steinbrecher, T.; Gohlke, H.; Cai, Q.; Ye, X.; Wang, J.; Hsieh, M. J.; Cui, G.; Roe, D. R.; Mathews, D. H.; Seetin, M. G.; Salomon-Ferrer, R.; Sagui, C.; Babin, V.; Luchko, T.; Gusarov, S.; Kovalenko, A.; Kollman, P. A.; *AMBER 12, University of California, San Francisco,* **2012**.

Chapter 3 (a)

Static and Dynamic Aspects of Supramolecular Interaction of Coumarin 153 and Fluorescein with Bovine Serum Albumin

Rajeev Yadav *et al*., *Aus. J. Chem*. **2012**, *65*, 1305.

The static and dynamic aspects of supramolecular interaction between coumarin 153 (C153) and fluorescein (FL) with bovine serum albumin (BSA) have been studied by spectroscopic techniques. Both the dyes found to form 1:1 complex with BSA with binding constants 2.9 ± 0.3 × 10^5 M^{-1} and 2.1 ± 0.2 × 10^5 M^{-1} for C153 and FL respectively. The binding site of C153 has been determined by steady-state FRET, site marker competitive experiment and molecular docking study. Our studies indicate that C153 binds to the domain IIIA of BSA whereas FL binds non-specifically. Denaturation characteristics of C153 and FL binding region of BSA was found to be very different than global denaturation. Furthermore, kinetics of binding has also been studied by stopped-flow method. The observed rate constants are found to be 8.8 sec^{-1} and 5.9 sec^{-1} for C153 and FL respectively.

3.1. Introduction

Molecular dyes are being used in great extent in clinical and medicinal applications in recent days.[1-4] The selective interaction of dye with a certain part of a massive complex has an enormous scope to pursue a site selective chemical modification without causing any change in the other part. In this aspect, some dyes like azo-, thiazine-, triphenylmethine- and acridine- are being used as antiseptic and other medicines.[5] Most of the drugs are generally transported into the required site through the circulatory system upon binding to a protein.[6] Human serum albumin (HSA) being most abundant protein in human circulatory system has been routinely studied for last few decades.[6-9] It transports a variety of endogenous and exogenous substances in circulatory system and plays an important role in the distribution and deposition of these substances.[7] Many drugs, including anti-coagulants, tranquillizers and general anesthetics are transported in the blood while bound to albumin.[6] As a consequence, the study of the interaction of drug and dyes with albumin is a long standing subject of interest.[8-15] Zhang *et al*. studied the interaction of malachite green with bovine serum albumin (BSA) and concluded that van der Waal's force and hydrogen bond play an important role in stabilizing the complex.[11a] Akbay *et al*. studied the interactions of two substituted hydroxychromone derivatives of coumarin with BSA by using fluorescence techniques. They showed that hydrogen bonding interaction were predominant in the formation of Coumarin–BSA complex.[14] In general, coumarin derivatives are important group of natural products and are found to be biologically active, having potent anti-cancer, anti-coagulant, chloretic, analgesic and diuretic properties.[17-20] Many studies have shown that some of coumarins also have anti-tumor activity against several human tumor cells.[21-23] Fluorescein is also a common fluorophore and it has been widely used in microscopy, forensics and serology to detect blood stain, etc. It is extensively used as a diagnostic tool in field of ophthalmology and optometry.[24] For such wide application, it is worth to study the interaction of coumarin and fluorescein with HSA. The parameters such as binding

stoichiometry, binding constant, binding site, binding kinetics are important parameters to characterize such supramolecular complexes.

On the other hand, bovine serum albumin (BSA) has been served as a model protein for this study because of its structural homology with HSA. BSA has 80% sequence homology with HSA and a repeating pattern of disulphide which are strictly conserved in both these serum albumin and is discussed in chapter 1.[25-32] Kosa *et al*. have investigated the binding parameters of some site specific drugs (e.g. warfarin, phenylbutazone, diazepam, ibuprofen) to variety of albumins (e.g. human, bovine, rabbit, dog and rat serum albumins) and showed that binding parameter of warfarin and ibuprofen to bovine albumin were passably similar to that in human serum albumin, whereas the binding parameters of phenylbutazone and diazepam to bovine albumin is different from human albumin.[33]

In the present study we investigate the static and dynamic aspect of binding characteristics of coumarin 153 (C153, scheme 3.1a) and fluorescein (FL, scheme 3.1b) with bovine serum albumin (BSA). Steady state absorption, emission and FRET have been used to extract the information regarding binding stoichiometry, binding constant and binding location inside the protein. The binding location has also been determined by the molecular docking study and compared with the experimental result. Binding kinetics has been determined using stopped flow technique. Unfolding behavior of different parts of BSA have also been investigated and compared with the global unfolding characteristics of the protein.

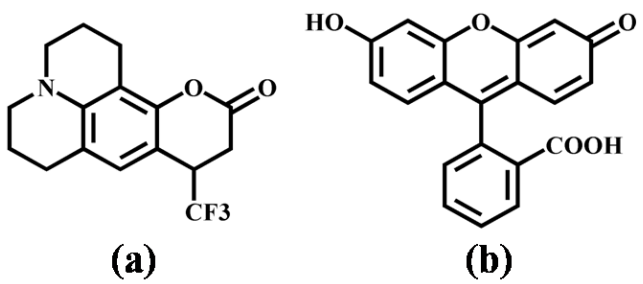

Scheme 3.1. (a) Molecular structure of coumarin 153. (b) Molecular structure of fluorescein.

3.2. Data Analysis

Binding stoichiometry between the fluorophore and BSA was determined by Job's method.[34,35] In this method, the concentration of the protein and dye were varied keeping the total concentration same. For the binding constant measurement, we kept the dye concentration fixed and measure the spectroscopic signal with increase in the protein concentration. The concentration of C153 and FL were determined from respective molar extinction coefficient of ε_{425nm} = 20,000 M^{-1} cm^{-1} and ε_{490nm} = 76,000 M^{-1} cm^{-1} respectively.[36, 37] For 1:1 complexation between protein (P) and dye (D) (as shown in equation 3.1) the value of binding constant between C153 and BSA was calculated from the fluorescence quantum yield of the system as a function of total protein concentration as given in equation 3.2.

$$P + D \rightarrow PD \qquad (3.1)$$

$$\phi = \frac{\phi_0 + \phi_C K[P_T]}{1 + K[P_T]} \qquad (3.2)$$

where ϕ is observed fluorescence quantum yield, ϕ_0 is quantum yield of sample without protein, ϕ_C is quantum yield of protein-dye complex, K is binding constant and $[P_T]$ is total protein concentration. For fluorescence quantum yield determination we used C153 in methanol (ϕ_f = 0.31) as a standard.[38,39]

In case of FL-BSA conjugate, the detectable change of absorbance was used to determine binding constant. For 1:1 binding between protein and dye the optical density of the system depends on the total protein concentration as,

$$OD = \frac{K[F_T][P_T]}{1 + K[P_T]}(\varepsilon_{FP} - \varepsilon_F) + [F_T]\varepsilon_F \qquad (3.3)$$

where OD is observed optical density of sample, $[F_T]$ is total fluorescein concentration, $[P_T]$ is total protein concentration, ε_F is molar extinction coefficient of fluorescein, ε_{FP} is molar extinction coefficient of FL-BSA complex and K is the

binding constant. At a particular concentration of dye and protein, the amount of free and bound dye can be determined as follows

$$C_f = \frac{[C_T]}{1 + K[P_T]} \tag{3.4}$$

Where C_f is free dye concentration in the dye protein mixture, $[C_T]$ is total concentration of dye, $[P_T]$ is total BSA concentration.

The binding site of C153 and FL in BSA has been determined by the site marker competitive experiment, steady-state FRET and also by molecular docking study. We have chosen two drugs warfarin and ibuprofen, which binds to two specific binding sites IIA and IIIA of BSA, respectively.[31,32] In site marker competitive experiment, a fixed concentration of BSA-dye conjugate is being titrated with the drug molecule and the changes in the absorption or emission were measured. The effect of drug molecule on the dye was determined by plotting the change of the spectroscopic signal as a function of drug concentration. Depending on the change of the signal, the probable binding site was determined. Steady-state FRET has been used to measure the distance of C153 from Trp in BSA. The efficiency (ε) of FRET has been calculated by using following equation:[40]

$$\varepsilon = 1 - \frac{I}{I_0} \tag{3.5}$$

Where I and I_0 are fluorescence intensities of Trp of BSA in absence and presence of C153. According to Förster theory, FRET efficiency (ε) is related to donor (Trp) - acceptor (C153) distance (r) as[40]

$$\varepsilon = \frac{R_0^6}{R_0^6 - r^6} \tag{3.6}$$

Where R_0 is the Förster distance between acceptor (C153) and donor (Trp of BSA), at which efficiency (ε) of energy transfer is 50%. Förster distance (R_0) for the present donor-acceptor pair (Trp in BSA-C153) was calculated using[40]

$$R_0 = 0.211[\kappa^2 n^{-4} \phi_D J(\lambda)]^{1/6} \qquad (3.7)$$

Where κ^2 is orientation factor taken as 2/3 by assuming randomize orientations of the donor and the acceptor,[40] n is the refractive index of the medium, which is 1.4 for macromolecules in water,[40] ϕ_D is the quantum yield of donor (Trp in BSA) is 0.32[16], and $J(\lambda)$ (in $M^{-1}cm^{-1}nm^4$) is the spectral overlap integral between the donor emission and the acceptor absorption as shown in equation 3.8.[40]

$$J(\lambda) = \frac{\int_0^\infty F_D(\lambda)\varepsilon_A(\lambda)\lambda^4 d\lambda}{\int_0^\infty F_D(\lambda)d\lambda} \qquad (3.8)$$

Where $F_D(\lambda)$ is the fluorescence intensity of donor in absence of acceptor (dimensionless quantity) and $\varepsilon_A(\lambda)$ is the molar extinction coefficient of acceptor ($M^{-1}cm^{-1}$) and λ is wavelength (nm).[40]

Computational modeling was carried out by using Autodock Tools 4.2. Here we docked C153 and FL into the HSA (PDB code: 1HA2) which gives the probable binding sight of these dyes inside the protein. The reason behind using HSA instead of BSA was the unavailability of PDB file of BSA in literature and BSA has 80% sequence homology with HSA.[25,26]

Protein unfolding study was carried out by measuring the change in circular dichroism (CD) signal of the protein or the absorbance or fluorescence signal of the bound dye, as a function of the denaturant concentration. A denaturant induced change of system properties as a function of denaturant concentration can be written as[41,42]

$$S = \frac{(S_0^N + m_F[D]) + (S_0^U + m_U[D])e^{-\frac{\Delta G_0 + m_{UF}[D]}{RT}}}{1 + e^{-\frac{\Delta G_0 + m_{UF}[D]}{RT}}} \quad (3.9)$$

where S is the observable (e.g. CD response, fluorescence intensity, absorbance, etc.), $[D]$ is concentration of denaturant, S_0^N and S_0^U are intercepts of folded and unfolded base line, m_F and m_U are the slopes of folded and unfolded base line and ΔG_0 is free energy change for denaturation in absence of denaturant. Here m_{UF} is slope of ΔG versus $[D]$ plot. The denaturant concentration ($[D]_{1/2}$) for 50% unfolding of the protein can be readily obtained as,

$$[D]_{1/2} = -\frac{\Delta G_0}{m_{UF}} \quad (3.10)$$

In the present study, we have used urea as the denaturant. The concentration of urea was varied from 0 to 9 M in the unfolding study by diluting a 10 M urea stock solution to avoid any dilution effect. For the overall unfolding of BSA, CD was used as observable. For the unfolding study of C153 binding site, C153 fluorescence has been used as the observable. However for FL binding site, we have used absorbance change as the observable for unfolding.

For the binding kinetics study, a fixed concentration of protein as well as dye was mixed in equal volume using stopped-flow technique and the change in fluorescence or absorbance was monitored as a function of time from the time of mixing. For 1:1 binding model, the observed fluorescence intensity or absorbance were related to 1st order rate constant as

$$F = A(1 - e^{-kt}) \quad (3.11)$$

where F is observed fluorescence intensity or absorbance for C153-BSA or FL-BSA complexes respectively. A is a constant depends on protein-dye complex, k is 1st order rate constant and t is time.

3.3. Results and Discussion

3.3.1. Complexation of C153 and BSA

3.3.1.1. Binding Stoichiometry and Binding Constant

The complexation between C153 and BSA has been monitored by the changes in the fluorescence of the C153 upon binding to BSA. The absorption spectrum of C153 in water shows a peak at 431 nm. Addition of BSA does not change the absorption spectrum of C153 much and the absorption maximum is found to be at 432 nm. However, on increasing BSA concentration the fluorescence maximum of C153 gradually blue shifted with an increase in the fluorescence intensity. Figure 3.1a shows the emission spectra of C153 with increasing concentration of BSA from 0 to 70 μM. C153 emission maxima shifts from 545 nm in water to 512 nm in presence of 70 μM BSA with a 3 times increase in fluorescence intensity. One can attribute this blue shift and fluorescence enhancement due to the encapsulation of C153 from aquous solution to the hydrophobic domains of BSA. Inside BSA internal motion of probe molecules is restricted and consequently the rate of non-radiative relaxation is also arrested resulting in the enhancement of fluorescence intensity of C153.[43,44] Job's plot clearly indicates a 1:1 complexation between C153 and BSA (Figure 3.1b). Figure 3.1c shows the quantum yield of C153 as a function of BSA concentration and has been fitted with equation 3.2 to find out the binding contant (*K*). For C153-BSA complex the observed value of binding constant (*K*) is $2.9 \pm 0.3 \times 10^5$ M^{-1} which is in the same order as observed by Samanta and co-workers[43a] and also by Kumar and co-workers.[43c] It is cleary seen from figure 3.1c that C153 (total concentration is 10 μM) almost completely binds to 30 μM BSA. At this concentration ratio it has been calculated that (using equation 3.4) about 90% C153 is bound to BSA. Hence we fix the concntration of BSA as 30 μM and C153 as 10 μM in all other experiments.

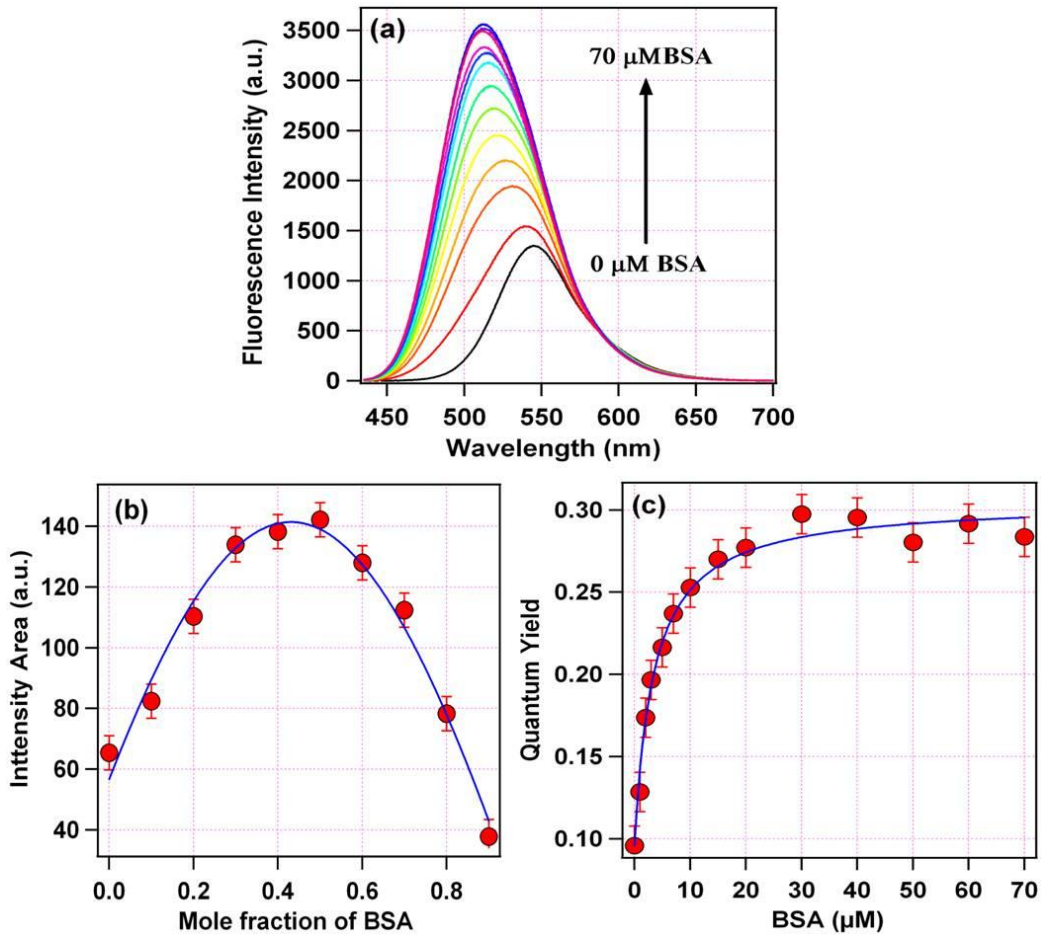

Figure 3.1. (a) Emission spectra of 10 μM C153 in presence of different concentration of BSA (varied from 0 to 70 μM) (λ_{ex} = 425 nm). (b) Job's plot for C153 binding to BSA. Total concentration of C153 and BSA was kept constant at 10 μM. (c) Plot of quantum yield of C153 against BSA concentration. Red filled circles with error bars indicate the experimental observed quantum yield and solid blue line is the best fit with equation 3.2. Here the error bars are obtained by averaging the associated errors of all the data points.

3.3.1.2. Identification of Binding Site Inside Protein

Site marker competitive experiment as well as molecular docking study was performed to determine the binding site of C153 inside BSA which was confirmed by FRET experiment. It is well documented that warfarin binds to domain IIA and ibuprofen binds to domain IIIA of human serum albumin.[31,32] In the present case, we have used bovine serum albumin which has 80% homology with HSA. Kosa *et al*. also showed that the binding site and binding affinity of the two drugs (i.e. warfarin and ibuprofen) in bovine serum albumin are sensibly similar that of human serum albumin.[33] The effect of these two drugs on the spectral

characteristic of the C153 in BSA was used to understand the binding site of C153 in BSA. Specifically it was determined by monitoring the spectral change of C153 in BSA on increasing concentration of warfarin and ibuprofen. In case of C153-BSA complex, increasing of warfarin concentration results in a 7% decrease in fluorescence quantum yield and emission maximum remains unchanged as shown in figure 3.2a. Interestingly, ibuprofen induced changes in fluorescence spectra of C153 bound BSA were much more pronounced. Here the fluorescence quantum yield decreases 25% with a red shift of emission maximum of 9 nm (figure 3.2b). The decrease in the fluorescence quantum yield as well as the red shift of the emission maximum of C153 in BSA in presence of ibuprofen clearly indicates that C153 binds to the subdomain IIIA of BSA.

We have also performed FRET experiment between the donor (Trp of BSA, λ_{ex} = 295 nm) and C153 to calculate the distance between Trp and C153 in the complex. Figure 3.3a shows the decrease in fluorescence intensity of the donor (Trp of BSA) with a concurrent increase in the acceptor (C153) fluorescence intensity on incresing concentration of C153. Such phenomenon is a clear indication of FRET. The overlap integral, $J(\lambda)$, and R_0 is calculated to be 4.43 × 10^{13} M^{-1} cm^{-1} nm^{-4} and 24.5 Å for the Trp-BSA and C153 donor acceptor pair. Finally, by using equation 3.5 and 3.6, the donor (Trp of BSA) and acceptor (C153) distance, *r*, is calculated to be 20.7 Å in the BSA-C153 complex. The probable binding site for C153 inside BSA was also investigated by molecular docking study. It shows that C153 binds to both binding sites that are located in domain IIA and domain IIIA of BSA. The average probable distance of C153 from Trp when it binds to domain IIA and domain IIIA were observed as 7 Å and 20 Å, respectively. It is to be noted that the distance between Trp and C153 in domain IIIA is same as we have calculated from the FRET measurement. The site marker compititive experiment along with FRET study clearly reveal that C153 binds to domain IIIA of BSA. Recently, Samanta and co-workers studied the binding of C153 in BSA theoretically by molecular docking method and found that it

selectively binds to the domain IIA of BSA.[43a] Our experimental data, however giving a different conclusion that C153 binds to domain IIIA of BSA.

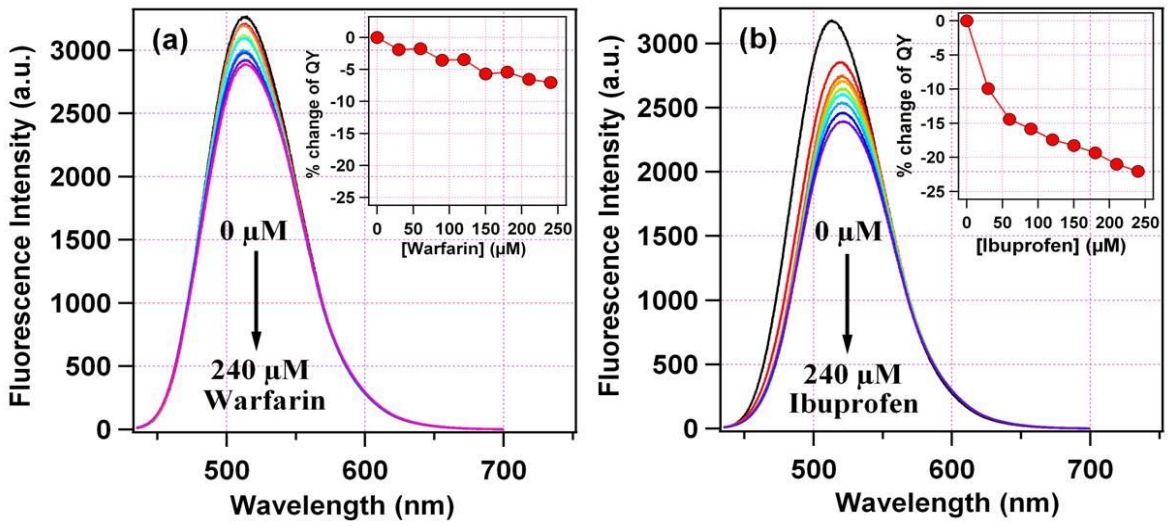

Figure 3.2. Effect of (a) warfarin and (b) ibuprofen binding on C153 bound BSA (a mixture of 10 μM C153 and 30 μM BSA). The concentration of warfarin and ibuprofen was varied from 0 to 240 μM (λex = 425 nm). Inset on each graph showing the percentage change of quantum yield of C153 upon drug binding against the drug concentration.

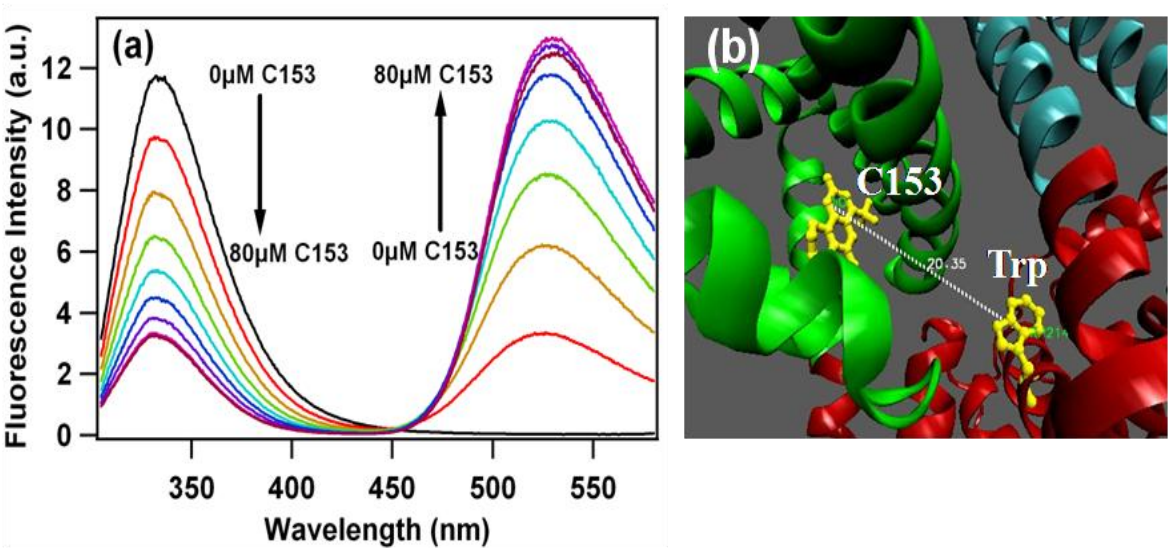

Figure 3.3. (a) Fluorescence spectra of 30 μM BSA in absence and presence of 10, 20, 30, 40, 50, 60, 70, 80 μM C153. The samples were excited at 295 nm. The arrows are showing the fall and rise of Trp and C153 fluorescence intensities respectively with increasing concentration of C153. (b) Location of C153 and Trp of HSA by computational modeling (Autodock Tools 4.2) study. The measured distance between Trp-HSA and C153 is about 20 Å.

3.3.1.3. Urea Induced Denaturation of BSA and C153-BSA Complex

The unfolding behavior of the global tertiary structure of BSA was monitored by cicular dichroism (CD) spectra of BSA on increasing concentration of urea. The CD-spectra of BSA (figure 3.4a) shows the presence of two bands at 209 nm and 222 nm.[45-47] The change in CD at 222 nm as a function of urea concentration (figure 3.4b) was fitted with equation 3.9 to estimate the free energy of unfolding of global BSA in absence of denaturant (ΔG_0^{glob}). The value is found to be 2.0 kcal mole^{-1}. The mid-point of unfolding was calculated to be at 4.9 M urea.

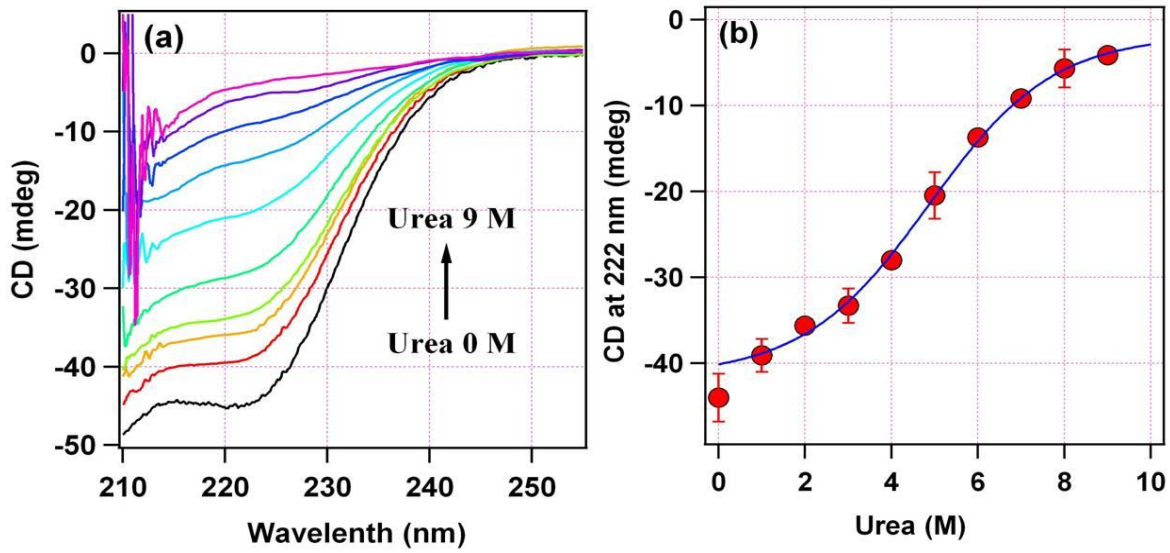

Figure 3.4. (a) Circular dichroism spectra 2 μM BSA with urea concentration varying from 0 to 9 M (b) Plot of CD value at 222 nm versus urea concentration. Solid blue line is the best fit of the data with equation 3.9.

For the determination of the free energy of unfolding for domain IIIA (C153 binding site) in absence of denaturant (ΔG_0^{IIIA}), we used C153 fluorescence intensity as the observable. The unfolding of BSA-C153 was monitored by change in fluorescence characteristics with increasing concentration of urea (figure 3.5a). The fluorescence intensity of C153 was found to decrease dramatically with urea concentration till 6 M with red shift of the emission maxima. Interestingly, untill 1.5 M urea the emission spectrum shows a blue shift of 1 nm then it starts shifting

to the longer wavelength. The blue shift at relatively low concentration of denaturant has also been observed previously.[48] Figure 3.5b shows the change in C153 emission intensity in BSA as a function of urea concentration. The free energy of domain IIIA unfolding in absence of denaturant (ΔG_0^{IIIA}) has been calculated by fitting the data using equation 3.9 and is found to be 2.2 kcal mol^{-1}. The midpoint of unfolding is observed at 3.6 M urea concentration. The results clearly suggest that domain IIIA is somewhat more unstable than overall BSA.

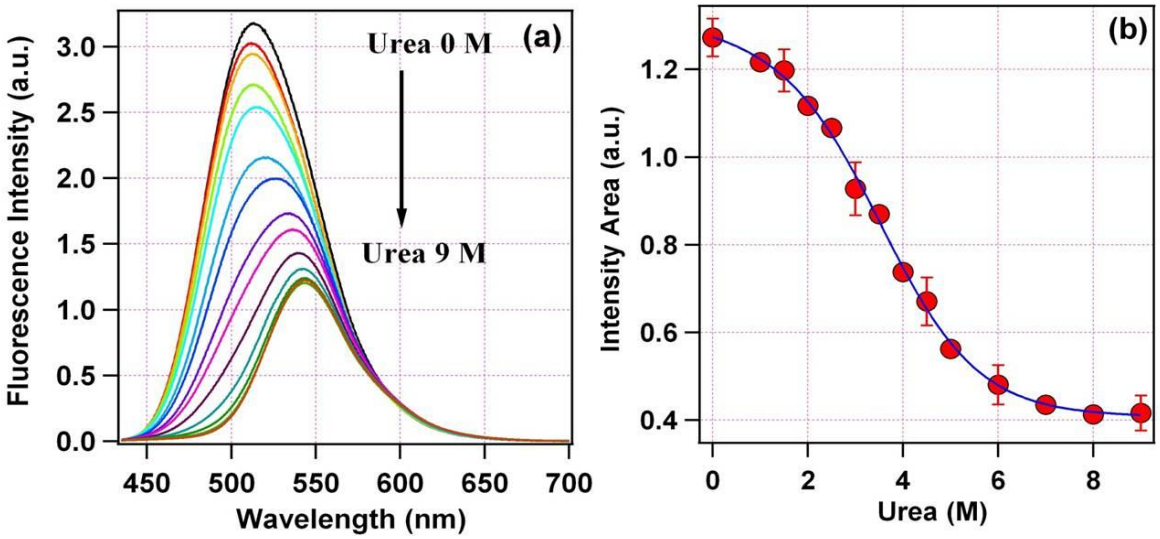

Figure 3.5. (a) Emission spectra of 10 μM C153 + 40 μM BSA with urea concentration vary from 0 M to 9 M (λ_{ex} = 425 nm) (b) Plot of fluorescence intensity area versus urea concentration. Solid blue line is the best fit of the data with equation 3.9.

3.3.1.4. Binding Kinetics

It is necessary to understand the dynamic aspects of interaction of C153 with BSA to fully characterize the complex. Using stopped-flow technique, we have studied the change in the fluorescence intensity of C153 on addition of BSA with time. The fluorescence intensity of C153 increases with time from the time of mixing due to the complaxation with BSA. The data was collected 10 times and avaraged and is shown in figure 3.6. Assuming a first order rate law, the data was fitted with equation 3.11 and the rate constant (k) of binding of C153 with BSA is found to be 8.8 sec^{-1}.

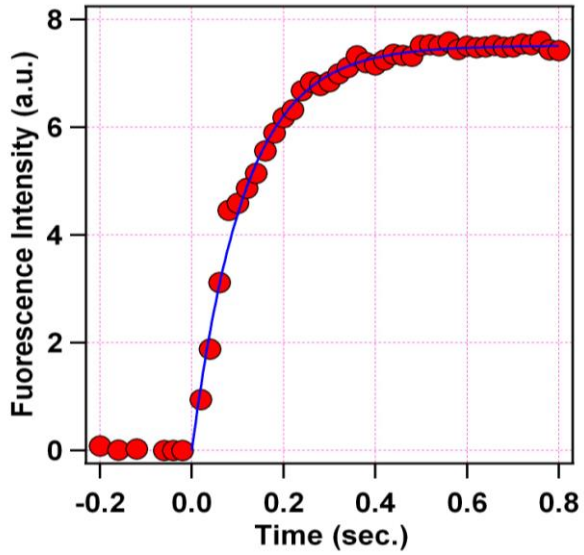

Figure 3.6. Plot of fluorescence intensity of 10 μM C153 + 50 μM BSA against time(sec.) at the time of mixing.

3.3.2. Complexation of FL with BSA

3.3.2.1. Binding Stoichiometry and Binding Constant

The complexation of fluorescein (FL) with BSA has been monitored by change in the absorption spectra of FL upon binding with BSA. The absorption spectrum of FL in water shows a peak at 482 nm with a shoulder at 453 nm. On increasing concentration of BSA, the absorption maxima of FL red shifted with increase in the absorbance (figure 3.7a). At 30 μM BSA, the absorption maxima is found to be at 505 nm. This increase in absorbance as well as red shifting is common for this type of dyes due to change of environment from aqueous medium to hydrophobic medium.[49,50] Mchedlov-Petrossyan and co-workers have studied the absoption of fluorescein in micellar media and found the absorption maximum shifts to 504.5 nm in cetylpyridinium chloride micelle.[49] Using this absorbance feature of fluorescein a Job's plot was constructed (Figure 3.7b), which clearly indicates 1:1 complex formation between FL and BSA. The change in absorbance of FL at 500 nm as a function of BSA concentration (Figure 3.7c) has been used to estimate the binding constant (*K*) of BSA-FL complex by fitting the data using equation 3.3. The binding constant (*K*) was found to be 2.1 ± 0.2 **x** 10^5 M^{-1}.

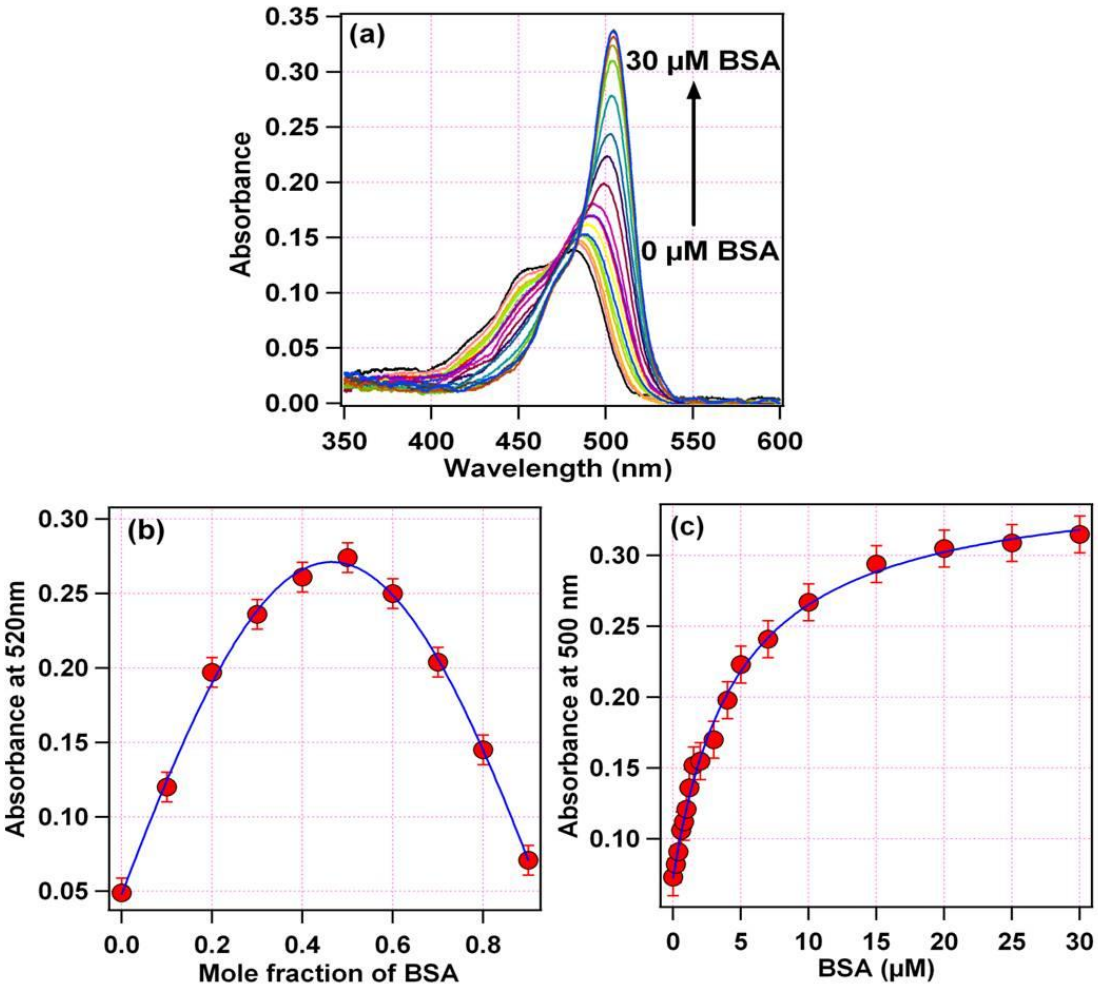

Figure 3.7. (a) Absorption spectra of 2 μM fluorescein with BSA concentration varying from 0 to 30 μM. (b) Job's plot for FL binding to BSA. Total concentration of fluorescein and BSA was kept constant at 30 μM. (c) Absorbance at 500 nm versus BSA concentration. Red filled circles indicate the experimental observed absorbance and solid blue line is the best fit with equation 3.3. Here the error bars are obtained by averaging the associated errors of all the data points.

3.3.2.2. Identification of Binding Site Inside Protein

To know where fluorescein binds inside BSA, both the site marker compititive experiment and molecular docking study have been performed. The FL binding site was monitored by change in absorption spectrum of FL-BSA complex on increasing concentration of wafarin and ibuprofen. Figure 3.8 shows the change of absorption spectra of Fl bound to BSA as a function of warfarin and ibuprofen concentration. The change of the absorption spectra of FL is almost same for both warfarin and ibuprofen. Urea induced denaturation study of FL-BSA complex

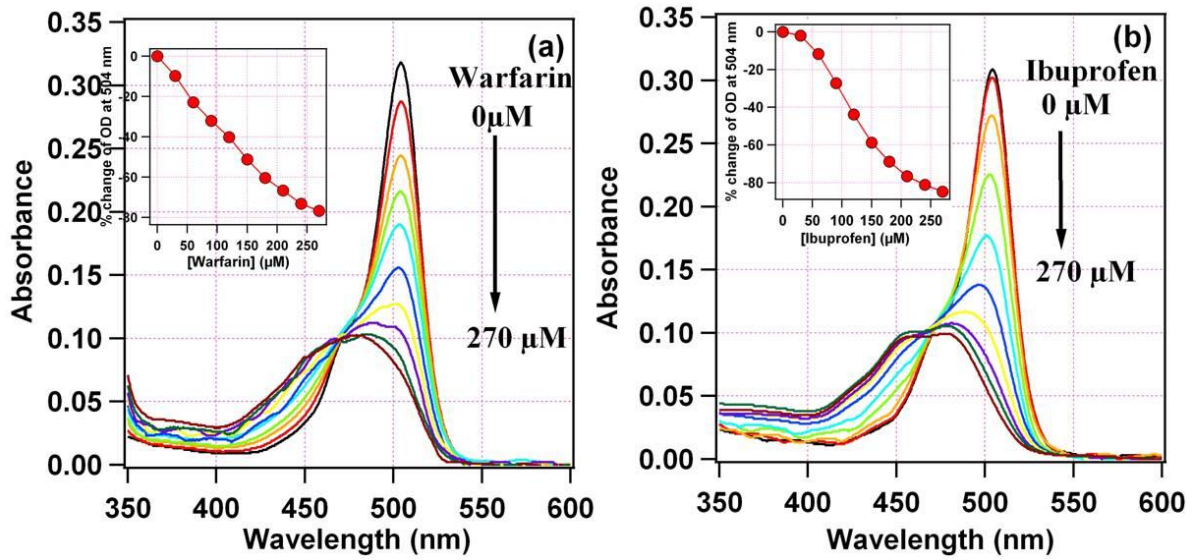

Figure 3.8. Absorption spectra of 2 µM fluorescein+30 µM BSA with (a) warfarin and (b) ibuprofen concentration varying from 0 to 270 µM. Inset: % Change of OD (at 504 nm) with respctive drug concentration.

reveals that denaturation is almost completed at 2.5 M urea concentration which is not possible if FL binds to the specific binding sites, either IIA or IIIA. We have also explored the FL binding site by molecular docking method. The docking study indicate that FL binds several places on the surface of the protein. It was also observed that it mostly binds at the surface of domain IIA. The similar change in absorption spectra of FL-BSA complex in the site marker experiment can also be explained for FL binds to the surface of BSA. Our experimental as well as docking results suggests that the binding of FL to BSA is a non-specific in nature.

3.3.2.3. Urea Induced Denaturation of FL-BSA Complex

Denaturation of FL bound BSA was studied by measuring absorption spectra of a sample having fixed concentration of BSA (30 µM) and FL (2 µM) with increasing concentration of urea. From figure 3.9a, it can be seen that on addition of urea the absorption maximum shifts to blue with decrease in absorbance. Decrease of absorbance with increasing concentration of urea indicates weakening of FL-BSA binding because of denaturation. Figure 3.9b shows how absorbance at 504 nm changes with increasing concentration of urea. The data was

fitted with equation 3.9 and the free energy of unfolding (ΔG_0) is found to be 2.9 kcal mol^{-1}. The mid-point of denaturation was observed at 1.5 M urea. This result indicates that a small amount of urea can denature the FL binding site of BSA. Easy denaturation of FL-BSA with urea as well as the non-specific binding nature of FL in BSA suggests that FL binds at the surface of BSA.

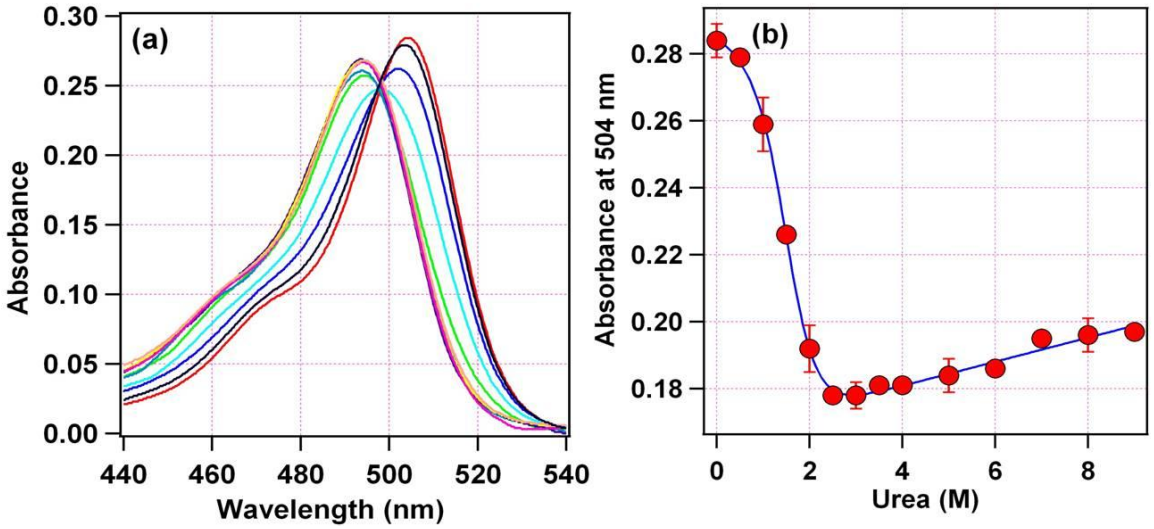

Figure 3.9. (a) Absorption spectra of 2 μM fluorescein + 30 μM BSA with urea conc varying from 0 to 9 M (b) Plot of absorbance (at 504 nm) vs urea concentration. Solid blue line is the best fit of the data with equation 3.9.

3.3.2.4. Binding Kinetics

To study the kinetics of binding between FL and BSA, both solution in equal volume was rapidly mixed by stopped-flow technique and the absorbance at 504 nm was monitored as a function of time. The averaged data of such 10 experiments is shown in figure 3.10. On fitting these data using equation 3.11, we estimate the rate constant (k) as 5.9 sec^{-1}.

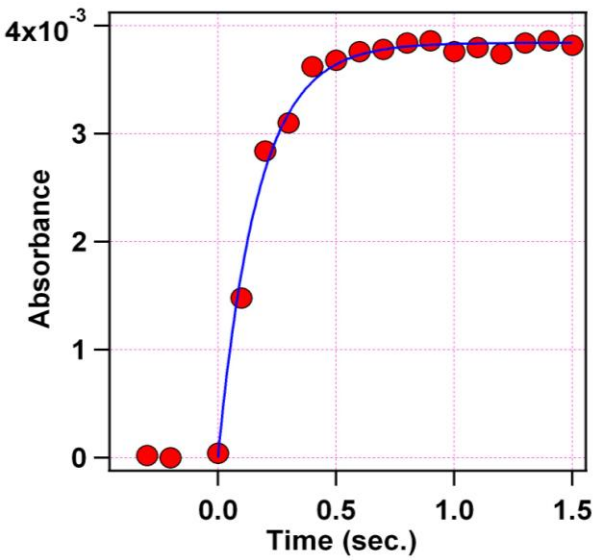

Figure 3.10. Plot of absorbance of 2 μM fluorescein + 30 μM BSA against time(sec) at the time of mixing.

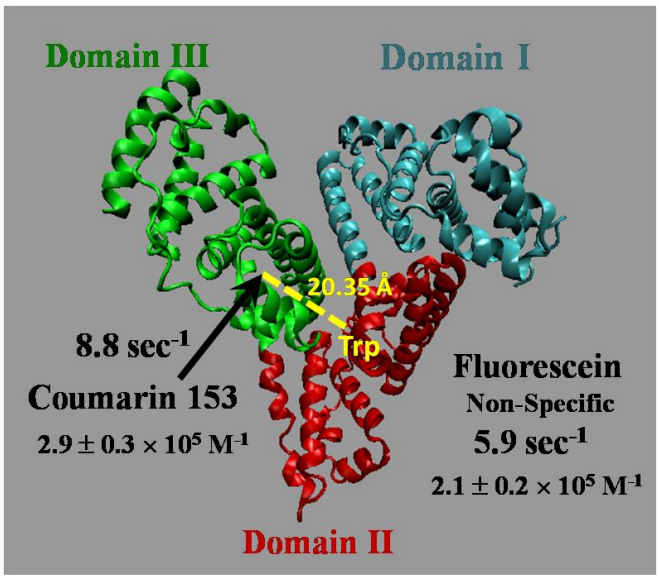

Scheme 3.2. Schematic represantation of binding parameters of coumarin 153 and fluorescein with BSA.

Table 3.1: Results of static and dynamic aspects of supramolecular interaction of coumarin 153 and fluorescein with bovine serum albumin at 27ºC.

	Binding Stoichio-metry	**Binding Constant $\times 10^5$ (M^{-1})**	**Binding Site**	**Denaturation Study**		**Rate Constant (sec^{-1})**
				ΔG_0 (kcal mol^{-1})	**$[D]_{1/2}$ (M)**	
BSA	-	-	-	2.0 ± 0.1	4.9	
C153-BSA	1:1	2.9 ± 0.3	Sub-domain IIIA	2.2 ± 0.4	3.6	8.8 ± 0.2
Fl-BSA	1:1	2.1 ± 0.2	Non-specific binbing	2.9 ± 0.4	1.5	5.9 ± 0.3

$[D]_{1/2}$ = Denaturant concentration for 50% unfolding of the protein.

ΔG_0 = Free energy change for unfolding of protein in absence of denaturant.

3.4. Conclusion

In the present work, the binding phenomenon of two fluorescent organic dye molecules namely, coumarin 153 (C153) and fluorescein (FL) with bovine serum albumin (BSA) was studied using spectroscopic techniques. The spectral characteristics of both C153 and FL is remarkably modified upon binding with BSA. All the results are sumarised in table 3.1 and scheme 3.2. Binding stoichiometry and binding constant for both the probe with BSA has been determined using steady-state absorption or emission studies. It has been found that both C153 and FL form 1:1 complex with BSA and the observed value of binding constants are 2.9±0.3 x 10^5 M^{-1} and 2.1±0.2 x 10^5 M^{-1}, respectively. Site marker competitive experiment, steady-state FRET and molecular docking study reveal that C153 binds to domain IIIA of BSA whereas FL binds at the surface of the protein. Urea induced denaturation study were done to understand the conformational stability of different sites of BSA compared to its global structure. The free energy of unfolding at zero denaturant concentration (ΔG_0) of global BSA is found to be 2 kcal mol^{-1} whereas for IIIA it is 2.2 kcal mol^{-1}. For non-specific FL-BSA complex, the free energy of unfolding at zero denaturant concentration (ΔG_0) is found to be 2.9 kcal mol^{-1}. The rate constants for binding of C153 and FL to BSA was estimated to be 8.8 sec^{-1} and 5.9 sec^{-1}, respectively by using stopped-flow technique. Overall, this work provides valuable information for binding of two important organic dye molecules and help to monitor the protein-probe binding more closely.

References

1. Kamat, B. P.; Seetharamappa, J. *Polish J. Chem.* **2004**, *78*, 723.
2. Cajlakovic, M.; Bizzarri, A.; Ribitsch, V. *Anal. Chim. Acta.* **2006**, *573-574*, 57.
3. Cheng, Z.; Levi, J.; Xiong, Z.,; Gheysens, O.; Keren, S.; Chen, X.; Gambhir, S. S. *Bioconjugate chem.* **2006**, *17*, 662.
4. Hameed, B. H.; El-Khaiary, M. I. *J. Hazard. Mater.* **2008**, *153*, 701.
5. Shreve, R. N.; Swaney, M. W; Riechers, E. H. *J. Am. Chem. Soc.* **1943**, *65*, 2241.
6. Rang, H. P.; Dale, M. M.; Ritter, J. *Mol. Pharmacol.* third ed, New York: Academic Press, **1995**.
7. Yamasaki, K.; Maruyama, T.; Kragh-Hansen, U.; Otagiri, M. *Biochim. Biophys. Acta* **1996**, *1295*, 147.
8. Flarakos, J.; Morand, K. L.; Vouros, P. *Anal. Chem.* **2005**, *77*, 1345.
9. Hushcha, T. O.; Luik, A. I.; Naboka, Y. N. *Talanta* **2000**, *53*, 29.
10. Kamat, B. P.; Seetharamappa J.; *J. Pharm. Biomed. Anal.* **2004**, *35*, 655.
11. (a) Zhang Y.; Zhou, B.; Zhang, X.; Huang, P.; Li, C.; Liu, Y. *J. Hazard. Mater.* **2009**, *163*, 1345.

    (b) Hu, Y.; Ou-Yang, Y.; Dai, C.; Liu Y.; Xiao, X. *Biomacromolecules* **2010**, *11*, 106.

    (c) Hu, Y.; Liu, Y.; Xiao, X. *Biomacromolecules* **2009**, *10*, 517.

    (d) Hu, Y.; Liu, Y.; Shen, X.; Fang, X.; Qu, S. *J. Mol. Struct.* **2005**, *738*, 143.
12. Deepa, S.; Mishra, A. K. *J. Pharm. Biomed. Anal.* **2005**, *38*, 556.
13. Shaikh, S. M. T.; Seetharamappa, J.; Kandagal, P. B.; Manjunatha, D. H.; Ashoka, S. *Dyes Pig.* **2007**, *74*, 665.
14. Akbay, N.; Topkaya, D.; Ergün, Y.; Alp, S.; Gök, E. *J. Anal. Chem.* **2010**, *65*, 382.
15. Stockwell, B. R. *Nature* **2004**, *432*, 846.
16. Vekshin, N. L. *J. Applied Spectroscopy* **1998**, *65*, 304.

17. Kalkhambkar, R. G.; Kulkarni, G. M.; Kamanavalli, C. M.; Premkumar, N.; Asdaq, S. M. B.; Sun, C. M. *Eur. J. Med. Chem.* **2008**, *43*, 2178.
18. Wu, L.; Wang, X.; Xu, W.; Farzaneh, F.; Xu, R.; *Curr. Med. Chem.* **2009**, *16*, 4236.
19. Basanagouda, M.; Shivashankar, K.; Kulkarni, M. V.; Rasal, V. P.; Patel, H.; Mutha, S. S.; Mohite, A. A. *Eur. J. Med. Chem.* **2010**, *45*, 1151.
20. Kulkarni, M. V.; Kulkarni, G. M.; Lin, C. H.; Sun, C. M. *Curr. Med. Chem.* **2006**, *13*, 2795.
21. Fylaktakidou, K. C.; Hadjipavlou-Litina, D. J.; Litinas, K. E.; Nicolaides, D. N. *Curr. Pharmaceu. Design* **2004**, *10*, 3813.
22. Borges, F.; Roleira, F.; Milhazes, N.; Santana, L.; Uriarte, E. *Curr.Med. Chem.* **2005**, *12*, 887-916.
23. Riveiro, M. E.; De Kimpe, N.; Moglioni, A.; Vazquez, R.; Monczor, F.; Shayo, C.; Davio, C. *Curr. Med. Chem.* **2010**, *17*, 1325.
24. Cohen, I. J. *J. Occup. And Env. Medicine* **1963**, *5*, 540.
25. Kragh-Hansen, U. *Pharm. Rev.* **1981,** *33*, 17.
26. Peters, T. *Adv. Prot. Chem.* **1985**, *37*, 161.
27. Klajnert, B.; Stanislawska, L.; Bryszewska, M.; Palecz, B. *Biochim. Biophys. Acta* **2003**, *1648*, 115.
28. Peters, T. J. *All About Albumin, Biochemistry, Genetic and Medical applications*, Academic Press, San Diago, **1996**.
29. He, X. M.; Carter, D. C. *Nature* **1992**, *358*, 209.
30. Bos, O. J.; Labro, J. F.; Fischer, M. J.; Witling, J.; Janssen, L. H. *J. Biol. Chem.* **1989**, *264*, 953.
31. Sudlow, G.; Birkett, D. J.; Wade, D. N. *Mol. Pharmacol.* **1976**, *12*, 1052.
32. Kragh-Hansen, U.; Chuang, V. T. G.; Otagiri, M. *Biol. Pharm. Bull.* **2002,** *25*, 695.
33. Kosa, T.; Maruyama. T.; Otagiri, M. *Pharm. Res.* **1997**, *14*, 1607.
34. Huang, C. Y. *Methods in Enzymol.* **1982**, *87*, 509.

35. Shobini, J.; Mishra, A. K.; Sandhya, K.; Chandra, N. *Spectrochim. Acta A* **2001**, *57*, 1133.
36. Kitamura, N.; Fukagawa, T.; Kohtani, S.; Kitoh, S.; Kunimoto, K.; Nakagaki, R. *J. Photochem. Photobiol. A: Chem.* **2007**, *188*, 378.
37. Mota, M. C.; Carvalho, P.; Ramalho, J.; Leite, E. *Int. Ophth.* **1991**, *15*, 321.
38. Seth, D.; Chakrabarty, D.; Chakraborty, A.; Sarkar, N. *Chem. Phys. Letter* **2005**, *401*, 546.
39. Jones II, G.; Jackson, W. R.; Choi, C.; Bergmark, W. R. *J. Phys. Chem.* **1985**, *89*, 296.
40. Lakowicz, J. R. Principles of Fluorescence Spectroscopy, third ed., Springer, New York.
41. Santoro, M. M.; Bolen, D. W. *Biochemistry* **1988**, *27*, 8063.
42. Street, T. O.; Courtemanche, N.; Barrick, D.; *Methods Cell Biol.* **2008**, *84*, 295.
43. (a) Bhattacharya, B.; Nakka, S.; Guruprasad, L.; Samanta, A. *J. Phys. Chem. B* **2009**, *113*, 2143.
    (b) Hazra, P.; Chakrabarty, D.; Chakraborty, A.; Sarkar N. *Biochem. Biophys. Res. Comm*. **2004**, *314*, 543.
    (c) Kumar, C. V.; Duff, M. R.; Jr., *Photochem. Photobiol. Sci*. **2008**, *7*, 1522.
44. Jones II, G.; Jackson, W. R. *Chem. Phys. Lett.* **1980**, *72*, 391.
45. Paul, B. K.; Samanta, A.; Guchait, N. *J. Phys. Chem. B* **2010**, *114*, 6183.
46. Chakrabarty, A.; Mallick, A.; Haldar, B.; Das, P.; Chattopadhyay, N. *Biomacromolecules* **2007**, *8*, 920.
47. Ahmed, B.; Parveen, S.; Khan, R. H. *Biomacromolecules* **2006**, *7*, 1350.
48. Sulkowska, A.; Rownicka, J.; Bojko, B.; Pozycka, J.; Zubik-skupien, I.; Sulkowski, W. *J. Mol. Struct.* **2004**, *704*, 291.
49. Mchedlov-Petrossyan, N. O.; Kleshchevnikova, V. N. *J. Chem. Soc. Faraday Trans.* **1994,** *90*, 629.
50. Göktürk, S. *J. Photochem. Photobiol. A: Chem.* **2005**, *169*, 115.

Chapter 3(b)

Temperature Dependent Binding Modes of Coumarin 152 with Human Serum Albumin

Rajeev Yadav *et al*., Manuscript under preparation

Present study describes the effect of temperature on binding parameters as well as mode of binding between coumarin 152 (C152) and human serum albumin (HSA). Site marker competitive experiment, Förster resonance energy transfer (FRET) and molecular docking study shows that C152 binds to the digitoxin binding site in domain III of HSA. Further, FRET and molecular dynamics simulations confirm that the binding location of C152 is independent of temperature (278 K to 323 K). It has been revealed that the binding affinity of C152 to HSA was almost unaffected until 298 K, afterward it decreases continuously on increasing temperature forming two distinct regions. Thermodynamic parameters for association indicate that strong electrostatic and hydrophobic interactions are operational at lower temperature region, whereas hydrogen bonding predominates at higher temperate region.

3.5. Introduction

Human serum albumin (HSA) is one of the most studied protein in the literature and is responsible for the transportation of a wide varieties of metabolites and drugs in our body.[1-7] The mechanistic study of the binding characteristics for a number of drugs and other ligands to HSA has been a major attention among several researchers in the last few decades.[3-7] The binding characteristics of a variety of coumarin derivatives with HSA was also studied because of their anti-cancer, anti-fungicidal, anti-tumor, and analgesics activities.[8] Coumarin dyes are also important for its high fluorescence quantum yield and can be used as marker in bio-imaging. Among all the coumarins, amino-coumarins are widely used as fluorescent dyes to monitor the change in microenvironment.[9]

In general, it has been revealed that the binding forces behind the protein-ligand interactions mainly involve the formation of hydrogen bonds, hydrophobic interactions, van der Waals forces, electrostatic forces, etc. and were characterized by the thermodynamic parameters of the binding process.[10] Mishra and co-workers have studied the temperature dependent interaction of coumarin 35 with HSA from 298 K to 323 K and found that the hydrophobic interaction is predominant in the complexation process.[9d] In another work, Seetharamappa and co-workers have studied the interaction of gemcitabine hydrochloride with bovine serum albumin (BSA) and HSA and showed that hydrogen bonding and hydrophobic interactions play a crucial role in the binding process.[12a] Zeng and co-workers have studied the interaction of 1-phenyl-3-(Coumarin-6-yl)-sulfonylurea with BSA and showed that hydrogen bonding and van der Waals forces play an important role in the formation of the complex,[11a] whereas Liu and co-workers revealed the existence of electrostatic interaction in the binding of berberine to HSA.[3b] In another article, they have showed that binding of the malachite green with BSA is driven by van der Waals forces and hydrogen bond formation.[3c] Recently, Mukherjee and co-workers have studied the interaction of tetracycline hydrochloride with three different proteins, HSA, BSA and Lysozyme (LYS) from 298 K to 308 K and

found that hydrophobic interactions are predominant in case of HSA and BSA, whereas both electrostatic as well as hydrophobic interactions are equally present in case of LYS.[12b] Later they have studied the pH dependent interaction of ciprofloxacin hydrochloride with BSA and showed that hydrophobic and van der Waal forces play an important role in the binding process.[12c] Zhang and co-workers have showed that hydrophobic interactions are predominant in binding of puerarin with HSA for a temperature range from 298 K to 310 K.[12d] Recently, Yi and co-workers have studied the interaction of porphyrins-4-hydroxycoumarins with BSA under the physiological conditions and showed that electrostatic forces are responsible for the complexation in the temperature range from 298 K to 310 K.[11b] Understandably, the nature of interaction for complexation differs case to case and also depends on the temperature of the system.[10-11]

Binding of coumarin 152 (C152) with serum albumin has also been studied quite rigorously in the past.[9d-f] Al-Soufi and co-workers have estimated the binding constant for C152 to BSA to be 0.23×10^5 M^{-1}.[9e] However, Samanta and co-workers have showed that the binding constant is about 1×10^5 M^{-1} and also determined that C152 binds to the domain IIA of BSA through molecular docking study.[9f] Mishra and co-workers have also showed the same binding site for C152 inside HSA using molecular docking study.[9d] However, they have reported a very high binding constant of 28×10^5 M^{-1} for the binding. This is clear that the measured value of binding constant between C152 and serum albumin differs a lot and is may be because of the strong temperature effect in the binding process. Clearly, a wide temperature variation will provide a better understanding about the temperature dependent interaction present in the systems. It is also worth to emphasize that in all the previous studies the binding location of C152 was estimated only by the molecular docking study. In the present study, we have used spectroscopic techniques, such as steady-state absorption and emission, Förster resonance energy transfer (FRET), site-marker competitive experiment and theoretical methods, such as molecular docking study and MD simulation, to

estimate the binding constant and binding site of C152 (scheme 3.3) with HSA for a wide temperature range from 278 K to 323 K. The temperature dependent study also helped us to vividly understand the nature of interactions in the binding process.

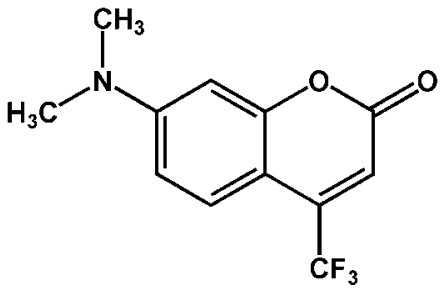

Scheme 3.3. Molecular structure of coumarin 152.

3.6. Data Analysis

All experiments have been done in 0.1 M sodium phosphate buffer (pH 7.4). The concentration of HSA was determined from its molecular weight of 66478 and for C152 concentration was determined from its molar extinction coefficient (ε_{403nm} = 20,401 M^{-1} cm^{-1}).[13a] Coumarin 480 in methanol (ϕ_f = 0.66) has been used as a standard for the fluorescence quantum yield measurement.[13b]

The data obtained from circular dichroism (CD) experiments were expressed as the percentage of α-helicity of HSA which is defined as.[14]

$$\%\alpha - helicity = \frac{MRE_{208nm} - 4000}{33000 - 4000} \times 100 \qquad (3.12)$$

where MRE_{208nm} is the mean residue elipticity at 208 nm in deg cm^2 $dmol^{-1}$, which is defined as

$$MRE = \frac{\theta \times M}{ncl} \qquad (3.13)$$

where θ is CD signal in mille degree, M is the molecular weight of HSA in gm $dmol^{-1}$, n is the number of amino acid residue, l is the path length of the quartz cell in cm and c is the concentration of the protein in gm lit^{-1}.

3.7. Results and Discussions

3.7.1. Circular Dichroism Spectra of HSA

In order to decipher the temperature dependent changes in the secondary structure of HSA, we have recorded the circular dichroism (CD) spectra of HSA in 0.1 M phosphate buffer (pH = 7.4) at different temperatures.[14] Figure 3.11a shows the CD spectra of HSA for different temperatures ranging from 278 K to 323 K. The two characteristic minima at 208 nm and 222 nm represent the α-helical nature of HSA.[14] Using equations 3.12 and 3.13, we have calculated % α-helicity of HSA at different temperatures and is found to be almost constant (~64 %) between 278 K and 288 K (Figure 3.11b and Table 3.2). On further increasing the temperature, α-helicity of HSA decreases slowly and becomes 58% at 323 K. The results indicate that there is mere changes in the secondary structure of HSA till 288 K and at higher temperature region, a very small deformation occurs.

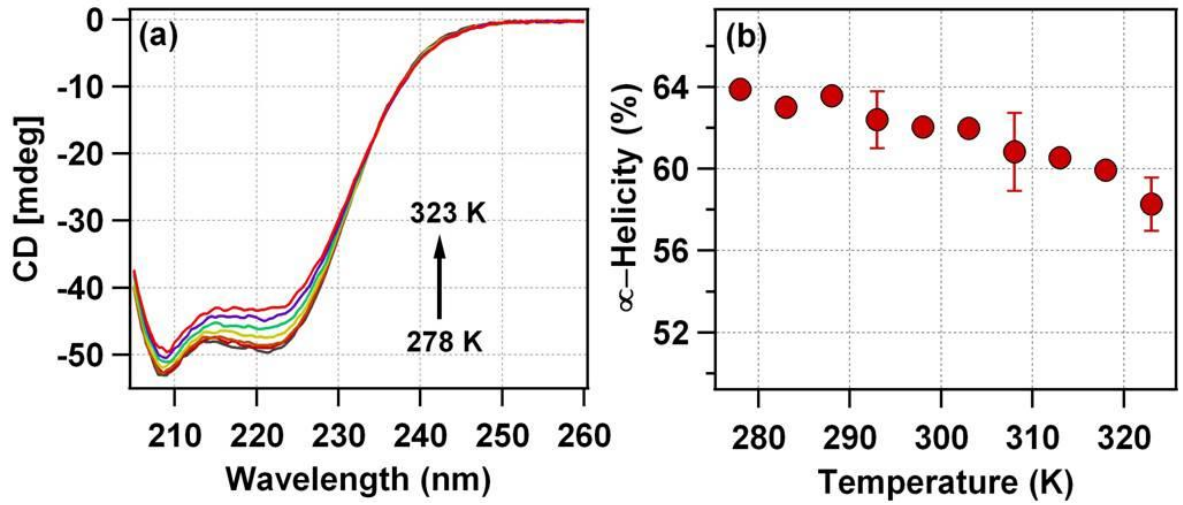

Figure 3.11. (a) Circular dichroism spectra of 5 μM HSA in pH 7.4 phosphate buffer from 273 K to 323 K. (b) Change of % α- helicity of HSA with temperature.

3.7.2. Binding Study of C152 with HSA

Interaction of C152 with serum albumin has already been studied at room temperature through its characteristic fluorescence enhancement upon binding.[9d-f] C152 has two excited singlet states namely, intra-molecular charge transfer (ICT)

and twisted intra-molecular charge transfer (TICT) states. ICT state is highly fluorescent whereas TICT state is non-fluorescent in nature.[15a] The formation of TICT state occurs via the twisting of the $–N(CH_3)_2$ group and consequently a complete charge transfer takes place in the system. Inside the confined protein environment, the formation of the TICT state gets hindered through the restrictions in the torsional motion of $–N(CH_3)_2$ group, and is the reason for the fluorescence enhancement.[9d,f]

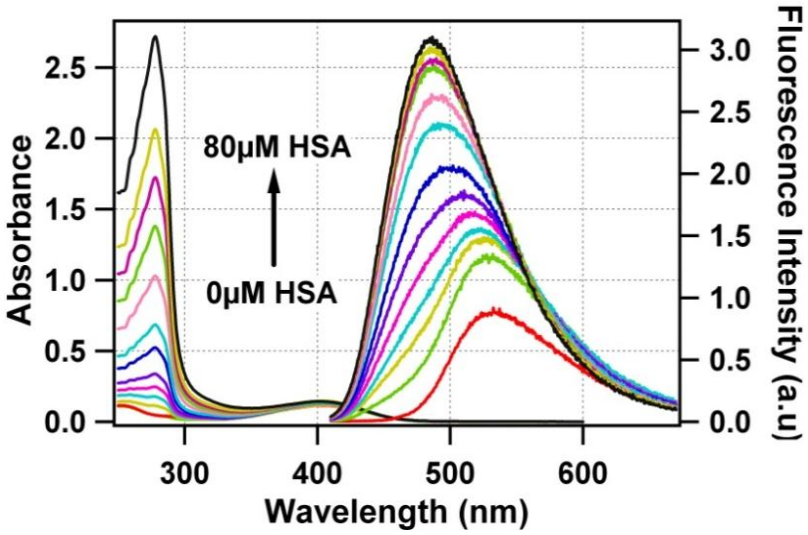

Figure 3.12. Steady state absorption (left axis) and emission (right axis) spectra of C152 (5μM) with increasing concentration of HSA at 298 K in pH 7.4 phosphate buffer.

We also have used the fluorescence enhancement method to study the binding process between C152 and HSA at a wide temperature range from 278 K to 323 K. The absorption and emission spectra of C152 in buffer solution are characterized by their maxima at 404 nm and 532 nm (λ_{ex} = 400 nm), respectively. The absorption maximum of C152 remains unchanged on addition of HSA whereas a blue shift of emission maximum was observed with a concomitant increase in the intensity (Figure 3.12). The blue shift of the emission spectra and the enhancement in fluorescence quantum yield is a clear indication of the binding process. Job's method was employed to calculate the binding stoichiometry by fixing the total concentration as 5 μM with varying concentration of HSA and

C152.[9d,15b] Figure 3.13 shows the change in fluorescence intensity at 450 nm with mole fraction of HSA at 293 K and 313 K. For both the temperatures, the maximum fluorescence intensity was observed for 0.5 mole fraction of HSA. This clearly indicates that C152 forms a 1:1 complex with HSA in the studied temperature region.

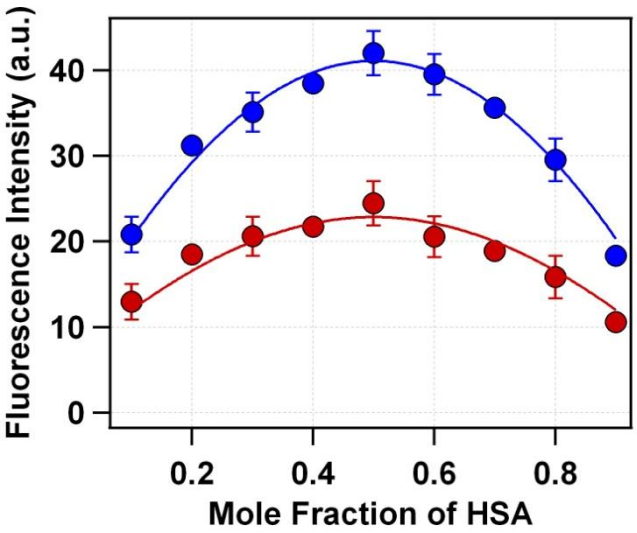

Figure 3.13. Job's plot for the complexation of C152 with HSA. Blue and red filled circles denote the observed fluorescence intensity of C152-HSA complex at 450 nm for 293 K and 313 K, respectively.

The fluorescence enhancement of C152 upon binding with HSA was used to calculate the binding constant of the process. At 278 K, the fluorescence quantum yield of C152 in 0.1 M sodium phosphate buffer (pH 7.4) is found to be 0.045, which monotonically increases on addition of HSA in the system and for 60 μM HSA the fluorescence quantum yield of C152 is found to be 0.15. Fluorescence lifetime of C152 also increased in this process. At 278 K, the average lifetime of C152 in 0.1 M sodium phosphate buffer (pH 7.4) is 0.75 ns, which increases to 5.1 ns on addition of 60 μM HSA. The fluorescence quantum yield and lifetime of C152 and its reliance on binding process is also found to depend on the temperature. At 323 K the fluorescence quantum yield and lifetime of C152 in 0.1 M sodium phosphate buffer (pH 7.4) are found to be 0.018 and 0.36 ns, which increase to 0.069 and 3.9 ns on addition of 60 μM HSA, respectively.

Figure 3.14 shows the dependence of fluorescence quantum yield of 5 μM C152 in buffer as a function of HSA concentration for 10 different temperatures ranging from 278 K to 323 K with an interval of 5 K. A least-square fitting of the data using equation 3.2 gives the binding constants between C152 and HSA. At 278 K the binding constant is found to be 1.47×10^5 M^{-1} which almost remain

constant till 298 K and decrease monotonously on further increase of the temperature. At 323 K the measured binding constant value is 0.79×10^5 M^{-1}. Figure 3.15a shows a plot of observed binding constants between C152 and HSA as a function of temperature and all the data are tabulated in table 3.2.

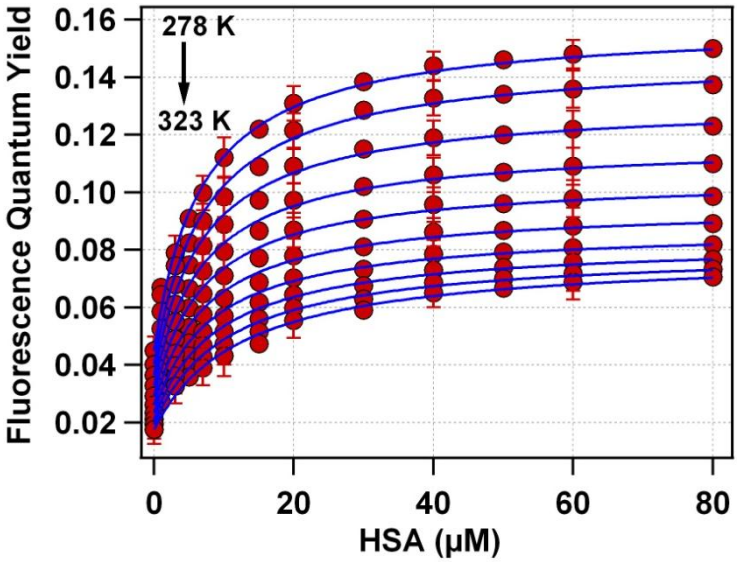

Figure 3.14. Plot of observed fluorescence quantum yield (red solid circles) with error bars against HSA concentration at different temperatures varying from 298 K to 323 K with an interval of 5 K and solid blue line is the best fit with equation 3.2.

To better understand the binding nature of C152 to HSA, thermodynamic parameters were estimated. The main thermodynamic parameters that play an important role for such interactions are free energy (ΔG°), entropy (ΔS°) and enthalpy (ΔH°) of binding and can be estimated by

$$\Delta G^0_{Binding} = -2.303RT \log K_b \qquad (3.14)$$

$$\Delta G^0_{Binding} = \Delta H^0 - T\Delta S^0 \qquad (3.15)$$

Where R is universal gas constant and K_b is the binding constant at each temperature. Free energy of binding (ΔG°) has been calculated by using equation 3.14 for different temperatures and is shown in figure 3.15b. The negative values of ΔG° at all the temperatures indicate the spontaneous nature of binding of C152 to HSA. The variation of ΔG° with temperature involves two distinct regions,

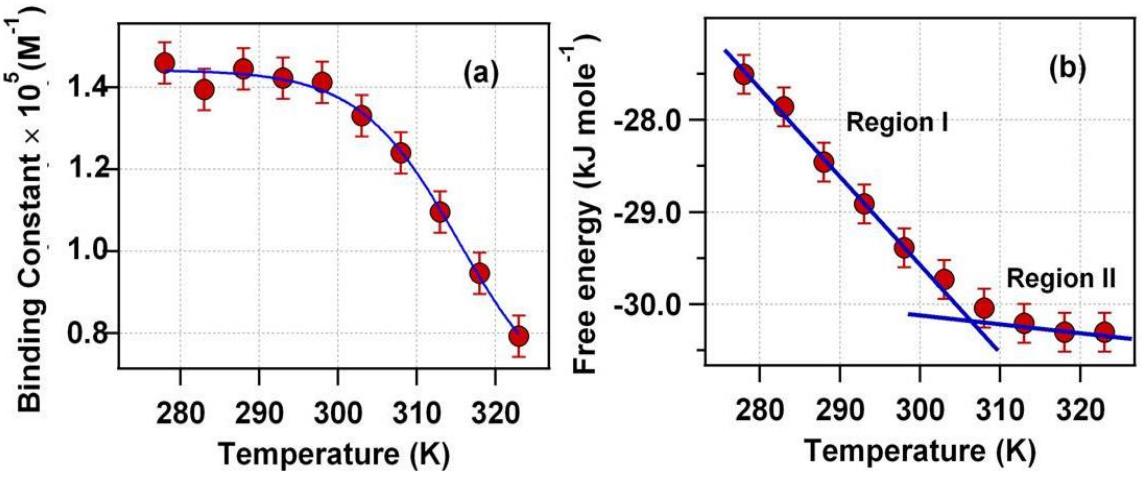

Figure 3.15. (a) Plot of binding constant for C152 with HSA as a function of temperature. Red filled circles are the experimentally observed binding constants and blue line is only the eye guide. (b) The change of free energy of binding of C152 to HSA as a function of temperature. Red filled circles are the calculated free energy of binding from binding constant by using equation 3.14 and blue lines are the fitted lines for both the regions with equation 3.15.

Table 3.2. α-Helicity of HSA, binding constant and thermodynamic parameter of binding for C152 to HSA, and distance between Trp and C152 bound to HSA at different temperatures.

Temperature (K)	**% α-Helicity**	**Binding Constant[A] × 10^5 (M^{-1})**	**Binding Free Energy[B] (kJ mol^{-1})**		**Trp-C152 bound to HSA distance (Å)**
278	63.9	1.47	-27.51	ΔH° = -0.49	20.9
283	63.0	1.38	-27.86	kJ mol^{-1}	21.3 ± 1.4
288	63.6	1.45	-28.46	ΔS° = 97	---
293	62.4 ± 1.4	1.42	-28.91	JK^{-1} mol^{-1}	21.4 ± 1.4
298	62.0	1.41	-29.39		---
303	61.9	1.33	-29.73		21.9
308	60.8 ± 1.9	1.24	-30.04	ΔH° = -27.2	22.8
313	60.5	1.10	-30.21	kJ mol^{-1}	---
318	59.9	0.95	-30.30	ΔS° = 9	21.1 ± 1.6
323	58.3 ± 1.3	0.79	-30.30	JK^{-1} mol^{-1}	20.1

[A] ± 0.05 × 10^5 , [B] ± 0.2

region I: from 278 K to 303 K and region II: from 308 K to 323 K, which is also shown in figure 3.15b. Further ΔS° and ΔH° has been calculated for these two regions, following equation 3.15, and all the thermodynamic parameters are summarized in table 3.2. This is to recall that a positive ΔH° and ΔS° values are

associated with hydrophobic association, whereas negative ΔH° and ΔS° values indicate predominant hydrogen bonding and van der Waals interaction in the binding process.[10] On the other hand, a positive ΔS° and very small (either positive or negative) ΔH° values are the characteristic of electrostatic interaction present in the system.[10] In the present case, the high positive value of ΔS° in the region I (278 K to 303 K) shows the interaction is entropically driven whereas for region II (308 K to 323 K) a high negative value of ΔH° indicating the binding is enthalpically driven. Based on the above result we propose that at lower temperature region the hydrophobic and electrostatic interactions dominate in the binding process and at higher temperature region hydrogen bonding interaction plays a crucial role.

Molecular Dynamics Simulations. To better understand the temperature dependent binding mechanism, atomistic molecular dynamics (MD) simulations at 293 K and 313 K have also been performed for aqueous solution of HSA complexed with C152 under the periodic boundary condition using Amber 9 for 2 ns.[16] The initial coordinate of HSA was obtained from the Protein Data Bank (1HA2)[17a] and for colligation of C152 to HSA, molecular docking study was performed using Autodock Tools 4.2.[17b] 20287 TIP3P water molecules[15c] were used to solvate whole system and 14 Na^+ ions were added for the neutralization. AMBER 9 and general AMBER force field (GAFF) were used to model the protein and C152 respectively.[16a-d,18a] Further procedure is same as given in chapter 2. After completion of 2 ns equilibration, MM-PBSA approach from Amber Tools 12 was used to estimate the biding free energy of C152 to HSA.[18b]

The results obtained from MD simulations are tabulated in table 3.3. At 293 K the value of binding free energy and electrostatic energy were observed as -181.1 kJ mol^{-1} and -23.6 kJ mol^{-1} respectively, that become -188.3 kJ mol^{-1} and -20.1 kJ mol^{-1} at 313 K. The average number of hydrogen bonds between C152 and HSA were found to be 1.25 and 1.30 at 293 K and 313 K respectively. The more negative value of binding free energy indicates that the binding process is more spontaneous at higher temperature which is in agreement with our experimental

results. It is to be noted that the value of binding free energy we got from MD simulations does not match with the experimental binding free energy because entropy contribution is not used in this calculation.[18b] The value of electrostatic interaction and average number of hydrogen bonds indicate that at lower temperature the electrostatic contribution is high whereas at higher temperature hydrogen bonding dominates in the binding process.

This is to emphasize that all the above discussions are valid only if the location of C152 is fixed in the huge HSA matrix over the temperature range under consideration. Consequently, we have determined the binding site of C152 in HSA at different temperatures as presented in the following section.

Table 3.3. Molecular dynamics simulation results for interaction of C152 with HSA at two different temperatures.

Tempera-ture (K)	Binding Free Energy (kJ mol^{-1})	Electrostatic energy (from MM force field) (kJ mol^{-1})	Average No. of H- Bonds Between C152-HSA	Distance between pairs within HSA (Å)		
				Trp214 – C152	Cys34-C152	Cys34-Trp214
293	-181.1	-23.6	1.25	20.52	40.32	35.7
313	-188.3	-20.1	1.30	21.67	40.12	35.6

3.7.3. Binding Site of C152 in HSA

In order to identify the binding site, the site marker competitive experiment and molecular docking study have been performed. The degree of change in the tryptophan fluorescence intensity of a drug-HSA complex with a varying concentration of C152 in the system has been used to determine the binding location of C152 in the site marker competitive experiment.[9c] We have chosen three drugs namely warfarin, ibuprofen and digitoxin as site markers, which specifically bind to three different binding sites, site I, II and III, respectively with similar binding constants.[1b,2a,7] Figure 3.16 (a,b,c) shows the fluorescence spectra of 30 μM HSA in absence and presence of 60 μM of these drugs and its

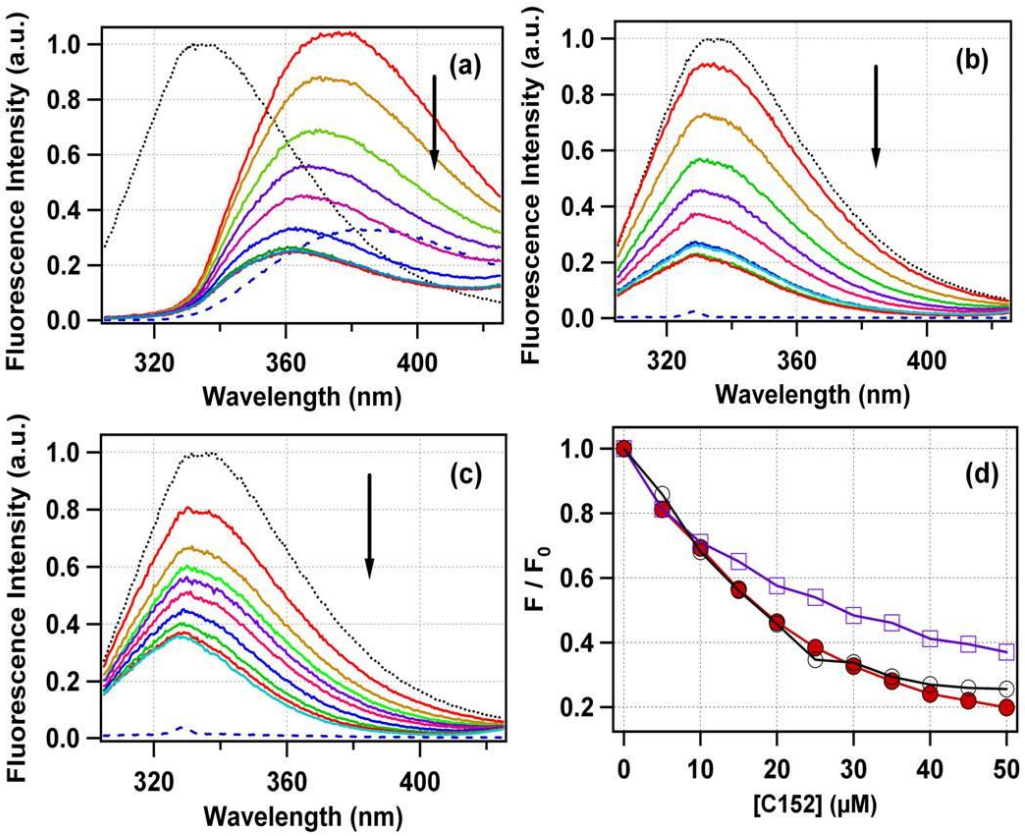

Figure 3.16. Fluorescence emission spectra of 30 μM HSA in pH 7.4 phosphate buffer in absence (……) and presence of 60 μM drug (- - - -) (a) warfarin (b) ibuprofen (c) digitoxin. The arrows show the decrease in fluorescence intensity of HSA with increasing concentration of C152 till 50 μM. (d) The change in emission intensity of HSA with C152 concentration in presence of warfarin (solid red circle), ibuprofen (blank circle) and digitoxin (blank squares).

dependence on addition of C152 at 298 K. In the presence of warfarin, the emission maximum is shifted towards lower energy region with a small increase in fluorescence intensity (figure 3.16a). However the presence of ibuprofen and digitoxin in HSA has a mere effect on its fluorescence properties as shown in figures 3.16b and 3.16c. In all three cases, the fluorescence intensity is found to decrease on addition of C152 in the system and the relative changes are shown in figure 3.16d. When ibuprofen and warfarin are present, the fluorescence intensity of HSA decreased to 20 % of its initial value on addition of 50 μM of C152. However in case of digitoxin, we noticed that the initial intensity decreased only to 40% in presence of 50 μM C152. This modest decrease of initial fluorescence in case of digitoxin indicates that C152 preferentially binds to the digitoxin binding

site which is present in domain IIIA of HSA. In two previous reports, Shobini *et al.*[9d] and Bhattacharya *et al.*[9f] have indicated that C152 binds to domain II A of serum albumin from their molecular docking study. However our experimental results suggest that C152 binds to domain IIIA. To clarify this we also have performed molecular docking study to probe the location of C152 in HSA and observed that the lowest energy conformer is one where C152 binds to the domain IIA of HSA. However the next 5 conformers of almost similar energy have C152 in domain IIIA. Thus molecular docking study also suggests that the most probable binding site of C152 in HSA is domain IIIA, which is in accordance with our experimental results.

Förster resonance energy transfer (FRET) experiment was further employed to confirm the binding site of C152 inside HSA by measuring the distance of C152 from the single Trp residue present in HSA. Using equations 3.5 to 3.8,[19] the Förster distance for the Trp-C152 pair has been calculated from the spectral overlap as shown in figure 3.17a. The overlap integral, $J(\lambda)$, was found to be 1.82 $\times 10^{14}$ $M^{-1}cm^{-1}$ nm^4 and the Förster distance (R_0) has been calculated as 25.92 Å.

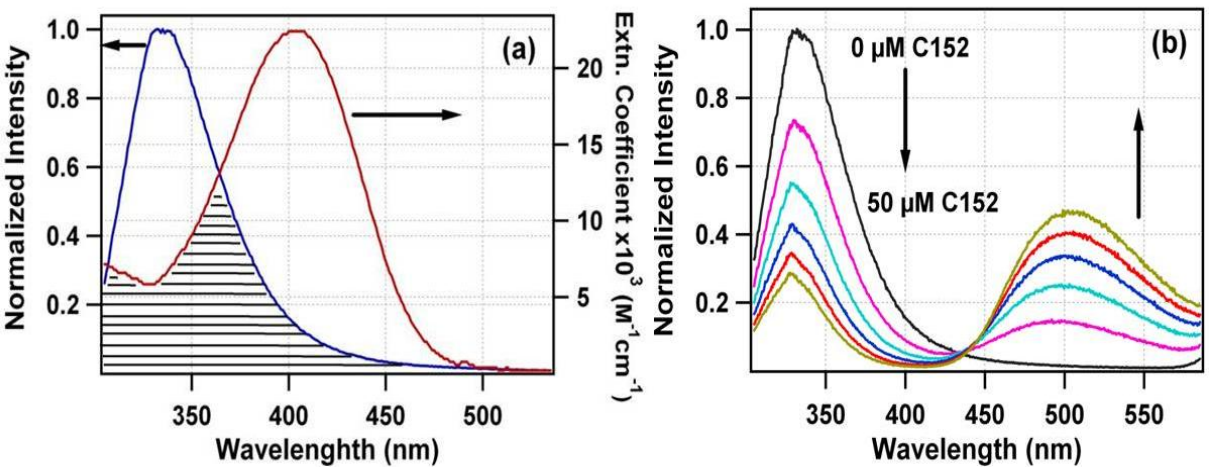

Figure 3.17. (a) Spectral overlap (shaded region) of normalized emission spectrum of donor (Trp of HSA) with absorption spectrum of C152. (b) Emission spectra of 30 µM HSA in pH 7.4 phosphate buffer in absence and presence different concentrations of C152 at 293 K. The arrows show the fall and rise in fluorescence intensity of HSA and C152 bound to HSA with increasing concentration of C152 respectively.

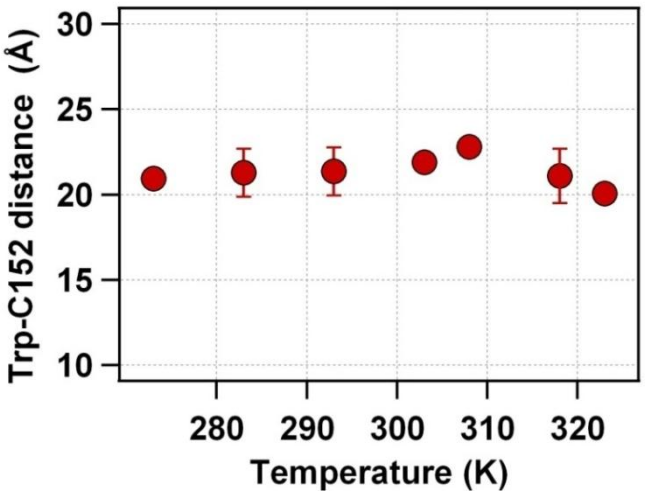

Figure 3.18. The variation of distance between Trp and C152 inside HSA as a function of temperature.

The decrease in the Trp fluorescence intensity on account of the energy transfer from Trp to C152 was monitored as a function of C152 concentration in the system and is shown in figure 3.17b. The FRET efficiency (ε) was estimated using the fluorescence intensity of donor in absence and presence of acceptor (C152 bound with HSA). For a total 81 % bound condition of C152 to HSA, we observed a FRET efficiency of 80 % at 293 K. From the known value of R_0 and estimated value of ε at 293 K, the distance between Trp and C152 in HSA was calculated to be 21.38 Å. The distance here we measured falls within the domain IIIA from the Trp residue, as evident from the crystal structure of HSA[15a] and thus confirms our observations that C152 binds to the domain IIIA of HSA.

To examine if there is any temperature dependence on the binding location of C152 in HSA, a temperature dependent steady state FRET experiment has been performed at seven different temperatures ranging from 278 K to 323 K. For each temperature the total bound C152 was maintained around 80 %. The measured distance is found to be almost independent on temperatures (see figure 3.18) signifying that the binding location of C152 inside HSA remain same over the temperature range under consideration. Further it was confirmed by MD simulation by measuring the Trp-C152, Cys34-C152 and Trp-Cys34 distance at two different temperatures (293 K and 313 K), which remain almost same as shown in table 3.3.

3.8. Conclusion

In the present work, the temperature dependent binding of coumarin 152 (C152) with human serum albumin (HSA) have been studied for a wide temperature range (from 278 K to 323 K) using spectroscopic techniques and the results were compared with computational studies. The spectroscopic results show that the binding affinity of C152 to HSA was almost unaffected until 298 K and decreases continuously on further increasing the temperature. Site marker competitive experiment, molecular docking study and Förster resonance energy transfer (FRET) experiment show that C152 binds to domain IIIA of HSA. The binding location of C152 is found to be independent on temperature (278 K to 323 K) through FRET experiment and molecular dynamics simulations. The calculated thermodynamic parameters show that at lower temperature the electrostatic and hydrophobic interactions predominate for association and at higher temperature hydrogen bonding interaction plays a crucial role in the binding process.

References:

1. (a) Peters, T. Jr. *All about albumin: Biochemistry, Genetics, and Medical Applications*, Academic press, San Diego, **1996**.
   (b) Kragh-Hansen, U.; Chuang, V. T. G.; Otagiri, M. *Biol. Pharm. Bull*. **2002**, *25*, 695.
   (c) Kosa, T.; Moruyama, T.; Otagiri, M. *Pharm. Res*. **1997**, *14*, 1607.
   (d) Hu, Y.; Ou-Yang, Y.; Dai, C.; Liu, Y.; Xiao, X. *Biomacromolecules* **2010**, *1110*, 6.
2. (a) He, X. M.; Carter, D. C. *Nature* **1992**, *358*, 209.
   (b) Curry, S.; Mandelkow, H.; Brick, P.; Franks, N. *Nature Struc. Biol*. **1998**, *5*, 827.
3. (a) Rang, H. P.; Dale, M. M.; Ritter, *J. Mol. Pharmacol.*, third ed., New York, Academic Press, **1995**.
   (b) Hu, Y.; Liu, Y.; Xiao, X. *Biomacromolecules* **2009**, *10*, 517.
   (c) Zhang, Y.; Zhou, B.; Zhang, X.; Huang, P.; Li, C.; Liu, Y. *J. Hazard Mater* **2009**, *163*, 1345.
4. (a) Hu, Y.; Liu, Y.; Shen, X.; Fang, X.; Qu, S. *J. Mol. Struct*. **2005**, *738*, 143.
   (b) Hushcha, T. O.; Luik, A. I.; Naboka, Y. N. *Talanta* **2000,** *53*, 29.
   (c) Kamat, B. P.; Seetharamappa, J.; *J. Pharm. Biomed. Anal*. **2004**, *35*, 655.
   (d) Deepa, S.; Mishra, A. K.; *J. Pharm. Biomed. Anal*. **2005**, *38*, 556.
   (e) Shaikh, S. M. T.; Seetharamappa, J.; Kandagal, P. B.; Manjunatha, D. H.; Ashoka, S. *Dyes Pigm*. **2007**, *74*, 665.
   (f) Akbay, N., Topkaya, D.; Ergün, Y.; Alp, S.; Gök, E. *J. Anal. Chem*. **2010**, *65*, 382.
   (g) Stockwell, B. R. *Nature* **2004**, *432*, 846.
5. (a) Dugiaczyk, A.; Law, S.; Dennison, O. E. *Proc. Natl. Acad. Sci. U.S.A.* **1982**, *79*, 71.
   (b) Carter, D. C.; Ho, J. X. *Adv. Prot. Chem*. **1994**, *45*,153.
6. (a) Sugio, S.; Kashima, A.; Mochizuki, S., Noda, M.; Kobayashi, K. *Prot. Eng*. **1999**, *12*, 439.

(b) Narazaki, R.; Maruyama, T.; Otagiri, M. *Biochim. Biophys. Acta.* **1997**, *1338*, 275.

7. (a) Sudlow, G.; Brikket, D. J.; Wade, D. N.; *Mol. Pharmacol*. **1975**, *11*, 824.

(b) Sjöholm, I.; Ekman, B.; Kober, A.; Ljungstedt-Pahlman, I.; Seiving, B.; Sjödin, T. *Mol. Pharmacol*. **1979**, *16*, 767.

8. (a) Kalkhambkar, R. G.; Kulkarni, G. M.; Kamanavalli, C. M.; Premkumar, N., Asdaq, S. M. B.; Sun, C. M. *Eur. J. Med. Chem.* **2008**, *43*, 2178.

(b) Wu. L.; Wang, X.; Xu, W.; Farzaneh, F.; Xu, R. *Curr. Med. Chem*. **2009,** *16*, 4236.

(c) Basanagouda, M.; Shivashankar, K.; Kulkarni, M. V.; Rasal, V. P.; Patel, H.; Mutha, S. S.; Mohite, A. A. *Eur. J. Med. Chem*. **2010**, *45*, 1151.

(d) Chinnakali, K.; Fun, H. K.; Sriraghavan, K.; Ramakrishnan, V. T. *Acta. Crystallogr*. **1998,** *C54*, 542.

(e) Fylaktakidou, K. C.; Hadjipavlou-Litina, D. J.; Litinas, K. E.; Nicolaides, D. N. *Curr. Pharm. Des.* **2004** , *10*, 3813.

(f) Borges, F.; Roleira, F.; Milhazes, N.; Santana, L.; Uriarte, E. *Curr. Med. Chem.* **2005**, *12*, 887.

(g) Riveiro, M. E.; De, Kimpe. N.; Moglioni, A.; Vazquez, R.; Monczor, F.; Shayo, C.; Davio, C. *Curr. Med. Chem.* **2010**, *17*, 1325.

9. (a) Bhattacharyya, K. *Acc. Chem. Res.* **2003**, *36*, 95.

(b) Das, K.; Jain. B.; Gupta, P. K. *Chem. Phys. Lett*. **2005**, *410*, 160.

(c) Yadav, R.; Das, S.; Sen, P. *Aust. J. Chem.* **2012**, *65*, 1305.

(d) Shobini, J.; Mishra, A. K.; Sandhya, K.; Chandra, N. *Spectrochim. Acta* A **2001**, *57*, 1133.

(e) Novo, M.; Al-Soufi, W. *11th International Electronic Conference on Synthetic Organic Chemistry*, ECSOC-11, **2007.**

(f) Bhattacharya, B.; Srinivas, S.; Guruprasad, L., Samanta, A. *J. Phys. Chem B.* **2009**, *113*, 2143.

(g) Wen, Y.; Liu, H.; Luan, F.; Gao, Y. *J. Luminesc*. **2011**, *131*, 126.

10. (a) Ross, P. D.; Subramanian, S. *Biochemistry* **1981**, *20*, 3096.

(b) Rahman, M. H.; Maruyama, T.; Okada, T.; Yamasaki, K.; Otagiri, M. *Biochem. Pharmacol.* **1993**, *46*, 1721.

11. (a) Liu, X.; Xi, P.; Chen, F.; Xu, Z.; Zeng, Z. J. *Photochem. Photobiol. B*, **2008**, *92*, 98.

(b) Yu, X.; Lu, S.; Yang, Y.; Li, X.; Yi, P.; *Spectrachim Acta A* **2012**, *91*, 113.

12. (a) Kandagal, P. B.; Ashoka, S.; Seetharamappa, J.; Shaikh, S. M. T.; Jadegoud, Y.; Ijare, O. B. *J. Pharm. Biomed. Anal.* **2006**, *41*, 393.

(b) Anand, U.; Jash, C.; Boddepalli, R. K.; Shrivastava, A.; Mukherjee, S. *J. Phys .Chem. B* **2011**, *115*, 6312.

(c) Anand, U.; Kurup, L.; Mukherjee, S. *Phys. Chem. Chem. Phys*. **2012**, *14***,** 4250.

(d) Zhang, G., Zhao, N.; Wang, L. *J. Luminesc*. **2011**, *131*, 2716.

13. (a) Ravi, M. *Proc. Ind. Acad. Sci. U.S.A.* **1998**, *110*, 133.

(b) Jones II, G.; Jackson, W. R.; Choi, C.; Bergmark, W. R. *J. Phys. Chem.* **1985** , *89*, 294.

14. Woody, R. W. *Theory of circular dichroism of proteins. In circular dichroism and conformational analysis of biomolecules*, G. D. Fasman, Ed., Plenum publishing corp., New York, p 25, **1996**.

15. (a) Nad, S.; Kumbhakar, M.; Pal, H. *J. Phys. Chem*. A **2003**, *107*, 4808.

(b) Beck, M. Y.; Nagypal, I. *Chemistry of complex equilibria*, Wiley, New York, **1990**, 112.

16. (a) Ponder, J. W.; Case, D. A. *Adv. Prot. Chem*. **2003**, *66*, 27.

(b) Case, D. A.; Cheatham, T.; Darden, T.; Gohlke, H.; Luo, R.; Merz, K. M.; Jr, Onufriev, A.; Simmerling, C.; Wang, B.; Woods, R. *J. Comput. Chem.* **2005**, *26*, 1668.

(c) Case, D. A.; Darden, T. A.; Cheatham, T. E.; III, Simmerling, C. L.; Wang, J.; Duke, R. E.; Luo, R.; Merz, K. M.; Pearlman, D. A.; Crowley, M.; Walker, R. C.; Zhang, W.; Wang, B.; Hayik, S.; Roitberg, A.; Seabra, G.; Wong, K. F.; Paesani, F.; Wu, X.; Brozell, S.; Tsui, V.; Gohlke, H.; Yang, L.; Tan, C.; Mongan, J.; Hornak, V.; Cui, G.; Beroza, P.; Mathews, D. H.; Schafmeister, C.;

Ross, W. S.; Kollman, P. A. AMBER 9, University of California, San Francisco, **2006**.

(d) Popelier, P. L. A.; Aicken, F. M. *ChemPhysChem*. **2003**, *4*, 824.

17. (a) Petitpas, I.; Bhattacharya, A. A.; Twine, S.; East, M.; Curry, S. *J. Biol. Chem*. **2001**, *276*, 22804.

(b) Morris, G. M.; Huey, R.; Lindstrom, W.; Sanner, M. F.; Belew, R. K.; Goodsell, D. S.; Olson, A. J. *J. Comput. Chem*. **2009**, *16*, 2785.

(c) Miyamoto, S.; Kollman, P. A. *J. Comput. Chem*. **1992** , *13*, 952.

18. (a) Wang, J.; Wolf, R. M.; Caldwell, J. W.; Kollamn, P. A.; Case, D. A. *J. Comput. Chem*. **2004**, *25*, 1157.

(b) Case, D. A.; Darden, T. A.; Cheatham, T. E.; III, Simmerling, C. L.; Wang, J.; Duke, R. E.; Luo, R.; Walker, R. C.; Zhang, W.; Merz, K.M.; Roberts, B.; Hayik, S.; Roitberg, A.; Seabra, G,; Swails, J.; Goetz, A. W.; Kolossváry, I.; Wong, K. F.; Paesani, F.; Vanicek, J.; Wolf, R. M.; Liu, J.; Wu, X.; Brozell, S. R.; Steinbrecher, T.; Gohlke, H.; Cai, Q.; Ye, X.; Wang, J.; Hsieh, M. J.; Cui, G.; Roe, D. R.; Mathews, D. H.; Seetin, M. G.; Salomon-Ferrer, R.; Sagui, C.; Babin, V.; Luchko, T.; Gusarov, S.; Kovalenko, A.; Kollman, P. A.; AMBER 12, University of California, San Francisco, **2012**.

19. (a) Lakowicz, J. R. 2006 *Principles of fluorescence spectroscopy*, 3rd edn., Springer: New York.

(b) Sytnik, A.; Litvinyuk. I. *Proc. Natl. Acad. Sci. U.S.A.* **1996,** *93*, 12959.

Chapter 4

Direct Observation of Intermediate State(s) in the Mechanistic Investigation of Domain Specific Protein-Surfactant Interaction

Rajeev Yadav *et al*., *Luminescence*, Submitted.

In the present work we have studied the interaction of two surfactants, an anionic (sodium dodecyl sulphate, SDS) and a cationic (cetyltrimethylammonium bromide, CTAB) with domain III of human serum albumin (HSA) using 8-anilino-1-naphthalene-sulphonate (ANS) as a fluorescent marker. The interaction of both the surfactants with HSA is found to be sequential in nature. The most important conclusion revealed from our study is that the nature of protein-surfactant interaction is not same throughout the entire protein. SDS is found to interact sequentially with the domain III of HSA having two detectable intermediate states in the binding process. In case of CTAB, we have observed only one intermediate state for its interaction with domain III. However, the overall conformational change of the HSA on addition of surfactants, studied by circular dichroism spectroscopy, and the ANS-Trp distance measurement by FRET could not resolve the presence of such intermediate states. The esterase activity of HSA in presence of different amount of surfactants is also in accordance with our above observation. Our study reveals that different parts of the multi-domain HSA have different affinity to the surfactants under consideration.

4.1. Introduction

It is now being well accepted that protein-surfactant assemblies can be served as an elegant model for the protein-lipid aggregate in the membrane of a living cell.[1] On this purview, the interaction of proteins with surfactants has been a subject of great interest for a long time.[2-11] In 1948 Duggan *et al*. for the first time showed the protective nature of sodium dodecyl sulfate (SDS) from urea induced denaturation of albumins.[2] In 1999 Moriyama *et al*. also reveal the protective nature of SDS till 0.2 mM concentration for bovine serum albumin (BSA) under urea induced denaturation.[3b] Further in 2008 Singh *et al*. showed the protective and unprotective nature of SDS at its low and high concentration, respectively, to the urea induced denaturation of BSA.[4b] Gelamo *et al*. studied the interaction of ionic surfactants with HSA and BSA and found a concentration dependent binding phenomena.[5] Mondal *et al*. have studied the interaction of SDS with HSA by using covalently attached external fluorescent probe and observed that on addition of SDS the local water dynamics in HSA became faster, which is attributed to the displacement of the buried water molecules in the immediate vicinity of the probe molecule.[9a] Vlasov *et al*. studied the interaction of cetyltrimethylammonium bromide (CTAB) with HSA at different pH values and revealed that the deepest denaturation of HSA reached at 4 mM of CTAB in a step wise fashion.[11b] Recently in 2010, Anand *et al*. studied the binding of SDS to HSA by probing the change in Trp fluorescence and found that the addition of surfactant takes place in a sequential manner as concentration of SDS is increased.[7a] This is to note that in most of the studies, HSA was used as the model protein, because of its key role in transport and deposition of varieties of metabolites and drugs in different parts of the body.[13-17]

As it can be seen in the literature, most of the researchers used the fluorescent property of single tryptophan unit (Trp) present in the domain IIA of HSA to study the HSA-surfactant interaction. As the fluorescence fluctuation is mainly attributed from the changes in local environment of the fluorophore, this

will only estimate the nature of interaction in the vicinity of the Trp i.e. domain II of HSA.[18] Nevertheless, for a big multi-domain protein, the effect of surfactants may be different for different domains of the protein and in the present work we will show how it is different in domain III of HSA. Domain III of HSA can be probed by 8-anilino-1-naphthalenesulphonate (ANS) fluorescence. Bagatolli *et al.* studied the binding of ANS to HSA by using diazepam and aspirin as a site marker and revealed that at very high concentration, ANS selectively binds to domain IIIA with high binding affinity ($K = 0.87 \times 10^6\ M^{-1}$) and also to domain IIA with low binding affinity ($K = 0.079 \times 10^6\ M^{-1}$).[19] However, at relatively low concentration regime (ANS to HSA < 10^3) it preferentially binds to domain IIIA of HSA.[20] The huge change in the fluorescence quantum yield of ANS on binding to HSA is an advantage for using ANS as a probe to study the effect of surfactant.[18c,d,20] It has been demonstrated that ANS has a non-planar configuration in the ground state and the locally excited (LE) state with the non-planar character is stable in the non-polar solvents, which gives a strong emission. However in polar solvents, the LE state undergoes a conformational change to a planar configuration forming the charge transfer (CT) state, which is non-fluorescent in nature.[21,22]

In the present study we have characterized the mechanistic pathway of interaction of anionic and cationic surfactants with the domain III of HSA using ANS as the domain marker. The results are also compared with the change in the global structure of HSA on addition of surfactants, using circular dichroism spectroscopy. The relative location of the ANS from Trp-214 and the relative esterase activity of HSA were also measured as function of surfactant concentration.

4.2. Data Analysis

During the experiment, the concentration of HSA and ANS (scheme 4.1) has been fixed as 50 μM and 30 μM respectively so that ANS can bind selectively to the domain III of HSA.[20] The relative fluorescence quantum yield of ANS in protein-surfactant assemblies has been determined from the change in the area under the fluorescence spectrum using ANS bound to HSA as a standard (ϕ_f^{ref} = 0.67).[19] The temperature during all the experiment was maintained at 25±1 °C.

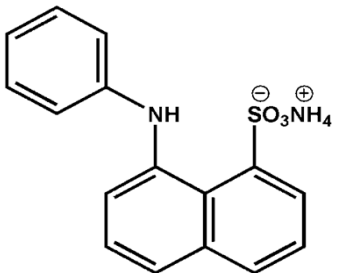

Scheme 4.1. Molecular structure of 8-Anilino-1-naphthalenesulfonic acid ammonium salt.

The change in the quantum yield of ANS bound to HSA with SDS was best fitted with four state model containing two intermediate states.

$$N \leftrightarrow I_1 \leftrightarrow I_2 \leftrightarrow U_1 \qquad (4.1)$$

Where I_1 and I_2 are the two intermediate states in between the native (N) and denatured (U_1) states of HSA. For such a four state model, the overall spectroscopic signal can be written as[24]

$$S = \frac{(S_N + S_{I1}\exp^{-X} + S_{I2}\exp^{-Y} + S_D\exp^{-Z})}{(1+\exp^{-X}+\exp^{-Y}+\exp^{-Z})} \qquad (4.2)$$

where, $X = (\Delta G_1^0 - m_1[\text{Surfactant}])/RT$

$$Y = (\Delta G_1^0 + \Delta G_2^0 - (m_1+m_2)[\text{Surfactant}])/RT$$

$$Z = (\Delta G_1^0 + \Delta G_2^0 + \Delta G_3^0 - (m_1+m_2+m_3)[\text{Surfactant}])/RT$$

and S_N, S_{I1}, S_{I2}, S_U are the values of the observable in the native, first intermediate, second intermediate and denatured state, respectively. $\Delta G_1{}^0$, $\Delta G_2{}^0$ and $\Delta G_3{}^0$ are the free energy change of each transition in the absence of denaturant. m_1, m_2 and m_3

are the slope of free energy change plotted against the surfactant concentration. The concentration of denaturant to unfold 50 % of the protein ($[D]_{1/2}$) can be calculated using the relation $[D]_{1/2} = \Delta G_i^0 / m_i$.

A three state model with one intermediate state was used to best fit the change in the quantum yield of ANS bound to HSA with the CTAB concentration.

$$N \leftrightarrow I_1^{'} \leftrightarrow U_2 \qquad (4.3)$$

Where U_2 is the CTAB induced denatured state of HSA. For this, the dependence of the signal with surfactant was modified accordingly.

We have also estimated the binding parameters between surfactants and HSA using modified Stern-Volmer equation as given below.[25]

$$\log[(F_0 - F)/F] = \log K + n\log[Q] \qquad (4.4)$$

Here *K*, *n* and *Q* stand for the binding constant, number of surfactant molecules and concentration of the surfactant respectively. F_0 and *F* are the fluorescence intensity of ANS bound to HSA in absence and presence of surfactant. The free energy of binding ($\Delta G^0_{binding}$) can be calculated by

$$\Delta G^o_{binding} = -2.303\, RT \log K \qquad (4.5)$$

The effect of surfactants on the esterase activity of HSA has been studied using steady state absorption spectroscopy. Here we have used *p*-nitrophenyl acetate (PNPA), which can be hydrolyzed efficiently in presence of HSA. However, the hydrolysis of PNPA in absence of HSA is not significant. The hydrolyzed product in this case is *p*-nitrophenol having a strong absorption at 400 nm with extinction coefficient of 16900 M^{-1} cm^{-1}.[26a-c] For this experiment 50 μM HSA has been treated with 25 μM PNPA in absence and presence of different concentrations of surfactants at room temperature and the absorbance at 400 nm was monitored after 5, 40, 120, 360 minutes of the mixing, and is corrected for hydrolysis of PNPA in absence of HSA.

4.3. Results and Discussion

4.3.1. Effect of SDS and CTAB on Global Structure of HSA

Circular dichroism (CD) spectroscopy probes the secondary structure of protein and is a widely used technique to monitor the overall conformation of a protein in solutions.[3b-d, 23] The changes in the secondary structure of HSA were monitored by change in CD signal on increasing concentration of surfactants (SDS and CTAB). The elipticity at 208 nm and 222 nm is a measure of α-helical content of HSA.[26d] It is important to note that CD spectra are associated to the overall secondary structure of protein hence it cannot provide the domain specific changes of HSA induced by surfactant molecules.

Figure 4.1a shows the CD spectra of HSA for different SDS concentrations ranging from 0 mM to 20 mM. In order to investigate the effect of added SDS on the structure of HSA, we have calculated the % α-helicity at each SDS concentration using equation 3.1 (chapter 3b). The change in α-helicity with increasing concentration of SDS is shown in figure 4.1b. This indicates that the helicity of HSA almost remain constant to ~65 % till 0.8 mM SDS. On further increase in the concentration of SDS, the α-helicity starts decreasing and become ~55 % at 3 mM SDS. No further change in α-helicity was observed on further increase in SDS concentration. The result indicates that SDS does not have any detrimental effect on the overall structure of HSA till 0.8 mM, and beyond this, SDS denatures the overall structure of HSA.

The interaction of CTAB with HSA has also been studied by CD spectroscopy and the spectra for different CTAB concentrations ranging from 0 mM to 10 mM are shown in figure 4.2a and the change in α-helicity with CTAB is shown in figure 4.2b. In this case, we observed that % α-helicity of HSA remains constant till 0.1 mM CTAB to ~65 % and then keep on decrease on increasing the concentration. Finally it saturates to ~52 % at around 2 mM CTAB concentration. Comparing the α-helicity in presence of SDS, we can see that the effect of CTAB

on global denaturation of HSA is much more drastic and it start affecting the overall structure at a much lower concentration than that of SDS. We have also recorded the CD spectra of the surfactants in absence of HSA and found that there was no signal appeared till 20 mM of surfactants. It confirms that the signals that we got for HSA in presence of SDS and CTAB were only contributed by HSA.

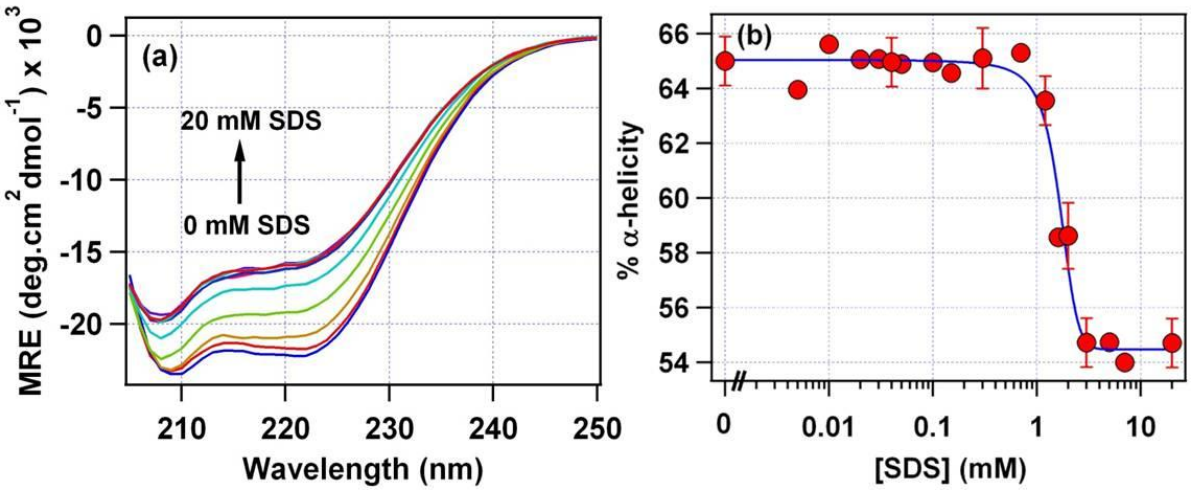

Figure 4.1. (a) Circular dichroism spectra of 5 µM HSA in pH 7.5 tris buffer in absence and presence of different concentration of SDS, (b) Change of % α- helicity of HSA with SDS concentration.

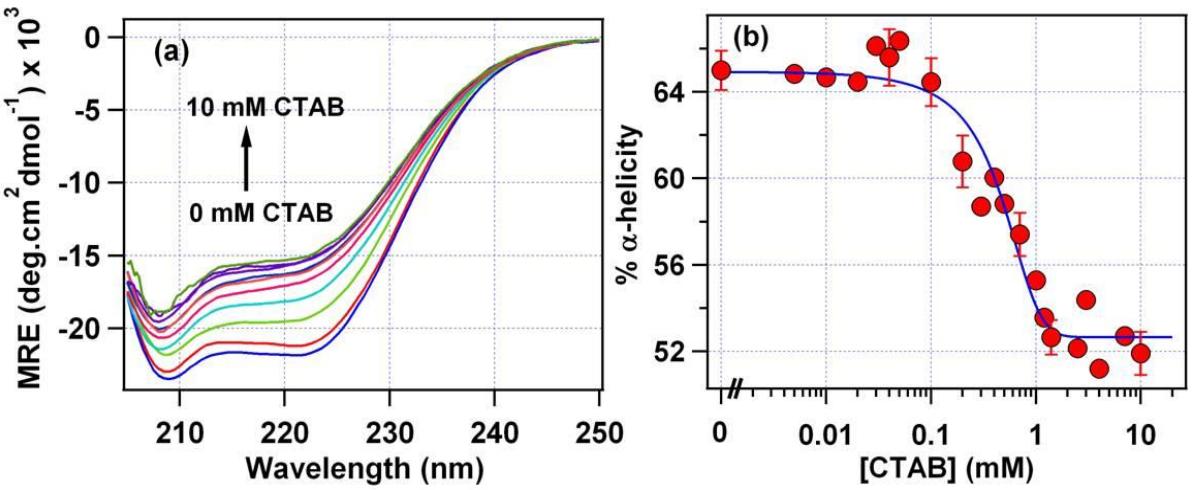

Figure 4.2. (a) Circular dichroism spectra of 5 µM HSA in pH 7.5 tris buffer in absence and presence of different concentration of CTAB, (b) Change of % α- helicity of HSA with CTAB concentration.

The change in the α-helicity of HSA was best fitted with the two state model ($N \leftrightarrow U_1/U_2$) during SDS and CTAB induced unfolding, using accordingly modified equation 4.2. From the fitting, ΔG^0 and m values have been observed as 2.67 kcal mol^{-1} and 1.61 kcal mol^{-1} mM^{-1}, respectively for SDS induced unfolding. Whereas, for CTAB induced unfolding these values have been observed as 0.82 kcal mol^{-1} and 2.15 kcal mol^{-1} mM^{-1}, respectively.

4.3.2. Effect of SDS on Domain III of HSA

As desired, the domain III of HSA has been specifically studied by ANS fluorescence as ANS selectively binds to domain III under the present experimental condition. The absorption spectrum of ANS in native state of HSA has maximum at 374 nm, which merely change on addition of SDS (Figure 4.3a). However, the fluorescence response depends strongly on the amount of SDS present in the medium. ANS displays an emission maximum of 464 nm with a very high fluorescence quantum yield of 0.67 when bound to HSA.[19] Upon addition of SDS up to 0.25 mM, there is a 2 % decrease in emission intensity at its maxima (the fluorescence quantum yield of ANS bound to HSA was almost unaffected, see table 4.1) with a 5 nm red shift (Figure 4.3b). These indicate that there is a change in the micro-environment around ANS binding site upon addition of 0.25 mM SDS. On the other hand, CD data (figure 4.1) shows that at this small concentration of SDS, there is also no change in the secondary structure of HSA. It can be concluded that in presence of such small concentration of SDS, the overall secondary structure of HSA is unaltered; however the microenvironment around ANS binding site in domain III is changed. On further increase in the concentration of SDS, the fluorescence quantum yield of ANS was found to decrease in stepwise fashion (figure 4.3c).

The step wise change of fluorescence quantum yield (ϕ_f) of ANS bound to HSA was best fitted with a four state model containing two intermediate states (equation 4.2) during SDS induced unfolding. From the fitting parameters, the ϕ_f

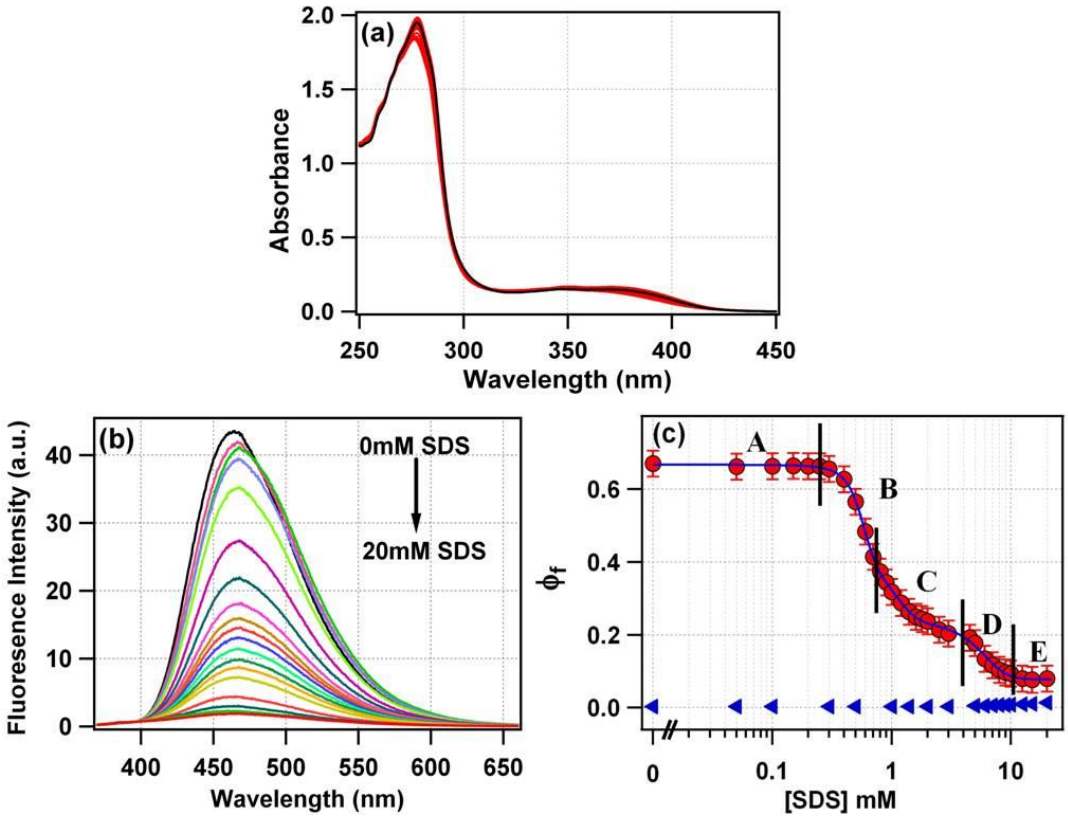

Figure 4.3. Steady-state (a) absorption and (b) emission spectra of 30 µM ANS in 50 µM HSA with increasing concentration of SDS from 0 to 20 mM. Here the black curve depicts the absorption and emission spectra of ANS in HSA without SDS. (c) The dependence of fluorescence quantum yield (ϕ_f) of ANS in buffer (blue triangle) and when bound to HSA (red circle) as a function of SDS concentration. Here the error bars are obtained by averaging the associated errors of all the data points.

Table 4.1. Fitting parameters for SDS/CTAB induced unfolding of domain III of HSA and the overall structure of HSA. (Unit of ΔG^0 is kcal mol^{-1}; Unit of m is kcal mol^{-1}M^{-1}; $[D]_{1/2}$ is the amount of SDS/CTAB in mM required for 50% unfolding).

		$N \leftrightarrow I_1 / N \leftrightarrow I'_1$			$I_1 \leftrightarrow I_2$			$I_2 \leftrightarrow U_1 / I'_1 \leftrightarrow U_2$		
		ΔG_1^0	m_1	$[D]_{1/2}$	ΔG_2^0	m_2	$[D]_{1/2}$	ΔG_3^0	m_3	$[D]_{1/2}$
Domain III of HSA	**SDS**	3.66	6.47	0.57	2.03	2.12	0.96	1.89	0.36	5.25
	CTAB	2.30	1.90	1.21	-	-	-	1.13	0.38	2.97
		$N \leftrightarrow U_1 / N \leftrightarrow U_2$								
		ΔG^0			m			$[D]_{1/2}$		
Overall HSA	**SDS**	2.67			1.61			1.66		
	CTAB	0.82			2.15			0.38		

value of I_1 and I_2 state is found to be 0.43 and 0.24, respectively. The ΔG^0 values have been observed as 3.64 kcal mol^{-1}, 2.03 kcal mol^{-1} and 1.89 kcal mol^{-1} for first transition ($N \leftrightarrow I_1$), second transition ($I_1 \leftrightarrow I_2$) and third transition ($I_2 \leftrightarrow U_1$), respectively. The *m* values have been observed as 6.47 kcal mol^{-1} mM^{-1}, 2.12 kcal mol^{-1} mM^{-1}, 0.36 kcal mol^{-1} mM^{-1} for the three transitions, respectively. The measured values of ΔG^0 and *m* for all the three transitions are shown in table 4.1. The change in the value of ϕ_f manifests the presence of all three transitions in the concentration range from 0.25 mM to 10 mM SDS (see figure 4.3c, red circles). However, it remains unchanged till 0.25 mM and beyond 10 mM SDS no further change was observed, indicating the absence of any alteration in the structure of HSA. Hence the step wise change of fluorescence quantum yield of ANS bound to HSA on addition of SDS, can be divided into five different regions as shown in figure 4.3c. Where all three transitions correspond to the region B, C, D respectively and the region A and E are for native as well as SDS induced denatured states of HSA. The value of ϕ_f of I_1 state that has been observed as 0.43 is corresponds to the value around 0.7 mM SDS, hence the first transition ($N \leftrightarrow I_1$) or region B exists in between ~0.25 to ~0.7 mM SDS. In this region the fluorescence quantum yield found to decrease rapidly, resulting the high values of ΔG^0 and *m*. Here the value of *m* reflects the power of a denaturant (SDS) to interact with the protein and effectively change its conformation. It is to emphasize that till 0.8 mM of SDS the secondary structure of HSA also remains unchanged as discussed in section 4.3.1. Hence the change observed in region B is due to the binding of SDS with domain III of HSA only. In the second transition ($I_1 \leftrightarrow I_2$) or in region C (~0.7 mM to ~4 mM SDS) the values of ΔG^0 and *m* have been decreased by ~1.5 and ~3 times than in the first transition respectively. The secondary structure of HSA in this region starts unfolding as observed in the CD study. This observed change in the CD signal might originate from overall structure of HSA. On further increase of SDS concentration between 4 mM to 10 mM (third transition or region D), the fluorescence quantum yield starts decreasing more

rapidly compared to region C and a blue shift in the emission maximum was observed. The blue shift indicates that ANS inside HSA is experiencing more hydrophobic environment which may be because of the presence of alkyl chains of SDS. In this region the value of ΔG^0 is almost same as in region C whereas the value of *m* has been decreased by ~6 times than in region C. A drastic fall in value of *m* from region B to region C indicates the decrease in the ability of SDS to interact with protein. At a higher concentration of SDS beyond 10 mM (region E), the emission maxima of ANS start shifting towards red side with a very small increase in quantum yield. In this region, SDS forms micelle and ANS may leave the protein and accumulated in the micelle giving a red shift in the emission maximum. To make a comparison with the effect of the surfactant only, the fluorescence quantum yield of ANS in tris-buffer as a function of SDS concentration in absence of the protein has been measured and is shown in the lower portion of figure 4.3c (blue triangles). The fluorescence quantum yield of ANS changes from 0.0034 in absence of SDS to 0.014 in presence of 20 mM SDS, which is negligible as compared the quantum yield of ANS bound to HSA in absence and presence of SDS. Hence it can be assumed that the change in fluorescence quantum yield of ANS in HSA with SDS concentration is due to the change in the local environment of ANS binding site in HSA, i.e. domain III of HSA.

To illustrate the mechanistic details of HSA-surfactant interaction, we have estimated the binding parameters between SDS and HSA using modified Stern-Volmer equation (equation 4.4). Figure 4.4 shows the change in $\log[(F_0\text{-}F)/F]$ with $\log[Q]$ which also clearly indicate the presence of five distinct regions (A to E) of sequential binding of SDS to HSA. The estimated values of *K*, *n* and $\Delta G^0_{binding}$ for region B, C and D are tabulated in table 4.2. We observed a strong and spontaneous binding of SDS to domain III of HSA in region B, characterized by the highest *K*, $\Delta G^0_{binding}$ and *n* values. In region C the binding of SDS is found to be non-cooperative in nature with low values of *K*, $\Delta G^0_{binding}$ and *n*. The relatively

high value of *K* and *n* in region D compared to region C infer that in this high concentration range of SDS, the binding is stronger than region C but less than region B.

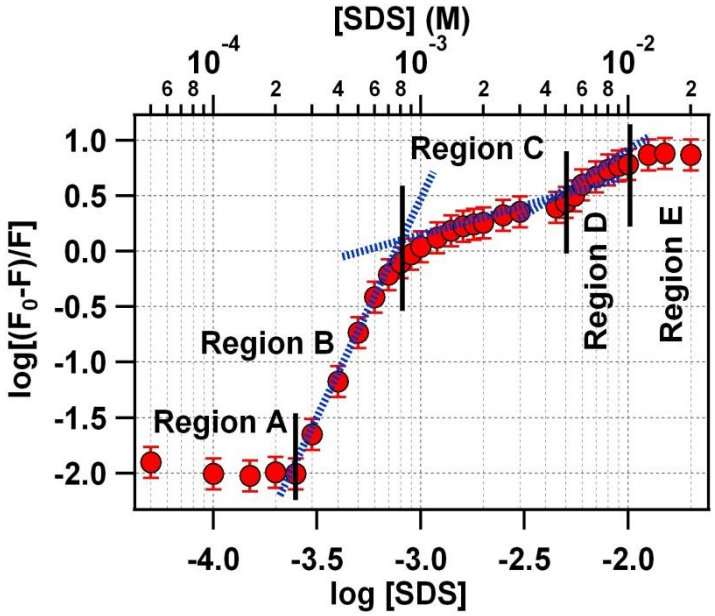

Figure 4.4. A plot of log[(F_0-F)/F] with log[Q]. F_0 and F are the fluorescence intensity of ANS in HSA in absence and presence of SDS. Different regions show the sequential binding stages of SDS to domain III of HSA. Blue dashed lines represent the fitting of the different regions as per equation 4.4. Here the error bars are obtained by averaging the associated errors of all the data points.

Table 4.2. Thermodynamic parameters of surfactant association with domain III of HSA.

Region	***K* (M^{-1})**	***n***	$\Delta G^0_{binding}$ **(kcal mol^{-1})**
	SDS		
Region B	1.4×10^{11}	4.0	-15.2
Region C	34.5	0.5	-2.1
Region D	9.9×10^{2}	1.1	-4.0
	CTAB		
Region B	6.7×10^{6}	2.5	-9.4
Region C	36.0	0.6	-2.1

This is to emphasize that recently Anand *et al*. shows the binding characteristics of SDS with HSA using Trp fluorescence as the marker.[7a] In this

case they have observed the specific effect of SDS on domain II of HSA. They also have seen that SDS binds to HSA in sequential manner depending on the total SDS concentration. Anand *et al*. observed the second region between 0.3 mM to 5 mM, which is 0.2 to 0.8 mM in the present study. Although in both the study, SDS shows a sequential interaction with HSA, but the domain of interest is different. The appearance of different regions in the two different studies has been assigned to the domain dependent interaction of SDS with HSA.

4.3.3. Effect of CTAB on Domain III of HSA

The absorption spectrum of ANS in HSA is found to be almost independent on addition of CTAB (Figure 4.5a), whereas we found that fluorescence response of ANS depends on CTAB concentration as shown in figure 4.5(b). The change in fluorescence quantum yield of ANS bound to HSA with varying concentration of CTAB is shown in figure 4.5c. It is clear that the effect of CTAB on the fluorescence properties of ANS bound to HSA is completely different from that we observed for SDS (scheme 4.2).

The change in fluorescence quantum yield (ϕ_f) of ANS bound to HSA with varying CTAB concentration was best fitted with a three state model containing one intermediate state. From the fitting parameters, the ϕ_f value of intermediate state is found to be 0.4. The ΔG^0 values for the first transition ($N \leftrightarrow I'_1$) and the second transition ($I'_1 \leftrightarrow U_2$) have been observed as 2.29 kcal $mol^{-1}$and 1.13 kcal mol^{-1}, respectively. The *m* values for these transitions are observed as 1.9 kcal mol^{-1} mM^{-1} and 0.38 kcal mol^{-1} mM^{-1}, respectively. These two transitions exist in between ~0.5 mM and ~10 mM of CTAB where the maximum change in the fluorescence quantum yield occurs. Hence the change of fluorescence quantum yield of ANS bound to HSA on addition of CTAB can be divided into four different regions as shown in figure 4.5c (red circles). In region A, which lasts till ~0.5 mM CTAB, the emission maximum of ANS in HSA is found to be unaffected with a small change of the fluorescence quantum yield implying that the

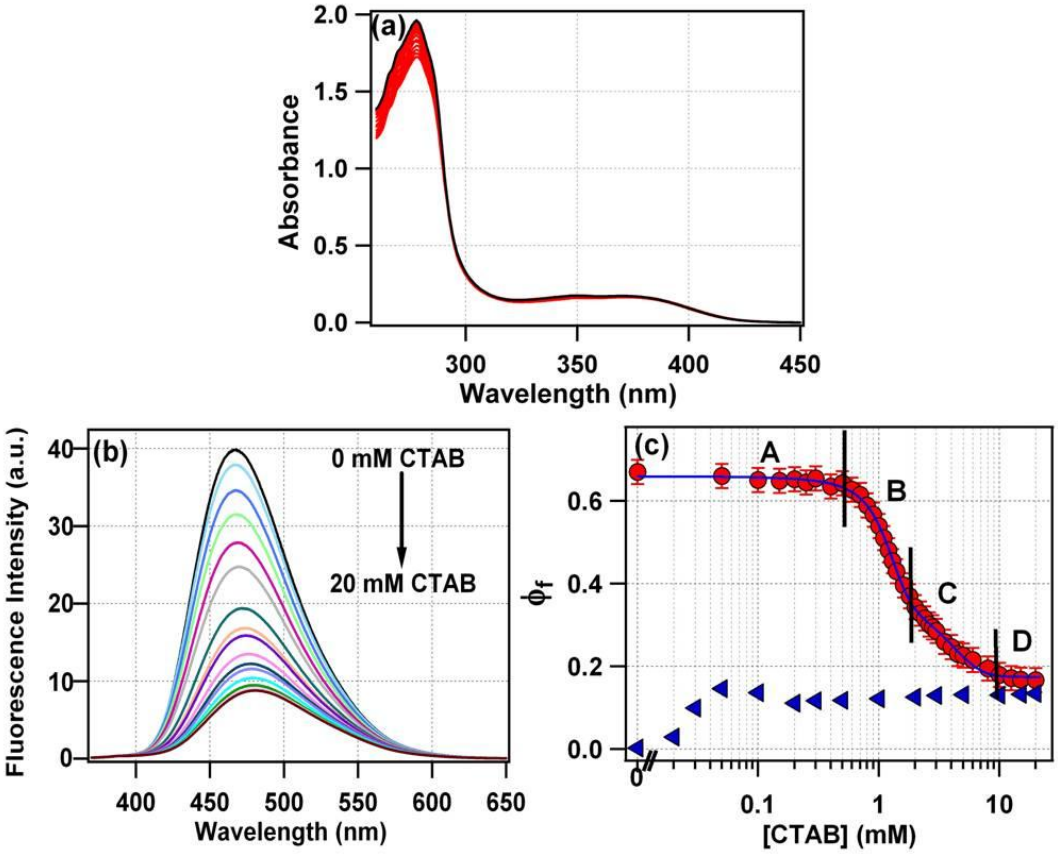

Figure 4.5. Steady-state (a) absorption and (b) emission spectra of 30 µM ANS in 50 µM HSA with increasing concentration of CTAB from 0 to 20 mM. Here the black curve depicts the absorption and emission spectra of ANS in HSA without CTAB. (c) The dependence of fluorescence quantum yield (ϕ_f) of ANS in buffer (blue triangle) and when bound to HSA (red circle) as a function of CTAB concentration. Here the error bars are obtained by averaging the associated errors of all the data points.

microenvironment of ANS in domain III of HSA is not affected much in this concentration range, unlike SDS. However, the CD data suggests a decrease in the helicity of HSA (figure 4.2b), consequently the destruction of the secondary structure, beyond 0.1 mM CTAB. Further addition of CTAB induces a drastic fall in fluorescence quantum yield of ANS and become saturate around 10 mM CTAB with an intermediate state (I'_1) around 2 mM. Hence the region B and C which correspond to the first and second transitions ranges from ~0.5 mM to ~2 mM CTAB and ~2 mM to ~10 mM CTAB respectively. At a higher concentration of CTAB beyond ~10 mM (region D), the fluorescence quantum yield remains constant. Same experiment has been done in absence of HSA, as a control. The

fluorescence quantum yield of ANS in tris-buffer is found to increase from 0.0034 to 0.14 till 0.5 mM of CTAB after that it remains constant as shown in the lower portion of figure 4.5c (blue triangles).

To illustrate the mechanistic pathway of HSA-CTAB interaction, we have constructed a plot of log $[(F_0\text{-}F)/F]$ against log $[Q]$ as shown in figure 4.6, which also clearly depicts four different regions (A to D) during the binding of CTAB to the domain III of HSA. The value of K, n and $\Delta G^0_{binding}$ for region B and C have been calculated using equation 4.4 and 4.5 and are tabulated in table 4.2. The binding of CTAB to the domain III of HSA is found to be very strong and spontaneous in nature in region B, characterized by highest values of K, negative $\Delta G^0_{binding}$ and n. In region C, the interaction of CTAB with domain III of HSA is weak in nature as compare to the region B.

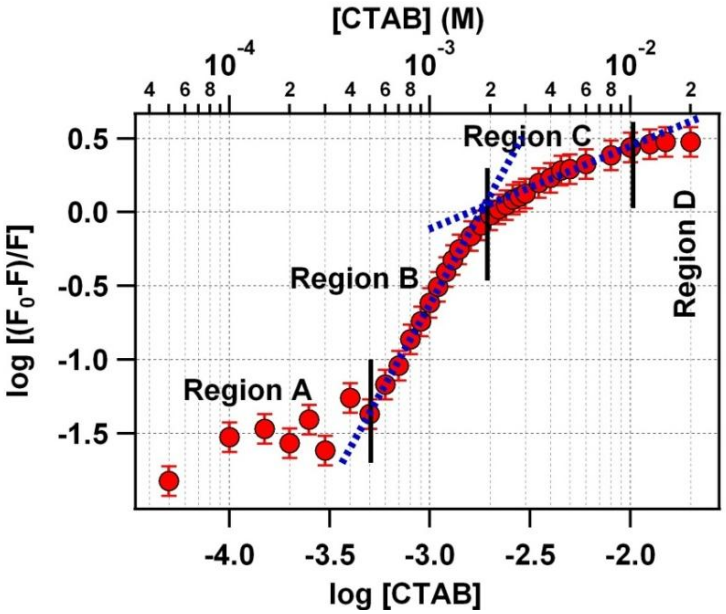

Figure 4.6. A plot of log[(F_0-F)/F] with log[Q]. F_0 and F are the fluorescence intensity ANS in HSA in absence and presence of CTAB. Different regions show the sequential binding stages of CTAB to domain III of HSA. Blue dashed lines represent the fitting of the different regions as per equation 4.4. Here the error bars are obtained by averaging the associated errors of all the data points.

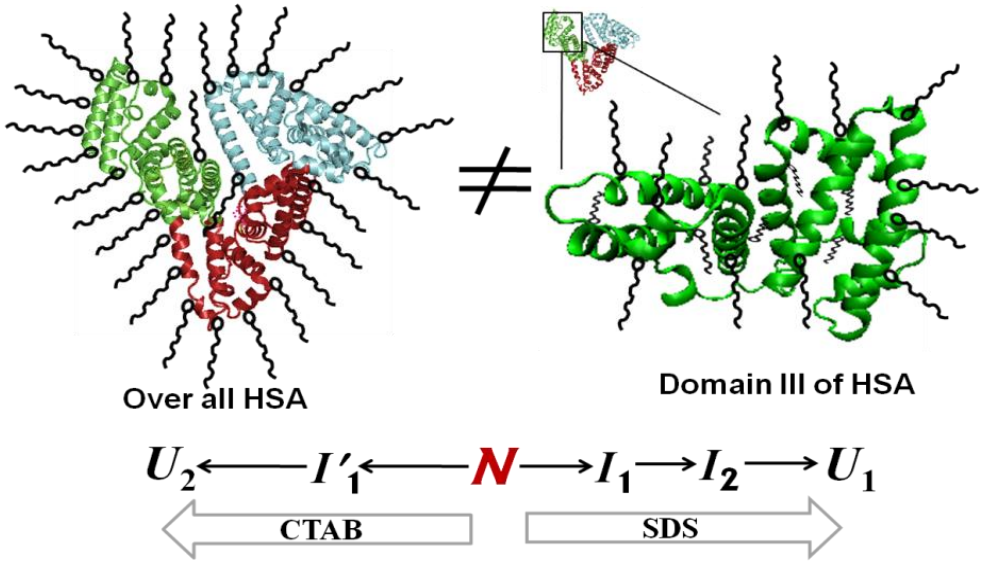

Scheme 4.2. SDS/CTAB induced denaturation process of domain III.

4.3.4. Effect of SDS and CTAB on Trp-ANS Distance

Förster resonance energy transfer (FRET) experiment was employed to monitor the distance between ANS and the only Trp-214 in HSA in the course of interaction with the surfactant molecules.[27] The changes in Trp-ANS distance with increasing concentration of SDS are shown in figure 4.7a. In absence of SDS the distance has been observed as 20 ± 0.4 Å and almost unchanged till 0.3 mM SDS. On further increase in the concentration of SDS, the Trp-ANS distance starts increasing and become ~23.5 Å at 1.5 mM SDS. No further change was observed on further increase in SDS concentration. Figure 4.7b shows the change in Trp-ANS distance with increasing concentration of CTAB. In this case, the distance (20 ± 0.4 Å) is almost unchanged until 0.4 mM CTAB; afterward it starts increasing gradually. At 10 mM CTAB the observed Trp-ANS distance is ~23.5 Å. This is to note that the donor (Trp) and accepter (ANS) are present in the domain II and III, respectively. As already pointed out, both the surfactants interact differently with domain II and III of HSA. Hence the observed dependence of Trp-ANS distance with the SDS and CTAB concentration must be because of the change in both the domains and thus is less informative.

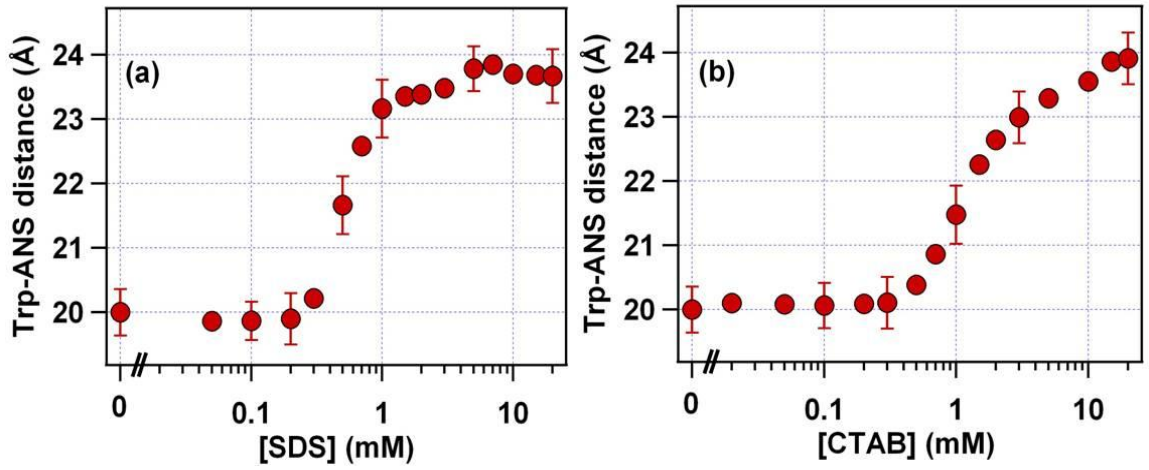

Figure 4.7. The variation of distance between Trp and ANS inside HSA as a function of (a) SDS and (b) CTAB concentration.

4.3.5. Effect of SDS and CTAB on Esterase Activity

From the above experimental results, it is evident that the structure of HSA altered upon interaction with the surfactants. In case of SDS, the overall secondary structure destroyed in an apparently two step fashion as the concentration of SDS increased, however, the local structural change of domain III is entirely different having two intermediate states, which was not detected in the secondary structure determination study. In case of CTAB, on the other hand, we have observed only one intermediate state while studying the domain III of HSA specifically. It is obvious that the disruption in the native form of HSA will influence its activity.[28] Thus it becomes crucial to probe how the activity of HSA changes with the addition of SDS and CTAB, which can be monitored by its esterase activity using PNPA.[26a-c] Masson and co-workers have studied the hydrolysis of PNPA with HSA and showed that the only one amino acid residue, Tyr-411, was acylated within the first 5 min of the reaction; while in 30 - 360 minutes reaction time, they have noticed partial acylation of additional 16-17 amino acid residues including Asp-1, Lys-4, Lys-12, Tyr-411, Lys-413 and Lys-414.[26b] To see the effect of SDS and CTAB on esterase activity of HSA, the absorbance of *p*-nitophenol, which is generated from the hydrolysis of PNPA upon treatment with HSA, has been monitored at 400 nm at 5 min, 40 min, 120 min, 360 min from the time of mixing.

During the first 5 minutes of the reaction, *p*-nitophenol has produced only by the reaction with Tyr-411, which is present in domain IIIA of HSA. Hence the absorbance at 400 nm at 5 min from the starting of the reaction will show the activity of domain III predominantly. Understandably, at higher reaction times, the overall protein will be involved in the hydrolysis process. In the present case, for the complete hydrolysis of 25 μM PNPA the absorbance at 400 nm has been calculated as 0.4225 using extinction coefficient of *p*-nitophenol at 400 nm as 16900 $M^{-1}cm^{-1}$.[26a-b] This absorbance value would be expected if the esterase activity is 100 %. In absence of surfactants the absorbance at 400 nm has been observed as 0.263, 0.326, 0.332, and 0.340 at 5 min, 40 min, 120 min and 360 min from the starting of the reaction, respectively for 50 μM HSA in 0.1M Tris-buffer, pH = 7.5 at 25 °C; and hence the relative activity of HSA is calculated to be 62 %, 77 %, 79 % and 80 % at respective times. The relative esterase activity for different reaction times (5 min to 360 min) with different concentrations of SDS and CTAB ranges from 0 mM to 20 mM are shown in figures 4.8a and 4.8b, respectively, which is corrected for without HSA. During first 5 min, the relative activity of HSA decreases from 62 % in absence of surfactants to about 3 % in presence of 20 mM SDS, and to 40 % in presence of 20 mM CTAB. The esterase activity in this time region mainly originates from domain IIIA of HSA. At longer reaction time, the esterase activity of HSA decreases with increase in the concentration of SDS, whereas, surprisingly the activity increases with increasing concentration of CTAB. At 360 min, the esterase activity becomes 44 % and 98 % in presence of 20 mM SDS and CTAB respectively. In presence of 20 mM SDS the relative activity has been observed as 3 %, 9 %, 19 % and 44 % at 5 min, 40 min, 120 min and 360 min of the reaction respectively (Figure 4.8a); whereas in presence of 20 mM CTAB the relative activity has been observed as 40 %, 94 %, 97 % and 98 % (Figure 4.8b).

It has been observed that during the first 5 minutes of the reaction, the dependence of relative esterase activity of HSA with increasing concentration of

SDS is very high. However, when the reaction is allowed to happen for longer time (360 min), the observed dependence is completely different. Similarly, the change in the relative esterase activity of HSA with increasing concentration of CTAB is entirely different for shorter and longer time of the reaction. As previously mentioned, in first 5 minutes the reaction occurs with Tyr-411, which is present in the domain III of HSA, whereas at longer time many amino acid residues throughout the whole protein takes part in the hydrolysis. Thus the esterase activity results clearly manifest that the response of domain III of HSA towards the surfactant molecules is different from the response of the overall protein, which we have noticed from our domain specific study in sections 4.3.2. and 4.3.3.

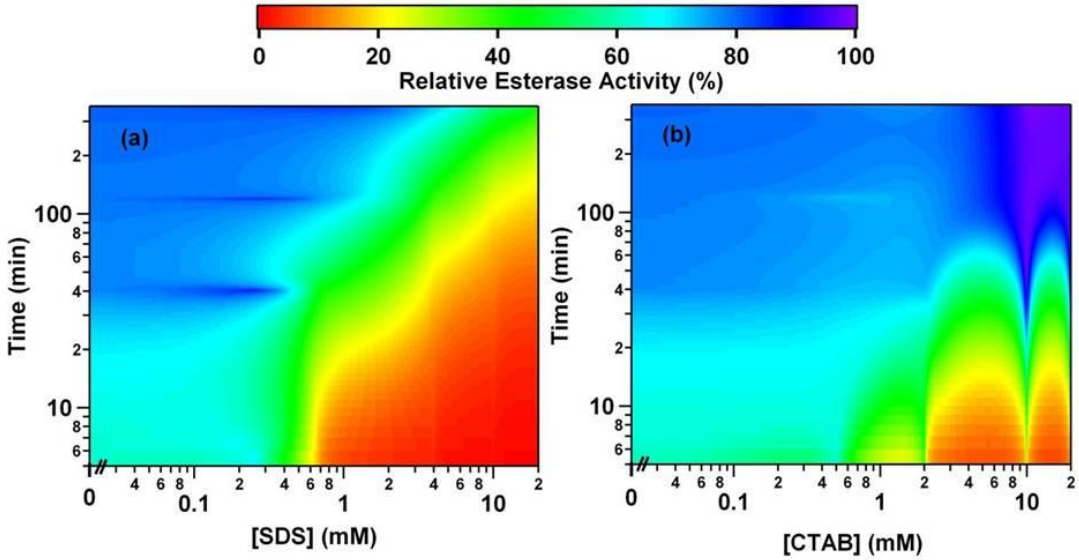

Figure 4.8. Change in the relative esterase activity of HSA with time and varying concentration of (a) SDS and (b) CTAB from 0 to 20 mM.

This is also note worthy to mention that the relative esterase activity of HSA increased from 80 % to 98 % in presence of 20 mM CTAB when the reaction was carried out for 360 minutes. Although, it is expected that on denaturation the activity will decrease, our result shows just the opposite behavior. Such an increase in the activity may be due to the unique protein-surfactant aggregates in this concentration ratio and need further study to understand it properly.

4.4. Conclusion

The present work elucidates the presence of intermediate state(s) in the interaction of anionic (SDS) and cationic (CTAB) surfactants with domain III of HSA using fluorescence spectroscopic techniques and ANS as fluorescent marker, which specifically binds to domain III of HSA (scheme 4.2). Interestingly, the signature of such intermediate state(s) was not observed when monitored by circular dichroism spectroscopy, which probes the global structural change of HSA, and distance of ANS from the Trp-214 in HSA. It reveals a continuous change in the global structure of HSA from its native state to the surfactant induced unfolded state without any involvement of intermediate state(s), unlike the domain III of HSA. The stepwise interaction of surfactants with domain III of HSA has been guided by the total concentration of surfactant present in the system. We have observed that surfactants interact more strongly at lower concentration region and on increase in the concentration the extent of interaction decreased. The relative esterase activity of HSA towards the hydrolysis of *p*-nitrophenyl acetate (PNPA) in presence of surfactants for different reaction time also supports our observation. It has been proposed that different parts of the multi-domain HSA have different affinities with the surfactants. This study is expected to provide useful insight into the site-specific interaction of the polar molecules in biological systems.

References:

1. (a) Singer, S. J.; Nicolson. G. L. *Science* **1972**, *175*, 720.
   (b) Lehninger, A. L.; Nelson, D. L.; Cox, M. M. *Principles of Biochemistry*, CBS Publications, New Delhi, **1987**.
2. Duggan, E. L.; Luck, F. M. *J. Biol. Chem*. **1948**, *172*, 205.
3. (a) Takeda, K.; Yamamoto, K. *J. Protein Chem.* **1990**, *9*, 17.
   (b) Moriyama, Y.; Takeda, K. *Langmuir* **1999**, *15*, 2003.
   (c) Moriyama, Y.; Takeda, K. *Langmuir* **2005**, *21*, 5524.
   (d) Moriyama, Y.; Watanabe, E.; Kobayashi, K.; Harano, H.; Inui, E.; Takeda, K. *J. Phys. Chem. B* **2008**, *112*, 16585.
4. (a) Hu, M.; Wang, X.; Wang, H.; Chai, Y.; He, Y.; Song, G. W. *Luminescence* **2012**, *27*, 204.
   (b) Singh, R. B.; Mahanta, S.; Guchhait, N. *Chem. Phys. Lett.* **2008**, *463*, 183.
   (c) Mahanta, S.; Singh, R. B.; Bagchi, A.; Nath, D.; Guchhait, N. *J. Luminescence* **2010**, *130*, 917.
   (d) Moyon, N. S.; Mitra, S. *J. Phys. Chem. B* **2011**, *115*, 10163.
5. (a) Gelamo, E. L.; *Spectrochim. Acta A* **2000**, *56*, 2255.
   (b) Gelamo, E. L.; Silva, C. H. T. P.; Imasato, H.; Tabak, M. Biochim. Biophys. Acta **2002**, 1594, 84.
6. (a) De, S.; Girigoswami, A.; Das, S. *J. Coll. Inter. Sci.* **2005**, *285*, 562.
   (b) Ding, Y.; Shu, Y.; Ge, L.; Guo, R. *Coll Surf A: Physicochem. Eng. Aspects* **2007**, *298*, 163.
   (c) Ospinal-Jimenez, M.; Pozzo, D. C. *Langmuir* **2012**, *28*, 17749.
7. (a) Anand, U.; Jash, C. *J. Phys. Chem. B* **2010**, *114*, 15839.
   (b) Anand, U.; Jash, C.; Mukherjee, S. *Phys. Chem. Chem. Phys.* **2011**, *13*, 20418.
8. (a) Kar, C.; Ojha, B.; Das, G. *Luminescence* **2013**, *28*, 339.
   (b) Mote, U. S.; Bhattar, S. L.; Patil, S. R.; Kolekar, G. B. *Luminescence* **2010**, *25*, 1.

9. (a) Mandal, U.; Ghosh, S.; Mitra, G.; Adhikari, A.; Dey, S.; Bhattacharyya, K. *Chem– An Asian J.* **2008**, *3*, 1430.
(b) Mukherjee, S.; Sen, P.; Halder, A.; Sen, S.; Dutta, P.; Bhattacharyya, K. *Chem. Phys. Let.* **2003**, *379*, 471.
10. (a) Chen, Z.; Liu, J.; Chen, X.; Zhang, T.; Han, Y. *Analyt. Sci*. **2007**, *23*, 1305.
(b) Chakraborty, A.; Seth, D.; Setua, P.; Sarkar, N. *J. Phys. Chem. B* **2006**, *110*, 16607.
11. (a) Vlasova, I. M.; Polyansky, D. V.; Saletsky, A. M. *Laser Phys. Lett*. **2007**, *4*, 890. (b) Vlasova, I. M.; Vlasov, A. A.; Saletsky, A. M. *J. Mol. Struct.* **2010**, *984*, 332.
(c) Vlasova, I. M.; Saletskii, A. M. *Mosc. Univ. Phys. Bull.* **2011**, *66*, 59.
12. (a) Peters, T. Jr. *All about albumin: Biochemistry, Genetics, and Medical Applications*, Academic press, San Diego, **1996**.
(b) Kragh-Hansen, U.; Chuang, V. T. G.; Otagiri, M. *Biol. Pharm. Bull.* **2002**, *25*, 695.
(c) Kosa, T.; Moruyama, T.; Otagiri, M. *Pharm. Res.* **1997**, *14*, 1607.
(d) Hu, Y.; Ou-Yang, Y.; Dai, C.; Liu, Y.; Xiao, X. *Biomacromolecules* **2010**, *11*, 106.
(e) Nanda, R. K.; Sarkar, N.; Banerjee, R. *J. Photochem. Photobiol. A: Chem.* ***2007***, *192*, 152.
13. (a) He, X. M.; Carter, D. C. *Nature* **1992**, *358*, 209.
(b) Curry, S.; Mandelkow, H.; Brick, P.; Franks, N. *Nature Struc. Biol.* **1998**, *5*, 827.
14. (a) Dugiaczyk, A.; Law, S.; Dennison, O. E. *Proc. Natl. Acad. Sci. U.S.A.* **1982**, *79*, 71.
(b) Carter, D. C.; Ho, J. X. *Adv. Protein Chem.* **1994**, *45*, 153.
15. Sugio, S.; Kashima, A.; Mochizuki, S.; Noda, M.; Kobayashi, K. *Protein Eng.* **1999**, *12*, 439.
16. Narazaki, R.; Maruyama, T.; Otagiri, M. *Biochim. Biophys. Acta* **1997**, *1338*, 275.

17. Sudlow, G.; Brikket, D. J.; Wade, D. N. *Mol. Pharmacol.* **1975**, *11*, 824.

18. (a) Bhattacharyya, K. *Chem. Commun.* **2008**, 2848.

(b) Bhattacharyya, K. *Acc. Chem. Res.* **2003**, *36*, 95.

(c) Yadav, R.; Sen, P. *Protein Sci.* **2013**, *22*, 1571.

(d) Pabbathi, A.; Patra, S.; Samanta, A. *ChemPhysChem*. **2013**, *14*, 2441.

19. Bagatolli, L. A.; Kivatinitz, S. C.; Aguilar, F.; Soto, M. A.; Sotomayor, P.; Fidelio, G. D. *J. Fluoresc.* **1996**, *6*, 33.

20. Bagatolli, L. A.; Kivatinitz, S. C.; Fidelio, G. D. *J. Pharm. Sci.* **1996**, *85*, 1131.

21. Kosower, E. M.; Kanety, H. *J. Am. Chem. Soc.* **1983**, *105*, 6236.

22. Upadhyay, A.; Bhatt, T.; Tripathi, H. B.; Pant, D. D. *J. Photochem. Photobiol. A: Chem* **1995**, *89*, 201.

23. Woody, R. W. *Theory of circular dichroism of proteins. In circular dichroism and conformational analysis of biomolecules,* G. D. Fasman, Ed.; Plenum publishing corp., New York, p. 25, **1996**.

24. Naidu, K. T.; Prabhu, N. P. *J. Phys. Chem. B* **2011**, *115*, 14760.

25. Xi-Zeng, F.; Rui-Xiang, J.; Yun, Q.; Xi-Wen, H. *Chem. J. Chinese. Univ.* **1996**, *17*, 866.

26. (a) Means, G. E.; Bender, M. L. *Biochemistry* **1975**, *14*, 4989.

(b) Lockridge, O.; Xue, W.; Gaydess, A.; Grigoryan, H.; Ding, S. J.; Schopfer, L. M.; Hinrichs, S. H.; Masson, P. *J. Biol. Chem.* **2008**, *283*, 22582.

(c) Ascenzi, P.; Gioia, M.; Fanali, G.; Coletta, M.; Fasano, M. *Biochem. Biophys. Res. Comm.* **2012**, *424*, 451.

(d) Kelly, S. M.; Price, N. C. *Curr. Prot. Pept. Sci.* ***2000***, *1*, 349.

27. (a) Sahu, K.; Mandal, S. K.; Ghosh, S.; Roy, D.; Bhattacharyya, K. *J. Chem. Phys.* **2006**, *124*, 124909.

(b) Yadav, R.; Das, S.; Sen, P. *Aust. J. Chem.* **2012**, *65*, 1305.

(c) Lakowicz, J. R. *Principles of fluorescence spectroscopy*, 3rd edn, Springer: New York **2006**.

28. Cordova, J.; Ryan, J. D.; Boonyaratanakornkit, B. B.; Clark, D. S. *Enzyme Microb. Technol.* **2008**, *42*, 278.

Chapter 5

Mechanistic Investigation of Domain Specific Unfolding of Human Serum Albumin and the Effect of Sucrose

Rajeev Yadav *et al*., *Protein Sci.* **2013**, *22*, 1571.

Present study is devoted to understand the unfolding mechanism of a multi-domain protein, human serum albumin (HSA), in absence and presence of sucrose by steady-state and time-resolved fluorescence spectroscopy with domain specific marker molecules and is further being substantiated by molecular dynamics simulation. In water, the domain III of HSA found to unfold first followed by domains I and II as the concentration of GnHCl is increased in the medium. The sequential unfolding behavior of different domains of HSA remains same in presence of sucrose; however, a higher GnHCl concentration is required for unfolding, suggesting stabilizing effect of sucrose on HSA. Domain I is found to be most stabilized by sucrose. The stabilization of domain II is somewhat similar to domain I, but the effect of sucrose on domain III is found to be very small. Molecular dynamics simulations also predicted a similar behavior of sucrose on HSA. The stabilizing effect of sucrose is explained in terms of the entrapment of water molecules in between HSA surface and sucrose layer as well as direct interaction between HSA and sucrose.

5.1. Introduction

The characterization of folding pathway of a multi-domain protein is a complex process by virtue of the presence of different domains, that folds/unfolds independently, and their mutual interactions to form the globally stabilized tertiary structure.[1-2] The complete understanding of the unfolding process require a detailed domain specific study and thus establish the complete denaturation landscape. Human serum albumin (HSA) is such a multi-domain protein with three different distinguishable domains and has been studied widely in the last few decades.[2-6-11] The single tryptophan (Trp, Scheme 5.1) unit of HSA is located in domain II and often the Trp fluorescence was used to study this domain selectively.[7,10] However, the selective study of domain III is rare in the literature as no intrinsic fluorophore is present in this domain.[12-14] Bagatolli *et al*. studied the binding of 8-anilino-1-naphthalenesulphonate (ANS, Scheme 5.1) in HSA and found that it selectively bind to the domain III with very high binding constant of 0.87×10^6 M^{-1} and proposed ANS as marker for domain III.[15] On the other hand, hemin (Scheme 5.1) is known to bind to domain I and can be used for the selective characterization of domain I.[16,17]

Since the function of proteins depends on their three-dimensional structure, several researchers put on their efforts to found suitable agent which combat the denaturation process under adverse condition.[18-22] Several sugars are found to act as a stabilizing agent for proteins and have been a subject of study for last few decades.[20-34] It has also been noticed that different sugars, eg. trehalose, sucrose, maltose, fructose, glucose, etc., have different stabilizing power for different proteins. There are some hypothesis regarding the stabilization of protein in presence of sugar given by different authors as - (i) The water replacement hypothesis;[23,24] according to which the stabilization occurs via the formation of hydrogen bonds between the sugar and the biomolecules, (ii) The water-entrapment hypothesis;[25] in this case, trapping of water molecules in between protein surface and sugar layer is the main stabilizing mechanism which slows

down the biological water, (iii) Mechanical-entrapment hypothesis;[33] here the entrapment of a particular biomolecular conformation takes place in a high viscous sugar matrix and, (iv) Broken glass hypothesis;[34] in this case, the direct interaction between protein and sugar takes place as well as water entrapment occurs in the system. Alfonso *et al*. demonstrated the stabilizing effect of trehalose on beta-lactoglobulin (BLG) by using fluorescence lifetime and fluorescence anisotropy measurements. They revealed that addition of trehalose shifts the midpoint of BLG denaturation profiles towards higher denaturant concentration with a 60% increase in the free energy of denaturation.[27] Their conclusion indicates the mechanical-entrapment hypothesis is in operation in this case. MD simulations of aqueous lisozyme in presence and absence of trehalose have been performed by Lins *et al*. and support the second hypothesis of water entrapment for the stabilization.[28] Whereas in 2010 Fedorov *et al*. showed that trehalose forms patches on the surface of lysozyme and support fourth hypothesis i.e. broken glass hypothesis.[34] It has been observed that the stabilization power of different sugars varies for different proteins. Trehalose was found to be a better stabilizing agent than sucrose for BLG, carboxy myoglobine, etc.[35], whereas, for azurin, the stabilizing power of sucrose is found to be higher than trehalose.[20] Sola-Penna and Roberto suggested that trehalose is more effective because it occupies at least 2.5 times larger volume than other sugars[31] and this stabilization is fully explained by the mechanical entrapment hypothesis.[28] In general, the stabilization effect of sucrose is almost same of the trehalose, if concentration of sucrose is almost 3 times higher than that of trehalose.[31]

Nevertheless, for a multi-domain protein the unfolding pathway of different domains in absence and presence of sucrose is expected to be different. However, such a study has not been performed in the past to the best of our knowledge and we intend to pursue this using HSA as the model multi-domain protein. In the present study we used guanidine hydrochloride as the denaturant to investigate the effect of sucrose on the denaturation profile of three different domains of HSA. We

also have performed atomistic molecular dynamics (MD) simulations and calculate the fluctuation of different domains of HSA to have a molecular level picture.

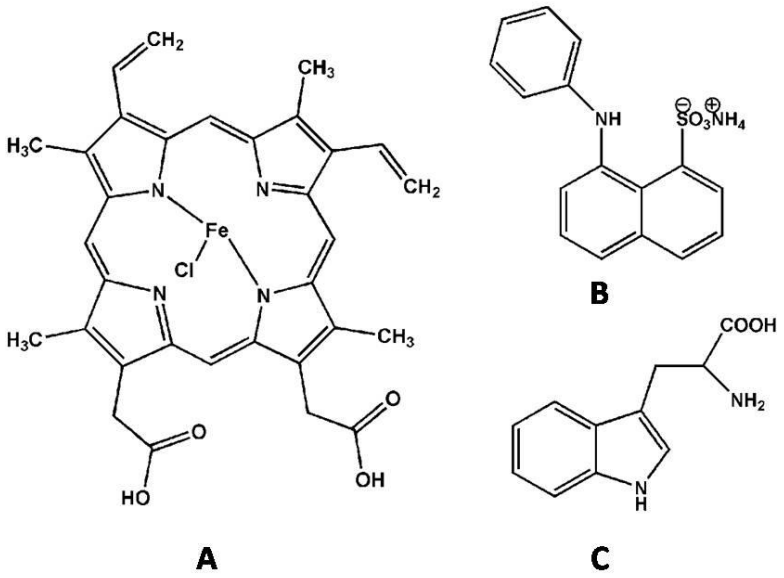

Scheme 5.1. Molecular structure of (a) hemin, (b) 8-anilinonaphthalene-1-sulphonic acid ammonium salt and (c) tryptophan.

5.2. Data Analysis

The unfolding of HSA was done by GnHCl as chemical denaturant and is known to follow a two step unfolding (N $\rightleftharpoons$ U), where N and U are the native and denatured states of HSA.[4] The equilibrium constant (*K*) of the native to denatured state transformation can be calculated as,[2a,2c]

$$K = \frac{\tau_N - \tau}{\tau - \tau_U} \quad or \quad \frac{FQ_N - FQ}{FQ - FQ_U} \tag{5.1}$$

where τ_N and τ_U are the fluorescence lifetimes of protein in folded and unfolded state respectively, whereas, FQ_N and FQ_U are the relative fluorescence quenching in the native and unfolded states respectively. Here, τ and FQ are the fluorescence lifetimes and relative fluorescence quenching of HSA at different denaturant concentration. The observed value of *K* was used to calculate free energy change (ΔG) between native and unfolded states using following equation.

$$\Delta G = -RT \ln K \qquad (5.2)$$

Where R is the universal gas constant (1.987 cal K^{-1} mol^{-1}) and T is the absolute temperature. The free energy change in the absence of denaturant (ΔG^0) can be calculated by extrapolation method by fitting the data observed in equation 5.2 as a function of denaturant using,[2a]

$$\Delta G = \Delta G^0 - m[D] \qquad (5.3)$$

where m is the slope, which measures the dependence of ΔG on denaturant. The concentration of denaturant to unfold 50% of the protein ($[D]_{1/2}$) can be written as,

$$[D]_{1/2} = \frac{\Delta G^0}{m} \qquad (5.4)$$

5.3. Results

5.3.1. Study of Domain III

Domain III of HSA has been studied by using the extrinsic fluorophore ANS.[15,36-41] Bagatolli *et al*. used diazepam and aspirin as a marker and revealed that ANS binds to domain IIIA with high affinity (K = 0.87 x 10^6 M^{-1}) and to domain IIA with low affinity (K = 0.079 x 10^6 M^{-1}).[28] Thus it is important to carefully choose the relative concentration of ANS to HSA, because at higher concentration it can also bind to the lower affinity site. At a relative concentration of ANS to HSA < 10^3 it preferentially binds to domain III[38] and in the present study ANS/HSA ratio is maintained at 0.5. The concentration of HSA is maintained at 10 μM for all the studies. This is to mention that at this ANS to HSA concentration ratio, the secondary structure of HSA remains unchanged. ANS in water is characterized with absorption maximum at 374 nm and emission maximum at ~520 nm with a very low fluorescence quantum yield of 0.003.[15] On binding to HSA, the fluorescence property of ANS changes dramatically with a

large blue shift of its emission maximum to 465 nm and increase in fluorescence quantum yield to 0.67, without much affecting its absorption characteristics. It is to be noted that the ANS have two emissive states; non-planar (NP) state where ANS remains non-planar and charge transfer (CT) state where molecule become planer and charge transfer takes place. In polar media, the locally excited (LE) state readily formed the non-emissive CT state and thus the fluorescence quantum yield of ANS in water is very low. In low polarity media, the emission predominantly occurs from the LE state which results in the blue shift of the emission maximum and increase in the fluorescence quantum yield.[36a] On denaturation the absorption spectrum of ANS does not change much, however, the fluorescence response of ANS is found to be depend strongly on denaturation. Till 1.5 M GnHCl the fluorescence quantum yield is found to decrease slowly with a mere change of its maximum. On further increase in GnHCl concentration, the fluorescence intensity decreases rapidly with a notable red shift of the emission maximum (Figure 5.1). To have a first look on the effect of sucrose on denaturation, we repeat the same experiment in presence of 1 M sucrose. The emission maximum of ANS in HSA with 1 M sucrose was observed at 464.5 nm with fluorescence quantum yield of 0.63 in native state which is almost similar in absence of sucrose. However, the effect of GnHCl is found to be completely different (Figure 5.1). In presence of sucrose, the emission maximum of ANS remains unchanged till 2.5 M GnHCl. To get a better picture on the effect of sucrose on denaturation pathway of domain III, we measured the fluorescence transients of ANS bound to HSA at different GnHCl concentration in absence and presence of sucrose, which are shown in figures 5.2a and 5.2b, respectively. The average lifetime of ANS bound to HSA with increase in the GnHCl concentration in absence and presence of sucrose are shown in figure 5.3 and are tabulated in table 5.1. ANS displays a triple exponential fluorescence decay behavior with three distinct lifetime components of 0.75 ns (0.01), 7.47 ns (0.15) and 18.13 ns (0.84) with an average lifetime of 16.36 ns in the native state of HSA, when no sucrose is present in the system. On denaturation, the fluorescence lifetime of ANS in HSA

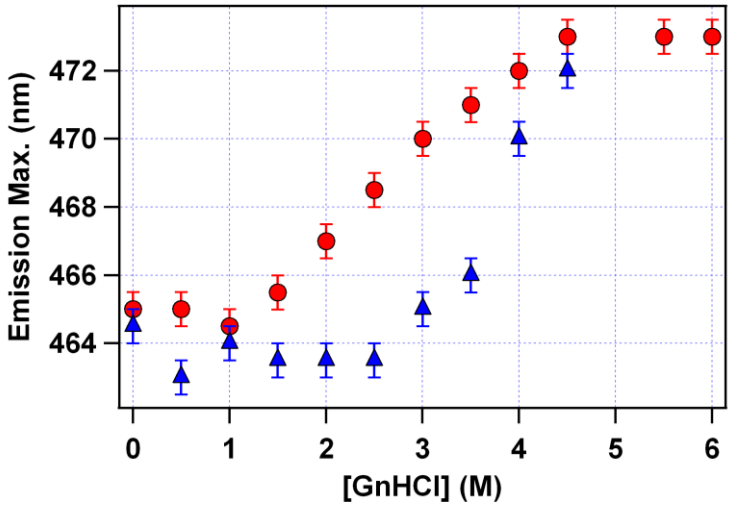

Figure 5.1. Plot of ANS emission maxima in the absence (●) and in presence (▲) of 1 M sucrose as a function of GnHCl concentration. Here the error bars are obtained by averaging the associated errors of all the data points.

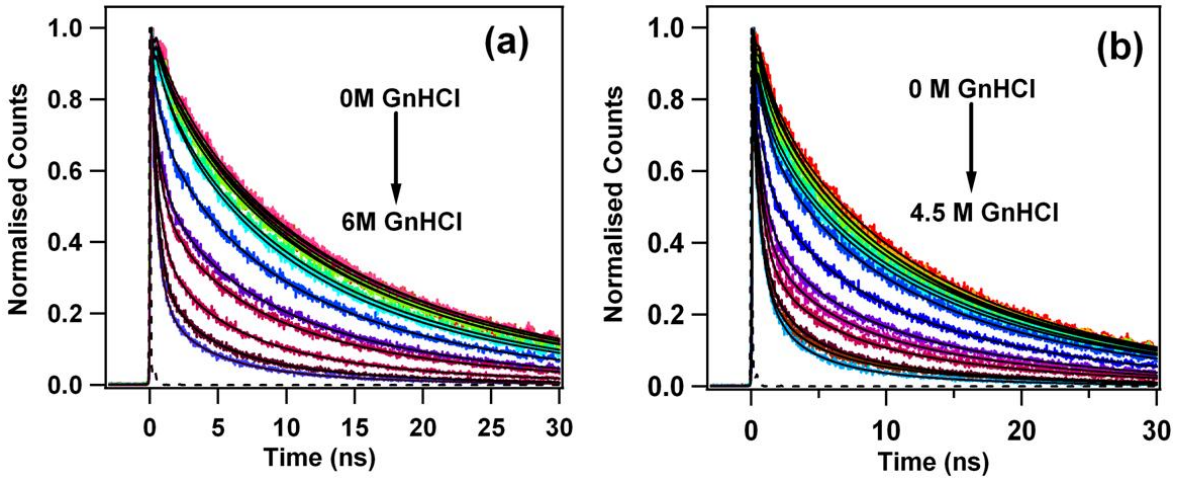

Figure 5.2. Fluorescence transients of ANS in HSA (λ_{ex} = 375 nm and λ_{em} = 470 nm) (a) in absence and (b) in presence of 1 M sucrose on increasing GnHCl concentration. Instrument response function is shown by dashed line. Solid lines represent the best fit to a tri-exponential function.

keeps on decreasing monotonically and at 3.2 M GnHCl, the three fluorescence lifetime components are 0.26 ns (0.27), 2.51 ns (0.44) and 7.05 ns (0.29) with an average lifetime of 3.22 ns. In presence of 1 M sucrose the average lifetime of ANS in native HSA is found to be 16.18 ns which is almost same as in absence of sucrose. However, at 3.2 M GnHCl the fluorescence lifetime of ANS is measured as 4.03 ns, which is 1.25 times higher compared to when sucrose is not present in

the medium. On further increasing the GnHCl concentration till 4 M, the average lifetime of ANS bound to HSA becomes 3.36 ns, which is very similar to the average lifetime of ANS in 3.2 M GnHCl when sucrose is absent. It shows that the denaturation profile of domain III of HSA in absence and presence of 1 M sucrose are different and a relatively high concentration of denaturant is required to unfold the domain III of HSA in presence of 1 M sucrose.

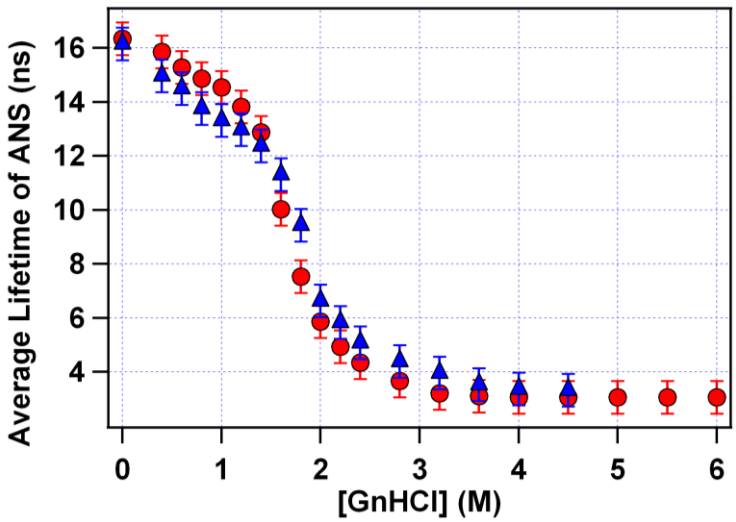

Figure 5.3. Plot of Average lifetime of ANS in HSA (●) in the absence and (▲) in the presence of 1 M sucrose as a function of GnHCl concentration. Here the error bars are obtained by averaging the associated errors of all the data points.

Table 5.1. Fluorescence lifetimes of ANS in HSA for different concentrations of GnHCl, in absence and presence of sucrose.

Sucrose (M)	**GnHCl (M)**	**τ_1 [a] (a_1) ns**	**τ_2 [a] (a_2) ns**	**τ_3 [a] (a_3) ns**	**$\langle\tau\rangle$ [a] (ns)**
0	0	0.75 (0.01)	7.47 (0.15)	18.13 (0.84)	**16.36**
0	1	0.63 (0.02)	6.21 (0.17)	16.72 (0.81)	**14.61**
0	2	0.35 (0.21)	3.36 (0.32)	10.12 (0.47)	**05.90**
0	3.2	0.26 (0.27)	2.51 (0.44)	07.05 (0.29)	**03.22**
0	4.5	0.23 (0.28)	2.03 (0.43)	07.29 (0.29)	**03.06**
1	0	0.52 (0.01)	5.73 (0.15)	18.23 (0.84)	**16.18**
1	1	0.53 (0.03)	5.05 (0.18)	16.03 (0.79)	**13.58**
1	2	0.39 (0.22)	3.45 (0.29)	11.32 (0.49)	**06.63**
1	3.2	0.31 (0.24)	2.19 (0.37)	08.07 (0.39)	**04.03**
1	4.5	0.32 (0.25)	2.04 (0.39)	07.22 (0.36)	**03.47**

$\langle\tau\rangle = a_1\tau_1 + a_2\tau_2 + a_3\tau_3$, [a] ± 0.2

5.3.2. Study of Domain II

The fluorescence properties of single tryptophan (Trp) residue in domain II of HSA is used to probe the unfolding behavior of this domain selectively. The absorption spectrum of HSA have the contribution from this single Trp solely around 290 nm region with its characteristic emission centered at 347 nm with a 295 nm excitation. On denaturation, the emission maximum of Trp changes with decrease in the fluorescence intensity. Till 1.75 M GnHCl, the emission maximum shows a 5.5 nm blue shift and then it starts shifting to the longer wavelength as is shown in figure 5.4. For 4.5 M GnHCl the maximum is observed at 357 nm. To investigate the effect of sucrose on the denaturation profile of domain II of HSA, same experiment has been performed in the presence of 1 M sucrose. In presence of 1 M sucrose, the Trp emission of native HSA is characterized with a maximum at 348 nm, which is almost similar as in the absence of sucrose, although there is a small decrease in the fluorescence intensity. Like in absence of sucrose, an initial blue shift of the emission maximum of Trp is also observed with increase in GnHCl concentration until 2.25 M. On further increasing the GnHCl concentration, the emission maximum start shifting to the red and at 4.5 M GnHCl concentration the emission maximum is found to be at 359 nm (see figure 5.4). At a first glance, this observation indicates sucrose also stabilizes the domain II of HSA. To better understand this behavior we measure the lifetime of Trp for different GnHCl concentration by recording the fluorescence transients. In bulk water, the fluorescence decay of Trp in HSA is biexponential in nature with two time constants of 3.12 ns (0.37) and 7.10 ns (0.63), having an average lifetime of 5.62 ns. The lifetime of Trp decreases monotonically with the increase in the GnHCl concentration. At 4.5 M GnHCl, the fluorescence decay can be best fitted with two time constants of 1.39 ns (0.46) and 3.51 ns (0.54) with an average lifetime of 2.54 ns. In presence of 1 M Sucrose, the average lifetime of Trp in HSA is found to be 6.63 ns and 3.08 ns in the native and unfolded (with 4.5 M GnHCl) state respectively. The observed fluorescence transients are shown in figures 5.5a and 5.5b and the data are tabulated in table 5.2. Figure 5.6 shows the variation of the

average lifetime of Trp in HSA as a function of GnHCl concentration. It can be readily seen that in absence of sucrose, domain II become fully denatured at 4.5 M GnHCl, which remains unchanged till 6 M of GnHCl. In presence of 1 M sucrose the average lifetime of Trp in HSA with 4.5 M GnHCl is clearly high compared to in the absence of sucrose. This indicates the protective nature of sucrose for domain II of HSA.

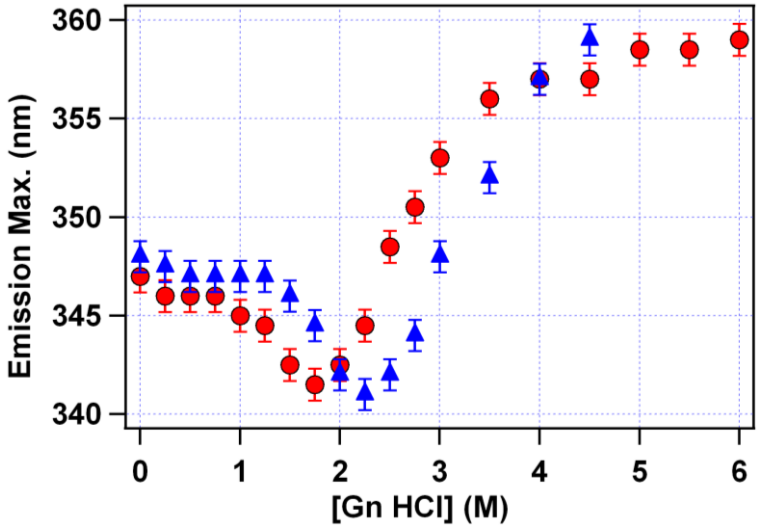

Figure 5.4. Tryptophan emission maxima in the absence (●) and in the presence (▲) of 1 M sucrose as a function of GnHCl concentration. Here the error bars are obtained by averaging the associated errors of all the data points.

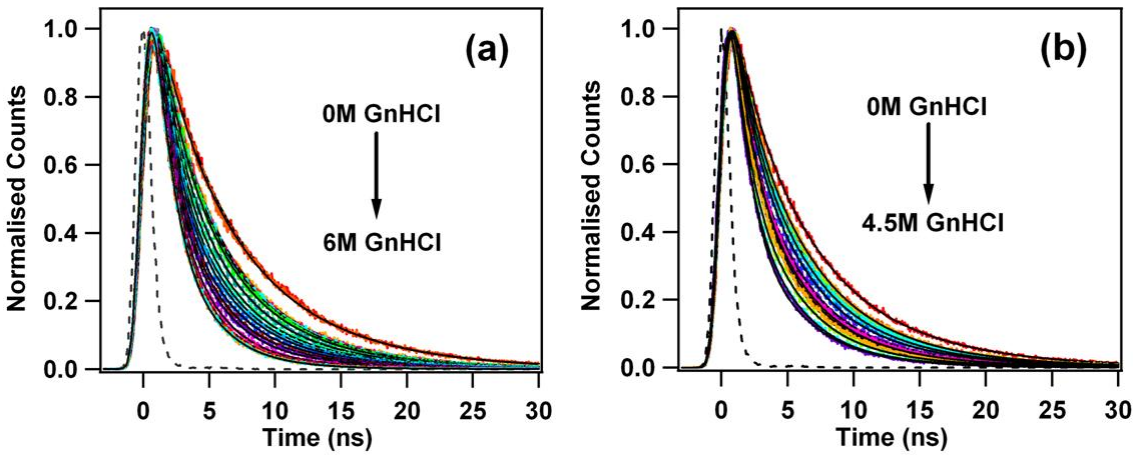

Figure 5.5. Fluorescence decays of tryptophan in HSA (λ_{ex} = 280 nm and λ_{em} = 350 nm) (a) in the absence and (b) in presence of 1 M sucrose on increasing GnHCl concentration. Instrument response function is shown by dashed line. Solid lines represent the best fit to a bi-exponential function.

Table 5.2. Fluorescence lifetimes of Trp in HSA for different concentrations of GnHCl, in absence and presence of sucrose.

Sucrose (M)	GnHCl (M)	τ_1 [a] (a_1) ns	τ_2 [a] (a_2) ns	$\langle\tau\rangle$ [a] ns
0	0	3.12 (0.37)	7.10 (0.63)	**5.62**
0	1	2.88 (0.34)	6.61 (0.66)	**5.33**
0	2	2.25 (0.43)	6.01 (0.57)	**4.39**
0	3	1.80 (0.52)	4.97 (0.48)	**3.32**
0	4.5	1.39 (0.46)	3.51 (0.54)	**2.54**
0	6	1.40 (0.47)	3.34 (0.53)	**2.42**
1	0	2.46 (0.24)	6.63 (0.76)	**5.63**
1	1	2.28 (0.27)	6.39 (0.73)	**5.28**
1	2	1.99 (0.33)	5.80 (0.67)	**4.54**
1	3	1.83 (0.41)	5.51 (0.59)	**4.00**
1	4.5	1.21 (0.38)	4.22 (0.62)	**3.08**

$\langle\tau\rangle = a_1\tau_1 + a_2\tau_2$

[a] $\pm$ 0.2

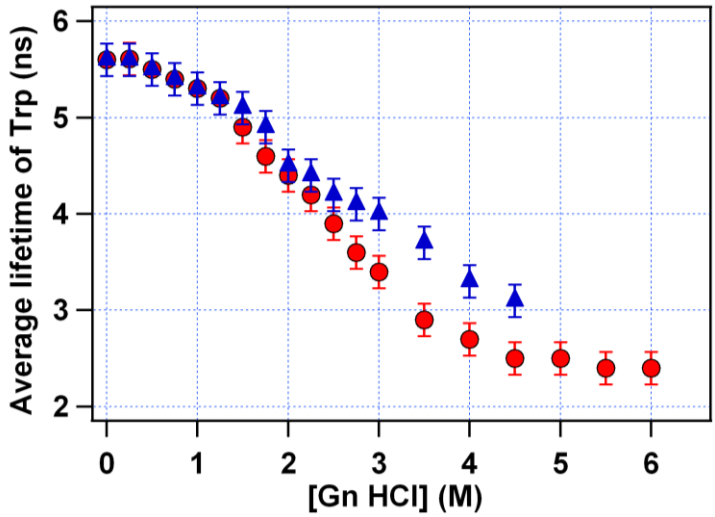

Figure 5.6. Plot of Average lifetime of tryptophan in HSA (●) in the absence and (▲) in the presence of 1 M sucrose with increase in the GnHCl concentration. Here the error bars are obtained by averaging the associated errors of all the data points.

5.3.3. Study of Domain I

To study of domain I, we have used hemin as quencher which selectively binds to the domain I of HSA.[13,16,17] Dockal *et al*. showed that hemin also binds to other secondary binding sites located in domain II and III of HSA at the molar ratio

of hemin/HSA as 2.[16] Hence, in the present study hemin/HSA ratio is maintained at 0.5. CD spectra confirm that at this low hemin concentration the secondary structure of HSA remains unchanged. Hemin quenches the intrinsic Trp fluorescence of HSA, which depends on the relative distance between them.[16,17] In native state, the relative fluorescence quenching of Trp with hemin is found to be 34.8%. On denaturation the relative fluorescence quenching of Trp by hemin decreases monotonically and at 4.5 M GnHCl it is found to be 6.8% which remain unchanged on further increase of GnHCl concentration. To understand the effect of sucrose on denaturation profile of domain I, we repeat the same experiment in presence of 1 M sucrose. The hemin mediated relative fluorescence quenching of HSA as a function of GnHCl shows a different behavior in presence of 1 M sucrose compared to otherwise as shown in figure 5.7 and table 5.3. In presence of 1 M sucrose the relative fluorescence quenching of native HSA is measured to be 35.8% and become 13.3% at 4.5 M GnHCl. This suggests that at 4.5 M GnHCl the domain I of HSA is less denatured in presence of sucrose compared to when sucrose is not present in the medium.

Table 5.3. Relative fluorescence quenching (%) at 340 nm of HSA for different concentrations of GnHCl, in absence and presence of sucrose.

Sucrose (M)	**GnHCl (M)**	**Relative Fluorescence Quenching (%)[a]**
0	0	**34.8**
0	1.25	**30.1**
0	2	**25.0**
0	3	**12.7**
0	4.5	**6.8**
0	6	**6.1**
1	0	**35.8**
1	1	**32.6**
1	2	**28.0**
1	3	**20.2**
1	4.5	**13.3**

[a] ± 2%

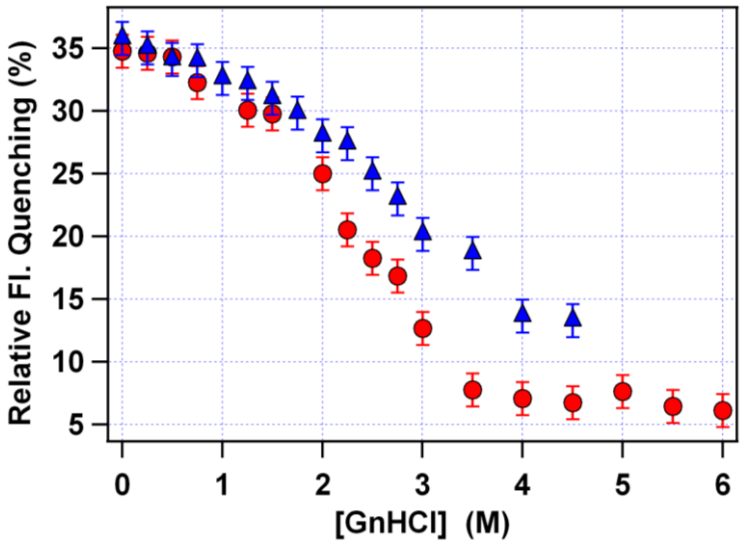

Figure 5.7. Relative tryptophan fluorescence quenching by hemin (●) in the absence and (▲) in the presence of 1 M sucrose as a function of GnHCl concentration. Here the error bars are obtained by averaging the associated errors of all the data points.

5.3.4. Molecular Dynamics Simulations

To have a molecular level understanding of the effect of sucrose on different domains of HSA, Atomistic molecular dynamics (MD) simulations at 300 K have been performed for aqueous solution of HSA in presence and absence of 1 M sucrose, under the periodic boundary condition. The initial coordinate of HSA was obtained from the Protein Data Bank (PDB ID: 1HA2).[42] For both cases, we have used Packmol[43] for fixing the protein at the center of a box with edges 104×66×106 $Å^3$ and were solvated with the TIP3P water molecules.[44] Sucrose molecules, when present, were uniformly distributed throughout the box with a distance of 5 Å from protein surface as well as from each other. The HSA-water system contains one HSA and 20837 water molecules, whereas the HSA-water-sucrose system contains one HSA, 420 sucrose and 6394 water molecules. For both the cases, solutions were neutralized by addition of 13 sodium ions. After minimization as shown in chapter 2, each system was equilibrated for 20 ps with restrained the protein and sucrose (when present). In case of HSA-water-sucrose a further 30 ps equilibration has been done holding the protein alone. Finally the MD simulation has been

carried out for 2.5 ns by maintaining the temperature at 300 K with the help of Langevin dynamics.[45]

It is to mention that during the course of the simulation, HSA remained in the folded state. The variation of potential energy and kinetic energy with time satisfied the energy conservation criteria in MD simulation and there was no change detected after an initial drift in total energy of the system for both the cases under investigation. The protein radius of gyration as well as solvent accessible surface area has also been calculated to see the compactness of protein structure in absence and presence of sucrose. Figure 5.8 shows the similar values of radius of gyration for HSA in absence and presence of sucrose as a function of time. Solvent accessible surface area for HSA has been calculated as 32238 $Å^2$ and 31456 $Å^2$ in absence and presence of sucrose respectively by using probe radius as 1.4 Å. The root mean-square atomic positional deviation (RMSD) as well as root mean-square atomic positional fluctuations (RMSF) have been calculated for α-carbon atoms of the protein after a proper alignment. The calculated RMSD and RMSF are shown in figures 5.9a and 5.9b, respectively. It has been observed that RMSD is small when sucrose is present in the system and it can be regarded as the stabilization of HSA by sucrose. The observed fluctuations in all residues are not uniform in either case. Radial distribution functions corresponding to the water in absence of sucrose as well as water and sucrose in presence of sucrose around the centre of geometry of HSA have also been calculated and shown in figure 5.10. It shows that some water molecules in presence of sucrose come closer to the protein

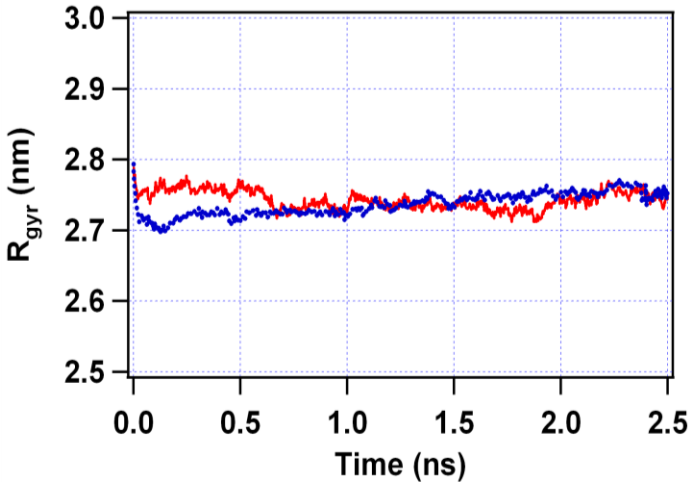

Figure 5.8. Radius of gyration (Rgyr) of HSA as a function of time in absence (red line) and presence (blue dotted line) of 1 M sucrose.

surface than in absence of sucrose. The average number of hydrogen bonds between the amino acid residues and water in different domains has also been calculated for both the cases. It shows that there was 27%, 40% and 38% increase in the number of hydrogen bonds for domain I, domain II and domain III respectively in presence of sucrose.

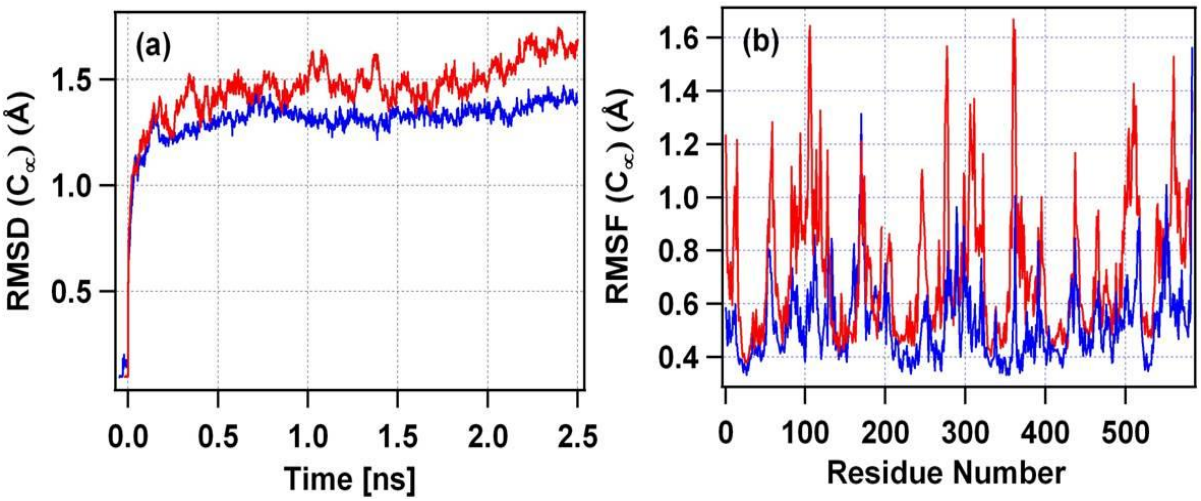

Figure 5.9. (a) Root mean square atomic positional deviation (RMSD) of α-C atoms of HSA as a function of time and (b) root mean square atomic positional fluctuations (RMSF) of α-C atoms of different amino acid residues of HSA averaged over 1.5 ns to 2.5 ns of MD simulation, in the absence (—, red line) and in the presence (—, blue line) of 1 M sucrose.

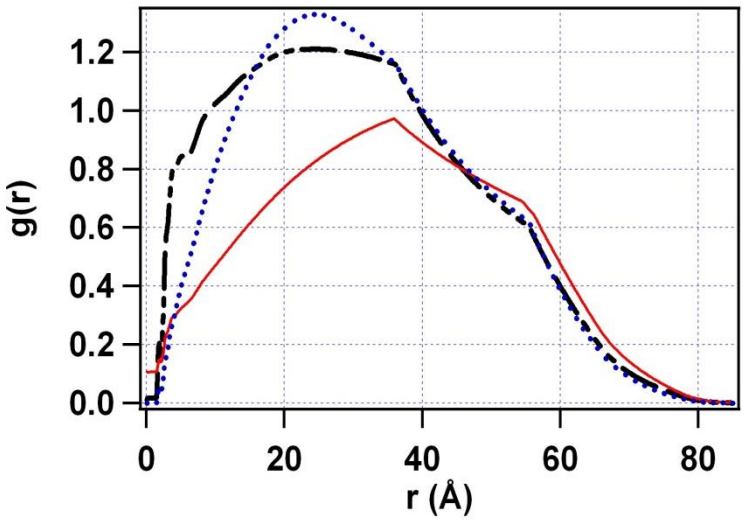

Figure 5.10. Radial distribution function for water around the center of geometry of HSA in absence of sucrose (—, red line), for water around the center of geometry of HSA in presence of sucrose (−•−, black line) and for sucrose around the center of geometry of HSA (•••••, blue line).

5.4. Discussion

The main aim of the present work is to investigate the unfolding mechanism of different domains of HSA and also to study the effect of sucrose therein. As mentioned above, we have used different marker molecules for different domains, namely hemin for domain I, intrinsic Trp-214 for domain II and ANS for domain III respectively. The change in the fluorescent response of a fluorophore in a protein matrix during its unfolding process is a well known phenomenon in the literature and is explained in terms of the increase in the non-radiative pathway of the fluorophore in more polar solvents (generally water) when exposed due to the unfolding of the protein which is the case for Trp and ANS in domain II and III, respectively.[14,36] For domain I the relative fluorescence quenching of Trp by hemin, which depends on their relative distance, has been used to monitor the unfolding process.

Using equation 5.1 and 5.2 first we have calculated the change in the free energy of unfolding for different GnHCl concentrations and consequently calculated $[D]_{1/2}$ (concentration of denaturant for 50% unfolding) using equation 5.3 and 5.4. The variation of ΔG as a function of GnHCl concentration for domain I, II and III is shown in figure 5.11 (a, b, and c) respectively. The linear dependence of ΔG on GnHCl concentration also confirms the two step unfolding process of HSA and is the case for individual domains. The estimated values of $[D]_{1/2}$ for domain I, II and III are 2.3 M, 2.4 M and 1.6 M GnHCl respectively. This clearly indicates the whole protein does not unfold uniformly and our results also suggest that domain III of HSA is most unstable and denatured first followed by almost simultaneous denaturation of domains I and II (scheme 5.2). This is to mention here, we have used the relative fluorescence quenching of Trp by hemin (reside in domain I of HSA) to study the unfolding behavior of domain I. Obviously, the change in the tertiary structure of domain II has also contributed to the domain I probing. In presence of sucrose, the $[D]_{1/2}$ values are also calculated

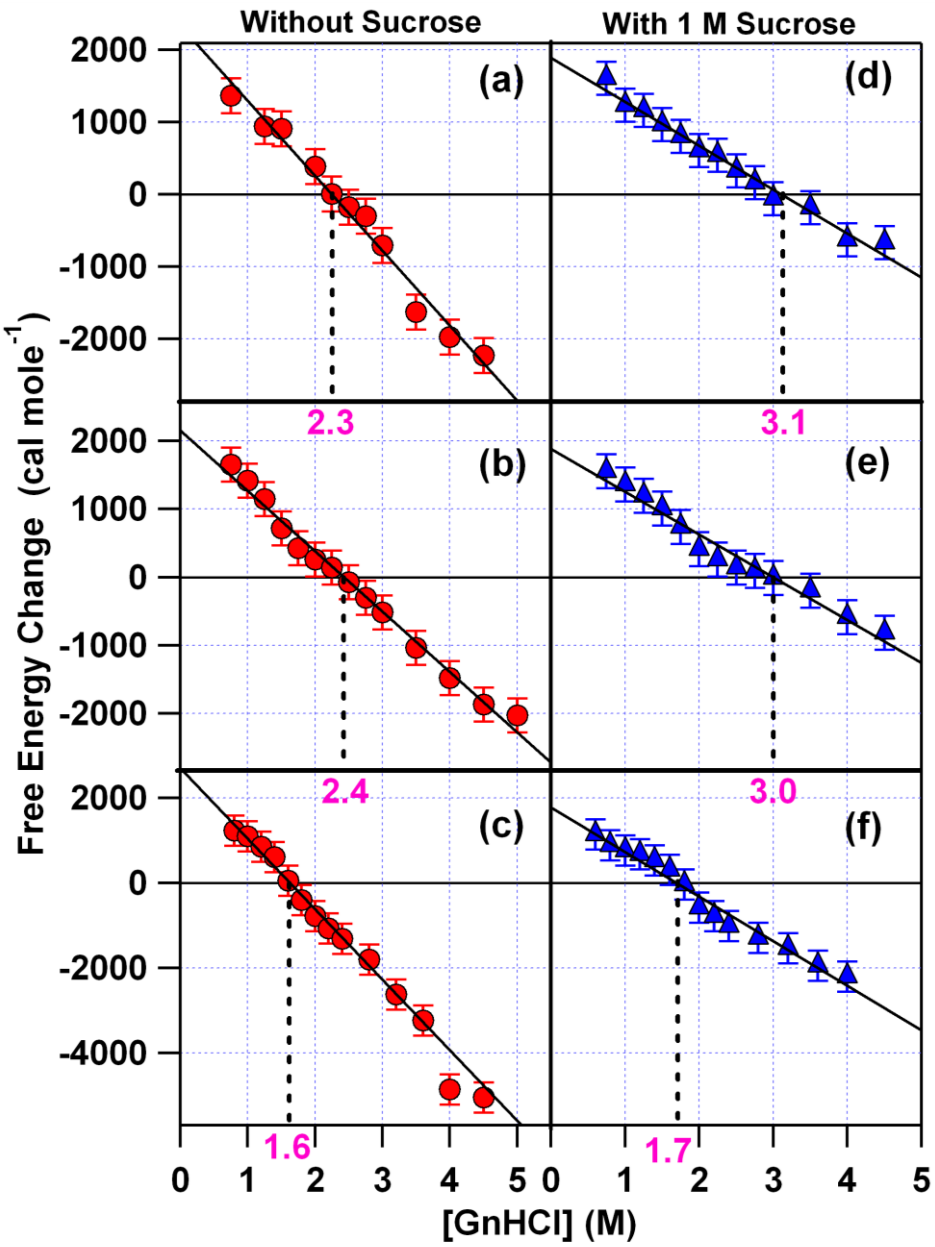

Figure 5.11. Free energy change during denaturation for domain I (a, d), domain II (b, e) and domain III (c, f) as a function of GnHCl concentration (●) in the absence and (▲) in the presence of 1 M sucrose. Solid lines represent the best fit with equation 5.3. Here the error bars are obtained by averaging the associated errors of all the data points.

in the same fashion and found to be 3.1 M, 3.0 M and 1.7 M GnHCl for domains I, II and III respectively (see figures 5.11 d, e and f). Here also the unfolding of domain III happens first followed by domains II and I. However, it is interesting to note that, the value of $[D]_{1/2}$ in presence of sucrose is found to be more compared to in the absence of sucrose, which is an indication of the sucrose mediated

stabilization of HSA towards its unfolding by GnHCl. The difference in the $[D]_{1/2}$ values ($\Delta[D]_{1/2} = [D]_{1/2}^{sucrose}-[D]_{1/2}^{water}$) for domain I, II and III are calculated to be 0.8 M, 0.6 M and 0.1 M GnHCl respectively. Understandably, the stabilization provided by sucrose for different domains of HSA are not same. Domain I gets more stability by sucrose followed by domain II and III. The low value of $\Delta[D]_{1/2}$ for domain III (0.1 M GnHCl) suggests a mere gain in stabilization for this domain which is not the case for other domains.

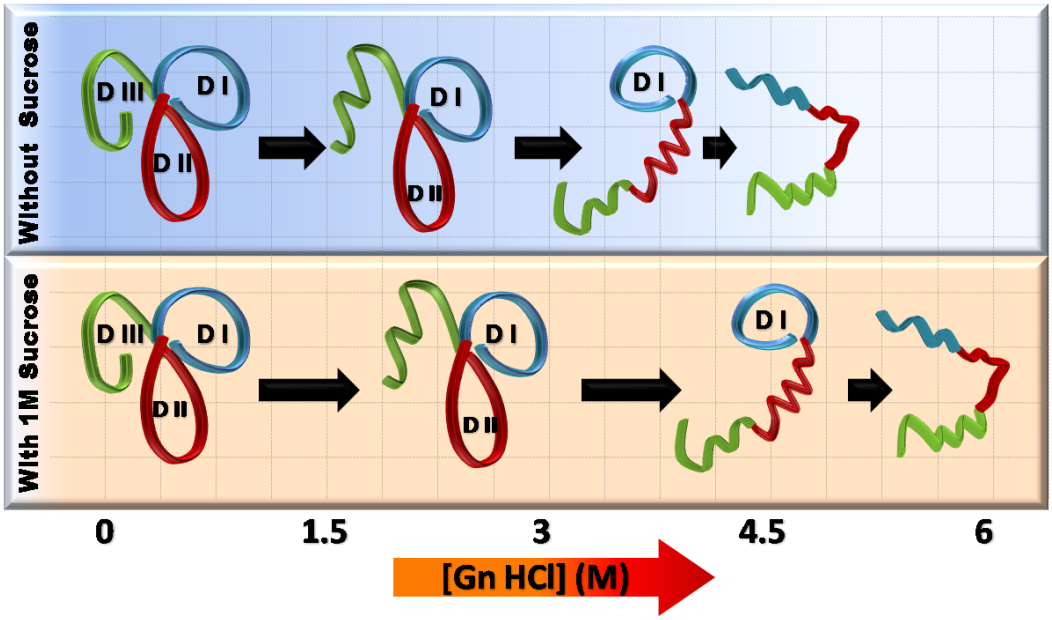

Scheme 5.2. Schematic representation for unfolding of all three domains of HSA as a function of GnHCl concentration and the effect of sucrose.

Molecular dynamics simulations also qualitatively represents the protective nature of sucrose on HSA unfolding, as evident from the lower and comparatively stable RMSD value of α - carbon atoms of HSA when sucrose is present in the system (see figure 5.9a). From figure 5.9b, we can see that the sucrose induced stabilization of RMSF values for different residues of HSA are not uniform in nature. For the hemin binding site of domain I (residue number 102 to 190) the average stabilization of RMSF value is found to be 0.14 Å, and for Trp environment in domain II (residue number 197 to 297) the value is calculated to be 0.16 Å. This is to note that the stabilization of the above two sites are almost same.

In case of ANS binding site in domain III (residue number 384 to 497) the stabilization of RMSF value is found to be 0.11 Å.[9,10a,17] MD simulation thus predicts the lowest sucrose mediated stabilization of domain III binding site of HSA compared to the other domains and is in good agreement with our experimental observations. The average number of hydrogen bonds formed by different amino acid residues of HSA with water and sucrose is also calculated from the MD trajectory. In presence of sucrose it has been seen that 15%, 11% and 13% of total sucrose molecules involves in hydrogen bonding with domain I, II and III, respectively and there is a 27%, 40% and 38% increase in number of hydrogen bonds with water compared to when sucrose is not present in the system. Radial distribution function also clearly indicate that water as well as sucrose molecules come closer to the surface of the protein molecule when sucrose is present in the system (see figure 5.10). This suggests that the broken glass hypothesis is in operation in the present case and manifests a differential stabilization of sucrose on different domains of HSA.

5.5. Conclusion

In conclusion, the present study reveals the domain wise unfolding mechanism of HSA by GnHCl in absence and presence of sucrose. HSA has three distinct domains I, II and III and were studied using different marker molecules specific for each domains. It was observed that, in water, domain III of HSA first gets unfold in the denaturation process. The domain I and II unfolds thereafter almost simultaneously (scheme 5.2). The $[D]_{1/2}$ values of domain I, II and III for GnHCl are estimated to be 2.3 M, 2.4 M, 1.6 M, respectively. In presence of sucrose the $[D]_{1/2}$ values are found to be 3.1 M, 3.0 M and 1.7 M GnHCl, respectively. The sequence of unfolding of HSA in presence of sucrose medium is found to be same as compared to otherwise, however the $[D]_{1/2}$ values are shifted at higher GnHCl concentration. Clearly, addition of sucrose impose restriction in the GnHCl induced unfolding process for all the three domains but with different extent. The domain I and II are found to be stabilized more by sucrose as compared to domain III. The relative change in the RMSD and RMSF values obtained from MD simulation study also supports our experimental observations. This is to conclude that the unfolding behavior of different domains of a big protein is not uniform and the stabilizing effect of a stabilizer is expected to be different for different domains. The increase in the number of hydrogen bonding between the amino acid residues and water as well as the participation of sucrose in hydrogen bonding with protein indicate that broken glass hypothesis is in operational in the stabilization process.

References

1. (a) Santoro, M. M.; Bolen, D. W. *Biochemistry* **1988**, *27*, 8063.
   (b) Klotz, I. M. *Proc. Natl. Acad. Sci. U.S.A.* **1996**, *93*, 14411.
   (c) Varshney, A.; Ahmad, B.; Khan, R. H. *Int. J. Biol. Macromol.* **2008** , *42*, 438.
2. (a) Muzammil, S.; Kumar, Y.; Tayyab, S. *Proteins: Structure, Function, and Genetics* **2000**, *40*, 29.
   (b) Ghosh, S.; Guchhait, N. *ChemPhysChem* **2009**, *10*, 1664.
   (c) Tanford, C. Adv. *Protein Chem.* **1968**, *23*,121.
   (d) Lilie, H.; Lank, K.; Rudolph, R.; Buchner, J. *Protein Science* **1993**, *2*, 1490.
   (e) Xu, Q.; Keiderling, T. A. *Protein Science* **2004**, *13*, 2949.
3. Kamal, J. K. A.; Zhao, L.; Zewail, A. H. *Proc. Natl. Acad. Sci. U.S.A.* **2004**, *101*, 13411.
4. Wallevik, K. *J. Biol. Chem.* **1973**, *248***,** 2650.
5. Chmelik, J.; Anzenbacher, P.; Chmelikova, J. *Collect Czech. Chem. Commun.* **1988**, *53***,** 411.
6. (a) Tayyab, S.; Siddiqui, M. U.; Ahmad, N. *Biochem Ed*. **1995**, *23***,** 162.
   (b) Khan, M. Y.; Agrawal, S. K.; Hangloo, S. *J. Biochem.* **1987**, *102*, 313.
   (c) Wang, Y.; Luo, Z.; Shi, X.; Wang, H.; Nie, L.; Huang, M. *Protein Science* **2011**, *20*, 2095.
7. Dugiaczyk, A.; Law, S.; Dennison, O. E. *Proc. Natl. Acad. Sci. U.S.A.* **1982**, *79*, 71.
8. (a) Peters, T. *All About Albumin: Biochemistry, Genetics, and Medical Applications,* Academic press, San Diego, **1996**.
   (b) Hu, Y.; Liu, Y.; Xiao, X. *Biomacromolecules* **2009**, *10*, 517.
   (c) Hu, Y.; Yang, Y.; Dai, C.; Liu, Y.; Xiao, X. *Biomacromolecules* **2010**, *11*,106. (d) Hu, Y.; Liu, Y.; Shen, X.; Fang, X.; Qu, S. *J. Mol. Struct.* **2005**, *738*, 143.
   (e) Kragh-Hansen, U.; Chuang, V. T. G.; Otagiri, M. *Biol. Pharm. Bull.* **2002**, *25-2*, 695.

(f) Kosa, T.; Maruyama, T.; Otagiri, M. *Pharma. Res.* **1997**, *14*, 1607.

9. Curry, S.; Mandelkow, H.; Brick, P.; Franks, N. *Nature Struc. Biol.* **1998**, *5*, 827.
10. (a) He, X. M.; Carter, D. C. *Nature* **1992**, *358*, 209.
    (b) Sudlow, G.; Birkett, D. J.; Wade, D. N. *Mol. Pharmacol.* **1976**, *12*, 1052.
11. Sugio, S.; Kashima, A.; Mochizuki, S.; Noda, M.; Kobayashi, K. *Protein Eng.* **1999**, *12*, 439.
12. Eleftheriou, N. M.; Brennan, J. D. *J. Sol-Gel Sci. Technol.* **2009**, *50*, 184.
13. Ahmad, B.; Ahmad, M. Z.; Haq, S. K.; Khan, R. H. *Biochim. Biophys. Acta* **2005**, 1750, 93.
14. Santra, M. K.; Banerjee, A.; Rahaman, O.; Panda, D. *Int. J. Biol. Macromol.* **2005**, *37*, 200.
15. Bagatolli, L. A.; Kivatinitz, S. C.; Aguilar, F.; Soto, M. A.; Sotomayor, P.; Fidelio, G. D. *J. Fluoresc.* **1996**, *6*, 33.
16. Dockal, M.; Carter, D. C.; Rüker, F. *J. Biol. Chem.* **1999**, *274*, 29303.
17. Zunszain, P. A.; Ghuman, J.; Komatsu, T.; Tsuchida, E.; Curry, S. *BMC Struct. Biol.* **2003**, *3*, 6.
18. (a) Cottone, G. *J. Phys. Chem. B* **2007**, *111*, 3563.
    (b) Abe, M.; Abe, Y.; Ohkuri, T.; Mishima, T.; Monji, A.; Kanba, S.; Ueda1, T. *Protein Science* **2013**, *22*, 467.
19. Dutta, U.; Cohenford, M. A. *Anal. Chim. Acta* **2006**, *558*, 187.
20. Strambini, G. B.; Balestreri, E.; Galli, A.; Gonnelli, M. *J. Phys. Chem. B* **2008**, *112*, 4372.
21. Miyawaki, O. *Biophys. Chem.* **2009**, *144*, 46.
22. Miyawaki, O. *Biochim. Biophys. Acta* **2007**, *1774*, 928.
23. Allison, S. D.; Chang, B.; Randolph, T. W.; Carpenter, J. F. *Arch. Biochem. Biophys.* **1999**, *365*, 289.
24. Carpenter, J. F.; Crowe, J. H. *Biochemistry* **1989**, *28*, 3916.
25. Belton, P. S.; Gil, A. M. *Biopolymers* **1994**, *34*, 957.

26. Lerbret, A.; Affouard, F.; Bordat, P.; Hedoux, A.; Guinet, Y.; Descamps, M. *Chem. Phys.* **2008**, *345*, 267.
27. Alfonso, L. D.; Collini, M.; Baldini, G. *Eur. J. Biochem.* **2003,** *270*, 2497.
28. Lins, R. D.; Pereira, C. S.; Hunenberger, P. H. *Proteins: Struc. Funct. Bioinfo.* **2004**, *55*, 177.
29. Bonincontro, A.; Bultrini, E.; Calandrini, V.; Cinelli, S.; Onori, G. *J. Phys. Chem. B* **2000**, 1*04*, 6889.
30. Lopez-Diez, E. C.; Bone, S. *Biochim. Biophys. Acta* **2004**, *1673*, 139.
31. Sola-Penna, M.; Meyer-Fernandes, J. R. *Arch. Biochem. Biophys.* **1998**, *360*, 10.
32. Sola-Penna, M.; Ferreira-Pereira, A.; Lemos, A. P.; Meyer-Fernandes, J. R. *Eur. J. Biochem.* **1997**, *248*, 24.
33. Sampedro, J. G.; Uribe, S. *Mol. Cell. Biochem.* **2004**, *256*, 319.
34. Fedorov, M. V.; Goodman, J. M.; Nerukh, D.; Schumm, S. *Phys. Chem. Chem. Phys.* **2010**, *13***,** 2294.
35. (a) Hottiger, T.; Virgilio, C. D.; Hall, M. N.; Boller, T.; Wiemken, A. *Eur. J. Biochem.* **1994**, *219*, 187.
    (b) Sola-Penna, M,.; Meyer-Fernandes, J. R. *Zeitschrift fur Naturforschung* **1994**, *51C*, 327.
36. (a) Upadhyay, A.; Bhatt, T.; Tripathi, H. B.; Pant, D. D. *J. Photochem. Photobiol. A: Chem.* **1995**, *89*, 201.
    (b) Santra, M. K.; Banerjee, A.; Krishnakumar, S. S.; Rahaman, O.; Panda, D. *Eur. J. Biochem.* **2004**, *271*, 1789.
    (c) Abou-Zied, O. K.; Al-Shishi, O. I. K. *J. Am. Chem. Soc.* **2008**, *130*, 10793.
    (d) Helms, M. K.; Petersen, C. E.; Bhagavan, N. V.; Jameson, D. M. *FEBS Lett.* **1997**, *408*, 67.
    (e) Devis, D. M.; McLockey, D.; Brich, D. J. S.; Gellert, P. R.; Kittlety, R. S.; Swart, R. M. *Biophy.s Chem.* **1996**, *60*, 63.
    (f) Lakowicz, J.R.; Gryczynski, I. *Biophys. Chem.* **1992**, *45*, 1.

37. Kamikubo, K.; Sakata, S.; Nakamura, S.; Komaki, T.; Miura, K. *J. Protein Chem.* **1990**, *9*, 461.
38. Bagatolli, L. A.; Kivatinitz, S. C.; Fidelio, G. D. *J. Pharmaceu. Sci.* **1996**, *85*, 1131.
39. Valsami, G. M.; Marcheras, P. E.; Koupparis, M. A. *Pharmaceu. Res*. **1991**, *8*, 888.
40. Takehara, K.; Yuki, K.; Shirasawa, M.; Yamasaki, S.; Yamada, S.; *Analyt. Sci.* **2009**, *25*, 115.
41. Kragh-Hansen, U. *Mol. Pharmacol.* **1988**, *34*, 160.
42. Petitpas, I.; Bhattacharya, A. A.; Twine, S.; East, M.; Curry, S. *J. Biol. Chem.* **2001**, *276*, 22804.
43. Martinez, L.; Andrade, R.; Birgin, E. G.; Martinez, J. M. *J. Comput. Chem.* **2008**, *30*, 2157.
44. Miyamoto, S.; Kollman, P. A. *J. Comput. Chem.* **1992**, *13*, 952.
45. Wu, X.; Brooks, B. R. *Chem. Phys. Lett.* **2003**, *381*, 512.

Chapter 6

Conformational Fluctuation Dynamics of Domain I of Human Serum Albumin in the Course of Chemically and Thermally Induced Unfolding Using Fluorescence Correlation Spectroscopy

Rajeev Yadav *et al*., *J. Phys. Chem. B.* **2014**, *118*, 5428.

The present study elucidates the involvement of conformational fluctuation dynamics during chemically and thermally induced unfolding of human serum albumin (HSA) by fluorescence correlation spectroscopic (FCS) study, time resolved fluorescence measurements and circular dichroism (CD) spectroscopic methods. Two fluorescent probes, tetramethylrhodamine-5-maleimide (TMR) and N-(7-dimethylamino-4-methylcoumarin-3-yl) iodoacetamide (DACIA) were used to selectively label the domain I of HSA through the reaction with cys-34 for these studies. The guanidine hydrochloride (GnHCl) induced global structural change of HSA is monitored through its hydrodynamic radius (r_H) and CD response, which is found to be two step in nature. In FCS experiment, along with the diffusion time component we have observed an exponential relaxation time component (τ_R) and has been ascribed to the concerted chain dynamics of HSA. Unlike in global structural change we found that the τ_R value changes in different manner in the course of the unfolding. The dependence of τ_R on the concentration on GnHCl was best fitted with a four state model, indicating the involvement of two intermediate states during the unfolding process, which were not observed through the CD response and r_H data. The fluorescence lifetime measurement also supports our observation of intermediate states during the unfolding of HSA. However, no such intermediate states were observed during thermally induced unfolding of HSA.

6.1. Introduction

Understanding the complex pathway of conformational changes during the folding/unfolding process of a protein is a major challenge in structural biology. A large numbers of experimental and theoretical studies have been performed to understand the unfolding pathway of proteins and are subject of considerable interest from last few decades.[1-11] It not only requires the structural characterization during the unfolding process but also the elucidation of the structural dynamics is necessary. The structural dynamics of side chain is expected to be different for the compact (native) and the loosen (unfolded) state of the protein. The time scale of such chain dynamics is in the order of nanosecond to microsecond and need to be studied for a wide time window. In the present scenario, fluorescence-based methods like fluorescence anisotropy decay kinetics and fluorescence correlation spectroscopy (FCS) have become powerful tools to investigate the protein conformational dynamics in this time range.[5-34]

FCS is an elegant technique for studying the conformational dynamics of proteins,[5-14] DNA,[19-22] RNA,[23, 24] polypeptides,[25] etc. in the sub-microsecond to second time scale, which is based on the temporal fluctuation in the fluorescence intensity of a fluorescent probe attached to such macromolecules in the observation volume. The fluctuations of fluorescent intensity observed in FCS results either from the translational diffusion of the molecule or other processes that are faster than the diffusion time, e.g. intersystem crossing, cis-trans isomerization, chemical reaction (e.g. quenching of fluorescence) etc. The intensity fluctuation of a fluorescent tag attached to a protein can also arises from the quenching of the fluorescence signal of the fluorescent tag by some amino acid residues (act as quenchers), which is momentarily brought closer to the fluorescent tag by the conformational fluctuation of the side chain, and can be studied by FCS.[26-28] Webb and co-workers have analyzed the conformational fluctuations of apomyoglobin as a function of acid-induced unfolding by FCS.[12] They have showed that as the pH of the medium decreases from 6.3 (native state) to 4.1 (molten globule state), both

the fluctuation time scales and their amplitudes increases. On further decrease in the pH to 2.6 (unfolded state), the longer fluctuation time component as well as its amplitude remain constant, however the amplitude of the shorter component increases from 11% to 17%.[12] They have reported the two time constants of conformational fluctuation of the native state as 8 μs and 100 μs. Samanta and co-workers have studied the effect of dimethylsulfoxide (DMSO) on the structure and the conformational dynamics of bovine serum albumin (BSA) labeled with fluorescein isothiocyanate (FITC) and observed that the hydrodynamic radius of BSA becomes almost double in presence of 40% DMSO. The observed conformational dynamics of BSA with a time constant of 35 μs have been explained in terms of self-quenching of FITC fluorescence.[13] Frieden and co-workers have studied the kinetics of conformational fluctuation of a intestinal fatty acid binding protein and showed that the conformational fluctuations have a relaxation time component of 35 μs at pH 7.3 and become 2.5 μs at pH 2.[5, 6]

Here we attempt to understand the structural fluctuations and conformational dynamics of domain I of HSA during thermally and chemically induced unfolding process through FCS. HSA consists three structurally similar α-helical domains I, II and III. Eeach is divided into two sub-domains (denoted as A & B) and have a unique characteristic for binding different drugs and metabolites.[35-39] It is known that the property of these domains are not identical and to understand the dynamics of the well studied HSA, one has to gain knowledge of individual domains. In our previous study, we have shown that the domain III of HSA unfolds first followed by domain I and II on addition of GnHCl in the medium and also the stabilization effect of sucrose on different domains of HSA are different.[40] Here, as first choice, we chose domain I of HSA that contains a free cys-34 residue, which allows site-specific labeling by thiol-reactive fluorophores.[31, 32, 36] Many of the researchers have studied the dynamics of domain I through the change in the fluorescence properties of chromophores that are covalently attached with cys-34 of HSA.[1, 10, 11, 31, 32] Bright and co-workers have studied the dynamics

of domain I of HSA through acrylodan covalently attached with cys-34.[32] Bhattacharyya and co-workers have studied the effect of room temperature ionic liquid (RTIL) on the size and conformational dynamics of domain I of HSA by FCS using fluorescent probe, 7-dimethylamino-3-(4-maleimidophenyl)-4-methylcoumarin (CPM) covalently attached with cys-34. They have observed that RTIL acts as denaturant when HSA is in native state; however it acts as a stabilizing agent in its unfolded state. Three time components have been ascribed to the conformational dynamics, among these, the two faster components were assigned for chain dynamics while the slowest component has been assigned for inter-chain interaction or concerted motion.[9]

In the present work, we have explored the progressive variation in the conformational fluctuation dynamics of domain I of HSA during its chemically and thermally induced unfolding process using FCS. To provide additional information and to validate the conclusion we have also used time resolved fluorescence and circular dichroism (CD) spectroscopy. Two fluorescent probes, N-(7-dimethylamino-4-methylcoumarin-3-yl) iodoacetamide (DACIA) and tetramethylrhodamine-5-maleimide (TMR) were used to selectively label the domain I of HSA through the reaction with cys-34.

6.2. Protein Labeling

The labeling of HSA with DACIA and TMR were carried out following Wang *et al.*'s method with minor modification (scheme 6.1).[1, 41] Two stock solutions of ~90 μM HSA were prepared in 50 mM phosphate buffer (pH 7.4) for each of the labeling dyes. Separately, the labeling dyes (DACIA and TMR) were dissolved in DMSO and added drop by drop to 6 ml of protein solution till a molar ratio of HSA to dye as 1:3.5. The mixture was then stirred gently at room temperature for 10 h followed by dialysis against 500 ml of 1:35 (vol/vol) DMSO and buffer (pH 7.4, 50 mM phosphate buffer) solution at 4 °C. The dialysis medium was replaced after each 12 h 4 times, after that the dialysis medium was

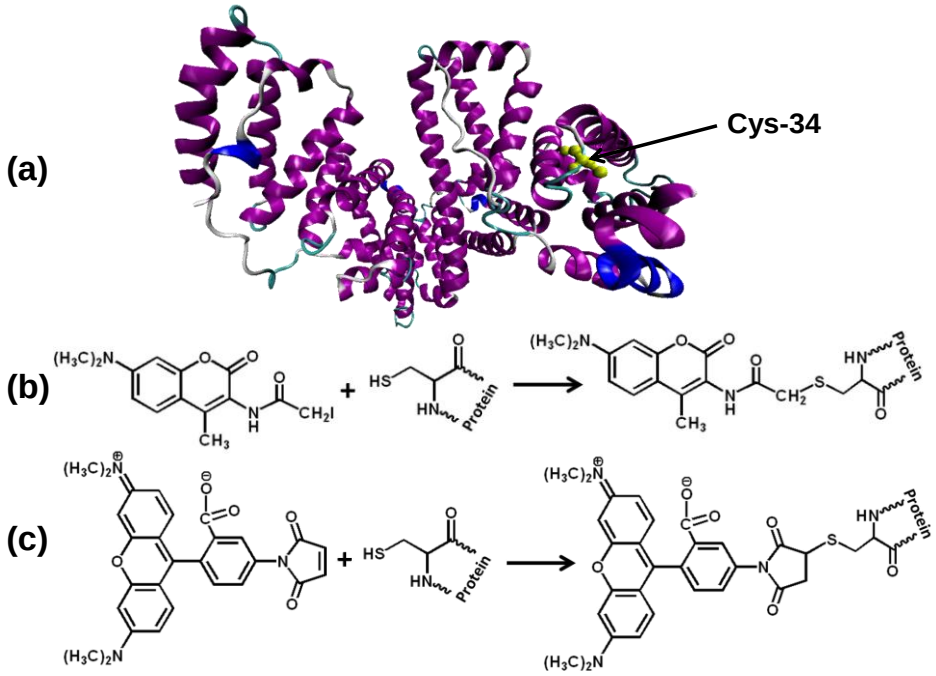

Scheme 6.1. (a) Schematic representation of human serum albumin (HSA) showing Cys-34 residue where fluorescent probes, DACIA and TMR have been covalently attached; reaction of (b) N-(7-dimethylamino-4-methylcoumarin-3-yl) iodoacetamide (DACIA) and (c) tetramethylrhodamine-5-maleimide (TMR) with cys-34 of HSA.

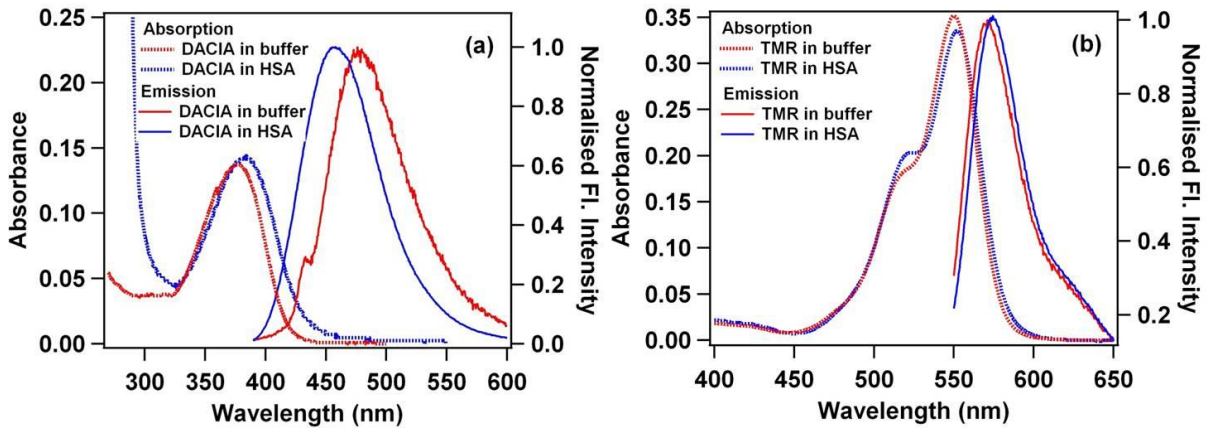

Figure 6.1. (a) Absorption and emission spectrum of free DACIA (red lines) and tagged with cys-34 of HSA (blue lines), (b) Absorption and emission spectrum of free TMR (red lines) and tagged with cys-34 of HSA (blue lines) in 50 mM phasphate buffer (pH 7.4).

replaced by only buffer (pH 7.4, 50 mM phosphate buffer) for 6-8 days. To check whether dialysis has completed or not, we have recorded the fluorescence spectra of each dialysed solution. The labeled protein was then concentrated using 10 kDa cut-off centrifugal filtration unit. The concentration ratio of HSA and attached dye

was estimated as ~1:0.6 for both the cases using absorbance of HSA, DACIA and TMR and the molar extinction coefficient as 36500 $M^{-1}cm^{-1}$, 24000 $M^{-1}cm^{-1}$ and 75000 $M^{-1}cm^{-1}$ respectively.[41-43] The absorption and emission spectrum of free DACIA and TMR in buffer and labeled with cys-34 of HSA are shown in figures 6.1a and 6.1b, respectively. In all the experiment the samples were prepared in 50 mM phosphate buffer (pH 7.4) and the concentration of HSA was maintained as 10 μM and 2 μM for time resolved fluorescence and circular dichroism (CD) measurements, respectively. However for FCS measurements the concentration of HSA was maintained as 40 nM. All the measurements were done at 298 ± 1 K if not stated otherwise.

6.3. Data Analysis

The time-resolved fluorescence intensity decays were collected at 455 nm and analyzed by deconvoluting the observed decays with the IRF to obtain the intensity decay function, manifested as a sum of three exponentials for the present study.[29]

$$I(t) = \sum_{i=1}^{3} fi \exp(-t/\tau_i) \qquad (6.1)$$

Where $I(t)$ is the fluorescence intensity at time t and f_i is the amplitude associated with the fluorescence lifetime τ_i and the sum of all f values is unity.

FCS measurements were performed on an instrument assembled in our laboratory, which has been described in chapter 2.

The autocorrelation function $G(\tau)$ of fluorescence fluctuations obtained from FCS experiment can be described as,[29]

$$G(\tau) = \frac{\langle \delta F(t) \delta F(t+\tau) \rangle}{\langle F(t) \rangle^2} \qquad (6.2)$$

where $\langle F(t) \rangle$ is the average fluorescence intensity, and $\delta F(t)$ and $\delta F(t+\tau)$ are the quantity of fluctuation in intensity around the mean value at time t and $t+\tau$ and are

given by

$$\delta F(t) = F(t) - \langle F(t) \rangle \,,\ \delta F(t+\tau) = F(t+\tau) - \langle F(t) \rangle \qquad (6.3)$$

For a single component system diffusing in only three dimensions in solution phase, the diffusion time (τ_D) can be obtained by fitting the correlation function $G(\tau)$ using following equation.[29]

$$G(\tau) = \frac{1}{N}\left(1+\frac{t}{\tau_D}\right)^{-1}\left(1+\frac{t}{\omega^2\tau_D}\right)^{-1/2} \qquad (6.4)$$

Where N is the number of particles in the observation volume and $\omega = \omega_z/\omega_{xy}$ which is the depth to diameter ratio of 3D Gaussian volume. If the diffusing species undergoes an association chemical reaction or conformational change, which modulate its fluorescence intensity, with a relaxation time τ_R, then the correlation function can be written as,[12]

$$G(\tau) = \frac{1-A+A\exp(-t/\tau_R)}{N(1-A)}\left(1+\frac{t}{\tau_D}\right)^{-1}\left(1+\frac{t}{\omega^2\tau_D}\right)^{-1/2} \qquad (6.5)$$

where A is the amplitude of the process defined by τ_R. The diffusion coefficient of the molecule can be calculated from the diffusion time (τ_D) and radius of the observation volume (ω_{xy}) using following equation.

$$D_t = \frac{\omega_{xy}^2}{4\tau_D} \qquad (6.6)$$

The structural parameter (ω) of the excitation volume was calibrated using a sample of known diffusion coefficient (Rhodamine 6G (R6G) in water, $D_t = 4.14 \times 10^{-6}$ cm^2 s^{-1}).[45] From the global analysis of the fluorescence correlation function of R6G of varying concentration, the observation volume has been estimated as 0.6 fL with a transverse radius of 292 nm.

Finally, the hydrodynamic radius (r_H) of the molecule was determined from the diffusion coefficient (D_t) using to the Stokes-Einstein equation as follows.[45]

$$r_H = \frac{k_B T}{6\pi\eta D_t} \qquad (6.7)$$

where k_B is the Boltzmann constant, T is the absolute temperature (298 K in the present study) and η is the viscosity of the medium.

Here we used TMR labeled HSA for FCS study. TMR labeled HSA was excited with 532 nm and the fluctuation of its fluorescence was measured as a function of GnHCl in our home built FCS system. Addition of GnHCl yields the changes in the viscosity and refractive index of the medium, which may affect the diffusion time in the observation volume. Refractive index mismatch can be corrected by adjusting the collar position of the objective as discussed in references 44, 46. In the present study, we have corrected the refractive index mismatch by adjusting the collar position of the objective from 0.14 in absence of GnHCl to 0.20 in presence of 6 M GnHCl. To determine the hydrodynamic radius of the protein accurately, viscosity correction has been done by measuring the diffusion time of R6G at each concentration of GnHCl as follows. [46, 47]

$$\frac{r_H^{HSA}}{r_H^{R6G}} = \frac{\tau_D^{HSA}}{\tau_D^{R6G}} \qquad (6.8)$$

Since R6G is rigid, its hydrodynamic radius (r_H^{R6G}) is independent on the viscosity of the medim. Whereas, the diffusion time of R6G molecule (τ_D^{R6G}) will change with the change in the viscosity of the system. The r_H value of R6G has been calculated from the known value of D_t (4.14×10^{-6} cm^2 s^{-1}) using equation 6.7. The diffusion time of free R6G have also been determined in presence of different concentrations of GnHCl for each experiment. The standardization with R6G molecule mimics the exact experimental condition to minimize the effect of viscosity.

6.4. Results

6.4.1. Circular Dichroism (CD) Spectroscopy

The CD spectrum of HSA exhibits two minima at 208 and 222 nm, signifying the α-helical signature of HSA.[48] Here, the change in the CD spectrum of HSA with increasing concentration of GnHCl is shown in figure 6.2a. At a high concentration of GnHCl we could not measure the CD spectra of HSA below 215 nm because of appreciable amount of absorbance by GnHCl. Figure 6.2b shows the change in CD signal (mdeg) at 222 nm with increasing concentration of GnHCl. It shows that there is no change in α-helicity of HSA till 1.5 M GnHCl. This indicates that the protein retains its helical structure till 1.5 M GnHCl. On further increase in the GnHCl concentration the CD signal at 222 nm starts changing rapidly and become almost constant at 5 M GnHCl. The result indicates that the secondary structure of HSA unfolds beyond 1.5 M GnHCl and the unfolding process completed at 4.5 M GnHCl. This is in good agreement with previous reports as given by Ahmad et. al and Santra et. al.[49, 50] Figures 6.3a and 6.3b show the change in the CD spectrum of HSA and CD signal (mdeg) at 222 nm with increase in temperature, respectively. It shows that the secondary structure of HSA remains unchanged till 310 K, afterwards, the helical structure starts destroying as the temperature increased. This also in agreement with the previous report by Rezaei-Tavirani et. al.[33]

6.4.2. Steady-State and Time Resolved Fluorescence Spectroscopy

To study the effect of GnHCl and temperature solely on domain I of HSA, a fluorescent tag method was used. The nature of the signal of a fluorophore is a function of its local environment. Here we have attached a solvatochromic dye (DACIA) to cys-34 residue present in the domain I of HSA. The absorption maximum of DACIA in 50 mM phosphate buffer (pH 7.4) shows a peak at 379 nm and emission maximum is at 478 nm. On labeling with HSA, the absorption maximum has been observed as 383 nm and the emission maximum of DACIA

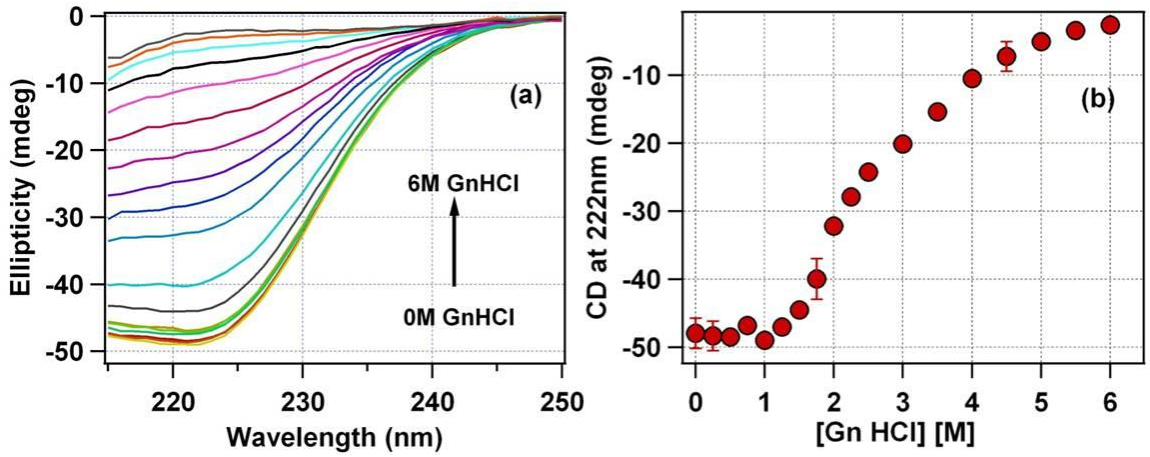

Figure 6.2. (a) Far-UV CD spectra of HSA in absence and in presence of different concentrations of GnHCl, (b) The change in the CD values at 222 nm with GnHCl concentration.

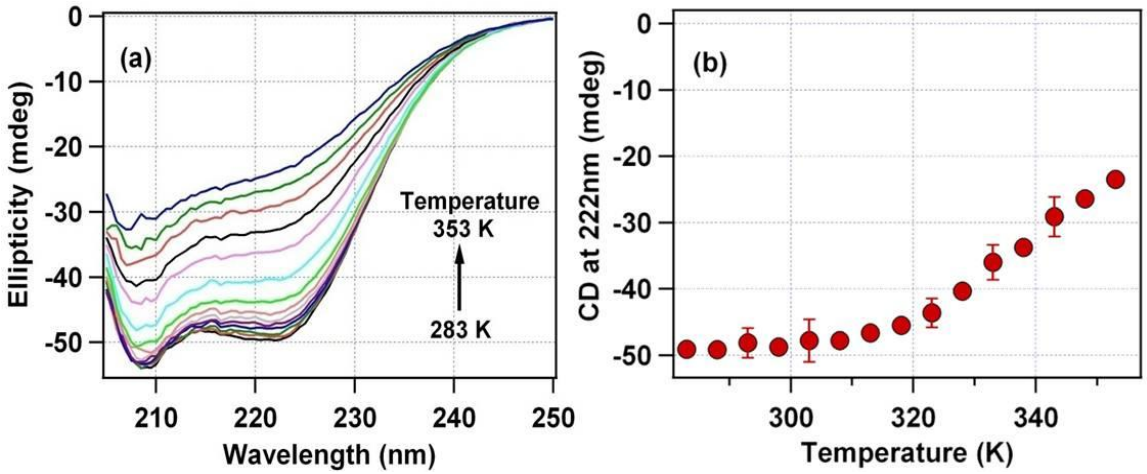

Figure 6.3. (a) Far-UV CD spectra of HSA at different temperatures, (b) The change in the CD values at 222 nm with temperature

changes dramatically with a large blue shift to 457 nm (figure 6.1a). On unfolding (both chemically and thermally), the absorption spectrum of DACIA does not change much; however, the fluorescence response of DACIA is found to be depends strongly on unfolding and shows an emission maximum of 478 nm and 461 nm in presence of 6 M GnHCl (at 298 K) and at 353 K, respectively. Along with the red shift in the emission maximum, the intensity of the fluorescence also decreased dramatically. For 6 M GnHCl, we have observed 1.3 times decrease in

the emission intensity from the native state whereas on increase the temperature to 353 K, the emission intensity decreased by 1.7 times from 298 K.

To understand the system in a better way, the fluorescence transients of DACIA labeled HSA were recorded in presence of different concentrations of GnHCl varied from 0 to 6 M (at 298 K) and at different temperatures ranging from 283 K to 353 K in absence of GnHCl. The lifetime of DACIA-HSA have been evaluated by fitting these transients with three exponential decay model (eq. 6.1). Figure 6.4a shows the fitted transients of DACIA labeled HSA using equation 6.1. The average lifetime of DACIA-HSA is found to depend strongly on GnHCl concentration as shown in figure 6.4b and table 6.1. This is to note that DACIA is covalently attached to domain I and the change in the average lifetime of DACIA is obviously due the change in the local environment of domain I of HSA during the unfolding process. In absence of GnHCl (at 298 K), the three time components of DACIA attached to HSA are 0.37 ns (0.03), 1.81 ns (0.22) and 4.28 ns (0.76) with an average lifetime 3.63 ns. As it can be seen in figure 6.4b, a shallow minimum is observed at 1.25 M GnHCl with an average lifetime of 3.28 ns. On further increase in GnHCl concentration to 1.75 M, the average lifetime increased to 3.32 ns. At 4.5 M GnHCl, the three time components are 0.13 ns (0.02), 1.65 ns (0.29) and 3.10 ns (0.69) with an average lifetime of 2.62 ns, which remains almost constant on further increase in GnHCl concentration (figure 6.4b, table 6.1). Figure 6.5a shows the fluorescent transients of DACIA labeled HSA at different temperatures (in absence of GnHCl), which is also observed to be tri-exponential in nature. At 283 K the three time components of DACIA are 0.29 ns (0.01), 1.81 ns (0.20) and 4.32 ns (0.79) with an average lifetime of 3.78 ns. The average lifetime found to decreases monotonically as the temperature raised. At 353 K, the three components are 0.78 ns (0.09), 1.90 ns (0.32) and 3.72 ns (0.59) with an average lifetime of 2.87 ns. Figure 6.5b shows the change in the average lifetime of DACIA labeled HSA in course of temperature induced unfolding process. As mentioned earlier, the change in the average lifetime of DACIA in HSA is mainly

because of the change in the local environment of domain I of HSA as DACIA is covalently attached to domain I. Interestingly, the dependence of average lifetime of DACIA in HSA is not same for chemically and thermally induced unfolding process. In case of chemically induced unfolding we have observed a shallow minimum, whereas in case of temperature induced unfolding no such minimum was observed.

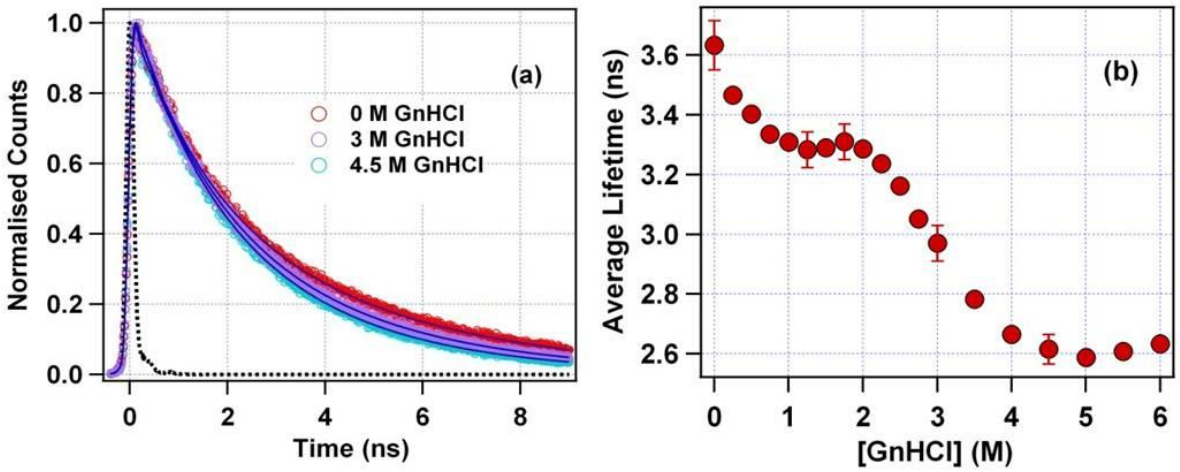

Figure 6.4. (a) Fluorescence transients of DACIA-HSA (λ_{ex} = 376 nm and λ_{em} = 455 nm) at four different concentration of GnHCl. Instrument response function is shown by dashed line. Solid lines represent the best fit to a tri-exponential function. (b) The change in average lifetime of DACIA-HSA as a function of GnHCl concentration.

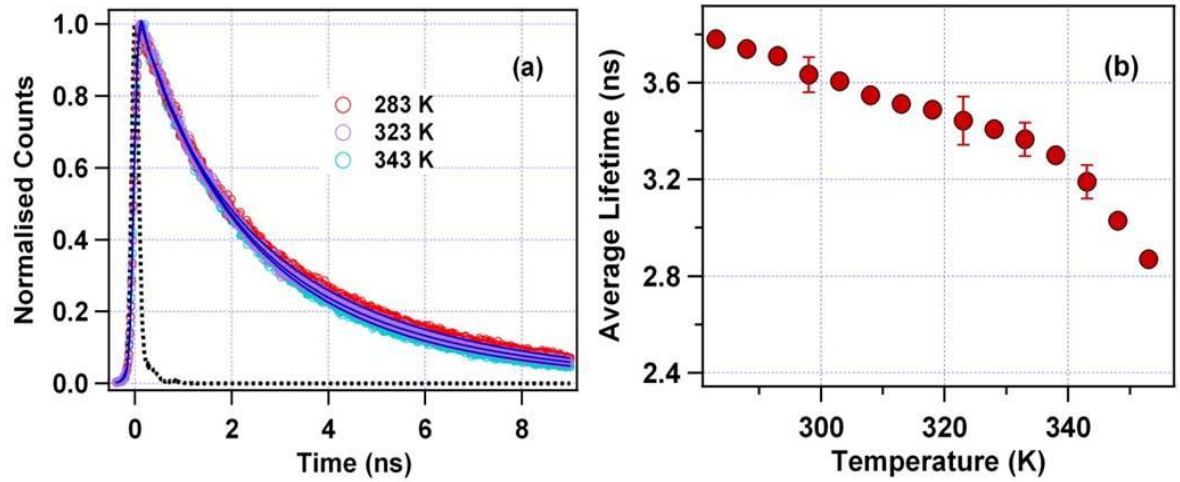

Figure 6.5. (a) Fluorescence transients of DACIA-HSA (λ_{ex} = 376 nm and λ_{em} = 455 nm) at three different temperatures. Instrument response function is shown by dashed line. Solid lines represent the best fit to a tri-exponential function. (b) The change in average lifetime of DACIA-HSA as a function of temperature.

Table 6.1. Average fluorescence lifetimes for DACIA labeled with HSA at different GnHCl concentrations and temperatures.

Average Lifetime			
GnHCl (M)	**<τ> (ns)**	**Temperature (K)**	**<τ> (ns)**
0	3.63 ± 0.08	**283**	3.78
0.25	3.47	**288**	3.74
0.5	3.40	**293**	3.71
0.75	3.33	**298**	3.63 ± 0.08
1	3.31	**303**	3.61
1.25	3.28 ± 0.06	**308**	3.55
1.5	3.29	**313**	3.51
1.75	3.30 ± 0.06	**318**	3.49
2	3.29	**323**	3.45 ± 0.1
2.25	3.24	**328**	3.41
2.5	3.16	**333**	3.37 ± 0.07
2.75	3.05	**338**	3.30
3	2.97 ± 0.06	**343**	3.19 ± 0.07
3.5	2.78	**348**	3.03
4	2.67	**353**	2.87
4.5	2.62 ± 0.05		
5	2.59		
5.5	2.61		
6	2.63		

6.4.3. Fluorescence Correlation Spectroscopy

FCS study has been done with TMR labeled HSA (attached to the same position where DACIA was tagged) in absence and presence of different concentrations of GnHCl varied from 0 to 6 M and at different temperatures varied from 283 K to 343 K. The fluorescence auto-correlation traces were first attempted to fit using equation 6.4, which contains only one diffusion component, and we found that the fitting was inappropriate. Our next attempt was to include a distribution in diffusion time to fit the observed autocorrelation traces. Here we have used Gaussian distribution model in our fitting equation as $G(\tau) = \sum a_i(\tau_{Di})(1+\tau/\tau_{Di})^{-1}(1+1/\omega^2\tau_{Di})^{-1/2}$, where $a_i(\tau_{Di}) = A_i \exp[-\{(\ln(\tau_{Di}) - \ln(\tau_P))/b\}^2]$, τ_P is the peak of the Gaussian distribution, b is the width of the distribution.[44, 51]

However, this model also fails to best fit the auto-correlation traces although the fitting is better than the fit using equation 6.4. The traces were best fitted to the equation 6.5, which has one diffusion time component along with one exponential relaxation time component (see figure 6.6 for some of the fitted auto-correlation curves). This implies that the source of the fluorescence intensity fluctuations is not only the diffusion of the TMR-HSA in and out of the observation volume but additionally guided by an exponential time component and has been assigned to the conformational changes of the protein within the observation volume.[12] A comparison of the fitting results, with only one diffusion component, with a distribution in diffusion time and one diffusion along with one exponential component, is shown in figures 6.7a and 6.7b for some GnHCl concentrations and for few temperatures, respectively. The knowledge of the diffusion component will shed light on the hydrodynamic radius of the protein through Stokes-Einstein relationship (equation 6.7), whereas the fluctuation relaxation time component gives the relaxation time for the conformational changes in the domain I of HSA. Bhattacharyya and co-workers as well as Samanta and co-workers also have observed such fluctuation relaxation time component for CPM labeled HSA and FITC labeled BSA, respectively.[9, 13]

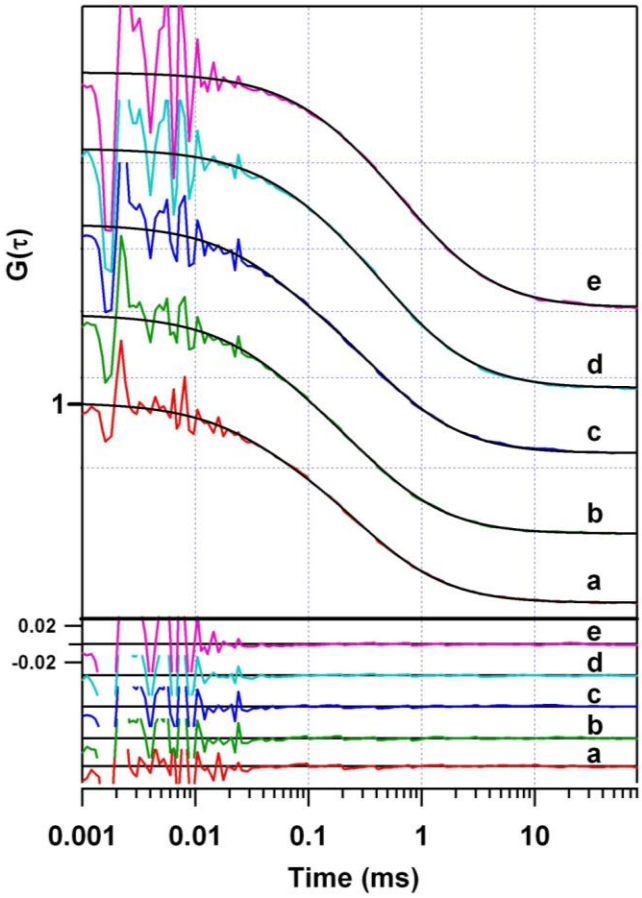

Figure 6.6. Autocorrelation curves of TMR-HSA in presence of 0, 1.1, 2, 3.5, 6 M GnHCl (a to e) with their best fit by equation 6.5 (1 Diffusion + 1 Component model). Lower portion of this figure shows the fitting residuals of respective curve.

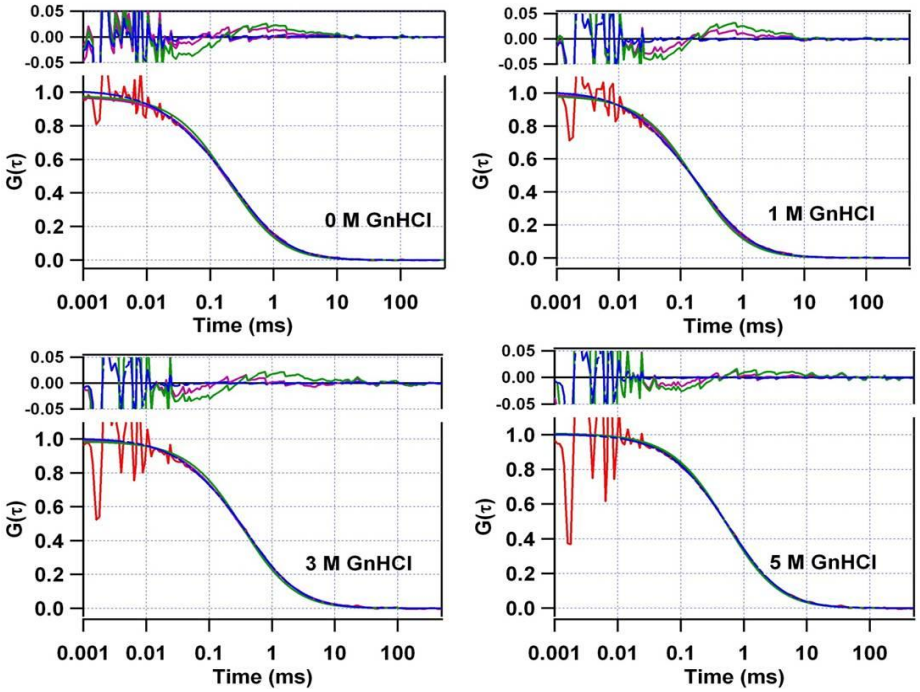

Figure 6.7a. Autocorrelation curves of TMR-HSA in presence of 0, 1, 3, 5 M GnHCl with their best fit by equation 6.4 (green lines), equation 6.5 (blue line) and Gaussian distribution model (orange line) for comparison. Upper portion of these figures show the fitting residuals of respective curve and respective fitting model.

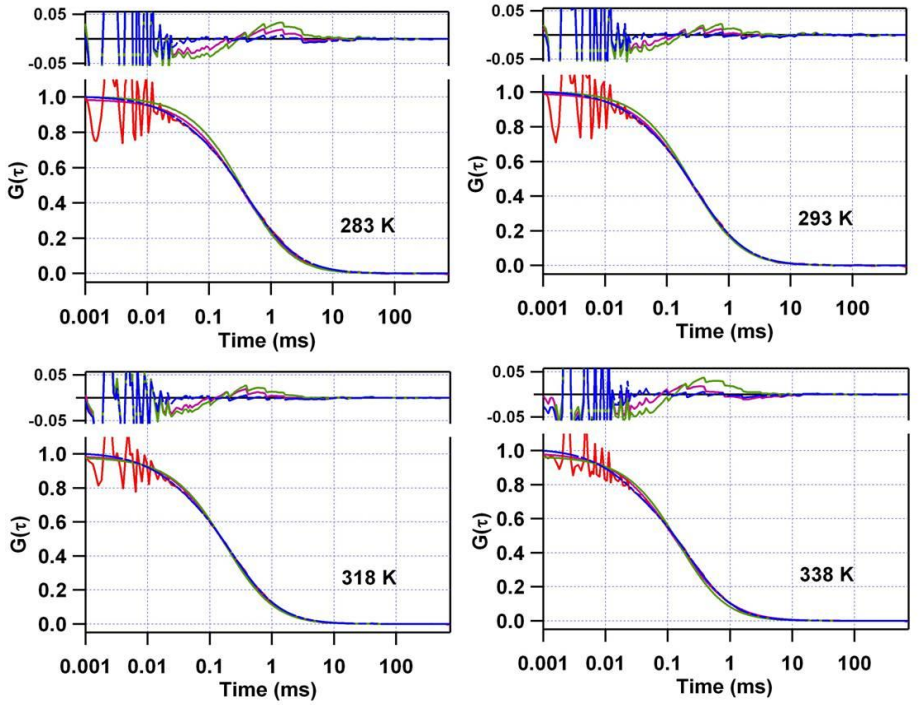

Figure 6.7b. Autocorrelation curves of TMR-HSA at 283 K, 293 K, 318 K and 338 K with their best fit by equation 6.4 (green lines), equation 6.5 (blue line) and Gaussian distribution model (orange line) for comparison. Upper portion of these figures show the fitting residuals of respective curve and respective fitting model.

6.4.3.1. Hydrodynamic Radius

The normalized fit lines of auto-correlation curves of TMR-HSA in presence of six concentrations of GnHCl at 298 K are shown in figure 6.8a and for five different temperatures in absence of GnHCl are shown in figure 6.8b. The correlation curve is found to shift towards the longer time region on increase in the concentration of GnHCl, indicating the slower diffusion (i.e. increase in the value of τ_D) of TMR-HSA on unfolding. Both the increase in the size of HSA upon unfolding and the increase in viscosity of the medium by presence of high amount of GnHCl are responsible for the slow diffusion of TMR-HSA. However, these curves are found to shift towards shorter time region on increasing temperature. This reverse behavior is because of the huge decrease in the viscosity of the sample with increase in the temperature that overcomes the effect of increase in the size of HSA upon thermal unfolding. The values of the experimentally measured τ_D have been employed to determine the diffusion coefficient (D_t) using equation 6.6 and the data are shown in figure 6.9a for GnHCl induced unfolding. In absence of GnHCl, the measured value of τ_D is 252 ± 15 μs corresponding to D_t as 84.4 ± 5.4 $\mu m^2 s^{-1}$. On addition of GnHCl, the τ_D value gradually become slower and at 6 M GnHCl the observed value is 712 μs with a D_t value of 29.9 $\mu m^2 s^{-1}$. Since the viscosity of the solution is changing on addition of GnHCl, the value of τ_D and D_t also incorporates the viscosity effect as already mentioned. The r_H value of HSA at each concentration of GnHCl has been determined after proper treatment of the τ_D value to correct the viscosity effect, as discussed in section 6.3 and are tabulated in table 6.2 and depicted in figure 6.9b. In the native state of HSA, the r_H value is found to be 39.1 ± 2.5 Å, which is in good agreement with early reports as 38.4 ± 2.0 Å by Chowdhury *et al.*[28] using FCS and 36 ± 1 Å by Galantini *et al.*[52] using small-angle x-ray scattering. Upon gradual addition of GnHCl to HSA, the value of r_H almost remains unchanged till 1.85 M; afterward it increases continuously till 4.5 M GnHCl and observed as 64.9 Å. At further higher concentration of GnHCl, the value of r_H remains almost unchanged (see figure 6.9b and table 6.2), indicating

that the overall structure of HSA is completely unfold at 4.5 M GnHCl which is in good agreement with our CD data. The value of r_H in unfolded state of HSA is also in good agreement with the previous reports as 61.0 ± 3.0 Å by Sasmal *et al.*[9] According to Wilkins *et al.*[53] the r_H value for protein containing N number of amino acids in native state as well as fully unfolded state can be obtained using the relations $r_H = (4.75 \pm 1.11)N^{0..29\pm0.02}$ Å and $r_H = (2.11 \pm 0.15)N^{0.57\pm0.02}$ Å respectively. Using these relations, the r_H of HSA (N ~ 585) has been calculated as 30.2 ± 10 Å and 79.7 ± 15 Å in native and fully unfolded state respectively. These numbers are also in good agreement with our observed values of r_H from FCS measurements.

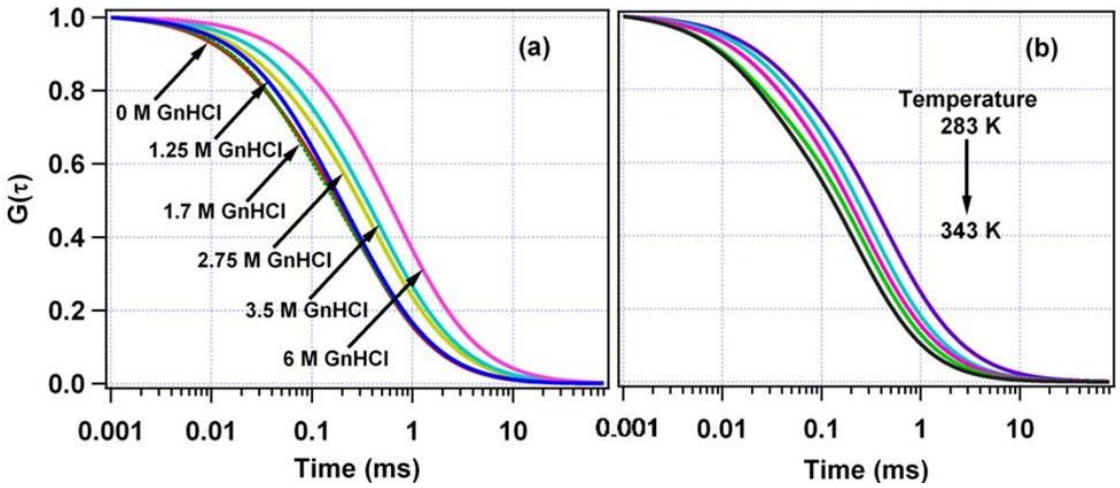

Figure 6.8. The normalized best fit lines of the autocorrelation curves of TMR-HSA GnHCl by equation 6.5 (1 Diffusion + 1 Component model) (a) in presence of 0, 1.1, 1.7, 2.75, 3.5, 6 M and (b) at different temperatures.

The values of diffusion coefficient (D_t) and hydrodynamic radii (r_H) have been determined for temperature induced unfolding of TMR-HSA after incorporating the effect of change in viscosity as temperature raised and are tabulated in table 6.3 and shown in figure 6.9c and 6.9d, respectively. At 283 K the value D_t and r_H has been observed as 57.7 $\mu m^2 s^{-1}$ and 41.0 Å, respectively. At 298 K the values of D_t and r_H are same as we observed for 0 M GnHCl, as 84.4 ± 5.4 $\mu m^2 s^{-1}$ and 39.1 ± 2.5 Å. On increase in the temperature to 343 K the D_t and r_H become 99.2 $\mu m^2 s^{-1}$ and 58.8 Å, respectively. It can be clearly seen that r_H values

at different temperatures are in between the values in native and unfolded states of HSA, hence in good agreement with previous reports.

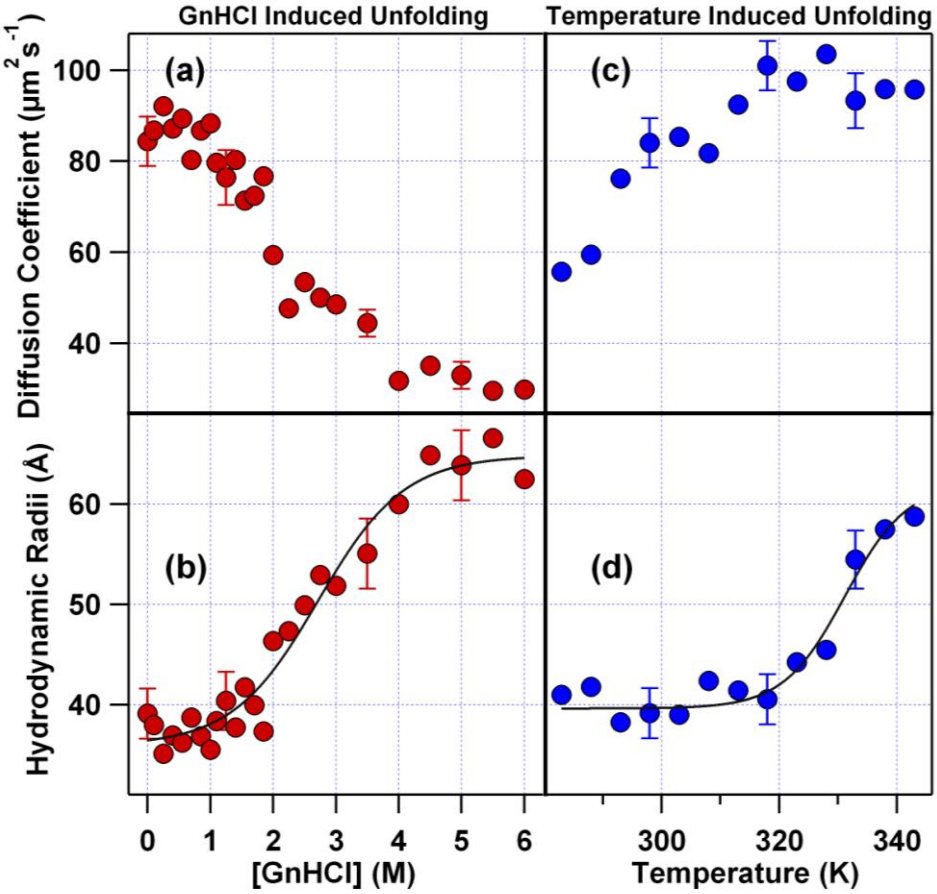

Figure 6.9. The change in diffusion coefficient, D_t and hydrodynamic radii, r_H of HSA as function of GnHCl concentration (a, b) and temperature (c, d). The solid line represents the data fitted into a two state model.

6.4.3.2. Conformational Dynamics

As stated earlier, the present FCS data are best fitted with a combination of diffusion (τ_D) and exponential time (τ_R) component as per equation 6.5. Like τ_D, the τ_R is also comprises the viscosity effect,[6] hence corrected for the viscosity following the method given by Mojumdar *et al.*[10] The corrected values of τ_R are shown in figures 6.10a and 6.10b for different GnHCl concentrations and temperatures respectively and are also tabulated in tables 6.2 and 6.3, respectively. In the native state of HSA, at 298 K, τ_R is observed as 27.5 ± 5 μs and remain

similar till 1 M GnHCl concentration. Afterwards an increment has been observed in the τ_R and reaches to 52.4 ± 6 μs at 1.25 M GnHCl. On further increase in the GnHCl concentration till 1.85 M, it decreased to 31.2 μs. The τ_R value again increases to 74.4 μs at 4.5 M GnHCl and remain similar till 6 M GnHCl. In absence of GnHCl, at 283 K, τ_R is observed as 27.0 μs and is almost unchanged till 333 K, afterward it increases slowly and become 36.0 μs at 343 K.

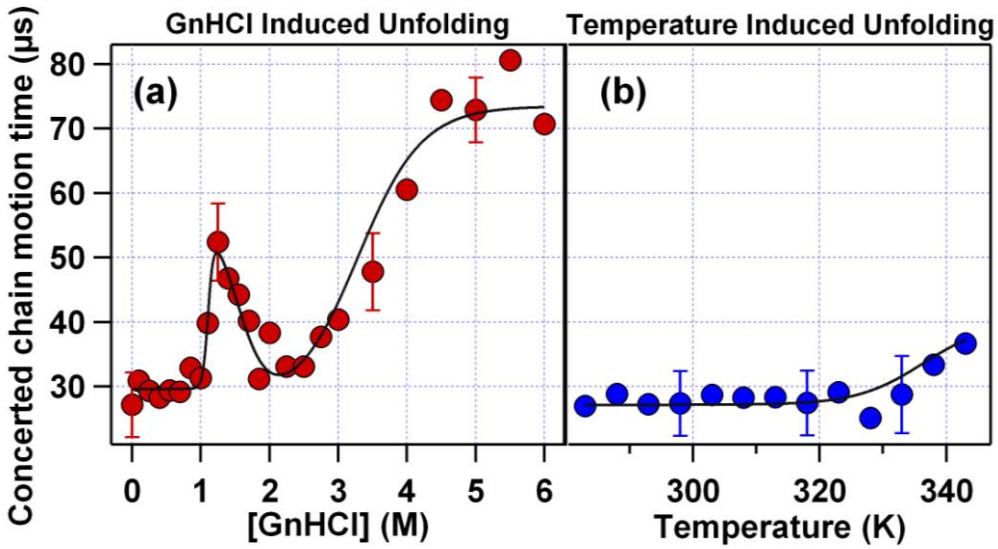

Figure 6.10. (a) Relaxation time component, τ_R corrected for viscosity and refractive index plotted as a function of GnHCl concentration (a) and temperature (b). The solid line represents the data fitted into a four state model using equation 6.10.

The exponential time component observed from autocorrelation curves in FCS experiment is in the time scale of 27-80 μs. Werner and co-worker have observed a ~30 μs time component of conformational dynamics of cytochrome c labeled with TMR in the intermediate state which is in dynamic equilibrium with unfolded state.[54] Webb and co-workers have observed a ~ 100 μs component in native and two components in the rang 30-200 μs in the acid unfolded state of apomyoglobin and ascribed as concerted chain motions.[12] Samanta and co-workers have observed the similar relaxation time component of 35-80 μs and correlated to the conformational dynamics of BSA in presence of DMSO.[13] Bhattacharyya and co-workers have observed three time components of conformational dynamics in

the range 3-200 μs for CPM labeled HSA and attributed as the chain dynamics of the protein (faster components) and concerted chain motion (slower component).[9] In another work they have showed the time component of 35-55 μs is for concerted chain motion of HSA in absence and presence of different GnHCl concentrations.[10] Hence, in accordance with the above mentioned reports, it can be concluded that the observed relaxation time constant of 27-80 μs is due to the concerted chain dynamics (concerted chain motion or inter-chain diffusion) of side chains of HSA and τ_R has been assigned to concerted chain dynamics of domain I of HSA.

Table 6.2. Diffusion coefficient (D_t), hydrodynamic radius (r_H) and concerted chain motion time (τ_R) for TMR labeled HSA at different GnHCl concentration.

GnHCl (M)	D_t ($\mu m^2 s^{-1}$)	r_H (Å)	τ_R (μs)
0	84.4 ± 5.4	39.1 ±2.5	27.5 ± 5
0.1	86.8	38.0	30.9
0.25	92.1	35.1	29.3
0.4	87.2	36.9	28.3
0.55	89.4	36.2	29.4
0.7	80.3	38.7	29.2
0.85	86.8	36.8	32.9
1	88.3	35.5	31.3
1.1	79.7	38.4	39.8
1.25	76.5± 6	40.4 ± 2.9	52.4 ± 6
1.4	80.3	37.7	46.8
1.55	71.4	41.7	44.2
1.7	72.4	39.9	40.2
1.85	76.7	37.3	31.2
2	59.4	46.3	38.3
2.25	47.7	57.3	33.1
2.5	53.5	49.9	33.1
2.75	50.1	53.0	37.7
3	48.6	51.9	40.4
3.5	44.5 ± 3	55.1 ± 3.5	47.8 ± 6
4	31.8	73.1	60.5
4.5	35.1	64.9	74.4
5	33.6 ± 3	63.9 ± 3.5	72.9 ± 5
5.5	29.6	66.5	80.6
6	29.9	62.5	70.7

Table 6.3. Diffusion coefficient (D_t), hydrodynamic radius (r_H) and concerted chain motion time (τ_R) for TMR labeled HSA at different temperatures.

Temperature (K)	D_t ($\mu m^2 s^{-1}$)	r_H (Å)	τ_R (μs)
283	55.7	40.9	27.0
288	59.5	41.8	28.8
293	76.2	38.2	27.2
298	84.4 ± 5.4	39.1 ± 2.5	27.5 ± 5
303	85.4	39.0	28.7
308	81.8	42.4	28.3
313	92.5	41.4	28.3
318	101.0 ± 5.4	40.5 ± 2.5	27.5 ± 5
323	97.5	44.2	29.1
328	103.5	45.5	25.1
333	93.3 ± 6	54.5 ± 2.9	28.7 ± 6
338	95.9	57.5	33.4
343	95.8	58.8	36.0

6.5. Discussion

The primary goal of the present study is to understand the involvement of conformational fluctuation in domain I during the GnHCl and temperature induced unfolding of HSA by FCS. The exponential time component observed in FCS experiment was assigned to the concerted chain motion dynamics in the domain I of HSA, whereas the other time component was assigned to the diffusion of the whole protein. The diffusional time component is a measure of the overall size of the protein and consequently the hydrodynamic radius (r_H) was calculated. During the course of the unfolding process, the overall dependence of r_H on the GnHCl concentration and temperature matches with the result obtained from the CD spectroscopy. Both studies indicate a two-state overall unfolding of HSA without the involvement of any stable intermediate state. However, as it can be seen in the fluorescence lifetime data, a shallow minimum was observed (see figure 6.4b) at 1.25 M GnHCl with a local maxima at 1.75 M GnHCl. Such observation hints towards the involvement of intermediate state(s) in the unfolding pathway of HSA

by GnHCl, whereas such signature of stable intermediate state(s) are absent in temperature induced unfolding process of HSA (see figure 6.5b). This is to note that fluorescence signal of the labeled fluorophore in HSA is mostly affected by its local environment. As here the fluorophore is tagged in domain I of HSA; we can assign the origin of the intermediate state because of subtle change in domain I of HSA. However, such kind of intermediate state was not detected through CD and by measuring the r_H value through FCS.

Table 6.4. Fitting parameters for GnHCl and temperature induced unfolding of TMR labeled HSA.

		$N \leftrightarrow I_1$			$I_1 \leftrightarrow I_2$			$I_2 \leftrightarrow D$		
		ΔG_1^0	m_1	$[D]_{1/2}$	ΔG_2^0	m_2	$[D]_{1/2}$	ΔG_3^0	m_3	$[D]_{1/2}$
GnHCl Induced Unfolding	τ_R	16.76	15.02	1.12	4.34	2.79	1.56	4.17	1.27	3.28
		$N \leftrightarrow D$								
		ΔG^0				m			$[D]_{1/2}$	
	r_H	2.35				0.87			2.70	
		$N \leftrightarrow D$								
Temperature Induced Unfolding		ΔG^0				m			$[T]_{1/2}$	
	τ_R	38.0				0.11			345.5	
	r_H	37.4				0.11			340.0	

Unit of ΔG^0 is kcal mol^{-1}; Unit of m is kcal $mol^{-1}M^{-1}$; $[D]_{1/2}$ and $[T]_{1/2}$ are the amount of GnHCl in M, and temperature in K required for 50% unfolding in GnHCl and temperature induced unfolding process, respectively.

The time component ascribed for concerted chain dynamics within the domain I of HSA originates from the fluctuation of fluorescence intensity of TMR through quenching by Tyr, His and Phe amino acid residues present in the side chains.[55] On denaturation, the time constant of the concerted chain motion dynamics is expected to increase as the side chain of domain I of HSA would take longer time to come close to TMR because it has to diffuse through a long path in the unfolded state than in the native state.[12, 13] The dependence of the time constant of the concerted chain dynamics (see figure 6.10a) also indicate the involvement of intermediate state(s) during the GnHCl induced unfolding, whereas such

observation was not noted from the temperature induced unfolding of HSA (see figure 6.10b).

The dependence of concerted chain motion time during the GnHCl induced unfolding was best fitted with four state model containing two intermediate states (see figure 6.10a)

$$N \leftrightarrow I_1 \leftrightarrow I_2 \leftrightarrow U \qquad (6.9)$$

where I_1 and I_2 are the two intermediate states in between the native (N) and unfolded (U) states of HSA. For such a four state model, the overall spectroscopic signal(s) can be written as[17]

$$S = \frac{(S_N + S_{I1}\exp^{-X} + S_{I2}\exp^{-Y} + S_U\exp^{-Z})}{(1+\exp^{-X}+\exp^{-Y}+\exp^{-Z})} \qquad (6.10)$$

Where, $X = (\Delta G_1^0 - m_1[GnHCl])/RT$

$$Y = (\Delta G_1^0 + \Delta G_2^0 - (m_1 + m_2)[GnHCl])/RT$$

$$Z = (\Delta G_1^0 + \Delta G_2^0 + \Delta G_3^0 - (m_1 + m_2 + m_3)[GnHCl])/RT$$

and S_N, S_{I1}, S_{I2}, S_U are the values of the observable of the native, first intermediate, second intermediate and unfolded state, respectively. $\Delta G_1{}^0$, $\Delta G_2{}^0$ and $\Delta G_3{}^0$ are the free energy change of each transition in the absence of denaturant. m_1, m_2 and m_3 are the slope of free energy change plotted against the GnHCl. The concentration of denaturant to unfold 50 % of the protein ($[D]_{1/2}$) can be calculated using the relation $[D]_{1/2} = \Delta G_i^0 / m_i$. From the fitting parameters, the concerted chain motion time of N, I_1, I_2 and U states are found to be 29.6 μs, 57 μs, 27 μs and 73.4 μs, respectively. The observed values of ΔG^0, m and $[D]_{1/2}$ for all three transitions are shown in table 6.4. The $[D]_{1/2}$ value for the first transition ($N \leftrightarrow I_1$), second transition ($I_1 \leftrightarrow I_2$) and third transition ($I_2 \leftrightarrow U$) are estimated as 1.12 M, 1.56 M and 3.28 M GnHCl, respectively. This clearly indicates the presence of two

intermediate states during unfolding process of HSA (Scheme 6.2) that exists in the initial concentration of GnHCl (till ~2 M GnHCl), which was not observed through CD and r_H values, where the variations could be best fitted with well accepted two state model, $N \leftrightarrow U$.[40, 50] The observed value of $[D]_{1/2}$ from the variation of r_H is found to be 2.7 M GnHCl concentration, which is in good agreement with the previously reported values.[40, 50] For temperature induced unfolding, the dependence of concerted chain motion time was best fitted with two state model $N \leftrightarrow U$ without the involvement of any intermediate state (see figure 6.10b).

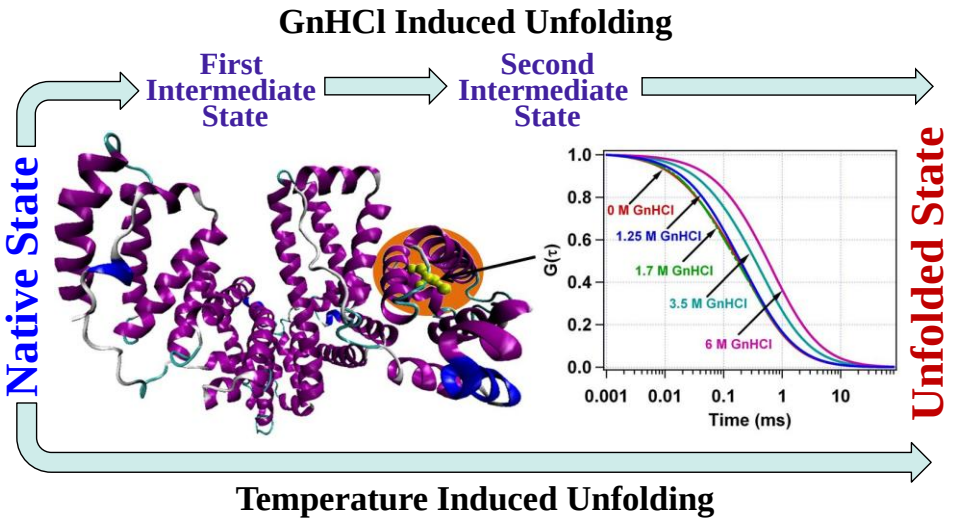

Scheme 6.2. Schematic representation of GnHCl and temperature induced unfolding process of HSA.

6.6. Conclusion

In the present study, FCS has been employed to study the global structural change as well as conformational dynamics of HSA during chemically and thermally induced unfolding through the covalently attached fluorescent tag (TMR) in domain I. The global structure of HSA has been associated with r_H value, which changes in a similar trend as observed through CD spectroscopy. The value of r_H has been observed as 39.1 ± 2.5 Å in the native state of HSA, and on addition of GnHCl it remains unchanged till 1.85 M, which become 64.9 Å in presence of 4.5 M GnHCl. In fluorescence correlation spectroscopic study, an exponential relaxation time component (τ_R) has been observed along with the diffusion time component, and is ascribed to the concerted chain dynamics of domain I of HSA. The time scale of concerted chain motion in the native state of HSA is found to be 27.5 ± 5 μs and remains similar till 1 M GnHCl. Afterwards an increment has been observed in the τ_R value which reaches to 52.4 ± 6 μs at 1.25 M GnHCl. On further increase in the GnHCl concentration till 1.85 M, the τ_R decreased to 31.2 μs. The τ_R value increases to 74.4 μs at 4.5 M GnHCl and remain similar till 6 M. Our analysis clearly indicates the involvement of two intermediate states during the GnHCl induced unfolding process of HAS, and domain I of HSA is primarily responsible for this subtle change in the overall structure of the protein in the intermediate states, as the fluorescent probe is located in the domain I of HSA. $[D]_{1/2}$ values for the first ($N \leftrightarrow I_1$), second ($I_1 \leftrightarrow I_2$) and third ($I_2 \leftrightarrow D$) transitions are estimated to be 1.16 M, 1.52 M and 3.0 M respectively. The fluorescence lifetime measurement also supports our observation of intermediate states during the GnHCl induced unfolding of HSA. However for thermally induced unfolding of HSA, no such intermediate states were observed. It has been realized that, to completely understand the unfolding mechanism of such massive proteins, one needs to study the different fragment separately.

References

1. Amisha, J. K.; Zhao, L.; Zewail, A. H. *Proc. Natl. Acad. Sci. U.S.A.* **2004**, *37*, 13411.
2. Klotz, I. M. *Proc. Natl. Acad. Sci. U.S.A.* **1996**, *93*, 14411.
3. Ghosh, S.; Guchhait, N. *ChemPhysChem* **2009**, *10*, 1664.
4. Anand, U.; Jash, C.; Mukherjee, S. *Phys. Chem. Chem. Phys*. **2011**, *13*, 20418.
5. Chattopadhyay, K.; Saffarian, S.; Elson, E. L.; Frieden, C. *Proc, Natl. Acad. Sci. U.S.A.* **2002**, *99*, 14171.
6. Chattopadhyay, K.; Elson, E. L.; Frieden, C. *Proc. Natl. Acad. Sci. U.S.A.* **2005**, *102*, 2385.
7. Haldar, S.; Mitra, S.; Chattopadhyay, K. *J. Biol. Chem*. **2010**, *285*, 25314.
8. Haldar, S.; Chattopadhyay, K. *J. Biol. Chem*. **2012**, *287*, 11546.
9. Sasmal, D. K.; Mondal, T.; Majumdar, S. S.; Choudhury, A.; Banerjee, R.; Bhattacharyya, K. *J. Phys. Chem. B* **2011**, *115*, 13075.
10. Mojumdar, S. S.; Chowdhury, R.; Chattoraj, S.; Bhattacharyya, K. *J. Phys. Chem. B* **2012**, *116*, 12189.
11. Das, D. K.; Das, A. K.; Mandal, A. K.; Mondal, T.; Bhattacharyya, K. *ChemPhysChem* **2012**, *13*, 1949.
12. Chen, H.; Rhoades, E.; Butler, J. S.; Loh, S. N.; Webb, W. W. *Proc. Natl. Acad. Sci. U.S.A.* **2007**, *104*, 10459.
13. Pabbathi, A.; Patra, S.; Samanta, A. *ChemPhysChem* **2013**, *14*, 2441.
14. Patra, S.; Santhosh, K.; Pabbathi, A.; Samanta, A. *RSC Advances* **2012**, *2*, 6079.
15. Rami, B. R.; Krishnamoorthy, G.; Udgaonkar, J. B. *Biochemistry* **2003**, *42*, 7986.
16. Jha, A.; Ishii, K.; Udgaonkar, J. B.; Tahara, T.; Krishnamoorthy, G. *Biochemistry* **2011**, *50*, 397.
17. Naidu, K. T.; Prabhu, N. P. *J. Phys. Chem. B* **2011**, *115*, 14760.
18. Fuentealba, D.; Kato, H.; Nishijima, M.; Fukuhara, G.; Mori, T.; Inoue, Y.; Bohne, C. *J. Am. Chem. Soc*. **2013**, *135*, 203.

19. Li, H. T.; Ren, X. J.; Ying, L. M.; Balasubramanium, S.; Klenerman, D. *Proc. Natl. Acad. Sci. U.S.A.* **2004**, *101*, 14425.

20. Jung, J.; Orden, A. V. *J. Am. Chem. Soc.* **2006**, *128*, 1240.

21. Edman, L.; Mets, U.; Rigler, R. *Proc. Natl. Acad. Sci. U.S.A.* **1996**, *93*, 6710.

22. Ishii, K.; Tahara, T. *J. Phys. Chem. B* **2013**, *117*, 11423.

23. Kim, H. D.; Nienhaus, G. U.; Ha, T.; Orr, J. W.; Williamson, J. R.; Chu, S. *Proc. Natl. Acad. Sci. U.S.A.* **2002**, *99*, 4284.

24. Kim, J.; Doose, S.; Neuweiler, H.; Sauer, M. *Nucleic Acids Res*. **2006**, *34*, 2516.

25. Neuweiler, H.; Doose, S.; Sauer, M. *Proc. Natl. Acad. Sci. U.S.A.* **2005**, *102*, 16650.

26. Neuweiler, H.; Banachewicz, W.; Fersht, A. R. *Proc. Natl. Acad. Sci. U.S.A.* **2010**, *107*, 22106.

27. Neuweiler, H.; Johnson, C. M.; Fersht, A. R. *Proc. Natl. Acad. Sci. U.S.A.* **2009**, *106*, 18569.

28. Chowdhury, R.; Chattoraj, S.; Mojumdar, S. S.; Bhattacharyya, K. *Phys. Chem. Chem. Phys*. **2013**, *15*, 16286.

29. Lakowicz, J. R. *Principles of Fluorescence Spectroscopy*, Third Ed.; Springer, NY, **2006**.

30. Jha, A.; Udgaonkar, J. B.; Krishnamoorthy, G. *J. Mol. Biol*. **2009**, *393*, 735.

31. Flora, K.; Brennan, J. D.; Baker, G. A.; Doody, M. A.; Bright, F. V. *Biophys. J.* **1998**, *75*, 1084.

32. Page, T. A.; Kraut, N. D.; Page, P. M.; Baker, G. A.; Bright, F. V. *J. Phys. Chem. B* **2009**, *113*, 12825.

33. Rezaei-Tavirani, M.; Moghaddaminia, S. H.; Ranjbar, B.; Amani, M.; Marashi, S. A. *J. Biochem. Mol. Biol*. **2006**, *39*, 530.

34. Sahu, K.; Mondal, S. K.; Ghosh, S.; Roy, D.; Bhattacharyya, K. *J. Chem. Phys.* **2006**, *124*, 124909.

35. Dugiaczyk, A.; Law, S.; Dennison, O. E. *Proc. Natl. Acad. Sci. U.S.A.* **1982**, *79*, 71.

36. Peters, T. Jr. *All About Albumin: Biochemistry, Genetics, and Medical Applications* Academic press: San Diego, **1996**.

37. He, X. M.; Carter, D. C. Atomic Structure and Chemistry of Human Serum Albumin. *Nature* **1992**, *358*, 209.

38. Curry. S.; Mandelkow, H.; Brick, P.; Franks, N. *Nature Struc. Biol*. **1998**, *5*, 827.

39. Sugio, S.; Kashima, A.; Mochizuki, S.; Noda, M.; Kobayashi, K. *Protein Eng.* **1999**, *12*, 439.

40. Yadav, R.; Sen, P. *Protein Sci*. **2013**, *22*, 1571.

41. Wang, R.; Sun, S.; Bekos, E.; Bright, F. V. *Anal. Chem.* **1995**, *67*, 149.

42. 2.3 Thiol-Reactive Probes Excited with Ultraviolet Light, Invitrogen.

43. Kwon, G.; Remmers, A. E.; Datta, S.; Neubig, R. R. *Biochemistry* **1993**, *32*, 2401-.

44. Pal, N.; Verma, S. D.; Singh, M. K.; Sen, S. *Anal. Chem*. **2011**, *83*, 7736.

45. Müller, C. B.; Loman, A.; Pacheco, V.; Koberling, F.; Willbold, D.; Richtering, W.; Enderlein, J. *Europhys. Lett*. **2008**, *83*, 46001.

46. Chattopadhyay, K.; Saffarian, S.; Elson, E. L.; Frieden, C. *Biophys. J*. **2005**, *88*, 1413.

47. Sherman, E.; Itkin, A.; Kuttner, Y. Y.; Rhoades, E.; Amir, D.; Haas, E.; Haran, G. *Biophys. J*. **2008**, *94*, 4819.

48. Kelly, S. M.; Price, N. C. *Curr. Prot. Pept. Sci*. **2000**, *1*, 349.

49. Ahmad, B.; Ahmad, M. Z.; Haq, S. K.; Khan, R. H. *Biochim. Biophys. Acta* **2005,** *1750*, 93.

50. Santra, M. K.; Banerjee, A.; Krishnakumar, S. S.; Rahaman, O.; Panda, D. *Eur. J. Biochem*. **2004,** *271*, 1789.

51. Sharma, S.; Pal, N.; Chowdhury, P. K.; Sen, S.; Ganguli, A. K. *J. Am. Chem. Soc*. **2012**, *134*, 19677.

52. Galantini, L.; Leggio, C.; Konarev, P. V.; Pavel, N. V. *Biophys. Chem*. **2010**, *147*, 111.

53. Wilkins, D. K.; Grimshaw, S. B.; Receveur, V.; Dobson, C. M.; Jones, J. A.; Smith, L. J. *Biochemistry* **1999**, *38*, 16424.

54. Werner, J. H.; Joggerst, R.; Dyer, R. B.; Goodwin, P. M. *Proc. Natl. Acad. Sci. U.S.A.* **2006**, *103*, 11130.

55. Hirano, M.; Takeuchi, Y.; Aoki, T.; Yanagida, T.; Ide, T. *J. Biol. Chem*. **2010**, *285*, 3777.

Chapter 7

Effect of Sucrose on Chemically and Thermally Induced Unfolding of Domain I of Human Serum Albumin: Solvation Dynamics and Time Resolved Fluorescence Anisotropy Study

Rajeev Yadav *et al*., Manuscript under preparation

The present study is devoted to understand the effect of sucrose on the solvation dynamics and orientation relaxation dynamics within the domain I of HSA during chemically and thermally induced unfolding. A fluorescent probe N-(7-dimethylamino-4-methylcoumarin-3-yl) iodoacetamide (DACIA), which selectively binds with domain I of HSA through cys-34, was used for this study. It has been observed that the average solvation time become slower in presence of sucrose in the initial concentration of GnHCl, however at higher concentration of GnHCl the effect of sucrose is almost negligible. The effect of sucrose was found to be maximum for 1.25 M GnHCl. Time resolved fluorescence anisotropy of DACIA labeled HSA was used to monitor the effect of sucrose on the local orientation motion of domain I of HSA through "wobbling-in-cone" model. It has been observed that in the initial concentration region of GnHCl (till 1.75 M), the effect of sucrose on the semicone angle is very small as compared to the higher concentration of GnHCl. The dependence of associated water dynamics and anisotropy decay clearly indicates that the solvation dynamics plays an important role in the stabilization process at the low concentration region; whereas environmental restriction is responsible for stabilizing the domain I of HSA at the higher concentration of GnHCl. However, we have observed a negligible stabilizing effect of sucrose towards the temperature induced unfolding of domain I of HSA in the present temperature range.

7.1. Introduction

Dynamics plays a crucial role in controlling the structure and activity of proteins.[1] The solvation dynamics of interstitial water of a protein is believed to be responsible for retaining its active structure even under perturbed condition. The relaxation of water molecules near the hydrophilic groups of a protein thus plays an important role in controlling the structure and functions of a protein. Such water molecules are known as biological water.[1-3] Recent experiments revealed that the dynamics of such water associated with protein is significantly retarded compared to the bulk water. The role of biological water in the stability of protein is therefore a subject of great interests in the protein folding problems in last two decades.[1-5] Many of the researchers have studied that dynamics of water molecules in the different states of proteins.[2-4] Roy and co-workers have studied the solvation dynamics in native and different non-native states of glutaminyl-tRNA synthetase (GlnRS) using covalently attached, acrylodan and observed that the solvation dynamics become faster as GlnRS goes from native to molten globule to the fully unfolded state.[2a] Zewail and co-workers studied the solvation dynamics of different domains of HSA using, acrylodan and prodan that covalently binds to cys-34 of domain I and non-covalently to domain II, respectively. They obtained the time scale of dynamically ordered water as 57 ps for domain I and 32 ps for domain II. On unfolding the of domain I, the time constant has been observed as 61 ps and 13 ps in the intermediate state and the unfolded state, respectively.[3b] Bhattacharyya and co-workers have studied of deuterium isotope effect on the structure and solvation dynamics of HSA using coumarin 153 (C153). They observed that the solvation of C153 bound to HSA in H_2O as well as D_2O was bi-exponential and showed that the solvation dynamics becomes slow in D_2O as compared in H_2O. In H_2O, the two time components have been observed as 7 ps (30%) and 350 ps (70%); whereas, in D_2O the time components are 4 ps (41%) and 950 ps (59%).[2b] In another work they have measured the effect of room temperature ionic liquid (RTIL) on the native and denatured state of HSA using CMP (7-dimethylamino-3-(4-maleimidophenyl)-4-methyl Coumarin) covalently attached to cys-34 of HSA

and observed an average solvation time of 650 ps in the native state of HSA, 260 ps in presence of 1.5 M RTIL, 60 ps in presence of 6 M GnHCl and 30 ps in presence of 1.5 M RTIL along with 6 M GnHCl.[2c]

Apart from solvation dynamics, time resolved fluorescence anisotropy is also an efficient tool for structural characterization of a protein.[6-10] Fluorescence anisotropy decays usually fit with a sum of exponentials that gives the information about overall and local motion of the fluorescence probe attached to the protein.[8a] Krishnamoorthy and co-workers have studied the motional dynamics of a covalently attached probe (acrylodan) to a protein (barstar) at various locations using fluorescence anisotropy decay. They have observed that the correlation times for global as well as local motion, which ranges from sub-nanoseconds to the hundreds of nanoseconds, depends on the location of the fluorophore and are also different for different forms of the protein.[6b] Bohne and co-workers have studied the photocyclodimerization of 2-anthracenecarboxylate (AC) in the chiral binding site of human serum albumin (HSA) and concluded that the long rotational correlation time of 36 ns for AC bound to HSA is responsible for the high enantiomeric excess in photocyclodemerization reaction.[7]

In our previous work, we measured the unfolding mechanism of different domains of human serum albumin (HSA) and also investigated the stabilizing effect of sucrose on each domain (chapter 5). We observed that the unfolding behavior and the extent of stabilization by sucrose on different domains are different. In another work, we have reported the change in the conformational fluctuation dynamics of domain I of HSA during chemically and thermally induced unfolding (chapter 6)[11] and observed two intermediate states during GnHCl induced unfolding of domain I of HSA, whereas the intermediate states were absent during temperature induced unfolding. In the present work, we have explored the effect of sucrose on the stability of domain I of HSA during its chemically and thermally induced unfolding process using solvation dynamics and fluorescence anisotropy decay. A fluorescent probes, N-(7-dimethylamino-4-

methylcoumarin-3-yl) iodoacetamide (DACIA) was used to selectively label the domain I of HSA.

7.2. Data Analysis

The labeling DACIA with cys-34 of HSA has been described in detail previously (section 6.2). For all the experiments, samples were prepared in 50 mM phosphate buffer (pH 7.4) and the concentration of HSA was maintained as 10 μM for fluorescence lifetime and anisotropy decay measurements. For circular dichroism (CD) measurements the concentration was maintained as 2 μM.

For time resolved fluorescence anisotropy and fluorescence lifetime measurements, samples were excited at 376 nm. The fluorescence transients were collected at magic angle polarization in a commercial TCSPC setup. The full width at half maxima of the instrument response function was measured about 110 ps. For time resolved anisotropy measurements, the decays were collected at 0° and 90° with respect to the excitation polarization with a definite time interval. The fluorescence transients were analyzed by deconvoluting with IRF and found to be tri-exponential in nature with the from,

$$I(t) = \sum_{i=1}^{3} fi \exp(-t/\tau_i) \qquad (7.1)$$

where $I(t)$ is the fluorescence intensity at time t and f_i is the amplitude associated with the fluorescence lifetime τ_i with $\sum f_i = 1$.

The time-resolved fluorescence anisotropy decays, $r(t)$, were analyzed as a sum of exponential terms as follows.[8]

$$r(t) = r_0 \sum_{j=1}^{n} \beta_j \exp(-t/\phi_j) \quad n = 2 \text{ or } 3 \qquad (7.2)$$

where r_0 is the limiting anisotropy in absence of rotational diffusion, β_j is the amplitude of the rotational correlation time ϕ_j, where $\Sigma\beta_j = 1$. In the present study,

some anisotropy decays could be fitted with this model (bi-exponential and tri-exponential function at time *t*), however a few anisotropy decays were found to have a dip and rise nature in it. In such cases, the anisotropy decays could not be fitted with the above mentioned model and requires a two component model as follows.[8]

$$r(t) = \sum_{k=1}^{2} a_k(t) r_k(t) \tag{7.3}$$

Where $a_k(t)$ is the fractional intensity of fluorescence transient of the component *k* and $r_k(t)$ is the anisotropy decay of component *k* and can be defined as,[8]

$$a_1(t) = \frac{\sum_{m=1}^{3} f_{1m} \exp(-t/\tau_{1m})}{\sum_{m=1}^{3} f_{1m} \exp(-t/\tau_{1m}) + \sum_{n=1}^{3} f_{2n} \exp(-t/\tau_{2n})} \tag{7.4}$$

$$a_2(t) = \frac{\sum_{n=1}^{3} f_{2n} \exp(-t/\tau_{2n})}{\sum_{m=1}^{3} f_{1m} \exp(-t/\tau_{1m}) + \sum_{n=1}^{3} f_{2n} \exp(-t/\tau_{2n})} \tag{7.5}$$

$$r_1(t) = r_0 \beta_{11} \exp(-t/\phi_{11}) + r_0 \beta_{12} \exp(-t/\phi_{12}) \tag{7.6}$$

$$r_2(t) = r_0 \beta_{21} \exp(-t/\phi_{21}) + r_0 \beta_{22} \exp(-t/\phi_{22}) \tag{7.7}$$

Here f_{1m} and f_{2n} are the relative amplitudes of the lifetimes τ_{1m} and τ_{2n}, respectively. ϕ_{11} and ϕ_{12} are the rotational relaxation times with their amplitudes β_{11} and β_{12} for the first component, whereas, ϕ_{21} and ϕ_{22} are the rotational correlation times with their amplitudes β_{21} and β_{22} for the second component. The amplitudes are related as,

$$\beta_{11} + \beta_{12} = \beta_{21} + \beta_{22} = 1 \tag{7.8}$$

The construction of time resolved emission spectra (TRES) from the steady state intensity and time resolved fluorescence decay parameters has already been described in chapter 2.

7.3. Results

7.3.1. Steady-State and Time Resolved Fluorescence Spectroscopy

To study the effect of sucrose on chemically as well as thermally induced unfolding of domain I of HSA, we used a covalently attached solvatochromic dye (DACIA) to cys-34 residue of HSA. Coumarin dyes are good markers and their emission maximum is very sensitive towards solvent polarity. The absorption maximum of DACIA in 50 mM phosphate buffer (pH 7.4) shows a peak at 379 nm; whereas on labeling with HSA it become 383 nm. However a large shift in the emission maximum has been observed which changes from 478 nm in 50 mM phosphate buffer to 457 nm in HSA.[12] The absorption spectrum of DACIA attached to HSA does not change much during chemically as well as thermally induced unfolding, however the fluorescence response of DACIA bound to HSA is found to be very much dependent on the unfolding (both chemically and thermally) of HSA. In the unfolded state the emission maximum shifts towards the low energy side and shows a maximum at 478 nm in presence of 4.5 M GnHCl, which remains constant till 6 M GnHCl (at 298 K). The emission maximum of DACIA tagged HSA is found to be 461 nm when the temperature is increased to 353 K. The red shift in the emission maximum is due to the higher exposure of the probe to bulk water, which is only possible when protein gets denatured. The change in the emission maximum shows that domain I of HSA is denatured completely till 4.5 M GnHCl, whereas the effect of temperature till 353 K is not so drastic. Similarly, in presence of 1 M sucrose the absorption maximum of DACIA bound to HSA was almost unaffected, whereas the emission maximum changes from 457 nm in the native state (298 K) to 476.5 nm in presence of 4.5 M GnHCl (298 K). On increase in the temperature till 353 K the emission maximum shifted to 460 nm. Sucrose was found to stabilize the domain I of HSA as is evidenced from the smaller red shift of emission maximum from the native state during unfolding process.

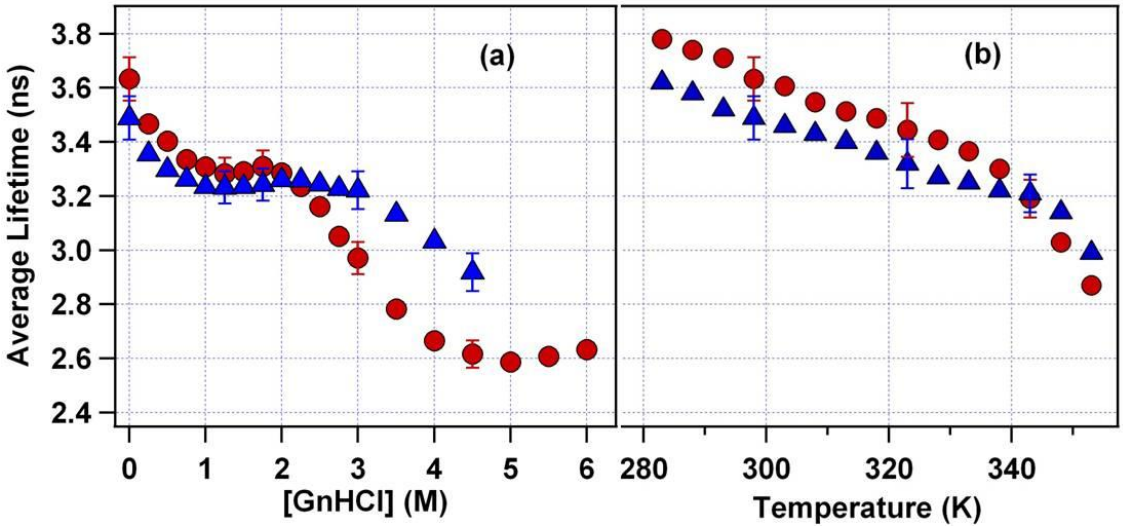

Figure 7.1. Change in the average lifetime of DACIA labeled HSA (●, red circles) in absence and (▲, blue triangles) in presence of 1 M sucrose as a function of (a) GnHCl concentration, and (b) temperature.

To get a better picture, we measured the lifetime of DACIA bound to HSA at different concentrations of GnHCl ranges from 0 to 6 M and at different temperatures ranging from 283 K to 353 K, both in absence and presence of 1 M sucrose and the data are depicted in figure 7.1 and also tabulated in table 7.1. In the native state of HSA and in absence of sucrose, the average lifetime has been observed as 3.63 ns which decreases to 2.6 ns on increase in the GnHCl concentration to 4.5 M with a dip and rise behavior in between, which has already been discussed in section 6.4.2. In presence of sucrose, the average lifetime of DACIA bound to HSA in native state is found to be 3.49 ns, which decreased to 2.92 ns at 4.5 M GnHCl. It shows that the denaturation is not completed at 4.5 M GnHCl in presence of sucrose and requires a higher GnHCl concentration for the complete unfolding. We also have measured the lifetime of DACIA labeled HSA at different temperatures ranging from 283 K to 353 K in absence as well as in presence of 1 M sucrose. Figure 7.1b shows the change in the average lifetime of DACIA-HSA with temperature in absence and presence of sucrose and the values are tabulated in table 7.1. At 283 K and in absence of sucrose, the average lifetime has been observed as 3.78 ns which become 2.87 ns at 353 K. However in presence of sucrose, the lifetime decreases from 3.62 ns at 283 K to 2.99 ns at 353 K. These

data clearly indicate the stabilizing effect of sucrose against thermally and chemically induced unfolding of HSA.

Table 7.1. Average fluorescence lifetimes for DACIA labeled HSA at different GnHCl concentrations and temperatures in absence and presence of 1 M sucrose.

Average Lifetime					
GnHCl (M)	**⟨τ⟩ (ns)**		**Temperature (K)**	**⟨τ⟩ (ns)**	
	0 M sucrose	**1 M sucrose**		**0 M sucrose**	**1 M sucrose**
0	3.63 ± 0.08	3.49 ± 0.08	**283**	3.78	3.62
0.25	3.47	3.36	**288**	3.74	3.58
0.5	3.40	3.30	**293**	3.71	3.52
0.75	3.33	3.26	**298**	3.63 ± 0.08	3.49 ± 0.08
1	3.31	3.24	**303**	3.61	3.46
1.25	3.28 ± 0.06	3.23 ± 0.06	**308**	3.55	3.43
1.5	3.29	3.24	**313**	3.51	3.4
1.75	3.30 ± 0.06	3.24 ± 0.06	**318**	3.49	3.36
2	3.29	3.26	**323**	3.45 ± 0.1	3.32 ± 0.09
2.25	3.24	3.26	**328**	3.41	3.27
2.5	3.16	3.24	**333**	3.37 ± 0.07	3.25 ± 0.07
2.75	3.05	3.23	**338**	3.30	3.22
3	2.97 ± 0.06	3.22 ± 0.07	**343**	3.19 ± 0.07	3.21 ± 0.07
3.5	2.78	3.13	**348**	3.03	3.14
4	2.67	3.03	**353**	2.87	2.99
4.5	2.62 ± 0.05	2.92 ± 0.07			
5	2.59				
5.5	2.61				
6	2.63				

7.3.2. Fluorescence Anisotropy Decay

GnHCl induced unfolding. We have measured the fluorescence anisotropy decay of DACIA labeled HSA in absence and presence of 1 M sucrose at 0 M, 1.25 M, 1.75 M, 3 M and 4.5 M GnHCl and are shown in figure 7.2a and 7.2b, respectively. In the native state of HSA, the measured fluorescence anisotropy decays were best fitted with two exponential function (equation 7.2) and the observed two time components with their amplitudes are observed as 0.5 ns (3%) and 44 ns (97%) in absence of sucrose; whereas in presence of sucrose the components are observed as

2.78 ns (4%) and 127 ns (96%). In both the cases, the slow time component was assigned to the global rotational motion of HSA, while the fast time component may involve the local orientational motion of DACIA molecule attached to the cys-34 of HSA. In presence of 1.25 M and 1.75 M GnHCl, the fluorescence anisotropy decays show a dip-and-rise behavior that can be fitted with the associated anisotropy decay model (equation 7.3) as described in section 7.2. In this model two rotational correlation times were chosen for each population. For the first population at 1.25 M GnHCl, the time components have been observed as 0.16 ns (6%) and 38 ns (94%) in absence of sucrose. In presence of 1 M sucrose these two time components are measured as 0.15 ns (6%) and 165 ns (94%). However, for the second population, the time components are found to be 0.17 ns (9%), 200 ns (91%) and 0.22 ns (4%), 1040 ns (96%) in absence and presence of 1 M sucrose, respectively. Similarly, at 1.75 M GnHCl for the first population, the time components have been observed as 0.19 ns (2%), 36 ns (98%) and 0.27 ns (4%), 228 ns (96%) in absence and presence of 1 M sucrose, respectively; and for the second population, the time components are observed as 0.19 ns (32%), 151 ns (68%) and 0.28 ns (6%), 940 ns (94%) in absence and presence of 1 M sucrose, respectively. In presence of 3 M and 4.5 M GnHCl, tri-exponential decay model (equation 7.2) was found to be sufficient to best fit the anisotropy decays. The three time component of the fluorescence anisotropy decay of DACIA labeled HSA in absence of sucrose are found to be 0.27 ns, 1.55 ns, 39 ns and 0.36 ns, 2.21 ns, 41 ns for 3 M and 4.5 M GnHCl, respectively. However in presence of 1 M sucrose, the three time components are observed as 0.40 ns, 1.22 ns, 238 ns and 0.66 ns, 4.57 ns, 314 ns for 3 M and 4.5 M GnHCl, respectively (see table 7.2). Here the extra time component was assigned to the segmental motion of the side chains of HSA, because at these concentrations of GnHCl the protein is almost unfolded. Here it is to be mentioned that the high viscosity of the medium in presence of 1 M sucrose may also contribute to the increase in rotational relaxation times.

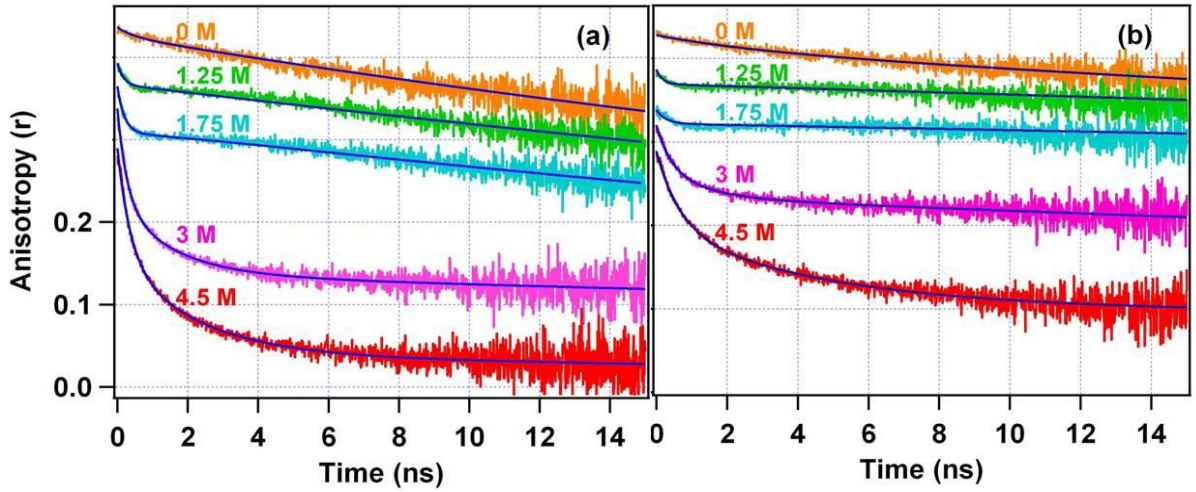

Figure 7.2. Time resolved anisotropy decays of DACIA labeled HSA in presence of 0 M (brown), 1.25 M (green), 1.75 M (cyan), 3 M (magenta) and 4.5 M (red) GnHCl concentrations. (a) in absence of sucrose, (b) in presence of 1 M sucrose. Solid blue line represents the best fit with the equations discussed data analysis section.

Table 7.2. Rotational correlation times with their amplitudes for DACIA labeled HSA at different concentrations of GnHCl in absence and presence of 1 M sucrose.

GnHCl (M)	Sucrose (M)	Native/Unfolded State				Intermediate State		
		ϕ_{11}[a] [ns] (α_{11})	ϕ_{12}[a] [ns] (α_{12})	ϕ_{13}[a] [ns] (α_{13})	θ°	ϕ_{21}[a] [ns] (α_{21})	ϕ_{22}[a] [ns] (α_{22})	θ°
0	**0**	0.50 (0.03)	—	44[b] (0.97)	**8.2**	—	—	
1.25	**0**	0.16 (0.06)	—	38[b] (0.94)	**11.6**	0.17 (0.09)	200[b] (0.91)	**14.3**
1.75	**0**	0.19 (0.02)	—	36[b] (0.98)	**6.6**	0.19 (0.32)	150[b] (0.68)	**28.6**
3	**0**	0.27 (0.35)	1.55 (0.28)	39[b] (0.37)	**44.8**	—	—	
4.5	**0**	0.36 (0.45)	2.21 (0.41)	41[b] (0.14)	**60.1**	—	—	
0	**1**	2.78 (0.04)	—	127[b] (0.96)	**9.4**	—	—	
1.25	**1**	0.15 (0.06)	—	165[b] (0.94)	**11.6**	0.22 (0.04)	1040[b] (0.96)	**9.4**
1.75	**1**	0.27 (0.04)	—	228[b] (0.96)	**9.4**	0.28 (0.06)	940[b] (0.94)	**11.6**
3	**1**	0.40 (0.15)	1.22 (0.12)	238[b] (0.73)	**25.9**	—	—	
4.5	**1**	0.66 (0.31)	4.57 (0.33)	314[b] (0.36)	**45.2**	—	—	

[a] ± 10 %, [b] as these values are >20 ns and all the intensity decays of DACIA in HSA completes till ~20 ns, hence the numbers can be misleading, θ is semicome angle as define in section 7.4

Temperature Induced Unfolding. To have a look on the conformational change of HSA during thermal induced unfolding and the effect of sucrose, we measured the fluorescence anisotropy decay of DACIA attached to HSA at different temperatures ranging from 283 K to 343 K in absence and presence of 1 M sucrose and are shown in figures 7.3a and 7.3b, respectively. Till 323 K the measured fluorescence anisotropy decay were best fitted with two exponential function (equation 2, with $n = 2$); whereas at higher temperature (333 K and 343 K), the decays were best fitted with three exponential decay model (equation 2, with $n = 3$) both in absence and presence of 1 M sucrose. At 283 K, the two time component with their amplitudes have been observed as 1.0 ns (3%), 40 ns (97%) and 1.5 ns (3%), 108 ns (97%) in absence and presence of 1 M sucrose, respectively. On increasing the temperature both the time components decrease with a small alteration in their amplitudes. At 303 K, these two time components and their amplitudes become 0.6 ns (4%), 36 ns (96%) and 1.48 ns (4%), 93 ns (96%); and at 323 K these were observed as 0.85 ns (3%), 27 ns (97%) and 1.06 ns (3%), 75 ns (0.97%) in absence and presence of 1 M sucrose, respectively. Similar to the GnHCl induced unfolding, the slow and fast time components were assigned to the global as well as local rotational motion of DACIA labeled with cys-34 of HSA. At higher temperature the decays were best fitted with three exponential function and at 343 K, the three time components are observed as 0.30 ns, 2.84 ns, 22 ns and 0.54 ns, 9.23 ns, 52 ns in absence and presence of 1 M sucrose, respectively (see table 7.3). We have observed that the longer component is much more temperature dependent and decreases with increase in the temperature. However with increase in the temperature the protein also get denatured and as a consequence the rotational relaxation time should increase as observed for GnHCl induced unfolding. The huge decrease in the viscosity of the sample with increase in the temperature may overcomes the effect of thermal unfolding and this can probably be the reason of decrease in rotational relaxation times with increase in the temperature of the medium.

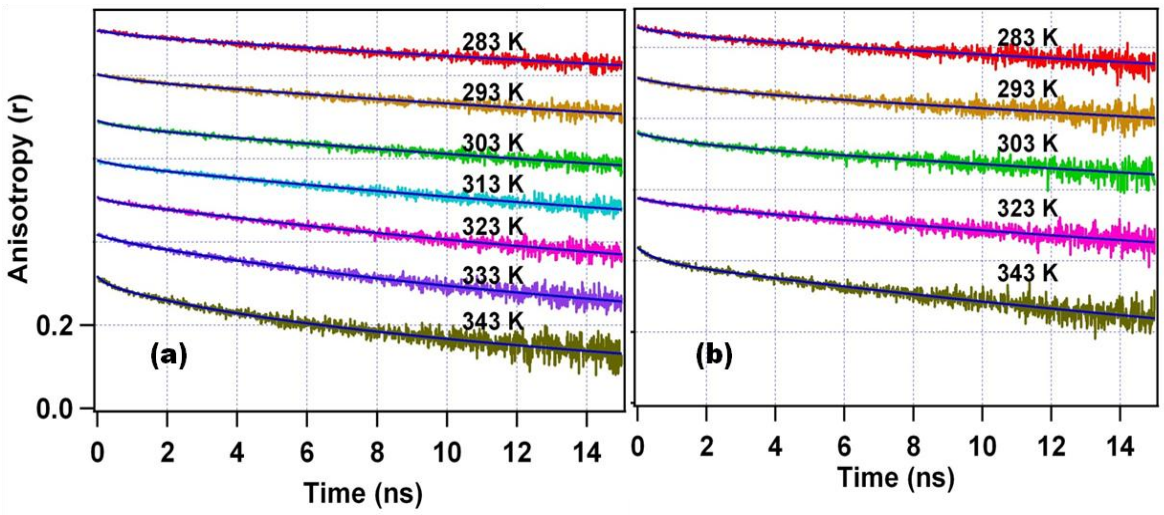

Figure 7.3. Time resolved anisotropy decays of DACIA labeled HSA at different temperatures, (a) in absence of sucrose, (b) in presence of 1 M sucrose. Solid blue line represents the best fit with the equations discussed data analysis section.

Table 7.3. Rotational correlation times with their amplitudes for DACIA labeled HSA at different temperatures in absence and presence of 1 M sucrose.

Temperature (K)	**Sucrose (M)**	**ϕ_{11}[a] [ns] (α_{11})**	**ϕ_{12}[a] [ns] (α_{12})**	**ϕ_{13}[a] [ns] (α_{13})**	**θ°**
283	**0**	1.00 (0.03)	—	40[b] (0.97)	**8.2**
293	**0**	0.8 (0.03)	—	44[b] (0.97)	**8.2**
303	**0**	0.6 (0.04)	—	36[b] (0.96)	**9.4**
313	**0**	0.6 (0.03)	—	35[b] (0.97)	**8.2**
323	**0**	0.85 (0.03)	—	27[b] (0.97)	**8.2**
333	**0**	0.51 (0.02)	6.06 (0.08)	25[b] (0.90)	**15.1**
343	**0**	0.30 (0.05)	2.84 (0.11)	22[b] (0.85)	**18.7**
283	**1**	1.48 (0.03)	—	108[b](0.97)	**8.2**
293	**1**	1.55 (0.04)	—	97[b] (0.96)	**9.4**
303	**1**	1.48 (0.04)	—	93[b] (0.96)	**9.4**
313	**1**	—	—	—	—
323	**1**	1.06 (0.03)	—	75[b] (0.97)	**8.2**
333	**1**	—	—	—	—
343	**1**	0.54 (0.06)	9.23 (0.04)	52[b] (0.90)	**15.1**

[a] ± 10 %, [b] as these values are >20 ns and all the intensity decays of DACIA in HSA completes till ~20 ns, hence the numbers can be misleading, θ is semicome angle as define in section 7.4

Here it is to mention that the excited state lifetime of DACIA in HSA is ~3 ns. This may give rise to a significant error in the longer rotational relaxation time for all the cases, which is always > 20 ns, as the fluorescence intensity decay

completes in ~20 ns time scale. Thus we could not determine the long component of the anisotropy decay accurately. Hence we will consider only the fast component for further discussion.

7.3.3. Solvation Dynamics

We also have studied the variation in the solvation dynamics of interstitial water molecules in domain I during chemically as well as thermally induced unfolding of HSA and the effect of sucrose on it using covalently attached DACIA to cys-34. Figure 7.4a shows the fluorescent transients of DACIA-HSA in 50 mM phosphate buffer (pH 7.4) at different wavelengths and in absence of sucrose (at 283 K). It clearly shows a fast decay at shorter wavelength side while rise is observed at longer wavelength side. Figure 7.4b shows the time resolved emission spectra (TRES) of DACIA-HSA at 283 K. At this temperature dynamic Stokes shift has been observed as 670 cm^{-1} and solvation completed in 11 ns.

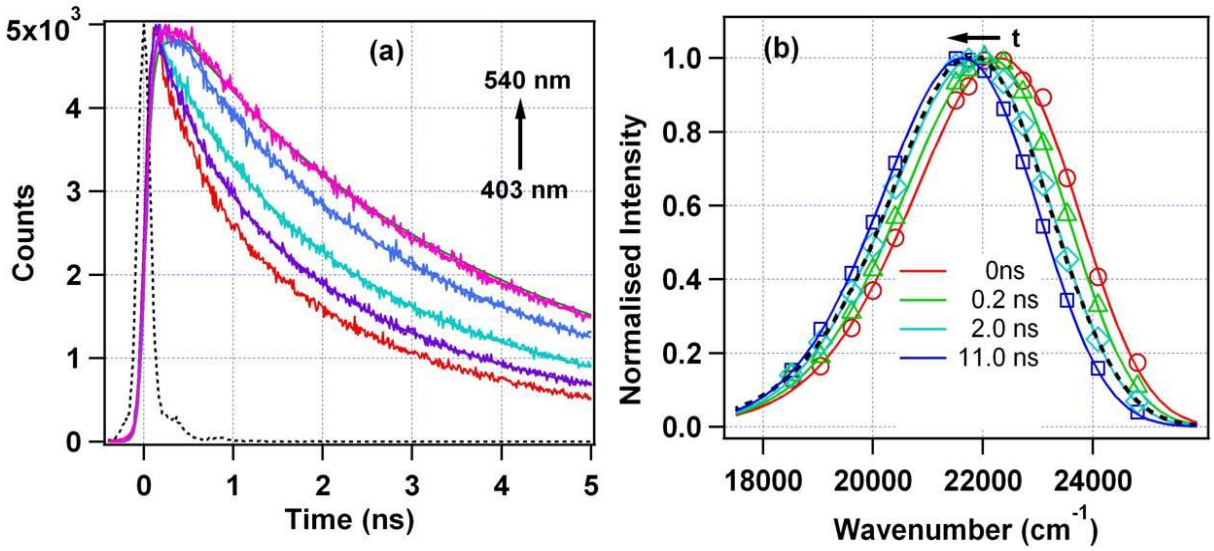

Figure 7.4. (a) Fluorescent transients of DACIA labeled HSA (λ_{ex} = 376 nm) at diferent wavelength ranges from 403 nm to 540 nm and at 283 K. (b) Time resolved emission spectra (TRES) of DACIA labeled HSA at 283 K. Dashed line is the steady state emission spectrum.

GnHCl Induced Unfolding. At room temperature, we recorded fluorescent transient of DACIA-HSA at 0 M, 0.25 M, 1.25 M, 1.75 M, 3 M and 4.5 M GnHCl

concentration, in absence and presence of 1 M sucrose. Wavelength dependence transients for all the cases show a rise at the red end, while only decay at the blue end. This clearly suggests a signature of solvation for all the systems. To estimate the solvation time, we have constructed TRES at each GnHCl concentration in absence and presence of 1 M sucrose. Few are shown in figure 7.5. The dynamic Stokes shift for the native HSA is observed as 560 cm^{-1} and 640 cm^{-1} in absence and presence of 1 M sucrose, respectively. The Stokes shift found to decrease with increase in the concentration of GnHCl for both cases, i.e. in absence and presence of 1 M sucrose as shown in table 7.4. At 4.5 M GnHCl the Stokes shift has been observed as 200 cm^{-1} and 300 cm^{-1} in absence and presence of 1 M sucrose, respectively.

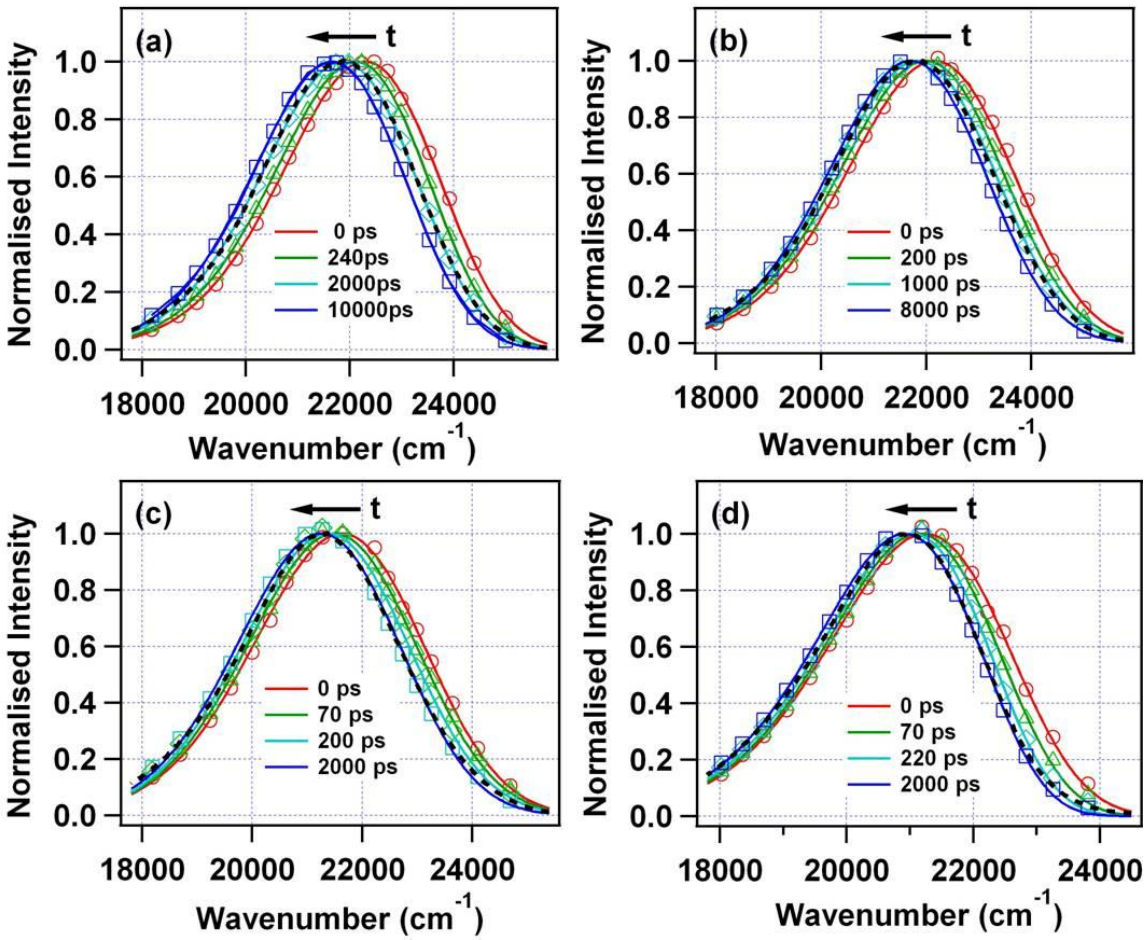

Figure 7.5. Time resolved emission spectra of DACIA labeled HSA at (a) 0 M, (b) 1.25 M, (c) 3 M, (d) 4.5 M GnHCl in presence of 1 M sucrose. Dashed line is the steady state emission spectrum of respective system.

Table 7.4. Decay parameters of $C(t)$ of DACIA labeled HSA at different concentrations of GnHCl in absence and presence of 1 M sucrose.

GnHCl (M)	Sucrose (M)	Stokes Shift[a] (cm^{-1})	Individual Fit				
			a_1	τ_1[b] (ps)	a_2	τ_2[b] (ps)	$\langle\tau_s\rangle$[c] (ps)
0	**0**	560	0.44	300	0.56	3800	**2300**
0.25	**0**	500	0.46	170	0.54	2300	**1300**
1.25	**0**	310	0.70	220	0.30	240	**230**
1.75	**0**	240	0.77	150	0.23	150	**150**
3	**0**	160	0.78	130	0.22	150	**150**
4.5	**0**	200	0.77	100	0.23	440	**180**
0	**1**	640	0.43	290	0.57	4100	**2500**
0.25	**1**	—	—	—	—	—	—
1.25	**1**	540	0.59	250	0.41	4000	**1800**
1.75	**1**	380	0.75	190	0.25	2300	**700**
3	**1**	380	0.73	130	0.27	340	**200**
4.5	**1**	300	0.75	150	0.25	730	**300**

[a] $\pm$ 50 cm^{-1}, [b] $\pm$ 10 % , [c] $\langle\tau_s\rangle = \sum a_i\tau_i$

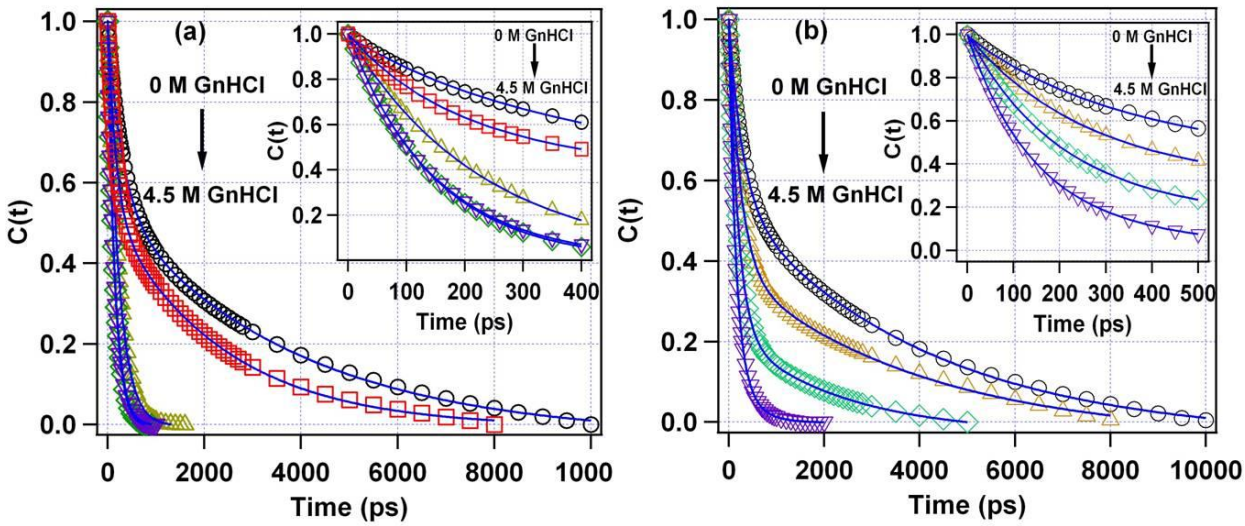

Figure 7.6. Decay of solvent response function**,** $C(t)$, of DACIA labeled HSA at different GnHCl concentrations ranging from 0 M to 4.5 M (a) in absence and (b) in presence of 1 M sucrose. Inset shows the $C(t)$ decays in the initial time.

The decays of solvent correlation function, $C(t)$ in absence and presence of 1 M sucrose are shown in figures 7.6a and 7.6b, respectively. The decay of $C(t)$ are fitted bi-exponentially and the decay parameters are summarized in table 7.4. In the native state of HSA, two time components of 300 ps and 3800 ps with an average

solvation time 2300 ps have been observed, which on increasing the GnHCl concentration decreases and become 100 ps and 440 ps with an average solvation time of 180 ps at 4.5 M GnHCl. However, in presence of 1 M sucrose the decrease in the solvation time is less as the concentration of GnHCl increased. The solvation time decreases from 2500 ps, in the native state to 300 ps at 4.5 M GnHCl in presence of 1 M sucrose.

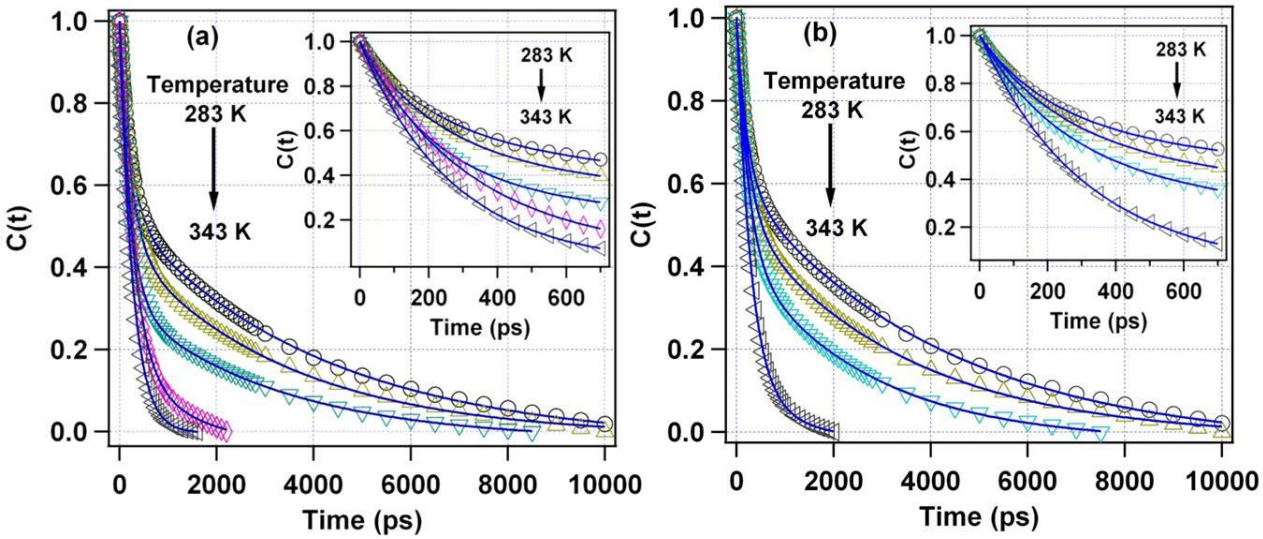

Figure 7.7. Decay of solvent response function**,** $C(t)$, of DACIA labeled HSA at different temperatures ranging from 283 K to 343 K (a) in absence and (b) in presence of 1 M sucrose. Inset shows the $C(t)$ decays in the initial time.

Temperature Induced Unfolding. Similar to the GnHCl, wavelength dependence transients of DACIA-HSA at different temperatures ranges from 283 K to 343 K also show a signature of solavtion for all the cases (at each temperature in absence and presence of 1 M sucrose). For all the systems, TRES have been constructed and the dynamic Stokes shift has been observed, which are shown in table 7.5. At 283 K the Stokes shift have been observed as 670 cm^{-1} and 770 cm^{-1}, which on increase the temperature till 343 K decreases to 270 cm^{-1} and 320 cm^{-1} in absence and presence of 1 M sucrose, respectively. Figure 7.7a and 7.7b exhibit the decays of $C(t)$ at different temperatures in absence and presence of 1 M sucrose, respectively. In the temperature range from 283 K to 323 K, the $C(t)$ decays are also bi-exponential in nature and the fitting parameters are summarized in table

7.5. At 283 K, the average solvation time, $\langle \tau_s \rangle$ has been observed as 2400 ps, which decreases with increasing the temperature and become 280 ps at 343 K. While, in presence of 1 M sucrose the value of $\langle \tau_s \rangle$ decreases from 2700 ps at 283 K to 400 ps at 343 K.

Table 7.5. Decay parameters of $C(t)$ of DACIA labeled HSA at different temperatures in absence and presence of 1 M sucrose.

Temperature	**Sucrose**	**Stokes Shift**[a]	**Individual Fit**				
(K)	**(M)**	**(cm^{-1})**	a_1	τ_1[b](ps)	a_2	τ_2[b](ps)	$\langle \tau s \rangle$[c] (ps)
283	**0**	670	0.44	230	0.56	4100	**2400**
293	**0**	620	0.48	250	0.52	3600	**2000**
303	**0**	510	0.53	230	0.47	3350	**1700**
313	**0**	490	0.60	240	0.40	3100	**1400**
323	**0**	410	0.67	220	0.33	3200	**1200**
333	**0**	320	0.81	290	0.19	1700	**550**
343	**0**	270	0.99	270	0.01	700	**280**
283	**1**	770	0.38	220	0.62	4200	**2700**
293	**1**	680	0.41	250	0.59	3600	**2200**
303	**1**	610	0.47	240	0.53	3400	**1900**
313	**1**	—	—	—	—	—	—
323	**1**	490	0.55	240	0.45	2600	**1300**
333	**1**	—	—	—	—	—	—
343	**1**	320	0.86	290	0.14	1200	**400**

[a] $\pm$ 50 cm^{-1}, [b] $\pm$ 10 % , [c] $\langle \tau s \rangle = \sum a_i \tau_i$

7.4. Discussion

The main aim of the present work is to understand the involvement of conformational dynamics and the solvation dynamics during chemically and thermally induced unfolding of domain I of HSA and also to study the effect of sucrose therein.

As mentioned, the fluorescence anisotropy has been used to measure the global as well as local orientational dynamics of HSA. The fitting parameters of anisotropy decays of DACIA tagged to cys-34 of HSA at each GnHCl concentration shows two rotational time components. The longer-lived time

component was assigned to the global rotational motion of HSA, while the shorter-lived rotational motion comprises of local orientation motion of DACIA inside HSA. The local orientation time in native state is 0.5 ns and decreased to 0.16 ns at 1.25 M GnHCl which become 0.36 ns in denatured state. As the local probe motion is faster than the global motion of the protein, the fluorescence anisotropy decay of DACIA tagged HSA was analyzed in terms of "wobbling-in-cone" model.[8-10] In this model, the semicone angle (θ) is associated with a cone within which a fluorescent molecule precesses during its excited state lifetime and can be written as,[8a,9]

$$\theta = \cos^{-1}\left[\frac{1}{2}\{(8\beta_S^{1/2}+1)^{1/2}-1\}\right] \qquad (7.9)$$

where β_s is the amplitude of the slowest rotational time component. The semicone angle is the measure of the local motion of the probe, which is associated with the local environment such as compactness of the protein. In absence of GnHCl, θ is found to be 8.2° which become 60.1° in presence of 4.5 M GnHCl (see figure 7.8a). This indicates that the probe is free to move in the denatured state of protein. Here it is to be noted that the value of θ increases to 11.6° at 1.25 M and again decrease to 6.6° at 1.75 M GnHCl, which is very similar to the value as in native state of HSA. In the previous work (chapter 6), we have showed that domain I of HSA follow a four state model containing two intermediate states during GnHCl induced unfolding, whereas in the temperature induced unfolding it follow a two state model without any intermediate state.[12] Convincingly, the present results also favors the presence of intermediate states during GnHCl induced unfolding. In presence of 1 M sucrose the θ value also shows a dip and rise behavior in the initial concentration of GnHCl. At 1.75 M GnHCl the semicone angle has been observed as 9.4°, which is equal when denaturant is absent. However at higher concentration of GnHCl the effect of sucrose is more, where the θ value has been observed as 45.2° at 4.5 M GnHCl as shown in figure 7.8a and values are given in table 7.2.

This indicates that the stabilization effect of sucrose is more for higher concentration of denaturant, i.e. the probe is not completely free to move as observed when sucrose was absent in the system.

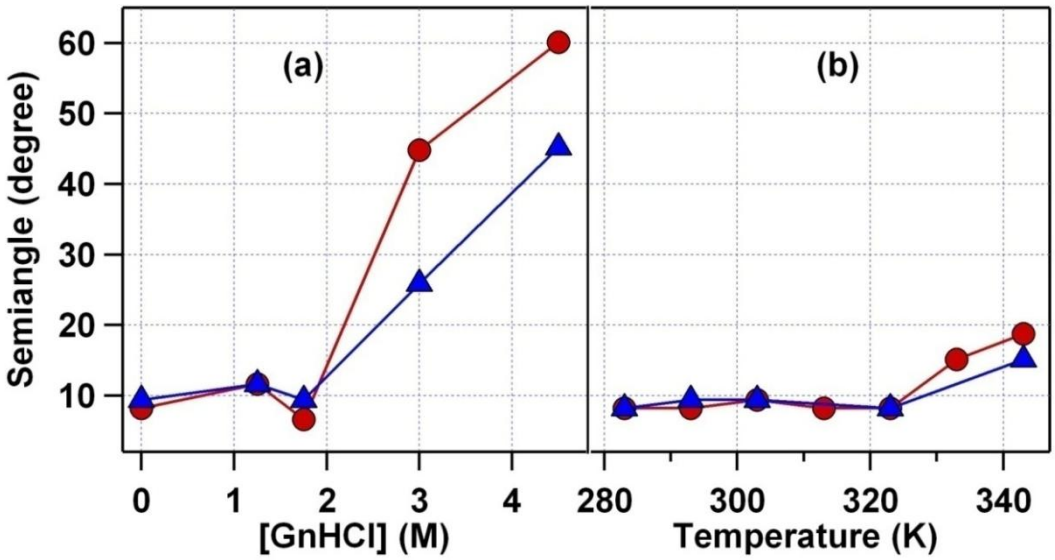

Figure 7.8. Change in the semicone angle (●) in absence and (▲) in presence of 1 M sucrose as a function of (a) GnHCl concentration and (b) temperature.

Similar to the GnHCl induced unfolding, the anisotropy decay of DACIA-HSA also shows two rotational time components at different temperatures ranges from 283 K to 323 K, whereas at higher temperature it has three time components. The faster time component, which was assigned for local orientation dynamics, decreases from 1 ns at 283 K to 0.30 ns at 343 K. To better understand this behavior we have calculated the semicone angle for DACIA-HSA at each temperature. At 283 K, θ is found to be 8.2° which is almost unaffected till 323 K and become 18.73° at 343 K as shown in figure 7.8b and the values are tabulated in table 7.3. This clearly shows that the structure of domain I of HSA remains unchanged till 323 K; afterward a small denaturation occurs in the structure. It is also in agreement with our previous results.[12] In presence of 1 M sucrose, the θ value, which is 8.2° at 283 K, also remains same till 323 K and become 15.1° at 343 K. This indicates that at 343 K, HSA does not denature appreciably.

The $C(t)$ decay of DACIA-HSA shows two solvation time components at each GnHCl concentration. A small change has been observed for the first component, which decreases from ~300 ps at 0 M GnHCl to ~100 ps at 4.5 M GnHCl, while a prominent change has been observed in the second component, which decreases from ~3800 ps at 0 M GnHCl to ~440 ps at 4.5 M GnHCl. The average solvation time decreases from 2300 ps at 0 M GnHCl to 180 ps at 4.5 M GnHCl as shown in figure 7.9a. These solvation time components can be assigned to the motion of the structured water molecules which are hydrogen bonded with the polar amino acid residues of the protein.[1,13,14] The slow solvation of these biological water molecules is responsible to retain the protein in its native form. The solvation becomes faster when it gets denatured as we observed at higher GnHCl concentration. As it can be seen, the effect of sucrose on solvation dynamics in HSA is almost negligible in its native state and fully denatured state. However for partially unfolded HSA, the effect of sucrose found to be prominent. For example, at 1.25 M GnHCl the solvation dynamics is retarded by 7.8 times in presence of sucrose. This suggests that the effect of sucrose on the solvation dynamics is more in the initial concentration of GnHCl.

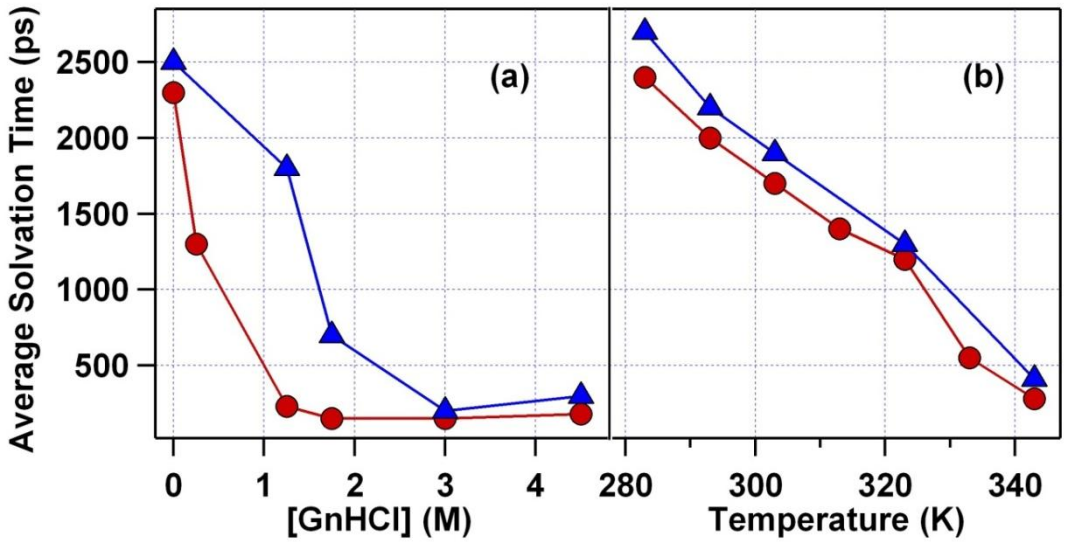

Figure 7.9. Change in the average solvation time (●) in absence and (▲) in presence of 1 M sucrose as a function of (a) GnHCl concentration and (b) temperature

Figure 7.9b shows the change in the average solvation time with temperature, in absence and presence of 1M sucrose. In absence of sucrose the average solvation time has been observed as 2400 ps at 283 K, which on increase in the temperature decreases continuously and become 280 ps at 243 K. In presence of 1 M sucrose it decreases form 2700 ps at 283 K to 400 ps at 343 K in a similar fashion. At all the temperatures, a marginal increase has been observed in the solvation time in presence of sucrose which is much less compared to the effect of sucrose on chemical denaturation. Hence for temperature induced unfolding, the solvation dynamics is almost unaffected by sucrose.

7.5. Conclusion

For this study, N-(7-dimethylamino-4-methylcoumarin-3-yl) iodoacetamide (DACIA) was selectively tagged with domain I of HSA. In absence of sucrose, the average solvation time, $\langle \tau_s \rangle$, in domain I of HSA has been measured as 2300 ps in the native state, 230 ps (~0.1 times of the native state) in presence of 1.25 M GnHCl, 150 ps (~0.07 times of the native state) in presence of 3 M GnHCl concentration, and remains almost unchanged at higher concentration of GnHCl. Whereas, in presence of 1 M sucrose, $\langle \tau_s \rangle$ value decreases from 2400 ps in native state to 1800 ps (~0.75 times of the native state) and to 200 ps (~0.08 times of the native state) in presence 1.25 M GnHCl and 3 M GnHCl, respectively and remains almost similar at higher concentration of GnHCl. The effect of sucrose was found to be maximum for 1.25 M GnHCl concentration. Time resolved fluorescence anisotropy of DACIA labeled HSA was also measured and the data was analysed using "wobbling-in-cone" model to investigate the local motion in domain I. In the native state of HSA, the semicone angle of the local motion has been observed as 8.2°, which become 60° (~7.3 time increase) at 4.5 M GnHCl concentration, in absence of sucrose. In the initial concentration of GnHCl (till 1.75 M), the effect of sucrose on the semicone angle is very small. However, the semicone angle appreciably decreased at higher concentration of GnHCl in presence of sucrose.

These observations clearly indicate that the solvation dynamics plays an important role in the stabilization process at low concentration region; whereas environmental restriction is responsible for stabilizing the domain I of HSA at the higher concentration of GnHCl. On the contrary, we have not observed any significant stabilizing effect of sucrose towards the temperature induced unfolding of domain I of HSA in the present temperature range.

References

1. (a) Pal, S. K.; Zewail, A. H. *Chem. Rev.* **2004**, *104*, 2099.
   (b) Bagchi, B. *Chem. Rev*. **2005**, *105*, 3197.
   (c) Wang, L.; Yu, X.; Hu, P.; Broyde, S.; Zhang, Y. *J. Am. Chem. Soc*. **2007**, *129*, 4731.
   (d) Winterburn, T. J.; Wyatt, D. M.; Phylip, L. H.; Bur, D.; Harrison, R. J.; Berry, C.; Kay, J. *J. Biol. Chem*. **2007**, *282*, 6508.
   (e) Friedman, R.; Fischer, S.; Nacliel, E.; Scheiner, S.; Gutman, M. *J. Phys. Chem. B* **2007**, *111*, 6059.
   (f) K. Bhattacharyya, *Chem. Commun*. **2008**, 2848.
2. (a) Samaddar, S.; Mandal, A. K.; Mondal, S. K.; Sahu, K.; Bhattacharyya, K.; Roy, S. *J. Phys. Chem. B* **2006**, *110*, 21210.
   (b) Das, D. K.; Mondal, T.; Mandal, U.; Bhattacharyya, K. *ChemPhysChem* **2011**, *12*, 814.
   (c) Chowdhury, R.; Mojumdar, S. S.; Chattoraj, S.; Bhattacharyya, K. *J. Chem. Phys*. **2012**, *137*, 55104.
3. (a) P. Sasisanker, A. Oleinikova, H. Weingartner, R. Ravindra, R. Winter, Phys. Chem. Chem. Phys. 2004, 6, 1899–1905.
   (b) Kamal, J. K. A.; Zhao, L.; Zewail, A. H. *Proc. Natl. Acad. Sci. U.S.A.* **2004**, *101*, 13411.
4. (a) Zhang, L.; Yang, Y.; Kao, Y. T.; Wang, L.; Zhong, D. *J. Am. Chem. Soc*. **2009**, *131*, 10677.
   (b) Kim, S.; Chung, J. K.; Kwak, K.; Bowman, S. E. J.; Bren, K. L.; Bagchi, B.; Fayer, M. D.; *J. Phys. Chem. B* **2008**, *112*, 10054.
5. (a) Pal, A.; Samanta, A. *J. Phys. Chem. B* **2007**, *111*, 4724.
   (b) Baker, S. N.; Zhao, H.; Pandey, S.; Heller, W. T.; Bright, F. V.; Baker, G. A. *Phys. Chem. Chem. Phys*. **2011**, *13*, 3642.
6. (a) Rami, B. R.; Krishnamoorthy, G.; Udgaonkar, J. B. *Biochemistry* **2003**, *42*, 7986.

(b) Jha, A.; Ishii, K.; Udgaonkar, J. B.; Tahara, T.; Krishnamoorthy, G. *Biochemistry* **2011**, *50*, 397.

7. Fuentealba, D.; Kato, H.; Nishijima, M.; Fukuhara, G.; Mori, T.; Inoue, Y.; Bohne, C. *J. Am. Chem. Soc*. **2013**, *135*, 203−209.
8. (a) Lakowicz, J. R. *Principles of Fluorescence Spectroscopy*, Springer, 3rd Ed. **2006**.

   (b) Jha, A.; Udgaonkar, J. B.; Krishnamoorthy, G. *J. Mol. Biol*. **2009**, *393*, 735-752.
9. a) Flora, K.; Brennan, J. D.; Baker, G. A.; Doody, M. A.; Bright, F. V. *Biophys. J*. **1998**, *75*, 1084-1096.

   (b) Page, T. A.; Kraut, N. D.; Page, P. M.; Baker, G. A.; Bright, F. V. Dynamics of loop 1 of domain I in human serum albumin when dissolved in ionic liquids, *J. Phys. Chem. B* **2009**, *113*, 12825-12830.

   (c) Quitevis, E. L.; Marcus, A. H.; Fayer, M. D. *J. Phys. Chem*. **1993**, *97*, 5762-5769.
10. (a) Sen, P.; Ghosh, S.; Sahu, K.; Mondal, S. K.; Roy, D.; Bhattacharyya, K. *J. Chem. Phys*. **2006**, *124*, 204905.

    (b) Sahu, K.; Mondal, S. K.; Ghosh, S.; Roy, D.; Bhattacharyya, K. *J. Chem. Phys*. **2006**, *124*, 204909.
11. Yadav, R.; Sen, P. *Protein Sci*. **2013**, 22, 1571-1581.
12. Yadav, R.; Sengupta, B.; Sen, P. *J. Phys. Chem. B* **2014,** DOI: 10.1021/jp502762t.
13. Chang, C. W.; Guo, L.; Kao, Y. T.; Li, J.; Tan, C.; Li, T.; Saxena, C.; Liu, Z.; Wang, L.; Sancar, A.; Zhong, D. *Proc. Natl. Acad. Sci. U.S.A*. **2010**, *107*, 2914.
14. Chang, C. W.; He, T. F.; Guo, L.; Stevens, J. A.; Li, T.; Wang, L.; Zhong, D. *J. Am. Chem. Soc*. **2010**, *132*, 12741.

Concluding Remarks and Future Outlook

In this thesis I have studied the domain specific response of multi-domain proteins towards molecular interactions, unfolding and dynamics using fluorescence based techniques. For these studies human as well as bovine serum albumin has been chosen as model protein, which contains three distinct domains. The main conclusion from the current work is that the properties of all three domains are different from each other and also from the overall protein in many perspectives as observed by circular dichroism (CD), UV-Vis, steady state and time resolved fluorescence spectroscopy and fluorescence correlation spectroscopic (FCS) study.

As most of the work in this thesis has been done at bulk level and revealed very useful information about molecular interactions, unfolding and dynamics for each domain of serum albumin. For better understanding these complex biological processes, it requires the knowledge at single molecular level. FCS is such a technique that has the capability to monitor the molecular interactions, unfolding and conformational change at the single molecular level.[1-6] We have recently constructed the FCS setup in our lab and studied the conformational fluctuation dynamics of domain I of HSA.[7] The FCS study for other two domain and molecular interactions and unfolding can also give a better information while studied at single molecular level.

For the present study we used different fluorescent marker for different domains of protein. Since the sensitivity change of fluorescent marker molecules towards environmental vary from molecule to molecule, hence as a future perspective one can use a single fluorescent molecule which can attached to the all part of a protein either by mutation or other.

References

1. Maiti, S.; Haupts, U.; Webb, W. W. *Proc. Natl. Acad. Sci. U.S.A.* **1997**, *94*, 11753.
2. Haustein, E.; Schwille, P. *Annu. Rev. Biophys. Biomol. Struct*. **2007**, *36*, 151.
3. Chattopadhyay, K.; Saffarian, S.; Elson, E. L.; Frieden, C. *Proc, Natl. Acad. Sci. U.S.A.* **2002**, *99*, 14171.
4. Chattopadhyay, K.; Elson, E. L.; Frieden, C. *Proc. Natl. Acad. Sci. U.S.A.* **2005**, *102*, 2385.
5. Sasmal, D. K.; Mondal, T.; Majumdar, S. S.; Choudhury, A.; Banerjee, R.; Bhattacharyya, K. *J. Phys. Chem. B* **2011**, *115*, 13075
6. Patra, S.; Santhosh, K.; Pabbathi, A.; Samanta, A. *RSC Advances* **2012**, *2*, 6079.
7. Yadav, R.; Sengupta, B.; Sen, P. *J. Phys. Chem. B* **2014,** DOI: 10.1021/jp502762t.

List of Publications

1. Microviscosity inside a Nanocavity: A Femtosecond Fluorescence Up-Conversion Study of Malachite Green.
   Shahnawaz Rafiq, **Rajeev Yadav**, Pratik Sen, *J. Phys. Chem. B* **2010**, *114*, 13988.

2. Femtosecond Excited-State Dynamics of 4-Nitrophenyl Pyrrolidinemethanol: Evidence of Twisted Intramolecular Charge Transfer and Intersystem Crossing Involving the Nitro Group.
   Shahnawaz Rafiq, **Rajeev Yadav**, Pratik Sen, *J. Phys. Chem. A* **2011**, *115*, 8335.

*3. Static and Dynamic Aspects of Supramolecular Interaction of Coumarin 153 and Fluorescein with Bovine Serum Albumin.
   Rajeev Yadav, Shyamashis Das, Pratik Sen, *Aust. J. Chem. **2012**, 65,* 1305.

4. Novel Chemosensor for the Visual Detection of Copper (II) in Aqueous Solution at the ppm Level.
   Vadapalli Chandrasekhar, Sourav Das, **Rajeev Yadav**, Sakiat Hossain, Rashmi Parihar, Ganesh Subramaniam, Pratik Sen, *Inorg. Chem*. **2012**, *51*, 8664.

*5. Mechanistic Investigation of Domain Specific Unfolding of Human Serum Albumin and the Effect of Sucrose.
   Rajeev Yadav, Pratik Sen, *Protein Sci.* **2013**, *22*, 1571.

6. Spectroscopic Study of Molecular Interactions in the Binary Mixture of Ethylacetoacetate and Tetrahydrofuran.
   Priyanka Yadav, **Rajeev Yadav**, *J. Chem. Cheml. Sci.* **2013**, *3*, 269.

7. Study of Molecular Interaction in Binary Liquid Mixtures of Ethyl Acetoacetate with Chloroform and Dimethylsulphoxide Using Excess Acoustic Parameters and Spectroscopic Methods.
   Priyanka Yadav, Manoj Kumar, **Rajeev Yadav**, *Phys. Chem. Liq.* **2014**, *52*, 31.

8. Multi-Pyrene Assemblies Supported on Stannoxane Frameworks: Synthesis, Structure and Photophysical Studies.
   Subrata Kundu, Ramesh K. Metre, **Rajeev Yadav**, Pratik Sen, Vadapalli Chandrasekhar, *Chem. Asian J.* **2014**, *9*, 1403.

*9. Conformational Fluctuation Dynamics of Domain I of Human Serum Albumin in the Course of Chemically and Thermally Induced Unfolding Using Fluorescence Correlation Spectroscopy.
Rajeev Yadav, Bhaswati Sengupta, Pratik Sen, *J. Phys. Chem. B*, **2014**, *118*, 5428.

*10. Direct Observation of Intermediate State(s) in the Mechanistic Investigation of Domain Specific Protein-Surfactant Interaction.
Rajeev Yadav, Shyamashis Das, Pratik Sen, *Luminescence*, Submitted.

*11. Effect of Sucrose on Chemically and Thermally Induced Unfolding of Domain I of Human Serum Albumin: Solvation Dynamics and Fluorescence Anisotropy Decay Kinetics Study.
Rajeev Yadav, Bhaswati Sengupta, Pratik Sen, Manuscript under preparation.

*12. Temperature Dependent Binding Modes of Coumarin 152 with Human Serum Albumin.
Rajeev Yadav, Pratik Sen, Manuscript under preparation.

13. Appearance of Slow Solvation Dynamics and Diffusion Coefficient in Methanol-Chloroform Binary Solvent Mixture: A Case of Synergistic Solvation in Mixed Solvents.
Shradhey Gupta, **Rajeev Yadav**, Bhaswati Sengupta, Shahnawaz Rafiq, Pratik Sen, Manuscript under preparation.

14. Natural Compound Inspired Synthesis of β-carboline Based Derivatives as Potent Anticancer Agents.
Shashi Dighe, **Rajeev Yadav**, Pratik Sen, Sanjiv Batra, Manuscript under preparation

15. Study of Sequential Interaction of Anionic and Cationic Surfactants with Drug Binding Site I of Human Serum Albumin.
Rajeev Yadav, Pratik Sen, Manuscript under preparation

* Included in thesis